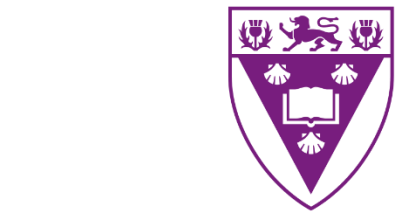

RHODES UNIVERSITY

Where leaders learn

The development of high-throughput assays to screen for potential anticancer and antimalarial compounds that target ADP-ribosylation factor 6 and its signalling machineries

A thesis submitted in fulfilment of the requirements for the degree of Master of Science in Biochemistry

Farrah Khan

January 2019

Abstract

ADP-ribosylation factors (Arfs) are small GTP-binding proteins that cycle between active GTP-bound forms and inactive GDP-bound forms. GDP/GTP cycling is regulated by large families of guanine nucleotide exchange factors (GEFs) and GTPase activating proteins (GAPs). ArfGEFs activate Arfs by mediating the exchange of GDP for GTP, while ArfGAPs terminate Arf function by stimulating the hydrolysis of the terminal phosphate group of GTP. Arf6 is a major regulator of endocytic trafficking and reorganization of the actin cytoskeleton in eukaryotic organisms. Owing to its participation in wide range of fundamentally distinct cellular processes, Arf6 may be a drug target for cancer and malaria amongst other diseases. As with cancer cells, rapid growth and viability of eukaryotic pathogens likely places a heavy burden on their endocytic pathways and a critical reliance on Arf6 activity. A putative malarial homolog of Arf6 (*Pf*Arf6) localises to numerous puncta along the periphery of the parasite in the mature trophozoite life stage of the parasite (T. Swart, MSc dissertation). Owing to highly inefficient parasite transfection procedures and a relative shortage of well described and validated parasite organelle markers, the possible functions of *Pf*Arf6 were explored using HeLa cells as a surrogate model for parasites by fluorescence microscopy of cells transfected with GFP-tagged *Pf*Arf6. Partial co-localisation was observed with the mammalian markers *Hs*Arf6 and LC3, which suggested possible roles in Arf6-dependent endocytosis and autophagy, respectively. While these possible roles are currently under investigation in parasites, an overall long-term goal which was initiated in this study was to determine whether *Pf*Arf6 is a valid drug target. To chemically validate *Pf*Arf6 as a drug target, a potent inhibitor needs to be identified. This requires the development of assays that may be employed for high-throughput screening of compound libraries. To support this goal, a novel plate-based assay was developed using human Arf6. The assay relies on the selective binding of an Arf effector protein domain (GGA3) fused to glutathione-S-transferase (GST), to His-tagged Arf6 immobilised on a nickel-coated plate. The assay format was developed and could robustly distinguish *Hs*Arf6-GDP (inactive) from *Hs*Arf6-GTP (active). Furthermore, it could be employed to detect the deactivation of Arf6 by ArfGAP1-stimualted GTP hydrolysis, but not Arf6 activation by ARNO-stimulated GDP/GTP exchange (ARNO is an ArfGEF). The ArfGAP1 deactivation assay was chemically validated using a known ArfGAP inhibitor, QS11. An improved assay was developed that employs JIP4 as an Arf6-specific binding partner instead of GGA3. In addition to superior performance, the alternative assay format could potentially be exploited for cancer drug discovery, since Arf6-JIP4 interaction has been implicated in cancer cell invasion and metastasis. Both assays may be employed to explore alternative ArfGEFs and ArfGAPs that act on Arf6 and contribute to the advancement of cancer. In parallel experiments, where development of *Pf*Arf6 assays was the focus, several issues arose. Firstly, we could not prepare GDP- and GTP-bound forms of *Pf*Arf6 since EDTA-mediated nucleotide exchange appeared to irreversibly destabilise the protein. However, *Pf*Arf6 activation (i.e. the preparation of

*Pf*Arf6-GTP) was possible when mediated by ARNO and assessed by tryptophan fluorescence kinetic assays, suggesting that *Pf*Arf6 may be expressed in GDP-bound form in *E. coli*. As with human Arf6, ARNO-mediated GDP/GTP exchange on *Pf*Arf6 was not detectable in the immobilised *Pf*Arf6-GGA interaction GST assay format. However, a more sensitive assay was developed which relies on the use of nickel-horseradish peroxidase to detect the binding of His-tagged *Pf*Arf6 to JIP4-GST immobilised on glutathione plates and could detect ARNO-mediated *Pf*Arf6 activation. Since we could not prepare *Pf*Arf6-GTP (that did not rely on the presence of the ArfGEF, ARNO), malarial ArfGAP deactivation studies were conducted using *Pf*Arf1 instead of *Pf*Arf6 in the GGA-GST interaction assay. Both *Pf*ArfGAP1and *Pf*ArfGAP2 stimulated GTP hydrolysis by *Pf*Arf1, but only the former was inhibited by the standard human ArfGAP inhibitor, QS11. The development of these simple, cost-effective assays can be used in the high-throughput screening of novel anticancer and antimalarial compounds that target Arf signalling machineries. In theory, the assay could be extended as a tool to identify novel inhibitors of the multitude of Arfs, ArfGEFs and ArfGAPs originating from any organism and hence has broad clinical significance.

Acknowledgements

I would like to thank my supervisor Professor Heinrich Hoppe, for his excellent supervision, guidance and encouragement throughout my postgraduate studies. Definitely the world's best supervisor!

To the present and past members of the research group thank you being part of an enjoyable working environment. To my colleagues in Arf – Tarryn Swart and Apelele Ntlansana, thank you for really being there through all the highs and lows of the project. The academic, technical and cleaning staff of the Department of Microbiology and Biochemistry, this project would not have been possible without the day-to-day running of the faculty.

To my parents, Isa and Nash Khan, I am so thankful for all your unwavering faith in me. To my big sister and big brother, Zaakira and Taariq Khan, thank you all your long-distance support.

To two of my most cherished friends, Lynn Wambua and Leigh-anne Derry, I cannot express how much our friendship has meant to me, but I will try my best: Lynn, the wind beneath my wings, the cytosine to my guanine, the single greatest person I've ever known. Your kindness and endless wisdom inspire me every day. I am so glad I forced my friendship on you. To say you have changed my life would truly be an understatement. Thank you for showing me the true meaning of friendship and I can only hope that one day this reacher can be as great as her settler. Leigh-anne, I love you. I always have, and I always will. I can't wait for the day we are all living together in our slightly haunted house ♥. On a more serious note, I genuinely look forward to many more adventures with the two of you.

The research was funded by the National Research Foundation (NRF), thank you for your financial support in the research presented here. Additional financial assistance from the Rhodes University Postgraduate Scholarship towards this research is hereby acknowledged. Opinions expressed, and conclusions arrived at, are those of the author and are not necessarily to be attributed to Rhodes University or the donor.

Table of contents

List of Abbreviations

ACT	Artemisinin combination therapy
ADAP	ArfGAP with dual PH domains
ADP	Adenosine diphosphate
AGE	Agarose gel electrophoresis
AGFG	ArfGAPs with FG repeats
ALPS	Amphipathic lipid packing sensor
AP	Adaptor protein
Arf	ADP-ribosylation factor
Arf6	ADP-ribosylation factor 6
ArfGAP	ADP-ribosylation factor GTPase activating protein
ArfGEF	ADP-ribosylation factor guanine nucleotide exchange factor
Arl	Arf-like GTPase
ARNO	Arf nucleotide binding site opener
ASAP	ArfGAP with SH3-domain, ANK repeat and PH domain-containing protein
ATP	Adenosine triphosphate
BAR	Bin-Amphiphysin-Rvs domain
BFA	Brefeldin A
BIG	BFA-inhibited GEFs
BRAG	Brefeldin-resistant ArfGEF
BRAG2/GEP100	Brefeldin-resistant ArfGEF 2 (also referred to as GEP100)
BSA	Bovine serum albumin
CADE	Caveolae-dependent endocytosis
CALM	Clathrin assembly protein
CCR5	C-C chemokine receptor type 5
CD4	Cluster of differentiation 4
CDE	Clathrin-dependent endocytosis
CDNB	2,4-Dinitrochlorobenzene
CFP	Cyan fluorescent protein
CHA	Common hydrophobic area
CHC	Clathrin heavy chain
CHO	Chinese hamster ovary cells
CLC	Clathrin light chain
CMV	Cytomegalovirus
COPI	Coatomer protein 1
CT-A1	Cholera toxin A1 subunit

CXCR4	Chemokine receptor type 4
DMSO	Dimethyl sulfoxide
DNA	Deoxyribonucleic acid
dNTP	Deoxyribonucleotide triphosphate
DTT	Dithiothreitol
DV	Digestive vacuole
E. coli	*Escherichia coli*
ECM	Extracellular matrix
EDTA	Ethylenediaminetetraacetic acid
EEA1	Early endosome antigen 1
EFA6	Exchange factor for Arf6
EGF	Epidermal growth factor
EMT	Epithelial-to-mesenchymal transition
EPEC/EHEC	Enteropathogenic and enterohaemorrhagic *Escherichia coli*
ER	Endoplasmic reticulum
ERC	Endocytic recycling compartment
FBS	Foetal bovine serum
FBX8	F-box only protein 8
FRET	Fluorescence resonance energy transfer
GBF	Golgi-Brefeldin A resistance factor
GDP	Guanosine diphosphate
GFP	Green fluorescent protein
GGA	Golgi-localised gamma adaptin-ear-containing, Arf-binding
GIT	G-protein-coupled receptor kinase-interacting ArfGAPs
GLUT1	Glucose transport 1
GLUT4	Glucose transporter 4
GSH	Glutathione
GSV	GLUT4 storage vesicles
GSα	G-protein α subunit
GTP	Guanosine triphosphate
HDS	Homology downstream of Sec7
HEK	Human embryonic kidney
HGF	Hepatocyte growth factor
HiFi	High fidelity
HIV-1	Human immunodeficiency virus 1
HRP	Horse radish peroxidase
HSV	Herpes simplex virus

HT	Hydrophobic triad
Hz	Hertz
IPTG	Isopropyl β-D-1-thiogalactopyranoside
JIP	c-Jun N-terminal kinase (JNK) interacting protein
JNK	c-Jun N-terminal kinase
Lat1	Large neutral amino acid transporter
LC3	Microtubule-associated proteins 1A/1B light chain 3B
LZII	Leucine zipper domain
MHC	Major histocompatibility complex
MHGCR	Hydroxymethylgutaryl-CoA-reductase
MKLP1	Mitotic kinesin-like protein 1
MKLP1-TD	Mitotic kinesin-like protein 1 terminal domain
MSI	Microsatellite instability
MT1-MMP	Membrane-tethered membrane type 1-matrix metalloproteinase
NAD	Nicotinamide adenine dinucleotide
NCBI	National centre for biotechnology information
Ni-NTA	Nickel-nitrilotriacetic acid
NM23-H1	Nonmetastatic protein 23 homolog 1
PA	Phosphatidic acid
PBS	Phosphate buffered saline
PCR	Polymerase chain reaction
Pf	*Plasmodium falciparum*
PH	Pleckstrin-homology
PI3K	Phosphatidylinositol 3-kinase
PIP_2	Phosphatidylinositol 4,5-biphosphates
PIP5K	Phosphatidylinositol 4-phosphate 5-kinase
PKC	Protein kinase C
PLD	Phospholipase D
PM	Plasma membrane
PPM	Parasites plasma membrane
PV	Parasitophorous vacuole
PVM	Parasitophorous vacuolar membrane
Rac1	Ras-related C3 botulinum toxin substrate 1
RBC	Red blood cell
RE	Recycling endosome
RFP	Red fluorescent protein
SDS	Sodium dodecyl sulfate

SDS-PAGE	Sodium dodecyl sulfate polyacrylamide gel electrophoresis
SMAP	Small ArfGAPs
TBS	Tris-buffered saline
TEMED	Tetramethylethylenediamine
TGF	Transcription growth factor
TGN	*Trans*-Golgi network
TMB	3,3',5,5'-Tetramethylbenzidine
Tris	Trizma base
V-ATPase	Vacuolar-type H^+-ATPase
WHO	World health organization
TRITC	Tetramethylrhodamine isothiocyanate

List of figures and tables

Chapter 1. Literature review.

ADP ribosylation factor 6, and its signalling machineries, as drug targets for cancer and malaria

ADP ribosylation factors (Arfs) are small (~20 kDa) guanosine triphosphate (GTP)-binding proteins (which are also referred to as GTPases) that are major regulators of vesicular trafficking and actin remodelling. GTP-binding proteins act as molecular switches that cycle between two conformations: an active GTP-bound form and an inactive guanosine diphosphate (GDP)-bound form. Arf guanine nucleotide exchange factors (ArfGEFs) mediate the exchange of GDP for GTP, thus activating Arfs, whereas Arf GTPase activating proteins (ArfGAPs) bind to Arf-GTP and stimulate the hydrolysis of the terminal phosphate of GTP, returning Arfs to their GDP-bound form. Active Arfs interact with effector proteins to mediate downstream cellular functions. ArfGEFs and ArfGAPs are also regulated via feedback loops in which active Arfs influence the efficiency of ArfGEFs and feed-forward signalling mechanisms where ArfGEFs selectively recruit effector proteins to promote specific cellular processes. In a similar, feed-forward regulatory system, effectors can influence the activation of ArfGAPs, which subsequently deactivate their cognate Arfs (**Figure 1**) (Jackson and Casanova, 2000; Randazzo and Hirsch, 2004; Vetter and Wittinghofer, 2001).

1. Nomenclature and classification of ADP-ribosylation factors

Arfs are part of the Arf GTPase subfamily in the Ras superfamily of small GTP-binding proteins (Takai et al., 2001). Arfs are present in a wide range of eukaryotes, but their nomenclature describes the six isoforms that exist in mammalian cells which are denoted Arf1-6. These mammalian isoforms are further categorized into three distinct classes based on amino acid sequence similarity (Tsuchiya et al., 1991). Class I contains Arf1-3. Class II Arfs share 80% sequence identity with class I and includes Arf4 and 5. Arf6 is the sole member of class III and shares only 64 - 69% sequence identity with other Arf isoforms. The relatively unique amino acid sequence appears to have resulted in the functional departure of Arf6 from other Arf isoforms. Although new functions for individual Arfs and their regulators (ArfGEFs and ArfGAPs) are constantly being elucidated, the core function of Arfs is to mediate the formation of vesicles that allow membrane and proteins to traffic between organelles in the secretory (Arf1 and related family members Arf2-5) (Volpicelli-Daley et al., 2005; Wieland and Harter, 1999) and endocytic (Arf6) pathways, in addition to the actin remodelling role of Arf6. Arf1 thus mediates the trafficking of secretory proteins between the Golgi apparatus and endoplasmic reticulum and between individual Golgi cisternae, as well as from the Golgi apparatus (*trans*-Golgi network) to endosomes. By contrast, Arf6 mediates endocytosis from the plasma membrane and the formation of

endosomes, as well as the recycling of endocytosed membrane/proteins back to the plasma membrane (D'Souza-Schorey et al., 1995; Kahn and Gilman, 1986; Logsdon and Kahn, n.d.).

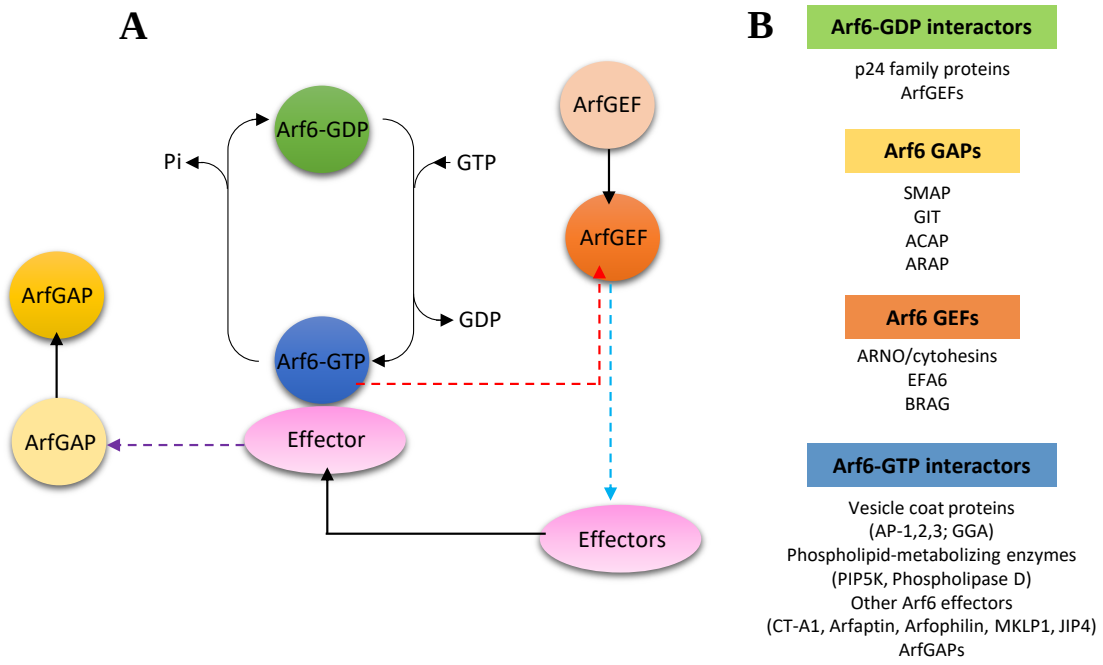

Figure 1: Regulation of Arf GTPases. **A:** Weak interactions with membranes promote the activation of Arf6-GDP (green). ArfGEFs (orange) promote the exchange of GDP for GTP resulting in the activated state of Arfs, Arf6-GTP (blue). In response to cellular requirements, ArfGAPs (yellow), exercise GTP-hydrolytic activity to return Arfs to their inactive, Arf-GDP form, by stimulating the release of the terminal phosphate in GTP (Pi). Activation signals initiate the conformational shift which promote ArfGEF (orange) activation from a pool of inactive ArfGEFs (light orange). Similarly, termination signals initiate the conformational changes that enhance ArfGAP (yellow) activation from a pool of inactive ArfGAPs (light yellow). Feedback loops in which the active Arf GTPase controls the efficiency of the ArfGEF (red broken line) and feed-forward signalling in which in which ArfGEFs select appropriate effectors that will be recruited for active Arf GTPases (light blue broken line) are higher-level regulatory mechanisms embedded in the GDP/GTP cycling of Arf GTPases. Similar feed-forward mechanisms demonstrated by effector proteins contribute to the activation of a specific ArfGAP (purple broken line). **B**: Known interactors of Arf6. Green: proteins that interact with Arf6-GDP. Yellow: ArfGAPs capable of promoting GTP-hydrolysis on Arf6. Orange: ArfGEFs capable of promoting GDP/GTP exchange on Arf6. Blue: proteins that interact with Arf6 (Adapted from Cherfils and Zeghouf, 2013).

2. Protein architecture of ADP-ribosylation factors

At the N-terminus, Arfs have an extension which folds into an amphipathic helix. The second residue in the N-terminal extension, glycine, is post translationally myristoylated which enhances it hydrophobicity. The hydrophobic N-terminus is critical for the interaction of Arfs with membranes (Antonny et al., 1997; Liu et al., 2009). Connected to N-terminal extension, is the G-domain via a linker region that is considerably shorter in Arfs than other members of the GTP-binding family. This constraint brings binding partners relatively closer to the membrane bilayer and has been posited as a possible reason why Arf binding partners are often coat proteins or lipid-modifying enzymes that shape or alter lipid bilayers (Gillingham and Munro, 2007; Lee et al., 2005; Neu et al., 1997).

The G-domain is a universal feature of all GTP-binding proteins which contains all the structural elements required for GDP/GTP cycling. The three major elements are the switch I, switch II and interswitch regions. The G-domain is composed of a central, six-stranded β-sheet surrounded by five α-helices (Pasqualato et al., 2002). The interswitch region consists of two connected β-strands located between the switch I and switch II regions. In the GDP-bound form the interswitch region adopts a retracted position. In this confirmation the N-terminal extension remains housed within a pocket in the protein core, reducing the potential for Arfs to interact with membranes. In the GTP-bound form the interswitch region undergoes a conformational shift which releases the N-terminal extension. In this state the N-terminal extension is free to interact with membranes. In addition to its effects on GDP/GTP cycling and membrane recruitment the switch I, switch II and interswitch region form a surface on one face of Arfs which forms the primary binding site for effector proteins (Vetter and Wittinghofer, 2001). A unique feature of Arf G-domains is the presence of two additional, highly conserved nucleotide binding sites – the N/TKxD and Gx_4GKS/T motifs. The N/TKxD motif binds to the base of the nucleotide and the Gx_4GKS/T motif recognises and interacts with the β, ɣ - phosphates of the nucleotide (Vetter and Wittinghofer, 2001).

Strict conversation in the switch, interswitch and nucleotide binding regions preserves classical GDP/GTP cycling and conserved effector binding residues within these regions usually indicates an effector protein capable of interacting with multiple Arfs. Chavrier and Ménétrey (2010) postulate that non-conserved residues at the boundaries of the conserved switch regions have resulted in the unique functional capabilities of Arf6. The carboxyl half of Arf proteins, which lack the highly conserved regions, accounts for most of the differences in amino acid residues between Arf6 and other isoforms (Stafford et al., 1996). Metazoan Arf6 homologs are distinguished by the presence of a glutamine-serine (QS) dipeptide signature adjacent to the Switch I domain of the protein (Al-Awar and Radhakrishna, 2000). A final distinguishing property of Arf6 is its pI range of 8.5 - 9.5. The pI range demonstrated by Arf6 imparts a net positive charge on the surface of the protein (Al-Awar and Radhakrishna, 2000). While the N-terminal myristate is required for binding of Arfs to membranes, it has been speculated that the combined effects of a net positive surface charge and the myristoylated tail retains Arf6-GDP on membranes to a much larger extent than Arf1-GDP (Cavenagh et al., 1996; Song et al., 1998).

3. GDP/GTP cycling of ADP-ribosylation factors

The regulatory roles of ArfGEFs and ArfGAPs ultimately affect the cellular functions mediated by Arfs. While ArfGEFs promote Arf functions, ArfGAPs rapidly terminate Arf function according to cellular requirements (Bos et al., 2007). Owing to the fact that Arf isoforms are more distantly related to each other than what is found between members of other small GTPase subfamilies, each Arf family member has their own set of ArfGEFs and ArfGAPs that regulate their activity (Kahn et al., 2008).

3.1. Guanine nucleotide exchange factors activate Arf GTPases

Weak interactions between inactive Arfs and membranes initiates the conformational transition required to activate Arf GTPases. Concurrently, ArfGEFs are recruited to the membrane by association and complete the conformational shift required to transition Arfs into their GTP bound state (Hongu and Kanaho, 2014; Jackson and Casanova, 2000). Crystallographic studies of Arfs in complex with ArfGEFs have provided insights into the precise molecular mechanisms of nucleotide exchange. An invariant glutamate residue (also referred to as the glutamic acid finger) in the Sec7 domain of ArfGEFs electrostatically and sterically competes with GDP and the coordinating magnesium ion in the nucleotide binding pocket of Arf GTPases (Béraud-Dufour et al., 1998; Renault et al., 2003). The repulsive forces exerted on GDP cause it to dissociate. The mechanism by which GTP subsequently binds to the nucleotide-binding site during Arf activation is not currently known, but it has been proposed that a series of intermediate complexes must exist for GTP entry to occur. Such complexes have been observed for DOCK9/Cdc42 small GTPases (Yang et al., 2009) but have not yet been elucidated for Arfs.

3.1.1. The Sec7 domain catalyses GDP/GTP nucleotide exchange

ArfGEFs, like Arfs, are found in a wide range of organisms including yeast, plants, protozoa, worms, flies, mammals and even certain bacterial pathogens. To date fifteen recognizable ArfGEFs are encoded for in the human genome. Individual members belong to five distinct ArfGEF families based on overall structure and domain organization: Golgi-BFA-resistance factor 1/BFA-inhibited GEFs (GBF/BIG), Arf nucleotide binding site opener (ARNO/cytohesin), exchange factor for Arf6 (EFA6), Brefeldin-resistant ArfGEF (BRAG) and F-box only protein 8 (FBX8) (Casanova, 2007). Although highly divergent in their overall sequence, these proteins share one common feature: a catalytic region containing ~ 200 amino acids called the Sec7 domain which has significant homology to the yeast Sec7p domain. The Sec7 domain is the minimal fragment required to promote the nucleotide exchange activity displayed by ArfGEFs (Béraud-Dufour et al., 1998; Jackson and Casanova, 2000).

3.1.2. Arf6-specific GEF families

Of the fifteen ArfGEFs that have been identified, eight individual ArfGEFs belonging to three ArfGEF families (ARNO/cytohesin, EFA6, BRAG) have demonstrated an ability to promote activation of Arf6 (Casanova, 2007). These families are considered low-molecular weight ArfGEFs (~ 45-50kDa in size) and share 77% sequence identity to one another. They also share common domain organization consisting of an N-terminal coiled-coil domain, the central Sec7 domain that is immediately adjacent to a phosphoinositide-binding pleckstrin-homology (PH) domain and regions rich in proline at the C-terminus (Paris et al., 1997). The PH domain is generally accepted as the region that facilitates binding of ArfGEFs to membranes (Cohen et al., 2007) and the proline-rich regions are speculated to be important for protein-binding although the binding partners have not yet been identified (Franco, 1999).

Interestingly, Cohen et al. (2007) demonstrated that Arf6-GTP recruits ARNO/cytohesin GEFs to the plasma membrane by binding to their PH domains. This result suggests that Arfs could interact with ArfGEF regions other than the Sec7 domain responsible for nucleotide exchange. Such results form part of the growing evidence that ArfGEF and ArfGAPs are not simply 'on and off switches' in Arf signalling as was previously envisioned but may have additional functions.

ARNO/cytohesins are the most highly characterized of the ArfGEFs and are primarily distributed at the plasma membrane (Frank et al., 1998). *In vitro* studies suggest that cytohesins/ARNO are capable of activating Arf6 but act more efficiently on class I Arfs. However, *in vivo* ARNO/cytohesins appear to co-localise preferentially with Arf6 at the cell periphery. Furthermore, overexpression of ARNO results in increase activation of Arf6 (Santy and Casanova, 2001). ARNO/cytohesins have been implicated in cell migration (Goldfinger et al., 2006) and vesicular transport processes such as docking and fusion of secretory vesicles (Caumont et al., 2000a). Lastly, it has been demonstrated that vacuolar-type H^+-ATPase (V-ATPase) interacts with ARNO and Arf6 in early endosomes suggesting a regulatory role in an endocytic degradative pathway (Hurtado-Lorenzo et al., 2006). The EFA family of ArfGEFs contains four mammalian proteins EFA6A-D (Sakagami, 2008). While EFA6A and EFA6C are expressed exclusively in the brain, EFA6B and EFA6D are ubiquitously expressed (Derrien et al., 2002; Sakagami, 2008). Unlike ARNO/cytohesins, EFA6 family members are highly specific for Arf6. The high selectivity for Arf6 has been demonstrated both *in vitro* and *in vivo* (Franco, 1999). EFA6 coordinates membrane recycling from the endocytic pathway and actin cytoskeleton reorganization (Derrien et al., 2002; Franco, 1999; Paleotti et al., 2005). The BRAG family of ArfGEFs comprises three members namely BRAG1, BRAG2/GEP100 and BRAG3 (Casanova, 2007). BRAG1 and BRAG3 are hypothesized to function exclusively in neurons (Inaba et al., 2004; Murphy et al., 2006). BRAG2/GEP100 is Arf6-specific and partially co-localises to endosomes and the cell periphery, suggesting a role in regulating endocytosis and the endocytic pathway (Dunphy et al., 2006; Hiroi et al., 2006).

3.2. Arf GTPase activating proteins deactivate Arfs

Arfs are key regulators of membrane trafficking during secretion and endocytosis and processes that require the rapid remodelling of actin networks such as phagocytosis and cell movement. ArfGAPs which terminate Arf GTPase function are thus integral modulators of these cellular processes (de Curtis, 2001; Donaldson and Jackson, 2000; Randazzo et al., 2007; Santy and Casanova, 2001; Turner et al., 2001). Because Arfs have very slow intrinsic GTPase activity, they require the rapid action of ArfGAPs to terminate processes according to cellular requirements (Cherfils and Zeghouf, 2013a). Elegant crystallographic studies using aluminium and beryllium fluorides (that interfere with GTP-hydrolysis) to mimic ArfGAP transition states have provided the currently accepted molecular mechanism for ArfGAP-stimulated GTP hydrolysis (Mittal et al., 1996; Wittinghofer, 1997). ArfGAPs capable of

inactivating Arfs have a conserved zinc-finger domain containing an invariant arginine residue. The arginine residue positions the conserved glutamine residue in the switch 2 region of the Arf GTPase, such that it can activate a single water molecule. The activated water molecule then nucleophilically attacks the terminal phosphate of GTP, causing its dissociation from the GTP binding site (Rittinger et al., 1997; Scheffzek et al., 2010). In Arf6 the conserved glutamine residue is at position 67 of the amino acid sequence (Cherfils and Zeghouf, 2013a).

3.2.1. The GAP domain stimulates GTP hydrolysis

While ArfGAPs are ubiquitously expressed in a diverse set of organisms, consensus nomenclature of the ArfGAP family of proteins is based on human ArfGAPs. To date 31 ArfGAPs have been identified and classified into 10 distinct families based on sequence similarity and domain organization between family members. The ten subfamilies are the ArfGAP1, ARFGAP2/3, ADAP, SMAP, AGFG, GIT, ASAP, ACAP, AGAP and ARAP (reviewed by Kahn et al., 2008). The hallmark of ArfGAPs is the ArfGAP domain which is described as the minimal fragment possessing the ability to stimulate Arf GTP-hydrolytic activity (Cukierman et al., 1995). The ArfGAP domain is ~ 130 amino acids in length and contains a characteristic C_4 type zing finger motif with spacing as described: $CX_2CX_6CX_2CX_4R$. The zinc finger motif houses an invariant arginine residue which has been posited as the catalytic element in the ArfGAP domain (Goldberg, 1999; Scheffzek et al., 2010). Of the ten subfamilies, at least one member from each of eight subfamilies have demonstrated the ability to trigger GTP-hydrolysis. However, the presence of two ArfGAP subfamilies that do not display this activity raises the possibility that ArfGAPs function in capacities other than the termination of Arf activity (Bharti et al., 2007; Hashimoto et al., 2004; Inoue and Randazzo, 2007). ArfGAPs have recently emerged as effectors and as scaffolds where protein complexes involved in cell signalling assemble (Gillingham and Munro, 2007; Inoue and Randazzo, 2007). Furthermore, Arl2 GAP which lacks the GAP domain but can stimulate GTP hydrolysis, suggests that GAP domain containing proteins maybe not represent the full repertoire of proteins capable of stimulating GTP hydrolysis in Arf GTPases. Such evidence shifts the prevailing paradigms around ArfGEFs, ArfGAPs and their canonical associations with Arf GTPases (Bowzard et al., 2007; Kahn et al., 2008).

3.2.2. Arf6-specific GAP families

ArfGAPs display various degrees of specificity for individual members of the Arf GTPase family. To date, nine ArfGAPs belonging to four ArfGAP subfamilies (SMAP, GIT, ACAP, ARAP) have demonstrated *in vitro* specificity for Arf6 (Donaldson and Jackson, 2011; Randazzo et al., 2007; Yamauchi et al., 2017). SMAPs have demonstrated regulatory roles in endocytosis (Arf6 is a major participant in endocytosis). SMAP1 and 2 are cytosolic and are recruited to membranes that form endocytic vesicles budding from early endosomes (Tanabe et al., 2006). Vesicles associated with SMAP2 have been shown to traffic towards the *trans*-Golgi network (TGN). During vesicle formation

they bind to clathrin heavy chains (CHC) as well as the clathrin assembly protein, CALM (Natsume et al., 2006). GITs are expressed ubiquitously but are most prominent in endothelial cells (Schmalzigaug et al., 2007). Unlike GITs, a direct interaction of ACAPs with Arf6 has been observed in cells. ACAP1 is associated with a clathrin coat which is regulated by Arf6 (Liu et al., 2009). ACAPs are known regulators of Arf6-depedendent actin remodelling and endocytosis (Inoue and Randazzo, 2007). Finally, although ARAPs demonstrate specificity for Arf6 in *in vitro* studies, they have only been indirectly linked to processes in which Arf6 is a known participant namely epidermal growth factor (EGF) receptor signalling, focal adhesion and lamellipodia formation (Inoue and Randazzo, 2007; Randazzo et al., 2007).

4. ADP-ribosylation factor protein interactions

In the protein's final conformation, the N-terminal helix, switch and interswitch regions all contribute residues to form the primary effector binding site on one face of all Arfs. This region can distinguish Arf-GDP from Arf-GTP. However, in their tertiary structures, Arf1-GTP and Arf6-GTP are virtually identical, raising the question which factors govern effector specificity. Although Arf1 and Arf6 share 78% sequence identity in their switch regions, minor differences in these regions account for the selectively of Arfs for Arf effectors, which themselves are a highly heterogenous family with unique structures that effectuate distinct downstream functions (Chavrier and Ménétrey, 2010; Ménétrey et al., 2007; O'Neal et al., 2005; Vetter and Wittinghofer, 2001). Currently known interactors of Arf6 discussed below are summarized below in **Figure 1**.

4.1. Proteins that interact with inactive Arf-GDP

In addition to ArfGEFs, the only other class of proteins known to interact with Arf1-GDP are p24-family proteins (Kaiser, 2000). The p24-family of proteins recruit coat proteins such as coatomer I and II (COPI and COPII) via sorting signals in their cytoplasmic domains, and mediate anterograde and retrograde transport in the early secretory pathway (between individual cisternae of the Golgi apparatus; Kaiser, 2000; Nie et al., 2003). *In vitro* and fluorescence resonance energy transfer (FRET) studies conducted in live cells were used to confirm the selectivity of p24-family proteins for Arf1-GDP as opposed to Arf1-GTP (Gommel et al., 2001; Majoul et al., 2001). Although effectors for Arf6-GDP have not yet been described (besides ArfGEFs), it is not inconceivable that similar effectors may exist that assist in the recruitment of Arf6-GDP to membranes involved in endocytic protein trafficking.

4.2. Proteins that interact with active Arf-GTP

Arf-GTP effector proteins are usually classified into one of three groups based on functional similarities: vesicle coat and adaptor proteins, phospholipid-metabolizing enzymes and ArfGAPs (as

previously discussed). Additional effector proteins have been identified that are not easily assigned to any of these three broader categories (Nie et al., 2003).

4.2.1. Vesicle coat proteins and adaptors

Vesicle coat and associated adaptor proteins are central to the well-established roles of Arfs in membrane trafficking (Nickel et al., 2002; Rothman, 2002; Springer et al., 1999). Coat proteins are recruited to membranes by Arf-GTP and induce vesicle formation on donor membranes, as well as concentrate cargo proteins in the budding vesicle (Kirchhausen, 2000). Fully formed vesicles bud from the donor membrane (ER and Golgi membranes) to form secretory vesicles trafficking within the secretory pathway, while endocytic vesicles bud from the plasma membrane. Deactivation of Arf-GTP by ArfGAPs triggers the dissociation of Arfs and coat proteins from vesicle membranes before their fusion to acceptor membranes (Brodsky et al., 2001). Coat proteins that are dependent on active Arf recruitment include coatomer, the clathrin/adaptor proteins (AP) 1,2 and 3 and clathrin/Golgi-localised, gamma adaptin ear-containing, Arf-binding (GGAs)1, 2 and 3. Coatomer is responsible for the formation of COPI vesicles that mediate retrograde transport between cisternae in the Golgi apparatus and between the Golgi and the ER, and coatomer subunits are thus effector proteins of Arf1. Similarly, AP-1 and the GGA coat proteins are Arf1 effectors that mediate the formation of secretory vesicles that transport lysosomal proteins from the *trans*-Golgi network (TGN) to endosomes (Boehm et al., 2001; Dell'Angelica et al., 2000; Donaldson et al., 1992; Ooi et al., 1998; Palmer et al., 1993; Robinson and Bonifacino, 2001; Stamnes and Rothman, 1993; Traub et al., 1993; Zhu et al., 1999). By contrast, AP-2 forms part of the clathrin coat that mediates the formation of endocytic vesicles during clathrin-dependent endocytosis. Arf6-GTP is involved in the recruitment of AP-2 to liposomes (Paleotti et al., 2005) which may contribute to the key role of Arf6 in endocytosis. Arf6-GTP also interacts with the β1-adaptin of AP-1 after its recruitment to immature secretory granules (AP-1 is involved in the formation of vesicles that recycle membrane/proteins from secretory granules and contribute to the maturation of the latter). In addition to AP-1 and 2, Arf6-GTP also associates with two subunits of the clathrin coat protein, AP-3. AP-3 is responsible for the trafficking of proteins from the TGN to lysosomes. However, it is important to note that while Arf6 demonstrated its binding potential to these adaptor proteins *in vitro*, no effector coat proteins for Arf6 have been identified *in vivo* (Austin et al., 2002) and the significance of the interactions may thus be questionable.

4.2.2. Phospholipid-metabolizing enzymes

The stimulation of phospholipid synthesizing enzymes increases the phosphoinositide population in membranes. The increase in phosphoinositides in membranes, in turn, regulates several signal transduction events within cells (Funakoshi et al., 2011). Arf1- and Arf6-GTP stimulate the activity of phosphatidylinositol 4-phosphate 5-kinase (PIP5K) as well as phospholipase D (PLD) (enzymes involved in phospholipid metabolism), which results in the production of the secondary lipid messenger

molecules phosphatidylinositol 4,5-biphosphates (PIP_2) and phosphatidic acid (PA) respectively. PIP_2 accumulation by Arf6-GTP stimulation of PIP5K regulates both actin and membrane dynamics - while PA only affects membrane trafficking (Czech, 2003; Honda et al., 1999; Melendez et al., 2001; Powner et al., 2002).

4.2.3. Other Arf6-GTP effectors

Arfs are defined as proteins that can activate cholera toxin (CT). Structurally related proteins that do not hold this ability are designated as Arf-like (Moss and Vaughan, 1995). CT is thus the first described Arf effector protein. The A1 subunit of cholera toxin (CT-A1) is an ADP-ribosyltransferase that catalyses the transfer of an ADP (adenosine diphosphate)-ribose moiety from nicotinamide adenine dinucleotide (NAD) to arginine 201 of the stimulatory G-protein α subunit ($G_S\alpha$) (Kahn and Gilman, 1986; Vanden Broeck et al., 2007). CT-A1 displays relatively low enzymatic activity *in vitro* but its affinity and activity towards $G_S\alpha$ increases upon interaction with active Arf6. CT-A1 binds to the switch and interswitch regions of Arf6 via hydrophobic interactions (O'Neal et al., 2005).

Arf6-GTP promotes the generation of cellular protrusions and ruffles by its interaction, and subsequent activation of Rac1 GTPase. Both Arf6-GTP and Rac1 GTPase bind to the effector protein Arfaptin 2 but the precise role of Arfaptin has not yet been elucidated (Brown et al., 2001; Franco, 1999; H. Radhakrishna, O. Al-Awar, Z. Khachikian, 1999). Although Arfaptin has promiscuous affinity for both Arf1- and Arf6-GTP, it has a higher affinity for Arf1-GTP than Arf6-GTP; while the effector protein Arfophilin is more selective for Arf6-GTP (D'Souza-Schorey et al., 1997; Shin et al., 2001). In this case, the interaction involves resides 37-80 in the amino acid sequence of human Arf6 (Shin et al., 1999). Arfophilin is speculated to be an effector molecule that bridges the functions of Arf6 and Rab11. Since Rab11 is responsible for the regulation of recycling endosomes, it is possible that the interaction of Arfophilin and Arf6-GTP contributes to the involvement of Arf6 in the recycling of proteins from the endocytic pathway back to the plasma membrane (Ai et al., 2010; Shin et al., 2001).

Arf6-GTP interacts with mitotic kinesin-like protein 1 (MKLP1) which recruits Arf6 to the midbody during cytokinesis. The midbody is a transient structure that is present just before cytokinesis comes to fruition. Cytokinesis cannot be completed in cells where Arf6 is depleted, indicating that Arf6 and its delivery to the midbody by MKLP1 are (likely) critical for the normal functioning of this process. MKLP1 interacts directly with Arf6-GTP through its terminal tail domain (MKLP1-TD). (Makyio et al., 2012).

c-Jun N-terminal kinases (JNK) interacting proteins (JIP) act as scaffolds for JNK cascade kinases and have been implicated in brain development, neuronal traffic, apoptosis and cytokinesis. Arf6-GTP regulates JIP3 and JIP4s interaction with kinesin-1 and dynein/dynactin motors which participate in endosomal recycling to the plasma membrane from the TGN (Koushika, 2008; Montagnac et al., 2009).

A leucine zipper (LZII) domain in JIP4 binds to residues within the interswitch and switch II regions of Arf6. This is first demonstration of an effector that can discriminate between Arf1 and Arf6 in an *in vitro* system (Isabet et al., 2009). The JIP4-Arf6 interaction has recently been flagged as a possible target for cancer therapeutics and will be discussed in detail later.

5. Cellular functions of ADP-ribosylation factor 6

Arf6 has two broad functions: membrane trafficking and actin remodelling. Arf6 membrane trafficking encompasses endocytosis, membrane recycling and regulated secretion. Owing to its ability to remodel the actin cytoskeleton, Arf6 also participates in membrane ruffle formation, invadopodia formation, neurite growth, phagocytosis, macropinocytosis, autophagocytosis and cell division. It is worth noting that the involvement of Arf6 in many of these processes, is often specific to different cell types (Aikawa and Martin, 2003; D'Souza-Schorey et al., 1995; Lawrence and Birnbaum, 2001; Peters et al., 1995; Tang et al., 2015).

5.1. Endocytosis, membrane recycling and regulated secretion

PIP5K and PLD, which are activated by Arf6, produce PIP_2's that accumulate in the inner leaflet of the plasma membrane. This provides the signal which initiates clathrin-dependent endocytosis (CDE) (Wenk and De Camilli, 2004). It has been proposed that Arf6-GTP and PIP_2 initiate the formation of endocytic invaginations by recruiting AP-2/ clathrin complexes to the plasma membrane. It is thought that AP-2 and clathrin then form a coat that mediates the invagination of the membrane to form a bud. To complete the formation of an endocytic vesicle, fission of the invagination from the membrane is mediated by the large GTPase dynamin that forms a contractile ring around the neck of the bud. This requires the kinase NM23-H1 (nonmetastatic protein 23 homolog 1). Arf6 binds and recruits NM23-H1 for dynamin-dependent fission of the vesicle (Palacios et al., 2002). SMAP1 has been identified as an Arf6-specific GAP which mediated Arf6's inactivation in the CDE pathway (Tanabe et al., 2006). The outcome of endocytosis is the internalization of both extracellular fluids and plasma membrane receptors. With regards to the latter, the role of Arf6-GTP in CDE has been demonstrated to contribute to the internalization of β2–adrenergic and leutinizing hormone receptors, as examples (Mukherjee et al., 2000). Endocytosis of signalling receptors contributes to the desensitization of cells to extracellular signalling molecules. In addition to CDE, Arf6 appears to participate in caveolae-dependent endocytosis (CADE). Arf6 is a common component of membrane fractions that are enriched with caveolae and the inhibition of Arf6 prevents signal transduction events that are usually facilitated by CADE (Lefort, 2003; Palacios et al., 2002). Finally, Arf6 is involved in the internalization of ligands by an additional endocytic pathway that is independent of clathrin, caveolae and dynamin. Mayor et al. (2014) describe this endocytic route as the Arf6-associated pathway. The incoming endosomes formed by this mechanism are distinct from the clathrin-coated subpopulation but share the eventual fate of fusion with

sorting endosomes (Brown et al., 2001; Naslavsky, 2003). A wide variety of cell-surface receptors that enter the cell via this pathway have been identified. These include the proteins involved in nutrient transport (Glut1, CD89, Lat1), immune function (MHC class I, CD1a), extracellular matrix interaction (CD44, CD147) and proteins that are anchored to the membrane by GPI (CD55 and CD59) (Eyster et al., 2011; Maldonado-Báez et al., 2013). D'Souza-Schorey and Chavrier, (2006) highlight the fact that although Arf6 mediates the entry and internalization of numerous receptors through several distinct endocytic routes, it is important to remember that its participation in each of these endocytic pathways may be dependent on the cell type.

The composition of sorting and recycling endosomes is that of several subsets of endosomes, which have entered the cell by a multitude of different endocytic pathways (D'Souza-Schorey and Chavrier, 2006; Maxfield and McGraw, 2004). In addition to internalising extracellular content, Arf6 is also responsible for the recycling of endocytosed proteins/membrane back to the plasma membrane. EFA6 (ArfGEF)-mediated activation of Arf6 has been shown to stimulate the return of extracellular ligands in Chinese hamster ovary cells (CHO) whereas inactive Arf6 mutants are unable to recycle these ligands back to the plasma membrane (D'Souza-Schorey et al., 1997; D'Souza-Schorey and Chavrier, 2006; David Padro and Tall, 2006). In HeLa cells Arf6 activity returns cell surface receptor proteins such as β1 integrin and transferrin present in recycling endosomes back to the cells peripheral membrane (Powelka et al., 2004). The ArfGAP ACAP1 has been implicated in the deactivation of Arf6 that is required to complete the recycling of β1 integrin and transferrin to the plasma membrane.

Although the main recognised role of Arf6 is in the endocytic pathway, there is evidence that it may play an additional role in regulated secretion. In pheochromocytes (neuroendocrine cells found in the medulla of adrenal glands which secrete catecholamines, adrenaline and noradrenaline) Arf6 localises to secretory vesicles and translocate to the plasma membrane when stimulated (Caumont et al., 2000b; Galas et al., 1997). Arf6 is also required in the insulin-stimulated secretion of glucose transporter 4 (GLUT4) receptors to the plasma membrane. In the absence of insulin, the GLUT4 receptor is sequestered in the endosomal system, the TGN and specialised storage compartments called GLUT4 storage vesicles (GSVs) which occur within the vicinity of TGN. Upon stimulation by insulin, GSVs are redistributed to the plasma membrane via recycling or sorting (early) endosomes and thus enhance the population of GLUT4 receptors at the cell surface (Holman and Cushman, 1994; Ploug et al., 1998; Rea and James, 1997; Zorzano et al., 1996). Arf6 recruits adaptor proteins to donor membranes, which in turn, interact with GSV components and clathrin to initiation the formation of GSVs. To date GGA, ACAP1, AP1 and AP3 are adaptor proteins that have been implicated in this process (Gillingham et al., 1999; Li et al., 2007; Li and Kandror, 2005; Utani, 2010). Millar et al. (1999) supported this notion by demonstrating that Arf6 peptides (peptides that mimic the myristoylated N-terminus) inhibited insulin-stimulated glucose transport and GLUT4 translocation to the plasma membrane.

5.2. Actin remodelling

The accumulation of PIP_2, as a result of Arf6-stimulation of PIP5K, recruits multiple actin-binding proteins to the plasma membrane (Hilpela et al., 2003). The inhibition of Arf6 has been shown to prevent the extension of pseudopods, and the process of phagocytosis indicating a critical reliance of these processes on Arf6 (Cavenagh et al., 1996; Niedergang et al., 2003; Uchida et al., 2001).

In addition, Arf6 is responsible for the uptake of extracellular content in larger endocytic invaginations called micropinosomes. Macropinocytosis resembles phagocytosis in that it requires actin rearrangements to form plasma membrane extensions, but this occurs over a larger surface area of the cell (pseudopod formation resulting in phagocytosis is limited to the plasma membrane immediately adjacent to the particle being phagocytosed).

During cell division, actin and membranes need to restructure accordingly to form the cleavage furrow. During cytokinesis, an increase in Arf6-GTP levels as well as the termination of cell division in cells where Arf6 was depleted by RNA interference, indicate that Arf6 is also an essential participant in the cell division/cytokinesis (Schweitzer and D'Souza-Schorey, 2005, 2002).

Arf6 also mediates rearrangements in the actin cytoskeleton via the activation of Rac1 (Ras-related C3 botulinum toxin substrate 1) GTPase or modulation of lipid metabolism. The ArfGEF ARNO promotes Arf6 activation which recruits Rac1, an actin regulatory element, to the plasma membrane where it modulates actin cytoskeleton reorganizations according to cellular requirements (Boshans et al., 2000; Radhakrishna et al, 1999; Santy et al., 2005). Arf6 also diminishes the effects of Rac1 on actin polymerization by recruiting it away from cell-cell contact sites. Cell-cell junctions, which are composed of actin, lose their integrity; the eventual effect is that cells acquire the ability to migrate (Palacios et al., 2002; Palacios and D'Souza-Schorey, 2003).

Lastly, Arf6 has been shown to regulate autophagy via its role in the generation of phosphatidylinositol 4,5-bisphosphates (PIP2s). In autophagy, targeted cytoplasmic constituents are isolated within an autophagosome (a double-membraned vesicle) and are targeted for digestion. Autophagosomes ultimately fuse with lysosomes where the contents are degraded. The generation of PIP2s at the plasma membrane, Golgi apparatus, endoplasmic reticulum (ER) and mitochondrial membranes has been proposed to contribute membranes to LC3-positive autophagosome precursor organelles by homotypic fusion (Bento et al., 2013; Brown et al., 2001; Moreau et al., 2012).

6. Clinical significance of Arf6 dysregulation

Aberrant Arf6 signalling (the dysfunction of Arf6 and/or its cognate ArfGEFs and ArfGAPs) has been implicated in several important communicable and non-communicable disease states. Owing to its broad clinical significance, Arf6 has become a prominent target. Navigen pharmaceuticals, a drug

discovery and development company based in Salt Lake City, Utah, has identified small molecule inhibitors of Arf6, that have shown efficacy against uveal melanoma, malignant sarcoma, acute lung injury, multi-drug resistant gram-negative bacterial pneumonia and diabetic retinopathy in *in vivo* models of these diseases. In December 2017, they created a subsidiary company, A6 pharmaceuticals, to focus on the advancement of the Arf6 inhibitor programme which suggests that Arf6 is continuing to gain traction as a prominent drug target. Arf6 has also been shown to play important roles in the pathogenesis of clinically important viruses human immunodeficiency virus (HIV-1; Garcia-Exposito et al., 2011) and herpes simplex virus (HSV; Nishi and Saigo, 2007), bacteria *Shigella flexeneri* (Garza-Mayers et al., 2015), *Yersinia pseudotuberculosis* (Wong and Isberg, 2003), *Chlamydia* (Balaña et al., 2005), *Listeria monocytogenes* (Ireton, 2007; Shen et al., 2000), enteropathogenic and enterohaemorrhagic *Escherichia coli* (EPEC/EHEC; Furniss et al., 2016; Szatmari et al., 2014; Wong et al., 2011), the fungal phytopathogen *Magnaporthe oryzae* (Wilson and Talbot, 2009) and the disease-causing protozoans *Trypanosoma cruzi* (Teixeira et al., 2015) and *Toxoplasma gondii* (Silva et al., 2009). These organisms will not be reviewed here. The scope of this study is Arf6 as a potential target for identification of novel anticancer and antimalarial therapies, as will be discussed below.

6.1.Cancer

Breast cancer and cervical cancer are some of the most commonly occurring diseases in South Africa, and with a 78% projected increase in cancer incidences by 2030 there is a strong urgency to develop novel chemotherapeutics (Sartorius et al., 2016). Since 70% of the total cancer-related deaths occur in Africa, Asia and South America it is especially crucial that novel, and more affordable, chemotherapeutics enter the market (Stewart et al., 2014).

Inhibition of Arf6 signalling has been shown to suppress cancer progression by numerous research groups (Grossmann et al., 2013a; Hashimoto et al., 2004; Morishige et al., 2008; Okada et al., 2015). As examples, Arf6 expression levels have been directly correlated to breast cancer invasiveness in several cell lines; this correlation was further supported by the significant reduction in invasiveness of Arf6 knock-down cell lines. Melanoma cells in mice models expressing a constitutively active Arf6 mutant (Q67L) appeared to have enhanced invasive properties (Grossmann et al., 2013a; Hashimoto et al., 2004; Hu et al., 2009). Interestingly the EFA family of ArfGEFs can both advance or repress cancer progression depending on the type of cancer and the type of EFA isoform. While EFA6A positively regulates cell invasion in glioma cells, EFA6B appears to supress cell invasion of certain breast cancer lines (Murphy and Courtneidge, 2011; Yamauchi et al., 2017).

Arf6 (and its associated ArfGEFs and ArfGAPs) have been most widely implicated in cancer progression for their contributions to tissue invasion and metastasis, although lesser roles in tumour angiogenesis and genome stability have also been identified (Hanahan and Weinberg, 2011; Okada et al., 2015; Sangar et al., 2014; Yamauchi et al., 2017). For epithelial cells to metastasize (disseminate

around the body) they need to acquire the ability to detach from their initial surrounding tumour cells and move to distal sites where new tumours can develop (formally known as tissue invasion and metastasis). Cancer cells acquire this ability by undergoing an epithelial to mesenchymal transition (EMT). EMT is the functional transition of an epithelial cell to a mesenchymal cell type which has an enhanced capacity to migrate (Hanahan and Weinberg, 2011). The molecular mechanisms by which Arf6 initiates local tissue invasion, including degradation of the extracellular matrix (ECM) have been well-studied.

Firstly, Arf6-GDP localises to cell-cell (adherens) junctions in polarised epithelial cells, hence, is important for cell adhesion. The ArfGAP SMAP1 also contributes, in this respect, through its regulatory role in the endocytosis of E-cadherin which is a central component of the adherens junction. Transcription growth factor (TGF)-β induced downregulation of E-cadherin appears to contribute to the loss of the adherens junction during EMT (Tanabe et al., 2006).

Secondly, Arf6-GTP's manipulation of the plasma membrane via actin remodelling, provides epithelial cells with the ability to form membrane protrusions which facilitate the movement of cancer cells. Arf6 is enriched in the invadopodia of metastatic cancer cells (Palacios et al., 2001). Invadopodia are actin rich structures which are also able to degrade the ECM (Nguyen et al., 2009). The ArfGEF BRAG2/GEP100-mediated activation of Arf6 regulates the location of the Arf6 downstream effector molecule AMAP1 which induces invadopodia formation (Morishige et al., 2008).

Lastly, Arf6 is involved in the regulated secretion of vesicles containing proteases that degrade the ECM (Schweitzer et al., 2011). Membrane-tethered membrane type 1-matrix metalloproteinase (MT1-MMP) is a key protease for collagen degradation in the collagen-rich ECM. Arf6-JIP4 interaction has been identified as a critical regulator in the delivery of MT1-MMP to the cell surface of tumour cells. Silencing Arf6 or JIP4 results in the mispositioning of endosomes carrying MTI-MMP, reduction in MT1-MMP exocytosis and ultimately reduces tumour cell invasion. In addition, Arf6 and MT1-MMP are up-regulated in tripe-negative breast cancers (Marchesin et al., 2015).

In addition to its contributions to cancer progression by tissue invasion and metastasis, Arf6 and its regulatory proteins have been linked to the hallmarks of genetic instability and tumour angiogenesis. Mutations in SMAP1 frequently arise in tumours associated with colorectal cancers displaying microsatellite instability (MSI) (Sangar et al., 2014). Sangar et al. (2014) subsequently demonstrated that inactivation of SMAP1 reduced cell invasiveness by hindering the epithelial-to-mesenchymal transition. Finally, The Arf6-specific ArfGEF Grp1 has been shown regulate hepatocyte growth factor (HGF)-dependent tumor angiogenesis (Okada et al., 2015).

Being prominent targets for cancer therapy, several small molecule inhibitors that target Arf6 signalling have been identified and have demonstrated the ability to repress cancerous phenotypes. SecinH3, a synthetic compound, was originally synthesized as an exclusive inhibitor of cytohesins (as opposed to other ArfGEFs). More recently, SecinH3 has been found to also inhibit nucleotide exchange activity of the Arf6-specific GEF, BRAG2/GEP100 (Grossmann et al., 2013b). In the original studies using SecinH3, systemic treatment of mice with the inhibitor resulted in the development of hepatic insulin resistance, one of the earliest clinical signs in the advancement of type II diabetes (Hafner et al., 2006). Although SechinH3 appeared to suppress pulmonary metastases of the glioma xenograft tumours in mice models, and inhibited tumour angiogenesis and growth in mice with melanoma and lung cancer, both mice-models showed signs of hepatic insulin resistance (Grossmann et al., 2013a; Hongu et al., 2016).

Statins were initially described as inhibitors of hydroxymethylgutaryl-CoA-reductase (MHGCR) in the mevalonate pathway (Endo et al., 1976; Goldstein and Brown, 1990). They have already been widely applied in the treatment of cardiovascular diseases by inhibiting *de novo* cholesterol synthesis, but have recently been shown to suppress proliferation, angiogenesis and metastasis, as well as promote normal cellular apoptosis (Yeganeh et al., 2014) . However, these effects have been attributed to the inhibition of the small GTPases Rho and Ras (Bouterfa et al., 2000; Deyonelle et., 2001). More recently statins have demonstrated roles in the inhibition of Arf6 trafficking. As a consequence of Rab11a inhibition, Arf6 trafficking to the plasma membrane (where it is activated) is blocked. Statins also block the activation of Arf6 by TGF-β and hepatocyte growth factor (HGF) which appears to inhibit breast cancer cell invasion (Morishige et al., 2008).

NAV-2729 is the only known inhibitor that binds directly to Arf6 and is predicted to target the GEF binding region of Arf6. By inhibiting Arf6 activation, NAV2729 appears to disrupt anchorage-independent growth of cancer cells and tumour angiogenesis as well as tumour growth in mice with uveal melanoma (Yoo et al., 2016).

To date, QS11 is the only reported inhibitor of an ArfGAP. While it inhibits the Arf1-specific ArfGAP1, ArfGAP1 has demonstrated an *in vitro* ability to deactivate Arf6-GTP. ArfGAP1 is inhibited by QS11 when Arf1- or Arf6-GTP is used as a substrate. Although QS11 has been reported to block the migration of breast cancer cells, the molecular mechanisms of this phenomenon have not yet been elucidated (Singh et al., 2015; Zhang et al., 2007; Zhu et al., 2012).

6.2. Malaria

6.2.1. The burden of malaria

We hope to exploit the wealth of knowledge surrounding human Arf6, in the functional characterisation of a putative malarial Arf6 homolog. Here we review likely roles for the putative Arf6 since, to our knowledge, the putative Arf6 gene has not yet been studied. Malaria is a mosquito-borne infectious disease caused by parasitic protozoans of the genus *Plasmodium*. Four species of *Plasmodium* infect humans, namely *vivax, ovale*, *malariae* and *falciparum. P. falciparum* is the most clinically important species since it contributes to the majority of global malarial incidences (Moorthy et al., 2007).

In 2015, 214 million incidences of *P. falciparum* malaria were reported. Five hundred thousand cases resulted in death, approximately 90% of which were in Africa. Such statistics reported annually by the World Health Organisation (WHO) has led to the belief that the malarial parasite is one of the most dangerous infectious agents in the world. In addition to high mortality rates, malaria has a crippling effect on human development in Central Africa where its occurrence is greatest (Gallup and Sachs, 2001).

The initial clinical manifestations of malarial infection is paroxysm. Paroxysm describes the cyclical occurrence of an abrupt feeling of coldness, followed by a high fever and finally sweating. Other symptoms of uncomplicated malaria include headache, cough, myalgia, vomiting, diarrhoea and jaundice (Beare et al., 2006). Since similar symptoms present in several other conditions such as flu, gastroenteritis and viral hepatitis, malaria is often, and easily, misdiagnosed. If a malarial infection is suspected after physical examination, the presence of the parasite can be confirmed by rapid diagnostic testing in a laboratory setting (Kattenberg et al., 2011; Nadjm and Behrens, 2012). However, rapid diagnostic testing, the funding and relevant facilities for these tests are not always available in Africa. As a result, physical examination remains the mainstay of malaria diagnosis, and with commonly held beliefs such as “a fever equals malaria unless proven otherwise”, it is not surprising the many patients are treated unnecessarily. This results in the waste of limited medical resources and provides the entryway for antimalaria drug resistance (Perkins and Bell, 2008; Yegorov et al., 2016). Frequent misdiagnosis of uncomplicated malaria during the incubation period, often leads to the rapid development of severe malaria (also referred to as falciparum malaria) in immune-compromised persons. Severe forms of malaria involve cerebral malaria (which can cause seizures and coma), respiratory failure, acute renal failure and severe anaemia amongst others. Consequences of the development of severe malaria during pregnancy are stillbirths, infant mortality, abortion and low birth weight (Bartoloni and Zammarchi, 2012; Caraballo and King, 2014). Co-infection of malaria with human immunodeficiency virus (HIV-1) appears to increase mortality. Korenromp et al. (2005) has even proposed that malaria is attributable to the HIV-1 epidemic in Sub-Saharan Africa. Considering the crippling nature of the clinical features of malaria, and the constant cycle of reinfection in malaria

endemic areas, it is hardly surprising that socio-economic progress in these areas is slow (Gallup and Sachs, 2001).

Even though malaria was once both treatable and preventable (White , 2006), the impact of the disease is now exacerbated by the various levels of resistance observed against all existing antimalarial drugs. Although the frontline treatment - artemisinin-based combination therapy (ACT) - is still efficacious in the treatment of malaria in Sub-Saharan Africa, reports of resistance in South East Asia have recently emerged (Hanboonkunupakarn and White, 2016). Furthermore, with the anticipated malarial vaccine still several years away from availability, the focus of antimalarial drug discovery has shifted to the elucidation of novel drug targets (Frearson et al., 2007; Neafsey, 2013; Riley and Stewart, 2013).

Since the full genome and proteome of *P. falciparum* is at our disposal, in theory the full arsenal of possible drug targets is also available for interrogation (Florens et al., 2002). Analysis of the parasite's genome has revealed sequences that have significantly high sequence similarity and identity to known mammalian ADP-ribosylation factor signalling machineries. While a homologous Arf1, ArfGAP and ArfGEF have been identified and partially characterised (Baumgartner et al., 2001; Cook et al., 2010; Senkovich and Chattopadhyay, 2004; Wiek et al., 2004), further interrogation of the parasites genome has resulted in the identification of an additional putative Arf6 and a second, putative ArfGAP protein encoding sequence. The focus here is the putative Arf6, but the additional Arf signalling machineries will be reviewed in detail as potential, novel antimalarial drug targets in Chapter 5.

6.2.2. The parasite lifecycle

P. falciparum has a complex lifecycle that requires two hosts for completion. Within the definitive host, the female *Anopheles* mosquito, the malarial parasite undergoes sexual development. The asexual cycle in humans culminates in the development of two forms of the parasite - asexual merozoites and sexual gametocytes (Talman et al., 2004). Parasite progeny that forgo mitosis to pursue gametocytogenesis in preparation of the sexual lifecycle enter peripheral circulation where they are ingested during a mosquito's blood meal. Although the mosquito will consume both merozoites and gametocytes, only gametocytes will survive and initiate the parasites sexual lifecycle within the insect host (**Figure 2**). Various stimuli in the mosquito host such as a temperature drop, increase in pH, suitable concentrations of calcium and the presence of mosquito-derived metabolic intermediates activates gametocytes, causing them to produce male and female gametes in the mosquito's midgut (Billker et al., 2004). The development of male gametocytes involves rapid cycles of DNA replication and result in eight flagellated microgametes on the surface of the male gametocyte (Sinden et al., 2010). Female gametocytes, which do not undergo DNA replication, enter the midgut where male gametes attach. Nuclear fusion of the male and female gametes results in the zygote which undergoes DNA replication and meiosis to develop into a motile ookinete that penetrates the midgut wall (Hurd et al., 2006; Janse

et al., 1986). Approximately 26-36 hours post-infection ookinetes traverse the midgut wall and invade the space between the midgut basal lamina and epithelial cells. Ookinete maturation proceeds by rapid cycles of karyokinesis and cytokinesis to give rise to thousands of sporozoites which are released into the haemocoel. Approximately 25% of sporozoites will migrate to the salivary glands of the mosquito and await transferal to the human host (Guttery et al., 2012).

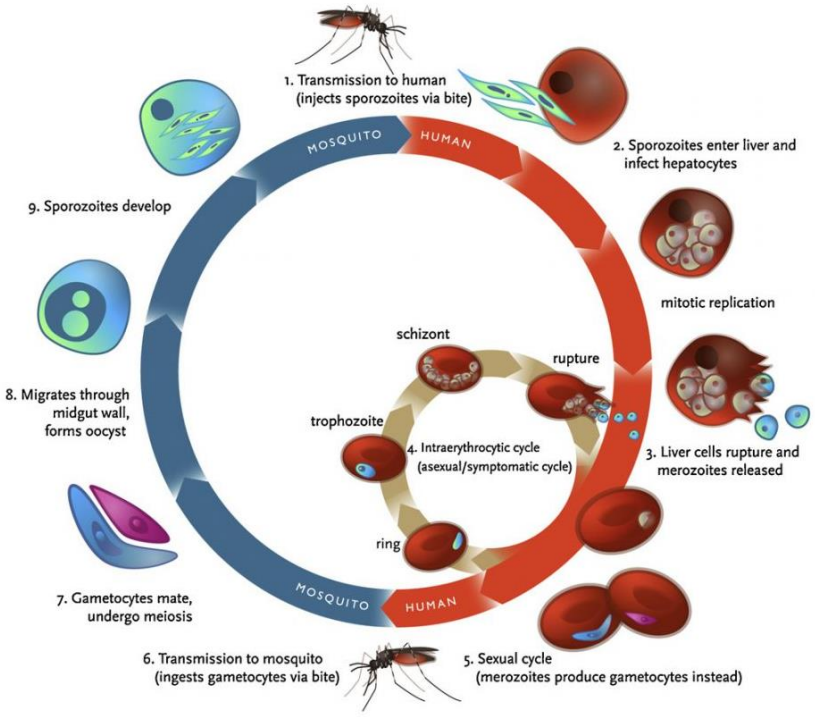

Figure 2: The lifecycle of *Plasmodium falciparum* (Klein, 2013). **1**. The *Anopheles* mosquito bites a human and injects sporozoites into the hosts bloodstream. **2**. Sporozoites migrate to the liver and invade hepatocytes. **3**. Inside hepatocytes sporozoites undergo rapid cycles of mitotic replication to produce tens of thousands of merozoite progeny. Merozoites exit hepatocytes and re-enter the bloodstream where they infect red blood cells to initiate the intraerythrocytic cycle of their lifecycle. **4**. Merozoites undergo drastic morphological changes into a ring form parasite before developing into trophozoites. Trophozoites rapidly acquire nutrients to facilitate its growth and eventual maturation into schizonts. Schizonts divide to produce 16-32 daughter merozoites which are released back into systemic circulation. A population of merozoites re-infect blood cells to complete additional rounds of asexual replication, while **5**. a smaller population develops into gametocytes. **6**. Gametocytes ingested by the mosquito undergo **7**. Gametogenesis to produce male and female gametes. These fuse to produce a zygote, which undergoes meiosis to produce an ookinete. **8**. The ookinete traverses the midgut wall of the mosquito and develops into an oocyst. **9**. The oocyst rapidly divides to produce daughter sporozoites which migrate to the salivary glands of the mosquito and await transferral to the human host.

In the secondary host (humans) the parasite undergoes asexual development. Infection in humans is initiated when sporozoites are transmitted into the hosts bloodstream during a mosquito's blood meal (Cowman et al., 2012). Sporozoites immediately proceed to the liver, where they leave systemic circulation by invading hepatocytes. Inside the hepatocyte, a single sporozoite undergoes schizogony (mitotic replication) to produce between 30 000 to 40 000 merozoites over a 140-hour period. The fully developed merozoites are packaged into merosomes which subsequently bud from hepatocytes and

enter the bloodstream. Merozoites are released into the bloodstream upon the disintegration of the merosome. Merozoites bind to and invade RBCs, which initiates the erythrocytic stages of malarial infection (Hisaeda et al., 2005). While the pre-erythrocytic stages of malarial infection is clinically silent, it is during cyclical invasion of erythrocytes in the intraerythrocytic stage that clinical symptoms of malaria manifest. Being the symptomatic stage of malarial infection the erythrocytic cycle is the most clinically important and the target of most antimalarial therapeutics (Delves et al., 2012). Intracellular merozoites undergo considerable morphological changes and differentiate into a ring stage form before developing into a trophozoite. Trophozoites, which have a characteristic ameboid shape, rapidly acquire nutrients from the host to facilitate organism growth. Once the trophozoites have acquired enough nutrients, organism growth ceases and karyokinesis occurs (called the schizont stage). Multiple divisions of the single haploid nucleus results in 16-32 dozen daughter nuclei which arrange along the periphery of the trophozoite (Hisaeda et al., 2005). During cytokinesis the plasma membrane invaginates around each daughter nucleus and the cell cytoplasm divides accordingly. The new daughter merozoites mature within the RBC causing the RBC membrane to rupture, releasing new merozoites into the bloodstream (Wickham et al., 2003). The majority of new merozoites invade new RBCs and undergo several more asexual erythrocytic cycles. A small fraction of merozoites develop into sexually dimorphic gametocytes which take 8-12 days to reach maturation. These mature gametocytes are capable of transfer back to the *Anopheles* mosquito host where sexual reproduction occurs (Liu et al., 2011).

6.2.3. Endocytosis in malarial parasites

During invasion of the RBC, merozoites become enclosed within a parasitophorous vacuolar membrane (PVM) derived from the RBC membrane (Haldar, 1998). While enclosure in the PVM and the RBC membrane allows the parasite to evade the host immune defence mechanisms it also restricts the parasites access to extracellular nutrients located in the blood plasma (Hanssen et al., 2012). The parasite circumvents this issue by ingesting the RBC cytoplasm (which is predominantly composed of haemoglobin) as a nutrient source by a process of endocytosis. The endocytosis process occurs approximately 12 hours after host cell invasion and is initiated in the mid-ring stage, accelerates significantly through the trophozoite stage and then decelerates and comes to a halt during cell division in the schizont stage (Deponte et al., 2012). The function of endocytosis is to provide a source of amino acids (as a result of haemoglobin catabolism) and to prevent the premature lysis of the host cell by providing space in the blood cell for the rapidly expanding parasite (Bakar et al., 2010; Lew et al., 2003; Tekwani and Walker, 2005).

Early studies on ‘the processes of malarial feeding’ proposed that endocytic invaginations at the parasite’s plasma membrane mature into cytosomes (endosome-like structures that are encapsulated in

the parasites plasma membrane (PPM) and the PVM) (Aikawa et al., 1966; Slomianny and Prensier, 1990). Double-membrane bound vesicles budding from cytosomes were proposed to migrate and fuse with and acidic digestive vacuole (DV), whereafter they are present as single membrane-bound vesicles in the DV lumen. Here, the vesicle contents are released, and haemoglobin degradation ensues (Yayon et al., 1983). However, recent studies have re-examined this hypothesis, and while the precise molecular mechanisms of malarial endocytosis are not fully understood several prevailing hypotheses have been put forward. Using serial thin-section electron microscopy, Elliott et al. (2008), indicated that during the ring-stage, parasites fold around the host cell cytoplasm as the first step in the biogenesis of the DV. This process is often referred to as the 'big gulp'. As the parasite matures, cytosome-derived vesicles and tubules carrying haemoglobin maintain haemoglobin uptake. In mature parasites they described an additional cytosome-independent endocytic pathway that is reminiscent of macropinocytosis (Elliott et al., 2008). Interestingly, Lazarus et al. (2008) put forward a vesicle-independent process of malarial endocytosis. They proposed that initial invaginations at the plasma membrane, rather than forming vesicles, elongate into tubular structures that appose the DV and remain connected to the parasites surface. Ultimately the tubules 'pinch off' and fuse with the DV to release their contents into the DV lumen (Lazarus et al., 2008).

While the organization of endocytosis in model organisms appears to be conserved, the precise molecular endocytic mechanisms that underly cytosomal endocytosis in malarial parasites are yet to be definitively determined. It has however been proposed that clathrin-mediated endocytosis, the most highly characterised 'canonical' system in mammalian cells, may not be responsible for cytosomal endocytosis in *P. falciparum.* This was proposed due to the lack of a characteristic clathrin "coat" around endocytic invaginations when viewed by electron microscopy (Bakar et al., 2010; Elliott et al., 2008). The parasite's genome also indicates several proteins which could potentially coordinate an endosomal network and are expressed during the asexual parasite stages. While a malarial Rab7 homolog has been characterised as a central regulator in the formation of early endosomes in malarial parasites (Elliott et al., 2008; Krai et al., 2014), there also exist additional homologs such as EEA1 and Arf6 that may be important elements in malarial endocytosis (Kari, M., PhD dissertation; Hoppe, H., *unpublished data*). In the interrogation of the putative malarial homolog of Arf6 (a major participant in endocytosis in other cell types), *Pf*Arf6, T.Swart (M.Sc dissertation) prepared transgenic parasites expressing GFP fusion constructs of the putative *Pf*Arf6 and determined its sub-cellular localization in the parasite by epifluorescence and confocal microscopy. Consistent with the vesicle-dependent hypotheses of malarial endocytosis, *Pf*Arf6-GFP localised to numerous puncta along the periphery of the parasite in the mature trophozoite life stage - which may be hypothesized to demarcate sites where endocytosis is being initiated - in addition to a more central intensely fluorescent single ring-like locus which was insensitive to the Golgi disruptors BFA and Golgicide. In the multinucleate schizont phase, the peripheral puncta disappeared, and the single central locus remained as a ring-like structure. The

localisation of *Pf*Arf6 under the treatment of drugs known to affect malarial endocytosis (chloroquine and mefloquine) was disrupted into a cytoplasmic pool, suggesting a possible role in endocytosis. (T.Swart, M.Sc. dissertation). The continuous degradation of haemoglobin is necessary for uninterrupted growth and proliferation of the parasite and hence make it an essential pathway that may be a potential target for new antimalarial drug discovery (Tekwani and Walker, 2005).

7. Motivation and overall aim of the study

The potential role of *Pf*Arf6 in this abovementioned process motivates this study. The goals were, firstly, to examine the possible functions of *Pf*Arf6 using HeLa cells as a surrogate model for parasites and, secondly, to establish plate-based *Pf*Arf6 assays that can be used to screen compounds for inhibitors that can in the longer term be used to chemically validate *Pf*Arf6 as a malaria drug target. To support the second goal, a novel plate-based assay was established using human Arf6. The assay was established using human Arf6 and the related accessory machineries since established Arf signalling inhibitors could be used to validate the assay. This may also be exploited for cancer drug discovery.

Chapter 2: Methods and materials

2.1. Preparation of DNA expression constructs

2.1.1. HeLa cell surrogate model constructs (pEGFP-N1-PfArf6 and pEGFP-N1-PfArf6 mutants)

The putative *P. falciparum* Arf6 coding sequence (PlasmoDB code: PF10_0337) was codon-optimised for human expression by GenScript (Hong Kong) and sub-cloned into the *Xho*I/*Kpn*I restriction sites of the pEGFP-N1 mammalian expression plasmid (Clontech) to create the pEGFP-N1-*Pf*Arf6 recombinant construct (T. Swart, M.Sc. dissertation). The pEGFP-N1-*Pf*Arf6^{Q67L} and the pEGFP-N1-*Pf*Arf6^{T27N} mutants of pEGFP-N1-*Pf*Arf6 were prepared by site directed mutagenesis and inverse PCR. The pmRFP-LC3 construct was a gift from Tamotsu Yoshimori (Addgene construct #21075), the TagRFP-T-EEA1 construct was a gift from Silvia Corvera (Addgene construct # 42635), the mRFP-CLC construct was a gift from Ari Helenius (Addgene construct #14435), the pcDNA3/hArf6(WT)-mCherry construct was a gift from Kazuhisa Nakayama (Addgene construct # 79422) and the DsRed-Rab5 WT construct was a gift from Richard Pagano (Addgene construct # 13050).

2.1.2. In vitro human Arf6 signalling assay constructs (pET-28a-CFP-HsArf6^{NΔ13}, pET-28a-CFP-HsArf1^{NΔ17}, pET-28a-ARNO^{Sec7}, pET-28a-ArfGAP1^{GAP}, as pGEX-4T1-JIP4^{LZ11} and pGEX-4T-2/hGGA3^{GAT})

The pET-28a-CFP construct, encoding cyan fluorescent protein (CFP) which was sub-cloned into the *Bam*HI/*Xho*I restriction sites of pET-28a, was previously prepared by F. Khan (2017). The pET-28a-CFP-*Hs*Arf6 ^{NΔ13} construct was prepared by sub-cloning the coding sequence for ^{NΔ13}*Hs*Arf6 (obtained from NCBI CAG46737.1) with a 3'-terminal stop codon and flanking *Nhe*I/*Bgl*II sites into the *Nhe*I/*Bam*HI restriction sites of the pET-28a-CFP construct (sub-cloning experiments are described in section 2.2 below). The pET-28a-CFP-*Hs*Arf1^{NΔ17} construct was prepared by T.Swart (PhD dissertation). The human cytohesin-2/ARNO protein sequence was obtained from NCBI (NP_004219.3). The Sec7 domain of cytohesins-2/ARNO (amino acids 51 – 253) was codon-optimized for expression in *E. coli* and cloned into pET-28a (*Nhe*I/*Xho*I sites) by Genscript. The construct will hereafter be referred to as pET-28a-ARNO^{Sec7}. The human ArfGAP 1 protein sequence was obtained from NCBI (NP_060679.1). The GAP domain of ArfGAP1 (amino acids 1 – 140) was codon-optimised for expression in *E. coli* and cloned into pET-28a (*Nhe*I/*Xho*I sites) by Genscript. The construct will hereafter be referred to as pET-28a-ArfGAP1^{GAP}. The human c-Jun-amino-terminal kinase-interacting protein 4 (JIP4) coding sequence was obtained from NCBI (NP_001124000.1). The leucin zipper (LZII) domain of JIP4 (amino acids 406 - 461) was codon-optimised for expression in *E. coli* and cloned into pGEX-4T1 (*Bam*HI/*Xho*I sites) by Genscript. The construct will hereafter be referred to as pGEX-4T1-

JIP4^{LZ11}. The pGEX-4T-2/hGGA3^{GAT} construct was used for the expression of the GAT domain of a human golgi-localized, gamma adaptin ear-containing, ARF-binding 3(GGA3)- GST fusion protein and was a gift from Kazuhisa Nakayama (Addgene construct # 79436).

2.1.3. In vitro malarial Arf6 signalling assay constructs (pET-28a-CFP-PfArf6$^{N\Delta17}$, pET-28a-CFP-PfArf1$^{N\Delta17}$, pET-28a-PfArfGAP1^{GAP}, pET-28a-PfArfGAP2^{GAP} and pET-28a-PfArfGEF^{Sec7})

The pET-28a-CFP-*Pf*Arf6$^{N\Delta17}$ construct was prepared by sub-cloning the coding sequence for $^{N\Delta17}$*Pf*Arf6 (PlasmoDB code: PF10_0337) with a terminal stop codon into the *Nhe*I/*Bam*HI restriction sites of pET-28a-CFP construct (the sub-cloning procedure is described in section 2.2. below). The pET-28a-CFP-*Pf*Arf1$^{N\Delta17}$ construct was prepared by T. Swart (PhD dissertation). The pET-28a-*Pf*ArfGAP1^{GAP} construct was prepared by sub-cloning the GAP domain (amino acids 1 – 161) of the putative malarial ArfGAP1 coding sequence (Senkovich and Chattopadhyay, 2004) obtained from PlasmoDB (PF3D7_1244600) with a terminal stop codon into the *Nhe*I/*Xho*I restriction sites of pET-28a-CFP construct (the sub-cloning procedure is described in section 2.2. below). The putative malarial ArfGEF (Wiek et al., 2004) was obtained from PlasmoDB (PF3D7_1442900). The Sec7 domain of the putative malarial ArfGEF (amino acids 1201 – 1739) was codon-optimised for expression in *E. coli* and cloned into pET-28a (*Nhe*I/*Xho*I sites) by Genscript. The construct will hereafter be referred to as pET-28a-*Pf*ArfGEF^{Sec7}. The putative malarial ArfGAP2 was obtained from PlasmoDB (PF3D7_0526200.1). The GAP domain of the putative malarial ArfGAP2 (amino acids 1 – 214) was codon-optimised for expression in *E. coli* and cloned into pET-28a (*Nhe*I/*Xho*I sites) by Genscript. The construct will hereafter be referred to as pET-28a-*Pf*ArfGAP2^{GAP}.

2.2. Molecular cloning

2.2.1. PCR amplification of the $^{N\Delta13}$HsArf6, $^{N\Delta17}$PfArf6 and PfArfGAP1^{GAP} coding sequences.

Forward primers were designed to amplify the *Hs*Arf6 and *Pf*Arf6 coding sequences (minus the sequences encoding for the conserved N-terminal hydrophobic extension). In addition to amplifying truncated versions of the $^{N\Delta13}$*Hs*Arf6 and $^{N\Delta17}$*Pf*Arf6 coding sequences, terminal stop codons were incorporated into the reverse primers to prevent the expression of Arf6-CFP fusion proteins (since these coding sequences were subcloned into the pET-28a-CFP construct). Finally, *Nhe*I/*Bgl*II restriction sites and the *Nhe*I/*Bam*HI restriction sites were incorporated into the forward and reverse primers for the amplification of $^{N\Delta13}$*Hs*Arf6 and $^{N\Delta17}$*Pf*Arf6 coding sequences, respectively, to facilitate cloning into the *Nhe*I/*Bam*HI sites of the pET-28a-CFP construct. The forward and reverse primers used to amplify the *Pf*ArfGAP1^{GAP} coding sequence were designed to incorporate terminal *Nhe*I and *Xho*I restriction sites respectively, to facilitate cloning into the *Nhe*I/*Xho*I sites of the pET-28a construct. All primers were synthesized by Integrated DNA technologies.

A 50 µL solution containing 1X KAPA HiFi fidelity buffer, 0.2 mM KAPA dNTP mix, 3 µM forward primer, 3 µM reverse primer, and 0.5 µL template DNA was heated to 94ºC for 2 minutes before 0.5 U KAPA HiFi polymerase was added. Following initial denaturing, 30 cycles of denaturation (for 40 seconds at 94ºC), annealing (for 45 seconds) and extension (for 2 minutes at 70ºC) preceded a final extension at 70ºC for 5 minutes (adapted from Mullis *et al*., 1986). PCR products were analysed by agarose gel electrophoresis (protocol provided in section 2.2.9). Confirmed PCR products were purified from the PCR reaction mix using a NucleoSpin Gel and PCR Clean-up kit (Macherey-Nagel) according to the manufacturer's instructions and stored at -20ºC.

Table 1: PCR products, primers and annealing temperatures (Hot start PCR)

PCR product	**Template DNA**	**Primers**		**Annealing temperature used** (ºC)
$^{N\Delta 13}$*Hs*Arf6	pARF6-CFP[1]	**F**	5'- GATCGCTAGCATGCGGATCCTCATGTTGGGC -3'	68ºC
		R	5'-GATCAGATCTTTAAGATTTGTAGTTAGAGGTTAACCATG- 3'	
$^{N\Delta 17}$*Pf*Arf6	pBluescript - (co) *Pf*Arf6[2]	**F**	5'- GATCGCTAGCGTGAGAATCCTGATCCTGGGC -3'	65ºC
		R	5'- GATCGGATCCTTACTTGATGTTATTGACCAGCCAG -3'	
*Pf*ArfGAP1^{GAP}	*Plasmodium falciparum* genomic DNA[3]	**F**	5'- GATCGCTAGCATGAATGCAGCCGCTGTAGAAC -3'	65ºC
		R	5'-GCATCTCGAGTTATGATGAAATAAAATCCGGTTCTTC- 3'	

1: Was a gift from Joel Swanson; Addgene construct # 11382)

2: *Pf*Arf6 codon-optimised for human cell expression and cloned into pBluescript by Genscript

3: Donated by Travis Basson

2.2.2. Site-directed mutagenesis to obtain the pEGFP-N1-^{Q67L}PfArf6 and pEGFP-N1-^{T27N}PfArf6 coding sequences.

To prepare constitutively active and inactive mutants of *Pf*Arf6 the single amino acid base substitutions Q67L and T27N respectively, were incorporated into the pEGFP-N1-*Pf*Arf6 construct. In addition to coding for the single amino acid base substitutions described above, primers were designed with 15 bp overlaps to facilitate ligation of the amplified constructs. An In-Fusion HD cloning kit (Takara, Clontech) was used for ligation. All primers were synthesized by Integrated DNA technologies.

A 50 µL solution containing 1X KAPA HiFi fidelity buffer, 0.2 mM KAPA dNTP mix, 3 µM forward primer, 3 µM reverse primer, and 0.05 µL parental template DNA (pEGFP-N1-*Pf*Arf6 construct) was heated to 94ºC for 2 minutes before 0.5 U KAPA HiFi polymerase was added. Following initial

denaturing, 30 cycles of denaturation (at 94°C for 40 seconds), annealing (for 45 seconds) and extension (70°C for 2 minutes) preceded a final extension at 70°C for 5 minutes. PCR products were purified from an agarose gel using a NucleoSpin Gel and PCR Clean-up kit (Macherey-Nagel) according to the manufacturer's instructions. Ligation was conducted according to the instructions for the In-Fusion ligation reaction in the In-Fusion HD EcoDry cloning kit (Clontech). Re-circularised constructs were transformed into competent *E. coli* XL-10 gold cells. Several colonies were propagated and screened for successful mutagenesis by sequencing alkaline lysis plasmid minipreps with the CMV forward primer (adapted from Carter, 1986). Sequencing was carried out by Inqaba Biotec (South Africa).

Table 2: PCR products, primers and annealing temperatures (Site-directed mutagenesis)

PCR product	**Template DNA**	**Primers**		**Annealing temperature used** (°C)
*Pf*Arf6 (Q67L)	pEGFP-N1-*Pf*Arf6	**F**	5'-GGAGGCCTGAGCTCCATCAGG-3'	67°C
		R	5'-GGAGCTCAGGCCTCCCAGGTC-3'	
*Pf*Arf6 (T27N)		**F**	5'-CAAGAACACCATCCTGAACAGAC- 3'	66°C
		R	5'-AGGATGGTGTTCTTGCCGGCG- 3'	

2.2.3. Evaluating DNA concentration and purity

The concentration (Abs_{260}) and purity ($Abs_{260/280nm}$) of purified DNA samples was determined using a NanoDrop 2000 spectrophotometer (Thermoscientific).

2.2.4. Ligation reactions

Target constructs were digested with the relevant restriction enzymes, resolved on an agarose gel and isolated from excised gel pieces using a NucleoSpin Gel and PCR Clean-up kit (Macherey-Nagel) according to the manufacturer's instructions. The concentrations and purities were evaluated. To 100 ng of the target construct, a 3-fold molar excess of the PCR product was added. The 3-fold molar excess was determined using the formula:

$$\text{3-fold molar excess } (ng) = 3 \text{ x } \frac{size\ of\ the\ PCR\ product\ (bp)}{size\ of\ the\ target\ construct\ (bp)} \text{ x } 100\ ng$$

The PCR products were cloned into the target constructs in 1X buffer for T4 DNA Ligase with 1 mM ATP in the presence of 1 µL T4 DNA ligase (New England BioLabs). Ligation reactions were conducted overnight in a mixture of ice and water (adapted from the methods of Western and Rose, 1991). The ligation products were transformed into competent *E. coli* XL-10 gold cells, several colonies

were propagated in overnight cultures and purified by alkaline lysis. Successful ligation products were screened for by conducting diagnostic restriction digestions on each alkaline lysis miniprep and analysing the products by agarose gel electrophoresis.

2.2.5. Preparing competent E. coli cells

XL-10 gold competent *E. coli* cells (Stratagene), BL21 (DE3) competent *E. coli* cells (New England BioLabs), Rosetta (DE3) competent *E. coli* cells (Novagen) and T7 Express lysY/Iq competent *E. coli* cells (New Egland BioLabs) were used in the study. Untransformed *E. coli* cells were propagated in Luria broth at 37ºC for 16 hours with continuous agitation. To 100 mL of Luria broth, 2.5 mL of the untransformed *E. coli* overnight culture was added (1 in 40 inoculum) and incubated at 37ºC with continuous agitation until the OD_{600nm} was 0.6 - 0.8. The cells were collected by centrifugation at 2152 *g* for 10 minutes at 4ºC and thereafter kept on ice. The cells were resuspended in 4 mL of ice-cold RF-1 buffer (100 mM KCl, 50 mM $MnCl_2$, 30 mM potassium acetate, 10 mM $CaCl_2$, 15% (v/v) glycerol) and incubated on ice for 20 minutes. The cells were collected by centrifugation at 1377 *g* for 10 minutes at 4ºC and resuspended in 3 mL ice-cold RF-2 buffer (10 mM HEPES, 10 mM KCl, 75 mM $CaCl_2$, 15% (v/v) glycerol) (Adapted from the methods of Tang *et al*., 1994). Aliquots were prepared in cryotubes and stored at -80ºC.

2.2.6. Transformation of competent cells

Competent *E. coli* cells were thawed on ice. To 50 µL of competent *E. coli* cells 1 µL alkaline lysis plasmid miniprep (or 10 µL ligation reaction) was added. The mixture was mixed briefly and incubated on ice for 25 minutes. Heat shock was conducted by incubating the mixtures at 42.5ºC for 1 minute and immediately incubated on ice for 5 minutes. To each transformation 500 µL Luria broth was added and the suspension incubated at 37ºC for 1 hour with gentle agitation. The cells were collected by centrifugation at 3099 *g* for 3 minutes and resuspended in 100 µL Luria broth. The resuspended cells were plated on Luria-agar plates containing 50 $\mu g.mL^{-1}$ kanamycin or ampicillin (depending on the constructs resistance marker). Once dry, the plates were incubated at 37ºC for 16 hours (Adapted from the methods of Bergmans *et al*., 1981).

2.2.7. Alkaline lysis plasmid miniprep

E. coli XL-10 gold cells harbouring target constructs stored as glycerol stocks (*E. coli* cultures in 15% (v/v) glycerol stored at -80ºC) were propagated in Luria broth containing 50 $\mu g.mL^{-1}$ kanamycin or ampicillin (depending on the constructs resistance marker). The culture was incubated for 16 hours at 37ºC with constant agitation. Approximately 3 mL of the bacterial culture was collected by centrifugation at 3 099 *g* for 3 minutes. The bacterial pellet was resuspended in GTE buffer (30 mM glucose, 25 mM Tris, 10 mM EDTA, 10 $\mu g.mL^{-1}$ RNase, pH 8.0) and lysed in lysis buffer (0.2 N NaOH,

1% (w/v) SDS). Cell lysis was terminated with neutralization buffer (42% (v/v) acetic acid, pH adjusted to 4.8 using KOH). Cellular debris was cleared by centrifugation at 16 873 *g* for 5 minutes. The cleared supernatant was transferred to a sterile Eppendorf tube, washed in absolute ethanol and washed in a 70% (v/v) ethanol solution. Ethanol was fully removed before the DNA pellet was dissolved in water by heating to 37°C for 10 minutes. Alkaline lysis minipreps were stored at -20°C.

2.2.8. Restriction digestion

All restriction digestions were conducted by incubating 10 µL of the target DNA (cleaned PCR products, target vectors or recombinant constructs) in a solution containing 1X ThermoScientific FastDigest buffer and 0.5 µL of each Thermoscientific FastDigest restriction enzyme required for 1 hour at 37°C (adapted from Cohen *et al*., 1973). Restriction digestion products were stored at -20°C until further use.

2.2.9. Agarose gel electrophoresis

All agarose gels were prepared by heating 0.8% (w/v) agarose in 1X TAE buffer (100 mM Tris, 100 mM acetate, 2 mM EDTA) or 1X TBE buffer (100 mM Tris, 100 mM boric acid, 2 mM EDTA) until fully dissolved. Once cooled 1.2 $\mu g.mL^{-1}$ ethidium bromide was added and the gel was left to set in a casting tray. Samples were prepared in sample loading buffer (5% (v/v) glycerol, 0.042 % (w/w) bromophenol blue in 1X TBE or 1X TAE buffer). Agarose gels loaded with samples were submerged in 1x TBE or 1x TAE buffer and run for 1.5 hours at 70 V alongside a Promega 1kb DNA ladder. Diagnostic gels for the analysis of PCR amplification and restriction digestions were visualised and photographed under UV light using a ChemiDoc XRS+ gel documentation system (Bio-Rad) (methods adapted from Meyers *et al*., 1976).

2.3. Mammalian cell culture, transfection and fluorescence microscopy

2.3.1. Routine cell culture

HeLa and HEK293 cells (Cellonex) were cultured in complete culture medium which consisted of DMEM with ultraglutamine and 4.5 $g.L^{-1}$ glucose (Lonza BioWhittaker), supplemented with 5% (w/v) penicillin/streptomycin/amphotericin B (Lonza) and 10% (v/v) heat-inactivated foetal bovine serum (FBS; Biowest) in sterile T25 or T75 cell culture flasks. Cultures were incubated at 37°C in a humidified incubator with 5% (v/v) CO_2. Once cells reached ~ 90% confluence, spent medium was aspirated off and the cells were briefly washed in filter sterilised 1X phosphate buffered saline (PBS). The cells were incubated in sufficient Trypsin-EDTA (Lonza; $680U.L^{-1}$ trypsin and $0.2g.L^{-1}$ EDTA) solution to cover the cell layer until complete cell detachment was observed by light microscopy. Suspended cells were subjected to 181 *g* centrifugation for 3 minutes and the supernatant aspirated off. Cell culture flasks

were reseeded with a 1:40 dilution of cells in complete culture medium and returned to the 37ºC incubator with humidified atmosphere of 5% CO_2.

2.3.2. Freezing and thawing stocks

HeLa and HEK cells were cryopreserved by resuspending cell pellets in 1 mL pre-cooled freezing medium (10% (v/v) DMSO, 90% (v/v) FBS) and subsequent storage at -80ºC. Cryopreserved cells were accessed for routine culture by thawing cells in freezing medium at 37ºC. Thawed cells were immediately washed in 15 mL prewarmed complete culture medium by resuspension and subsequent centrifugation at 181 *g* for 3 minutes. Washed cells were seeded into cell culture flasks and routine culturing continued.

2.3.3. Transient transfection for live cell imagining

Approximately 1 x 10^4 HeLa or HEK cells in 100 uL complete culture medium were plated in each of ten wells in 96-well flat bottom plates and incubated until cell confluence reached 70 - 90%. Transfections were conducted using X-fect Transfection Reagent (Clontech). The transfection mixture was prepared by mixing 5 μg of transfection construct in 50 μL X-fect buffer. To this, 1.5 μL X-fect polymer was added and the transfection mixture incubated at room temperature for 10 minutes. To each of the 10 wells in the 96-well plate, 5 μL transfection mixture was added. The cells were incubated with the transfection mixture for 3 hours at 37ºC in humidified atmosphere with 5% CO_2. The medium was aspirated off and 100 μL fresh complete culture medium was added to each well. The transfected cells were returned to the incubator for 24 hours before analysis.

2.3.4. Transient transfection for fixed cell imagining

Approximately 0.6 x 10^5 HeLa or HEK cells in 500 μL complete culture medium was plated in four wells (containing glass coverslips) of a 24-well plate and incubated until cell confluence reached 70 - 90%. Transfections were conducted using X-fect Transfection Reagent (Clontech). The transfection mixture was prepared by mixing 5 μg of the transfection construct in 100 μL X-fect buffer (for co-transfections 2.5 μg of each construct was used). To this, 1.5 μL X-fect polymer was added and the transfection mixture incubated at room temperature for 10 minutes. To each of the four wells, 25 μL transfection mixture was added. Cells were incubated with transfection mixture for 3 hours at 37ºC in humidified atmosphere with 5% CO_2. The medium was aspirated off and 750 μL fresh complete culture medium was added to each well. The transfected cells were returned to the incubator for 24 hours before being processed for microscopy.

2.3.5. Chloroquine treatment

Chloroquine treatment was conducted on HeLa cells transfected with pmRFP-LC3, or co-transfected with pmRFP-LC3 and pEGFP-N1-*Pf*Arf6. Chloroquine (Sigma-Aldrich) stock solutions were prepared in water, filtered sterilised into sterile Eppendorf tubes and stored at -20^{o}C until use. Chloroquine treatment was conducted 16 hours post-transfection. Complete culture medium was removed and fresh culture medium containing 100 μM chloroquine was added to the cells and culturing continued for 24 hours. Control cells were incubated in medium without chloroquine. Cells were subsequently fixed as described in section 2.3.7 and viewed as described in section 2.3.9.

2.3.6. Haemoglobin endocytosis assay

Blood was collected from human volunteers in 10 mL vacutubes containing EDTA as anticoagulant (ethical approval obtained from the Rhodes University ethics committee: 2011Q4-1). Red blood cells (RBCs) were lysed by adding 3 volumes of water to one volume of packed RBCs. Following lysis, the suspension was mixed with an equal volume of 2X PBS. The resulting 1X PBS suspension was centrifuged for 2 minutes at 460 *g* to remove resealed RBC ghosts, and the haemoglobin containing supernatant (hereafter referred to as the haemoglobin solution) was aspirated, filter sterilized and stored at 4^{o}C. Twenty-four hours post-transfection HeLa cells expressing *Pf*Arf6-EGFP were incubated for 1 hour under normal culture conditions, in culture medium without FBS containing 20% (v/v) haemoglobin solution. Control cells were incubated in parallel in medium without haemoglobin. Cells were washed three times in pre-warmed 1X PBS by gentle agitation for 1 minute each. Cells were subsequently fixed with paraformaldehyde and cellular membranes were permeabilized by incubating for 2 minutes in 0.1% (v/v) Triton X-100 in 1X PBS. Thereafter the cells were incubated for 15 minutes in 0.15 M glycine (in water), blocked for 20 minutes in incubation buffer (1% (w/v) BSA, 0.1% (v/v) Tween 20 in 1X PBS), incubated for 1 hour at room temperature in a 1:400 dilution rabbit anti-haemoglobin antiserum (Sigma-Aldrich) in incubation buffer, washed in wash buffer (0.1% (w/v) BSA, 0.1% (v/v) Tween 20 in 1X PBS) and finally incubated for 40 minutes at room temperature in a 1:200 dilution of anti-rabbit TRITC antibodies (Jackson ImmunoResearch) in incubation buffer. Cells were washed four times before they were stained with Hoechst and mounted on coverslips.

2.3.7. Cell fixation, Hoechst staining and mounting on coverslips

Cell fixation was conducted as follows: complete culture medium was aspirated off, and cells were washed three times in 500 μL of pre-warmed 1X PBS by gentle agitation for 2 minutes each. Cells were immediately fixed in 250 μL of 4% (w/v) cold paraformaldehyde in 1X PBS by incubating the cells for 10 minutes at ambient temperature. The paraformaldehyde was removed and the cells were washed three times in 500 μL of 1X PBS by gentle agitation for 2 minutes each. Nuclei were stained with 1

μg.mL^{-1} Hoechst 33342 in 1X PBS by incubation for 10 minutes with gentle agitation. The Hoechst solution was removed and the cells were washed three times in 500 μL of 1X PBS by gentle agitation for 2 minutes. The coverslips containing the fixed immobilised cells were removed from the 24 well plate, briefly rinsed in water, air dried and mounted in Fluoroshield (Sigma-Aldrich) on glass microscope slides. Mounted coverslips were stored in the dark for 2 days before further use.

2.3.8. Immunofluorescence microscopy

HeLa cells transfected with pEGFP-N1-*Pf*Arf6 were used for co-localisation study of *Pf*Arf6-GFP with endogenous EEA1. After cells were fixed in 4% (w/v) paraformaldehyde, they were permeabilized for 15 minutes in permeabilization buffer (5% (w/v) BSA, 10% (w/v) sucrose, 0.1% (v/v) Triton X-100 in 1x PBS). Cells were incubated in a 1:250 dilution of goat anti-EEA1 polyclonal primary antibodies in permeabilization buffer for 4 hours at room temperature, followed by a 30-minute secondary antibody incubation in a 1:250 dilution of donkey anti-goat Alexafluor 546. All antibodies were obtained from Santa Cruz Biotechnology. Cells were subsequently fixed with paraformaldehyde, stained with Hoechst and mounted on microscope slides in mounting medium.

2.3.9. Fluorescence microscopy

Cells transiently transfected for live cell imagining were incubated in 1 μg.mL^{-1} Hoechst for 10 minutes before being viewed live on a Zeiss AxioVert.A1 FL-LED inverted microscope with a 40X objective. Cells that were fixed, stained with Hoechst and mounted in mounting medium were viewed on an Olympus BX61 upright fluorescence microscope either with a 40X objective or with a 100X oil immersion objective.

2.4. Bacterial protein expression and purification

2.4.1. Small scale expression

Expression constructs transformed into BL21 (DE3) competent *E. coli* cells (New England BioLabs), Rosetta (DE3) competent *E.coli* cells (Novagen) or T7 Express lysY/Iq competent *E.coli* cells (New England BioLabs) were propagated in Luria broth containing 50 μg.ml^{-1} kanamycin or ampicillin at 37^{o}C for 16 hours with continuous agitation. To 7.2 mL of Luria broth containing 50 μg.ml^{-1} kanamycin or ampicillin, 0.8 mL of the relevant overnight culture was added (1 in 10 inoculum) and incubated at 37^{o}C with continuous agitation until the OD_{600nm} value fell between 0.5 – 0.9. Protein expression was induced by adding 1 mM IPTG to the expression culture and typically conducted for 3 hours at 37^{o}C or 16 hours at 16^{o}C. The bacterial cells were collected by centrifugation at 5 000 *g* for 10 minutes and washed in 2 mL wash buffer (50mM Tris-HCl (pH 8.0)). The resuspended pellet was centrifuged again at 5 000 *g* for 10 minutes and stored at -80^{o}C overnight. Hereafter all steps were conducted on ice and

all buffers used were ice-cold. The frozen pellet was thawed for 10 minutes and resuspended in 1 mL wash buffer. The cells were lysed with 2 $mg.mL^{-1}$ lysozyme for 30 minutes, and by two cycles of sonication at 60 Hz for 45 seconds each with 1 minute resting periods. The cell lysate was centrifuged at 5 000 *g* for 10 minutes to separate the insoluble and soluble fractions. The insoluble fraction was resuspended in 1 mL wash buffer. All fractions were prepared for SDS-PAGE analysis and stored at -20ºC until further use.

2.4.2. Large scale expression

To 250 mL of Luria broth containing 50 $\mu g.mL^{-1}$ kanamycin or ampicillin, 2.5 mL of the relevant overnight culture was added (1 in 100 inoculum) and incubated at 37ºC with continuous agitation until the OD_{600nm} value fell between 0.5 - 0.9. Protein expression was typically induced by adding 1mM IPTG to the expression culture and conducted for 3 hours at 37ºC. The bacterial cells were collected by centrifugation at 5 000 *g* for 10 minutes and the pellet was washed in 20 mL of Ni-NTA equilibration buffer (50 mM Tris-HCl, 20 mM Imidazole, pH 8.0) or glutathione equilibration buffer (1x PBS containing 1 mM PMSF) for His-tagged and GST-tagged fusion proteins respectively. The resuspended pellet was centrifuged again at 5 000 *g* for 10 minutes, the supernatant discarded, and the pellet stored at -80 ºC overnight.

2.4.3. Cell lysis

Cell lysis was conducted on ice using ice-cold buffers. The frozen pellet of the large-scale expression culture was thawed on ice for 30 minutes, before being resuspended in 10 mL Ni-NTA equilibration or glutathione equilibration buffer. The cells were lysed in 2 mg. mL^{-1} lysozyme in equilibration buffer for 30 minutes on ice, and by 2 cycles of sonication at 60Hz for 1 minute each with 1-minute resting periods on ice. The cell lysate was centrifuged at 14 000 *g* for 30 minutes to separate the insoluble and soluble fractions.

2.4.4. Preparation of Ni-NTA and glutathione agarose columns

Ni-NTA fast start kit (Qiagen) columns were stored at 4 ºC in storage solution (50% ethanol in water). The column was washed in one volume water and was conditioned in two volumes of Ni-NTA equilibration buffer before purification. After purification the Ni-NTA column was washed twice in water and stored in storage solution at 4ºC until further use. To prepare glutathione agarose gel, 70 mg of lyophilised glutathione agarose powder (Sigma-Aldrich) was hydrated in 14 mL water overnight at 4ºC. The beads were washed in 10 volumes of water and stored in glutathione storage buffer (2 M NaCl, 1 mM sodium azide in water) at 4ºC until further use. Before purification the column was washed in one volume of water and equilibrated in two volumes of glutathione equilibration buffer. After purification the column was washed in two volumes of water, one volume of glutathione cleansing

buffer 1 (0.1 M borate, 0.5 M NaCl in water, pH 8.5 using NaOH), one volume of water, one volume of glutathione cleansing buffer 2 (0.1 M acetate, 0.5 M NaCl in water, pH 4.5 using acetic acid), one volume of water and stored in glutathione storage solution at 4°C until further use.

2.4.5. Protein purification by Ni-NTA affinity chromatography

The soluble fraction was filtered through a 0.45 µm filter and again through a 0.2 µm filter. A 60 µL sample of the filtered lysate was collected and stored on ice. The filtered lysate was applied to the equilibrated Ni-NTA column. A 60 µL sample of the flow-through was collected and stored on ice for subsequence SDS-PAGE analysis. The column was washed twice in 5 mL Ni-NTA equilibration buffer. A 60 µL sample of the flow-through from each wash was collected and stored on ice. Bound proteins were eluted into 3 mL Ni-NTA elution buffer (50 mM Tris-HCl, 500 mM imidazole, pH 8.0). A 60 µL sample of the eluate was collected and stored on ice. The eluate was stored on ice until desalting.

2.4.6. Protein purification by glutathione affinity chromatography

The soluble fraction was filtered through a 0.45 µm filter and again through a 0.2 µm filter. A 60 µL sample of the filtered lysate was collected and stored on ice for subsequent SDS-PAGE analysis. The filtered lysate was applied to the equilibrated glutathione agarose column. A 60 µL sample of the flow-through was collected and stored on ice. The column was washed twice in 5 mL glutathione equilibration buffer. A 60 µL sample of the flow-through from each wash was collected and stored on ice. Bound proteins were eluted into 3 mL glutathione elution buffer (10 mM reduced glutathione, 50 mM Tris-HCl, pH 9.5). A 60 µL sample of the eluate was collected and stored on ice. The eluate was stored on ice until desalting.

2.4.7. Desalting and protein storage

A PD-10, Sephadex™ G-25 M desalting column (GE Healthcare), was equilibrated with 5 volumes assay buffer (25 mM HEPES, 150 mM KCl, 1 mM $MgCl_2$, 1 mM DTT, pH 7.4). The eluate was applied to the desalting column and allowed to penetrate the resin. Purified proteins were desalted into 3.5 mL assay buffer. A 60 µL sample of the desalted purified protein was collected and stored on ice for SDS-PAGE analysis. Purified, desalted proteins were stored in 40% (v/v) glycerol at -20°C.

2.4.8. Protein concentration

Desalted proteins were concentrated using a Centrisart I column (Sigma-Aldrich). The desalted fraction was added to the column, incubated on ice for 5 minutes and centrifuged at 2500 *g* for 40 minutes at 4°C using a Megafuge 1.0R (Heraeus) benchtop centrifuge. 60 µL sample of the concentrated protein fraction was collected and stored on ice for SDS-PAGE and Bradford assay analysis.

2.4.9. Bradford assay

The concentration of the desalted purified protein was determined alongside a BSA protein standard curve. A two-fold dilution series ranging from 0.075 – 1.25 $mg.mL^{-1}$ BSA in assay buffer was prepared and stored at -20°C until use. To 5 µL of assay buffer, BSA protein standards and desalted purified protein, 250 µL Bradford reagent (Sigma-Aldrich) equilibrated to room temperature was added in a 96-well plate and incubated at room temperature for 5 minutes. The absorbance at 595 nm was determined for each sample in a Spectramax plate reader. A BSA standard curve with an R^2 value ≥ 0.99 was used to extrapolate the concentration of the desalted purified proteins.

2.5. SDS-PAGE and Western blotting

2.5.1. SDS-PAGE

To 60 µL of the sample to be analysed, 20 µL of 4X SDS sample loading buffer (0.25 M Tris, pH 6.8, 4.2% (w/v) SDS, 40% (v/v) glycerol, 4% (v/v) β-mercaptoethanol, 1% (w/v) bromophenol blue in water) was added and boiled for 5 minutes at 95 °C. The samples were loaded in the wells of a 4% (w/v) acrylamide stacking gel (0.125 M Tris, pH 6.8, 0.1% (w/v) SDS, 4% (w/v) acrylamide, 0.1% (w/v) *bis*-acrylamide, 0.05% (w/v) ammonium persulfate, 0.0012% (v/v) TEMED in water). Typically, proteins were resolved through a 12% (w/v) acrylamide resolving gel (0.38 M Tris, pH 8.8, 0.1% (w/v) SDS, 12% (w/v) acrylamide, 0.27% (w/v) *bis*-acrylamide, 0.0035% (w/v) ammonium persulfate, 0.0007% (v/v) TEMED in water) alongside a colour protein standard broad range molecular weight marker (New England Biolabs). Gels ran for 90 minutes at 120V in 1X SDS running buffer (25 mM Tris, 192 mM Glycine, 0.1% (w/v) SDS in water) (Laemmli, 1970). Gels were stained in Coomassie stain (0.25% (w/v) Coomassie blue R-250, 45 % (v/v) methanol, 10% (v/v) acetic acid in water) for 1 hour at 37 °C with agitation. Stained gels were destained in destain solution (40% (v/v) methanol, 10% (v/v/) acetic acid in water) until bands were visible. Gels were photographed using a Chemidoc XRS+ gel documentation system and software (Bio-Rad).

2.5.2. Western blotting

Proteins resolved on a polyacrylamide gel were transferred onto an Amersham Hybond™ ECL nitrocellulose blotting membrane at 90V for 1 hour at 4°C while submerged in transblot buffer (25 mM Tris, 192 mM Glycine, 20% (v/v) methanol in water). The membrane was washed in water, stained for 5 minutes with Ponceau S stain (0.1% (w/v) Ponceau S, 1% (w/v) glacial acetic acid in water) and rinsed in Ponceau S destain (1% (v/v) glacial acetic acid in water) until clear.

2.5.3. Detection of GFP-tagged proteins

Tris-buffer saline was prepared with 40 mM Tris, 150 mM NaCl in water and the pH was adjusted to 7.4 (TBS). The blot was blocked for 40 minutes in incubation buffer (0.1% (v/v) Tween 20, 1% (w/v) BSA, 2% (w/v) milk powder in TBS) at ambient temperature, incubated with 1 μg/mL B-2 mouse monoclonal anti-GFP primary antibodies (Santa Cruz Biotechnology) in incubation buffer overnight at 4°C, then washed in wash buffer (0.1% (v/v) Tween 20 in TBS). The membrane was incubated with a 1:5000 dilution of horseradish peroxidase-conjugated goat anti-mouse secondary antibody (SeraCare) in incubation buffer for 1 hour, washed in three volumes of wash buffer, covered in TMB membrane peroxidase substrate (SeraCare) and rinsed in water after bands became visible on the blot.

2.5.4. Detection of His-tagged proteins

The blot was blocked in 20 mL incubation buffer (0.1% (v/v) Tween-20, 1% (w/v) BSA, 10 mM imidazole in TBS) overnight at 4°C. The blot was probed with a 1:5000 dilution of HisDetector Nickel-HRP (SeraCare) for 1 hour at ambient temperature. The blot was washed in three volumes of wash buffer (0.1% (v/v) Tween-20, 10 mM imidazole in TBS), covered in TMB membrane peroxidase substrate (SeraCare) and rinsed in water after bands became visible on the blot.

2.5.5. Detection of GST-tagged proteins

The blot was blocked for 40 minutes in incubation buffer (0.1% (v/v) Tween 20, 1% (w/v) BSA, 10 mM reduced glutathione in TBS) at ambient temperature. The blot was probed with a 1:1000 dilution of rabbit anti-GST primary antibodies (Sigma-Aldrich) in incubation buffer overnight at 4°C, washed in three volumes of wash buffer (0.1% (v/v) Tween 20, 10 mM reduced glutathione in TBS) and incubated in 1:5000 dilution anti-rabbit HRP conjugated secondary antibodies (SeraCare) for 1 hour at ambient temperature. The blot was washed in three volumes of wash buffer, covered in TMB membrane peroxidase substrate (SeraCare) and rinsed in water after the bands became visible on the blot.

2.6. Nucleotide exchange and intrinsic tryptophan fluorescence

Nucleotide exchange was conducted by incubating 1 μM $^{N\Delta13}$*Hs*Arf6, 50 μM GDP or GTP, 5 mM EDTA in assay buffer at 37°C for 60 minutes with gentle agitation. $^{N\Delta13}$*Hs*Arf6-GDP and $^{N\Delta13}$*Hs*Arf6-GTP complexes were stabilised by adding 20 mM $MgCl_2$ and incubating for 5 minutes with gentle agitation at ambient temperature. Nucleotide exchange for $^{N\Delta17}$*Hs*Arf1 was conducted by incubating 1 μM $^{N\Delta17}$*Hs*Arf1, 50 μM GDP or GTP and 2 mM EDTA at 25°C for 60 minutes with gentle agitation. $^{N\Delta17}$*Hs*Arf1-GDP and $^{N\Delta17}$*Hs*Arf1-GTP complexes were stabilised by adding 3 mM $MgCl_2$ and incubating for 5 minutes with gentle agitation at ambient temperature. Intrinsic tryptophan fluorescence was measured as a continuous reading at ambient temperature or an end-point reading at an excitation

wavelength of 298 nm and an emission wavelength of 340 nm in a SpectraMax® M3 (Molecular Devices) plate reader. Each biological replicate was conducted in technical triplicate.

2.7. Immobilised interaction assays

2.7.1. Ni-NTA immobilised Arf6-GGA GST interaction assay

To pre-blocked Ni-NTA HisSorb plates (Qiagen, Germany), 50 µL of 1 µM Arf GTPase pre-loaded with GDP or GTP (human Arf1, human Arf6, malarial Arf1 or malarial Arf6) was immobilised by continuous agitation for 30 minutes at 4°C. GST-GGA^{GAT} was added to a final concentration of 1 µM in a total volume of 100 µL and incubated for a further 90 minutes at 4°C with constant agitation. The proteins were removed, and the wells washed in two volumes (100 µL each) of wash buffer (0.1% (v/v) Tween-20 in assay buffer). The wells were subsequently washed in four volumes (100 µL each) of assay buffer and incubated in 200 µL GST substrate master mix (2 mM reduced L-glutathione, 1 mM 2,4-Dinitrochlorobenzene (CDNB) in 1X PBS) equilibrated to 25°C for 30 minutes. The absorbance at 340 nm was measured in a SpectraMax® M3 (Molecular Devices) plate reader. Each biological replicate was conducted in technical triplicate. The Ni-NTA immobilised Arf6-JIP4 GST interaction assay was conducted similarly by replacing GST-GGA^{GAT} with GST-JIP4^{LZII}.

2.7.2. Glutathione immobilised JIP4-Arf6 interaction assay

In round-bottom plates 1 µM GST-JIP4^{LZII} was incubated with 1 µM Arf GTPase pre-loaded with GDP or GTP (human Arf1, human Arf6, malarial Arf1 or malarial Arf6) in assay buffer in a total volume of 100 µL for 60 minutes with continuous agitation at ambient temperature. Concurrently, pre-blocked glutathione coated plates (Thermo Scientific) were washed in three volumes (100 µL each) of assay buffer containing 0.05% (v/v) Tween-20. Thereafter the protein mixtures were immobilised to the glutathione coated plate by transferring the reaction mixtures from the round-bottom plate and incubating with continuous agitation for 60 minutes at ambient temperature. The plate was washed in three volumes (100 µL each) of assay buffer containing 0.05% (v/v) Tween-20 and then incubated for 1 hour at ambient temperature with constant agitation in assay buffer containing 0.05% (v/v) Tween 20, 1% BSA (w/v) and HisDetector Nickel-HRP (Sera Care) diluted 1: 10 000. The plates were washed in three final volumes (100 µL each) of wash before and subsequently incubated in 100 µL SureBlue Reserve (Sera Care) for 30 minutes at 25°C. The absorbance at 340 nm was measured in a SpectraMax® M3 (Molecular Devices) plate reader. Each biological replicate was conducted in technical triplicate.

2.8. GEF-mediated GDP/GTP exchange assays

In round-bottom plates 1 µM Arf GTPase pre-loaded with GDP (human Arf1, human Arf6, malarial Arf1 or malarial Arf6) was incubated with 0.20 µM ARNO^{Sec7} and 50 µM GTP in assay buffer in a total

volume of 50 µL at 37ºC for 30 minutes with continuous agitation. The reactions were subsequently transferred to a nickel-coated plate and the Ni-NTA immobilised Arf6-GGA GST interaction assay (section 2.7.1) was employed to determine the activation status of the ArfGTPases following the GEF activation assay.

2.9. GAP-mediated GTP hydrolysis assays

In round-bottom plates 1 µM Arf GTPase pre-loaded with GTP (human Arf1, human Arf6, malarial Arf1 or malarial Arf6) was incubated with 0.15 or 0.20 µM ArfGAP (GAP domains for human Arf, or the putative malarial ArfGAPs) in assay buffer in a total volume of 50 µL at 37ºC for 30 minutes with continuous agitation. The reactions were subsequently transferred to a nickel-coated plate and the Ni-NTA immobilised Arf6-GGA GST interaction assay (section 2.7.1) was employed to determine the activation status of the ArfGTPases following the GAP deactivation assay.

2.10. Statistical analyses

Where appropriate, comparisons between datasets were made using unpaired t-tests to calculate P-values using the online, GraphPad *t-test* calculator. P-values below 0.05 were regarded as indicating significant differences between compared mean values.

Chapter 3: Functional exploration of a putative malarial ADP-ribosylation factor 6 by expression in HeLa cells.

3.1. Introduction

An ongoing interest of the research group is to explore the molecular mechanism of protein secretion and endocytosis in *Plasmodium falciparum* by characterizing malarial parasite homologues of proteins known to be involved in these processes in other cell types (Arf1 and Arf6 respectively). The predicted *P. falciparum* Arf1 (*Pf*Arf1) homolog displays high sequence similarity to the human Arf1 (with a sequence identity of 76%, and sequence similarity of 89%), while the predicted *P. falciparum* Arf6 (*Pf*Arf6) homolog displays a sequence identity of 48%, and sequence similarity of 70%. The principal approach in assessing the function of these proteins was to create transgenic parasites expressing GFP-tagged versions of the putative Arf GTPases and determining their sub-cellular localization in the parasite by epifluorescence and confocal microscopy. Localisation studies of the putative *Pf*Arf1 and *Pf*Arf6 as GFP tagged constructs in malarial parasites revealed that *Pf*Arf1-GFP localised to a structure reminiscent of the Golgi apparatus – a single punctate locus in trophozoites which multiplies during the schizont stage as the nucleus and parasite divides and dissipates upon treatment with the Arf1 inhibitors Brefeldin A (BFA) and Golgicide (T. Swart, manuscript in preparation). *Pf*Arf6-GFP, by contrast, localised to numerous puncta along the periphery of the parasite in the mature trophozoite life stage - which may be hypothesized to demarcate sites where endocytosis is being initiated - in addition to a more central intensely fluorescent single ring-like locus which was insensitive to the Golgi disruptors BFA and Golgicide. In the multinucleate schizont phase, the peripheral puncta disappeared, and the single central locus remained as a ring-like structure. The localisation of *Pf*Arf6 under the treatment of mefloquine, a drug known to affect malarial endocytosis, was disrupted into a cytoplasmic pool, suggesting a possible role in endocytosis. (T.Swart, M.Sc. dissertation). Co-transfection of the malarial Arf1 with a Golgi marker in malarial parasites would aid in the identification of the hypothesized Golgi-like structure. In principle, the same approach may be used to define *Pf*Arf6 localisation in parasites. The expression of recombinant proteins in *P. falciparum* is a significantly lengthy and demanding procedure due to the low transfection efficiencies displayed by the malarial parasite (Hasenkamp et al., 2012). As indicated above, validation of a localisation pattern observed for putative proteins requires a second transfection with an established organelle marker. The obstacles encountered by the current transfection methods is significantly compounded by the requirement of co-transfection. In the case of *Pf*Arf6, the problem of definitively identifying the localisation of the protein in parasites is further compounded by the relative shortage of well described and validated parasite organelle markers. For example, definitive markers of endocytic sites are not available, and the central ring-like structure demarcated by *Pf*Arf6-GFP does not resemble known endocytic organelles. In an attempt to circumvent

these difficult methods a supporting approach was developed. The strategy was to express GFP-tagged malarial Arf GTPases (codon-optimized for mammalian expression) in mammalian cells and determine their localization and effects on the cells – a method that we termed the HeLa cell surrogate model (HCSM). T. Swart expressed *Pf*Arf1-GFP and characterised the localisation pattern observed in HeLa cells by co-transfection with a Golgi apparatus (Golgi) marker. Experimentally this was a simple procedure because HeLa cells have very high transfection efficiencies and transient expression experiments suffice (as opposed to the need to prepare stably transfected cell lines, as is required in *P. falciparum* transfection experiments). *Pf*Arf1-GFP strictly localised to the Golgi in HeLa cells, thus faithfully recapitulating its parasite function. It further suggests that *Pf*Arf1 is able to interact with the human Arf1 regulatory proteins in HeLa cells, which is likely a reflection of its high sequence homology to its human counterpart. The question arose whether the HCSM could be employed to infer the parasite function of *Pf*Arf6. The work presented in this chapter employs the HeLa cell surrogate model to determine possible functions of the putative *Pf*Arf6 through the use of co-transfection and fluorescence microscopy.

3.2. Aims and objectives

Aim of the study: Use HeLa cells as a model for malarial parasites to conduct co-localisation studies with the putative malarial Arf6.

Specific questions/objectives and experimental approaches:

1. Is the putative malarial Arf6 homolog (*Pf*Arf6) capable of expression in HeLa cells?
   The expression of the *Pf*Arf6-GFP fusion protein in HeLa cells was determined by Western blot analysis.
2. What is the localisation pattern of *Pf*Arf6 in HeLa cells and to which structures does it localise?
   The localisation pattern of *Pf*Arf6-GFP in HeLa cells was determined by epifluorescence and/or confocal microscopy. To explore the possible functions of *Pf*Arf6 in HeLa cells, co-localisation studies were conducted by co-transfecting *Pf*Arf6-GFP and markers for Arf6-dependent endocytosis, clathrin-dependent endocytosis, fluid-phase endocytosis and autophagocytosis (known cellular functions of Arf6 in other cell types).
3. Is the observed localisation pattern of *Pf*Arf6 related to the cancerous phenotype of HeLa cells?
   The localisation pattern of *Pf*Arf6-GFP in a non-cancerous cell line (HEK293 cells) was observed by epifluorescence and/or confocal microscopy.

3.3. Results

***Pf*Arf6-GFP is capable of expression in HeLa and HEK293 cells.** The coding sequence for the putative malarial Arf6 (*Pf*Arf6) was codon-optimized for mammalian expression and sub-cloned into the mammalian expression vector pEGFP such that the GFP tag was fused to the C-terminus of *Pf*Arf6. To assess whether *Pf*Arf6-GFP was capable of expression in HeLa cells, HeLa cells were transfected with the pEGFP-N1-*Pf*Arf6 construct or the pEGFP-N1 control construct. Transfected cells were lysed in sample buffer, the proteins resolved on an SDS polyacrylamide gel and then transferred to a nitrocellulose membrane. GFP-tagged proteins were probed for using polyclonal mouse anti-GFP primary antibodies and goat anti-mouse secondary antibodies conjugated to horseradish peroxidase (HRP). GFP-positive bands were visualised using TMB membrane peroxidase substrate. The pEGFP-N1 transfected cells contained a single GFP-positive band at approximately 26 kDa, while the pEGFP-N1-*Pf*Arf6 transfected cells produced two GFP-positive bands at approximately 47 kDa and 38 kDa (**Figure 3A**). This result indicated that the *Pf*Arf6-GFP recombinant protein, which has a predicted size of 46 kDa, was expressed in HeLa cells. The detection of the C-terminally fused GFP tag suggests that the fusion protein was translated to fruition. Therefore, the lower molecular weight 38 kDa band likely represents a version of the protein shortened at the N-terminus. This could be the result of proteolytic cleavage in the intact transfected HeLa cells, or possibly degradation by released proteases in the lysate.

To determine whether *Pf*Arf6-GFP displayed a distinct localisation pattern, transfected HeLa cells were observed by epifluorescence microscopy. To investigate whether the *Pf*Arf6-GFP fusion protein was producing a localisation pattern that was directed by *Pf*Arf6 function, transfections with the pEGFP-N1 plasmid lacking the *Pf*Arf6 gene were conducted as a negative control. GFP was observed throughout the nucleus and cytoplasm (**Figure 3B**), whereas the *Pf*Arf6-GFP fusion protein displayed a unique localisation pattern. The change in localisation patterns observed when the *Pf*Arf6 coding sequence was introduced to the plasmid suggests that the localisation pattern observed for *Pf*Arf6-GFP was directed by the function of *Pf*Arf6. Two distinct morphologies were observed – *Pf*Arf6-GFP localised either to punctate structures or to ring-like structures with a distinct lumen. In terms of cellular distribution, the punctate and ring-like *Pf*Arf6-GFP structures were consistently observed dispersed in the cell cytoplasm (**Figure 3C**).

An additional consideration in the interrogation of expression of *Pf*Arf6-GFP in HeLa cells was the fact that cancerous cells often exhibit considerably different cellular biology to non-cancerous mammalian cells (Hanahan et al., 2000). To investigate whether the punctate and ring-like structures to which *Pf*Arf6-GFP localised were related to a cellular process that is specific to the cancerous phenotype, expression of *Pf*Arf6-GFP in a non-cancerous mammalian cell type, human embryonic kidney (HEK) cells, was conducted. *Pf*Arf6-GFP was capable of expression in HEK cells (**Figure 3A**). Localisation of GFP and *Pf*Arf6-GFP in HEK cells was similar to the findings in HeLa cells. GFP was observed in

the nucleus and cytoplasm (**Figure 3B**), while *Pf*Arf6-GFP reproduced punctate and ring-like structures in HEK cells **(Figure 3C**). This suggested that the localisation of *Pf*Arf6-GFP was not specific to the cancerous phenotype.

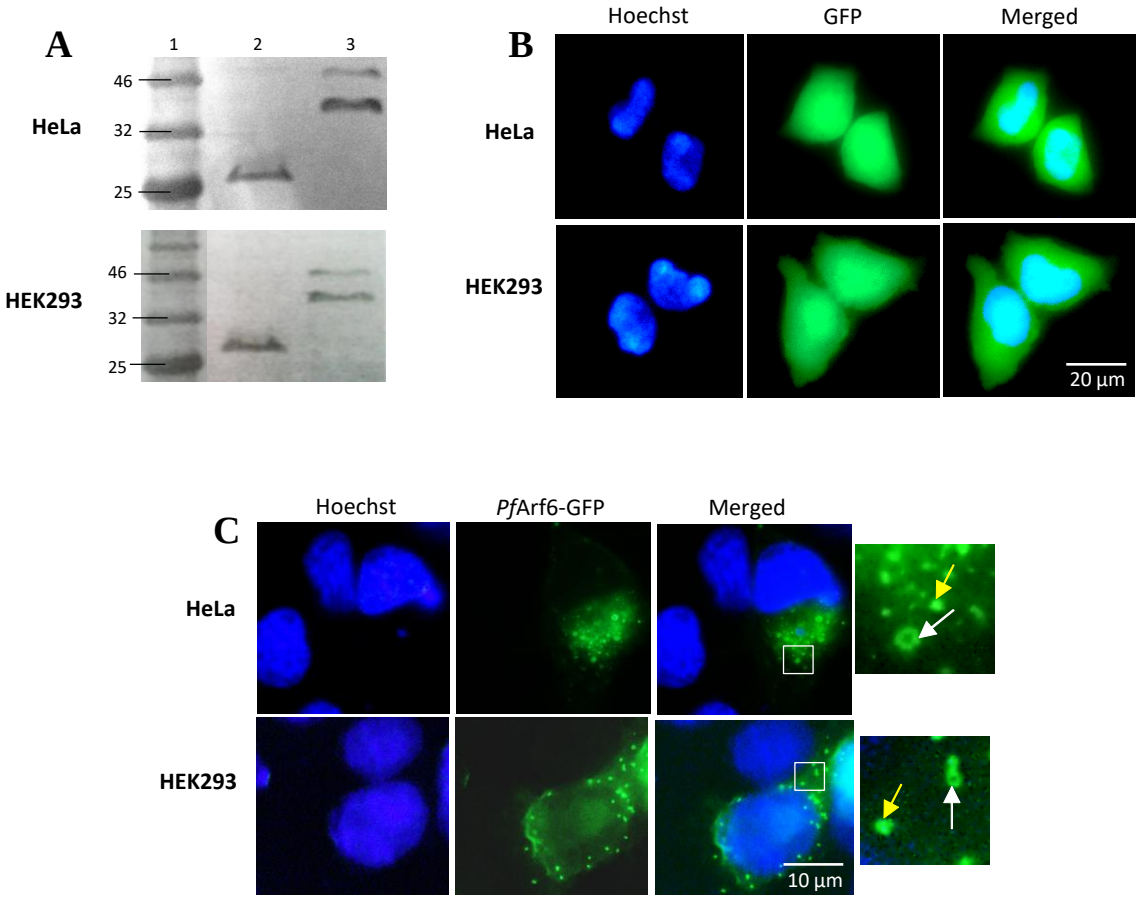

Figure 3: Expression of *Pf*Arf6-GFP fusion protein in HeLa and HEK293 cells. **A:** Western blot analysis of HeLa and HEK293 cell lysates from cells expressing GFP or *Pf*Arf6-GFP. Polyclonal mouse anti-GFP primary and goat anti-mouse secondary antibodies conjugated to HRP were used for immunodetection. Lane 1: New England BioLabs colour protein standard broad range molecular weight marker with bands sized in kilodaltons (kDa). Lane 2: Cells expressing GFP. Lane 3: Cells expressing *Pf*Arf6-GFP. **B**: HeLa and HEK293 cells expressing GFP as a negative control were viewed live on a Zeiss AxioVert.A1 FL-LED inverted microscope with a 40X objective. **C**: HeLa and HEK293 cells expressing *Pf*Arf6-GFP were fixed with paraformaldehyde and viewed on an Olympus BX61 upright fluorescent microscope with a 100X objective and immersion oil. Nuclei were visualised by staining with Hoechst 33342. *Pf*Arf6-GFP localised to punctate structures (*yellow arrow in inset*) and ring-like structures with a distinct lumen (*white arrow in inset*) in the cell cytoplasm.

***Pf*Arf6-GFP partially co-localises with markers for Arf6-dependent endocytosis, but not clathrin-dependent or fluid-phase endocytosis.** To investigate the possible function demonstrated by *Pf*Arf6 in HeLa cells by defining its localization, *Pf*Arf6-GFP structures were interrogated as endocytic vesicles that form part of the Arf6-associated endocytic pathway (Mayor et al., 2014). As such, human Arf6 was used to track plasma membrane invaginations and endocytic vesicles associated with *Hs*Arf6. Human Arf6 fused to mCherry (hArf6(WT)-mCherry) was used as the marker protein. HeLa cells were co-transfected with pEGFP-N1-*Pf*Arf6 and hArf6(WT)-mCherry, fixed with paraformaldehyde, stained with Hoechst and visualised by epifluorescence microscopy. Representative images of the co-localisation studies demonstrated that human Arf6 partially co-localised with *Pf*Arf6-GFP punctate structures (**Figure 4A** *yellow arrow*). This result suggested that *Pf*Arf6-GFP may be associated with Arf6-dependent endocytosis in HeLa cells.

To support or refute this notion, the structures were subsequently interrogated as early endocytic invaginations that form part of the clathrin-dependent endocytic pathway. Clathrin light chain (CLC) is a protein subunit that forms part of the clathrin triskelion and was used as a marker protein (Legendre-Guillemin et al., 2002). CLC derived from mice fused to mRFP was co-transfected with pEGFP-N1-*Pf*Arf6 in HeLa cells. The cells were subsequently fixed with paraformaldehyde, stained with Hoechst and visualised by epifluorescence microscopy. Clathrin coated vesicles (CLC-mRFP) occurred at the cell periphery, with a separate population adjacent to the nucleus (**Figure 4B** *first panel*). These results are consistent with the known function of clathrin – namely in coating endocytic invaginations at the plasma membrane and vesicles budding from the *trans*-Golgi network (TGN). The population at the cell periphery, presumably those involved in the formation of early endocytic invaginations (**Figure 4B** *red arrow*), was distinct from *Pf*Arf6-GFP puncta (**Figure 4B** *green arrow*). While there were distinct *Pf*Arf6-GFP puncta in the area adjacent to the nucleus (**Figure 4B** *second panel*) this region also contained an extensive concentration of CLC and likely represented vesicles budding from the TGN. This result suggested that *Pf*Arf6-GFP did not co-localise to clathrin-coated endocytic vesicles and supported the partial localisation of *Pf*Arf6-GFP with the clathrin-independent, Arf6-associated endocytic pathway.

As a final possible endocytic uptake route, fluid-phase endocytosis was investigated. To achieve this, a novel method was developed. Haemoglobin is sufficiently large that it would be internalized by endocytosis (as opposed to transport across the lipid membrane) in a non-specific manner (since mammalian cells do not have haemoglobin-specific transmembrane receptors) and thus would be trafficked through all the organelles of the fluid-phase endocytic pathway before digestion in lysosomes (Kou et al., 2013; Rejman et al., 2004). It thus acts as a fluid-phase marker of organelles along the endocytic pathway. HeLa cells expressing *Pf*Arf6-GFP were incubated with a solution containing free haemoglobin. After the incubation, the cells were fixed and haemoglobin containing structures were

detected with anti-haemoglobin rabbit and anti-rabbit TRITC conjugated antibodies (**Figure 4C** *left panel*). The haemoglobin-positive puncta in the cells were absent in cells that were not incubated with haemoglobin (**Figure S36A**). Haemoglobin-containing puncta were also not detected in immunofluorescence controls where primary antibodies were omitted (**Figure S36B**). The haemoglobin positive structures (*red arrow*) did not co-localise with *Pf*Arf6-GFP puncta (**Figure 4C** *green arrow*) suggesting that *Pf*Arf6-GFP did not localise to organelles that form part of the fluid-phase endocytic pathway in HeLa cells.

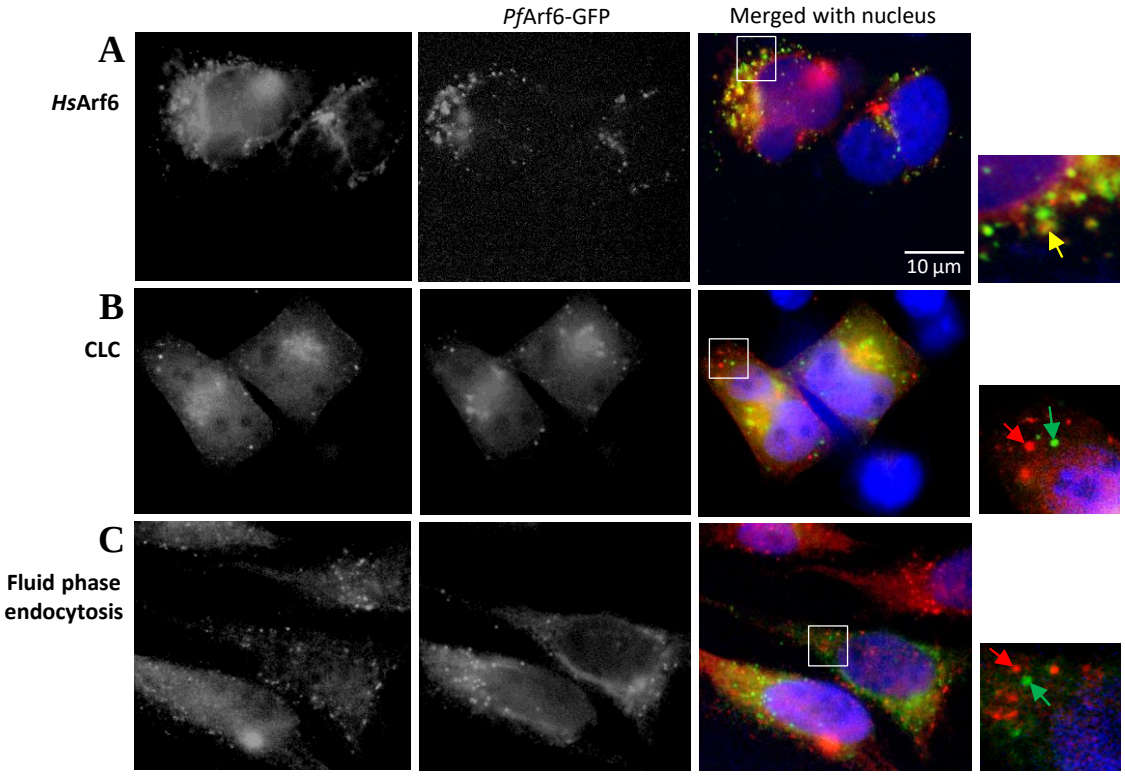

Figure 4: Co-localisation studies of *Pf*Arf6-GFP with marker proteins for different endocytic pathways. **A**: *Pf*Arf6-GFP partially co-localises with human Arf6, a marker protein for Arf6-assoicated endocytic vesicles in HeLa cells (*yellow arrow*). **B**: *Pf*Arf6-GFP (*green arrow*) and clathrin light chain (CLC) (*red arrow*) a marker protein for clathrin-associated early endocytic vesicles do not co-localise at the cell periphery in HeLa cells. **C**: HeLa cells transfected with pEGFP-N1-*Pf*Arf6 incubated in a solution containing free haemoglobin. Endocytosed haemoglobin was detected with anti-haemoglobin rabbit polyclonal primary and anti-rabbit TRITC conjugated secondary antibodies. Nuclei were visualised by staining with Hoechst 33342 and cells were viewed on an Olympus BX61 upright fluorescent microscope with a 100X objective and immersion oil. *Pf*Arf6-GFP (*green arrow*) does not co-localise with haemoglobin internalized by fluid-phase endocytosis (*red arrows*) in HeLa cells.

***Pf*Arf6-GFP partially co-localises with autophagosomes in HeLa cells.** To investigate whether *Pf*Arf6-GFP structures represent autophagosomes, microtubule-associated protein 1A/1B-light chain 3 (LC3) was used as a marker protein to track autophagosomes. LC3 is abundant in the nucleus even though it functions primarily in autophagosomes present in the cytoplasm. During nutrient-rich conditions, LC3 is distributed in both the nucleus and the cytoplasm (incorporated into autophagosomes). Nutrient deprivation triggers autophagy and promotes the redistribution of LC3 from the nucleus to the cytoplasm where it subsequently associates with autophagosomes. Nutrient starvation thus increases the number of LC3-positive autophagic structures observed in the cytoplasm (Huang & Liu, 2015). To investigate co-localisation between *Pf*Arf6-GFP and the LC3 marker protein used to track autophagosomes, it was crucial to also study possible co-localisation under conditions where autophagy was induced. Therefore, the objective was to express *Pf*Arf6-GFP in HeLa cells with enhanced levels of autophagy. Nutrient deprivation and treatment with an autophagy inducer such as rapamycin should produce the desired effect of enhanced autophagy (Asano et al., 2014; Parker et al., 2016). An additional option was to treat HeLa cells expressing *Pf*Arf6-GFP with chloroquine, a drug that blocks the fusion of autophagosomes to lysosomes, resulting in an accumulation of autophagosomes (Sigismund et al., 2008). To establish a method for inducing autophagy, HeLa cells expressing LC3-pmRFP were deprived of nutrients, treated with rapamycin or treated with chloroquine. The cells were subsequently fixed with paraformaldehyde, stained with Hoechst and analysed by epifluorescence microscopy. Attempts to promote autophagy by nutrient deprivation (incubation in Hank's balanced salt solution - a solution made up to physiological pH and isotonic salt concentration lacking nutrients) and treatment with the autophagy inducer rapamycin were not successful. No clear differences in LC3 distribution were observed (*results not shown*). However, chloroquine treatment clearly redistributed nuclear LC3-pmRFP to the cytoplasm where it incorporated to distinct autophagosomes (**Figure 5A** *bottom panel*). Chloroquine stock solutions were prepared in water; therefore a vehicle control was omitted. In untreated cells LC3-pmRFP localised to both the nucleus and the cytoplasm (**Figure 5A** *top panel*). In cells treated with chloroquine LC3-pmRFP was observed exclusively in the cytoplasm (**Figure 5A** *bottom panel*). Therefore, to investigate the possible function of *Pf*Arf6 in autophagocytosis, HeLa cells were co-transfected with *Pf*Arf6-GFP with LC3-pmRFP under routine culture conditions (untreated) or under chloroquine treatment. The cells were subsequently fixed with paraformaldehyde, stained with Hoechst and analysed by epifluorescence microscopy. In untreated cells, a pool of LC3-pmRFP was present in the nucleus, as well as in a few distinct LC3-pmRFP positive autophagosomes in the cytoplasm (**Figure 5B** *top panel*). In chloroquine treated cells LC3-pmRFP redistributed to the cytoplasm and was associated with an increased amount of autophagosomes (**Figure 5B** *bottom panel*). While *Pf*Arf6-GFP partially co-localises with LC3-pmRFP under untreated conditions (**Figure 5B** *top panel, yellow arrow*), an apparent increase in co-localisation was observed under chloroquine treatment (**Figure 5B** *top panel, yellow arrow*). Taken together, the results suggested that *Pf*Arf6-GFP participates in autophagy in HeLa cells.

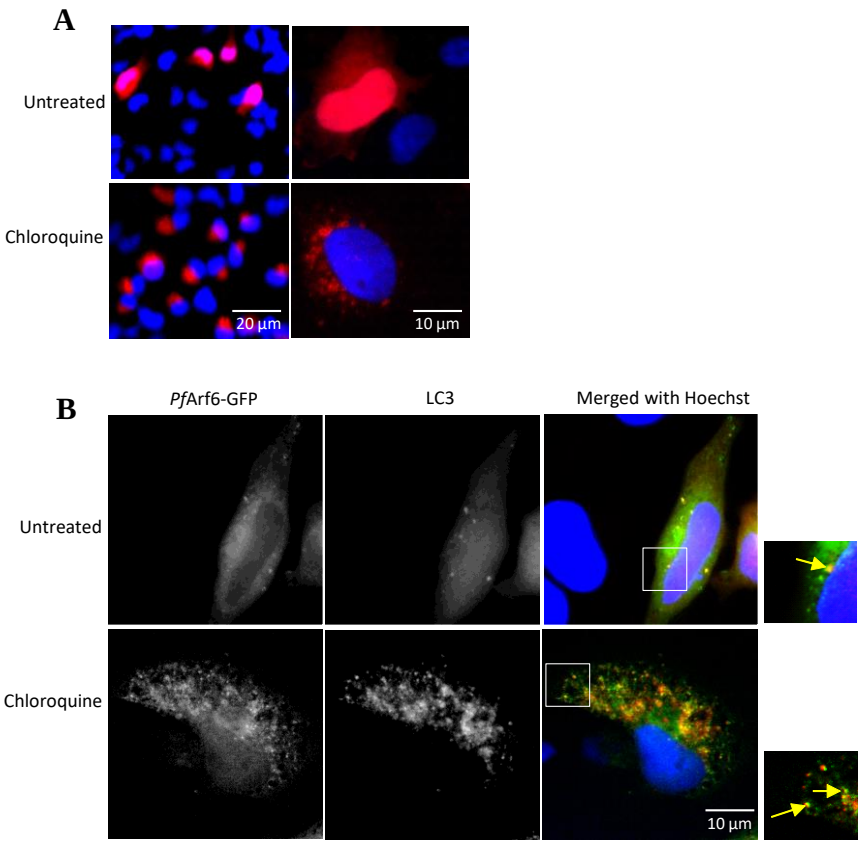

Figure 5: Co-localisation studies of *Pf*Arf6-GFP with an autophagosome marker protein. **A**: Microtubule-associated protein 1A/1B-light chain 3 (LC3) fused to pmRFP (LC3-pmRFP) was used as a marker protein for autophagosomes. *Top panel*: Untreated HeLa cells expressing LC3-pmRFP. *Bottom panel*: HeLa cells expressing LC3-pmRFP treated for 24 hours with 100 µM chloroquine. *Left panel*: HeLa cells viewed with a 40X objective. *Right panel*: HeLa cells viewed with a 100X objective. **B**: *Top panel*: Untreated HeLa cells co-expressing LC3-pmRFP and *Pf*Arf6-GFP. *Pf*Arf6-GFP punctate structures partially co-localised with LC3-pmRFP in the cytoplasm (*yellow arrow*). *Bottom panel*: HeLa cells co-expressing LC3-pmRFP and *Pf*Arf6-GFP treated for 24 hours with 100 µM chloroquine. An apparent increase in the co-localisation between LC3-pmRFP and *Pf*Arf6-GFP puncta was observed (*yellow arrows*). HeLa cells were fixed with paraformaldehyde, stained with Hoechst 33342 and viewed on an Olympus BX61 upright fluorescent microscope with a 40X of 100X objective and immersion oil.

An increase in *Pf*Arf6-GFP structures was observed when constitutively active and inactive *Pf*Arf6-GFP mutants were expressed in HeLa cells. Although *Pf*Arf6-GFP punctate structures co-localised with marker proteins for Arf6-associated endocytosis and autophagocytosis, co-localisation of *Pf*Arf6-GFP ring-like structures with markers for clathrin-dependent endocytosis (CDE), Arf6-associated endocytosis, fluid-phase endocytosis or autophagocytosis was not observed. Since these structures had not been identified with any of the markers associated with functions of Arf6 in other cell types, it raised the possibility that the ring-like structures may be artefactual, *i.e.* structures that are not normally present in HeLa cells but induced by the over-expression of *Pf*Arf6-GFP in the cells. One possibility is that the *Pf*Arf6-GFP ring-like structures represented aggregates of *Pf*Arf6-GFP. An alternative possibility was that the structures were induced by overactivation of *Pf*Arf6-GFP, *i.e.* the presence of an abnormally high preponderance of GTP-bound versus GDP-bound *Pf*Arf6. The effect of overactivation of Arf GTPases may be studied using constitutively active mutants. Constitutively active mutants of Arf GTPases are GTP-bound and are unable to hydrolyse the terminal phosphate of the nucleotide which, under normal conditions, returns the Arf GTPases to their inactive, GDP-bound state. Constitutively active mutants of Arf6 are prepared by mutating the glutamine residue at position 67 in the amino acid sequence to a leucine residue (Arf6-Q67L). On the other hand, constitutively inactive mutants of Arf6 are prepared by mutating the threonine residue at position 27 in the amino acid sequence to an asparagine residue (Arf6-T27N). Constitutively inactive Arf6 mutants are unable to exchange GDP for GTP, thus are 'locked' in their GDP-bound, inactive state (D'Souza-Schorey et al., 1998). Expression of a constitutively active human Arf6 (HsArf6-Q67L) in HeLa cells prevents Arf6 vacuoles from fusing with early and sorting endosomes. As a result, *Hs*Arf6-Q67L grape-like vacuoles accumulate within the cytoplasm (Naslavsky, 2003; Sannerud et al., 2011). Morphologically, these grape-like vacuoles are also spherical with a distinct lumen, thus strongly resembling the ring-like structures observed when *Pf*Arf6-GFP is expressed in HeLa cells. If a predominant subpopulation of wild-type *Pf*Arf6-GFP is locked in an active state, thus inducing the formation of the vacuoles, it raises the possibility that *Pf*Arf6-GFP is, at least in some cases, not effectively regulated by the ArfGAPs present in HeLa cells (ArfGAPs should stimulate the return *Pf*Arf6-GTP to its GDP-bound form). To explore whether the putative *Pf*Arf6 protein is effectively regulated in HeLa cells (specifically by mammalian ArfGAPs), sequences encoding constitutively active and inactive mutants containing single amino acid substitutions (of residues that are conserved between human Arf6 and malarial Arf6) were prepared by inverse PCR. PCR products were recircularised by ligation, transformed into competent *E. coli* cells, propagated and purified by plasmid miniprep. Plasmids containing the mutated coding sequences were validated by DNA sequencing. The wild-type *Pf*Arf6 sequence was successfully mutated to encode the constitutively active *Pf*Arf6 (Q67L) and constitutively inactive *Pf*Arf6 (T27N) mutants (**Figure 6**). HeLa cells were subsequently transfected with the plasmids containing the wild-type *Pf*Arf6-GFP (control), constitutively active *Pf*Arf6-GFP (Q67L) or constitutively inactive *Pf*Arf6-GFP (T27N) sequences. Initial observations of the transfected cells led to the impression that expression

of the mutants resulted in an increase in the number of *Pf*Arf6-GFP structures (**Figure 7A**). To test the hypothesis, three biological replicates, containing three technical replicates each, was conducted for each transfection. Each technical replicate involved counting the total number *Pf*Arf6-GFP containing structures (including both puncta and rings) in fifteen randomly selected cells. The average number of structures per cell (SPC) was calculated for each technical replicate. The three technical replicates were averaged, and the data was normalized to produce a relative number of structures per cell (RSPC) for the wild-type, active mutant and inactive mutant (*i.e.* the wild-type *Pf*Arf6 was normalised to 1). The mean RSPC of the three biological replicates was subjected to statistical analysis by a student's t-test. The observed increase in the number of *Pf*Arf6-GFP structures in HeLa cells transfected with active and inactive mutants (as opposed to the wild-type) was statistically significant ($\rho < 0.05$ for both mutants) (**Figure 7B**).

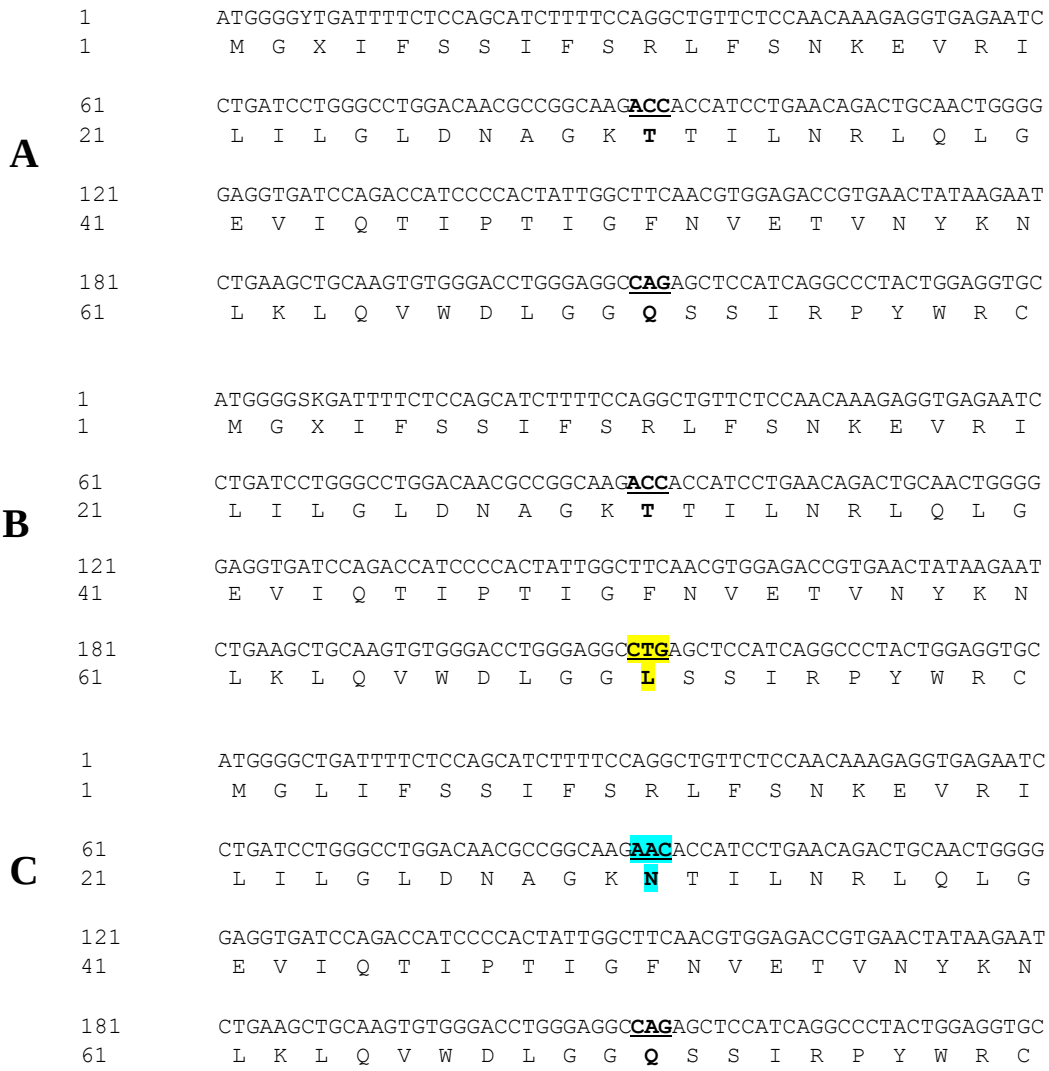

Figure 6: Validation of the site-directed mutagenesis of *Pf*Arf6 by DNA sequencing. Single nucleotide substitutions were incorporated into the amplicon of *Pf*Arf6-GFP by inverse PCR. Re-circularised amplicons were used to transform *E. coli* and plasmids isolated from transformed colonies. Sequencing of the plasmids was conducted using a CMV forward primer at Inqaba Biotech (South Africa). **A**: The wild-type *Pf*Arf6 coding sequence containing codons for glutamine (Q) and threonine (T) residues in position 67 and 27 respectively (underlined and in boldtype). **B**: The A/T mutation encoding the substitution of glutamine with leucine in position 67 of the protein sequence (Q67L) (highlighted in yellow) produced the coding sequence for *Pf*Arf6 (Q67L) which is routinely used to study a constitutively active, GTP-bound form of human Arf6 proteins. **C**: The C/A mutation encoding the substitution of threonine with asparagine in position 27 of the protein sequence (T27N) (highlighted in cyan) produced the coding sequence for *Pf*Arf6 (T27N) gene which is routinely used to study a constitutively inactive, GDP-bound form of human Arf6 proteins.

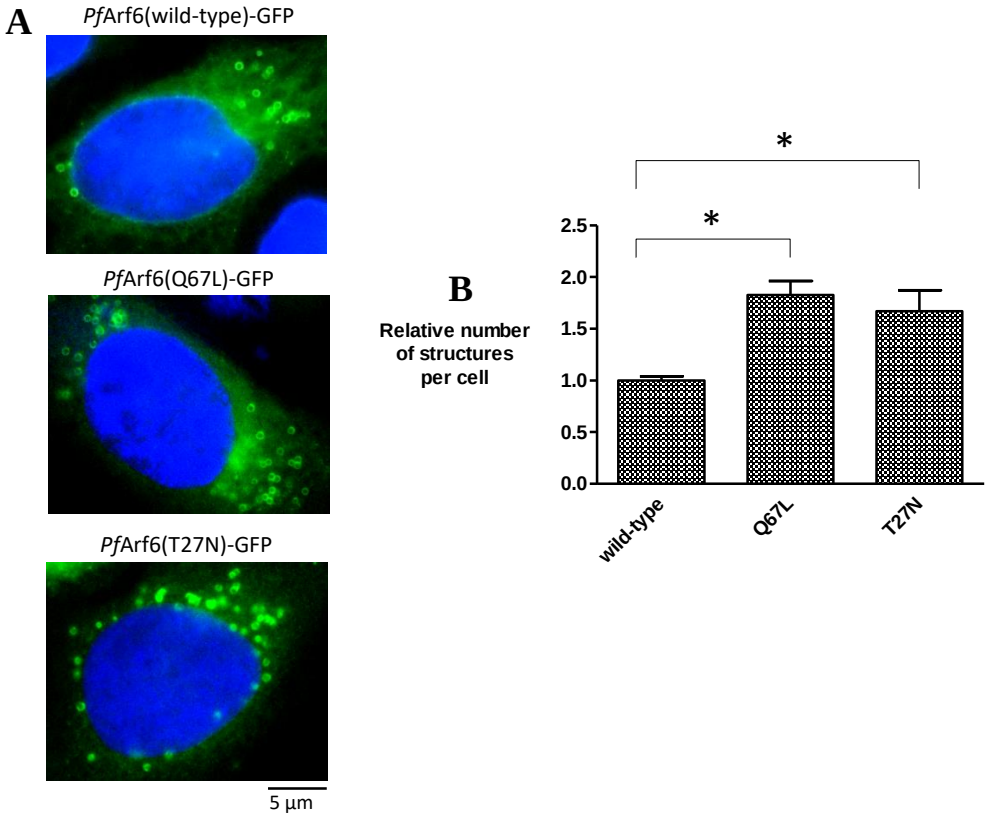

Figure 7: Expression of constitutively active and inactive *Pf*Arf6-GFP mutants in HeLa cells. **A**: Representative images of HeLa cells expressing wild-type *Pf*Arf6-GFP, constitutively active mutant *Pf*Arf6(Q67L)-GFP and constitutively inactive *Pf*Arf6(T27N)-GFP. Cells were fixed with paraformaldehyde, stained with Hoechst 33342 and viewed on an Olympus BX61 upright fluorescent microscope with a 100X objective and immersion oil. **B**: The average number of *Pf*Arf6-GFP structures per cell increased, relative to the wild-type, when expressing a constitutively active, Q67L (*$\rho < 0.05$, n = 9) and inactive mutant, T27N (*$\rho < 0.05$, n = 9) of *Pf*Arf6 in HeLa cells.

3.4. Discussion and future work

While the fact that the *Pf*Arf6-GFP plasmid was capable of expression, and that the structures to which *Pf*Arf6-GFP localised were not influenced by GFP fusion or the cancerous phenotype, speaks to the practicality of the HCSM, it is also important to bear in mind that heterologous expression systems may not indicate the native functions of proteins, in this case *Pf*Arf6. Similar localisation patterns of *Pf*Arf6-GFP in the parasite and HeLa cells may tempt the proposal that the true function of *Pf*Arf6 was realised in HeLa cells, but confirmation of this conclusion still requires a definitive identification of the subcellular structures represented by the *Pf*Arf6-GFP puncta in parasites. Co-localisation studies in parasites requires prioritization since co-transfections are significantly lengthy, demanding procedures with low transfection efficiencies (transfections usually take about 6 weeks until ready for analysis) and any co-localisation pursued by immunofluorescence would require the use of specially reared antibodies (Hasenkamp et al., 2012; Langsley and Chakrabarti, 1996).

In mammalian cells, endocytosis begins with the formation of invaginations at the plasma membrane (PM). Dynamin, a large GTPase, polymerises around the 'neck' of the invagination and upon hydrolysis of GTP it severs the invagination from the plasma membrane to form an endocytic vesicle. Endocytic vesicles deliver endocytosed material to early (or sorting) endosomes. Soluble cargo is delivered to late endosomes and finally to lysosomes. Soluble cargo in the lysosome is digested by hydrolytic enzymes (reviewed by Doherty and McMahon, 2009). In contrast, a proportion of membrane proteins and membrane delivered to the early endosome are recycled back to the PM to initiate additional rounds of endocytosis. Membrane recycling occurs via an endocytic recycling compartment (ERC). Some membrane cycling occurs directly form early endosomes to the PM or are transported to the *trans*-Golgi network (TGN) and returned to the PM in constitutive secretory vesicles budding from the TGN. Vesicles containing lysosome-resident hydrolases bud from the TGN, transition through the early/sorting endosome and are ultimately delivered to lysosomes (reviewed by Grant and Donaldson, 2009). Endocytosis is either mediated by plasma membrane receptors (receptor-mediated endocytosis) or is non-specifically mediated (fluid-phase endocytosis). In receptor-mediated endocytosis, plasma membrane proteins have exoplasmic domains that function as receptors for specific ligands in the extracellular medium. The cytoplasmic domains contain endocytic motifs that recruit coat proteins which mediate the formation of the early invagination. Receptor-mediated endocytosis results in the rapid concentration of endocytic cargo in invaginations and, as result the rate of endocytosis is considerably higher than fluid-phase endocytosis which internalises cargo that enters invaginations by 'chance' (any proteins that just happen to be within the vicinity during the formation of endocytic vesicles) (reviewed by Stahl and Schwartz, 1986). Clathrin-mediated endocytosis is a mode of receptor-mediated endocytosis where the formation of the invagination is mediated by the coat protein clathrin and is also dynamin-dependent. In addition to the extensively characterised clathrin-mediated endocytic

pathway, several clathrin-independent pathways have been described. These include caveolin- and flotillin-dependent and Arf6-dependent endocytosis (Doherty and McMahon, 2009). Unlike caveolin and clathrin, which are coat proteins, Arf6 is a membrane-binding protein that recruits coat proteins to the membrane. Although the incoming endocytic vesicles from the clathrin-dependent, fluid-phase and Arf6-associated pathways are distinct, they share the same fate in that they fuse to form the early/sorting endosome where they are sorted for recycling or degradation (Naslavsky, 2003).

Since *Hs*Arf6 is associated with endocytic vesicles budding at the cell surface in several endocytic pathways, and that its participation in each pathway in cell-dependent (Radhakrishna and Donaldson, 1997), the study commenced by exploring which endocytic pathways, available at the cell surface of metazoan cells, *Pf*Arf6-GFP puncta and ring-like structures were associated with in HeLa cells. The partial co-localisation of *Pf*Arf6-GFP with *Hs*Arf6 suggested that *Pf*Arf6 was associated with endocytic vesicles that form part of the Arf6-associated pathway. The lack of co-localisation between *Pf*Arf6-GFP and clathrin light chain supported this finding, since Arf6-dependent endocytosis is clathrin-independent (Radhakrishna and Donaldson, 1997). Arf6-dependent endocytosis is also dynamin-independent (Mayor et al., 2014), but co-localisation studies of *Hs*Dynamin1-RFP and *Pf*Arf6-GFP were not fruitful. HeLa cells transfected with *Hs*Dynamin1-RFP displayed significant bleed-through which made it impossible to distinguish *Pf*Arf6-GFP structures from the marker protein. Reductions in the amount of *Hs*Dynamin1-RFP plasmid DNA used resulted in very weakly expressed *Hs*Dynamin1-RFP which were difficult to visualise without drastic overexposure and ultimately affected the proper interpretation of the data (*results not shown*). These experiments could, alternatively, be explored by immunofluorescence and would serve to support the notion that *Pf*Arf6-GFP is exclusively participating in Arf6-associated endocytosis and not clathrin- or caveolin-dependent endocytosis (which is also dynamin-dependent) (Mayor et al., 2014). Initially, *Pf*Arf6-GFP puncta and ring-like structures were investigated as endocytic vesicles trafficking through the cell following internalization by fluid phase-endocytosis using tetramethylrhodamine isothiocyanate (TRITC) fused to Dextran (TRITC-Dextran). Very weak signals were occasionally observed, and once again made the data difficult to interpret. In retrospect, paraformaldehyde fixation and permeabilization may have contributed to the loss of staining and alternative measures could be attempted. However, in the alternative method that was developed using haemoglobin uptake and immunodetection, the lack of co-localisation between *Pf*Arf6-GFP and haemoglobin internalized by fluid phase-endocytosis suggested that *Pf*Arf6, at least in HeLa cells, did not play a role in fluid-phase endocytosis. A final avenue to interrogate *Pf*Arf6-GFP structures as participants in the Arf6-associated endocytic pathway was to co-localise the structures with cargo proteins known to traffic through this distinct route (candidates are listed in Chapter 1, section 5.1).

Prior to fusion with the early/sorting endosomes, Arf6-GTP inactivation causes Arf6-GDP to dissociate from the incoming endocytic vesicle (Mayor et al., 2014). The ring-like structures observed when expressing the wild-type *Pf*Arf6-GFP (which had not yet been co-localised with any marker protein)

raised the possibility that these structures may be artefacts of protein over-expression or represent *Pf*Arf6-GFP that, at least in some instances, is not being effectively regulated by mammalian ArfGEFs and ArfGAPs. Overexpression of the constitutively active *Hs*Arf6-Q67L mutant traps Arf6 in internal vacuolar structures (Naslavsky, 2003; Sannerud et al., 2011). Expression of a constitutively active version of *Pf*Arf6-GFP resulted in a significant increase the number of *Pf*Arf6-GFP positive structures in the cell. This result might suggest that *Pf*Arf6-GFP (wild-type) was, in some cases, not effectively inactivated by human ArfGAPs and the lack of inactivation was enhanced by the expression of the constitutively active mutant *Pf*Arf6(Q67L)-GFP. However, this hypothesis does not account for the increase in *Pf*Arf6-GFP positive structures observed when expressing a constitutively inactive mutant *Pf*Arf6 (T27N). Which raises the question of whether *Pf*Arf6-GFP 'locked' in its GDP-bound state (T27N mutation) would similarly accumulate in vacuolar structures owing to *Pf*Arf6-GFP not being effectively activated by human ArfGEFs. Dell'Angelica et al. (2000) and Sannerud et al. (2011) proposed that a cytosolic localisation of the *Hs*Arf6-T27N mutant is favoured, although it also occurs in tubular membranous structures. Reasonable candidates for structures in which *Pf*Arf6-GFP 'locked' in its GDP-bound state might become trapped would be the recycling endosome (RE) or the endocytic recycling compartment (ERC), since *Hs*Arf6-GDP is recruited to these structures to facilitate the recycling of cargo and membranes back to the plasma membrane (Naslavsky, 2003). It is even possible that the *Pf*Arf6-GFP punctate structures may also represent recycling endosomes returning to the plasma membrane rather than budding from it. To test this hypothesis *Pf*Arf6-GFP could be co-localised with Rab11 (a marker for the ERC) and Rab35 (a marker for the RE) (Barral et al., 2012; Eyster et al., 2009; Kouranti et al., 2006; Mayor et al., 2014; Radhakrishna and Donaldson, 1997; Sato et al., 2008). However, Donaldson and Jackson (2000) strongly emphasise that the interpretation of constitutively active and inactive mutants of Arf6 should be considered cautiously since blocking Arf6's GDP/GTP cycle may alter its native function.

More recently, *Hs*Arf6 has also been implicated in autophagosome biogenesis (Moreau et al., 2012). Autophagy is a major cellular degradation pathway that involves the engulfment of cytoplasmic contents into double-membrane vesicles called autophagosomes. Autophagosomes and its contents are transported to and fuse with lysosomes where they are degraded. Akin to the formation of early endosomes by homotypic fusion of endocytic vesicles, pre-autophagic structures (called phagophores) form first and fuse to form the autophagosome (Mizushima et al., 2008; Ravikumar et al., 2009; Xie and Klionsky, 2007). Phagophores derive membranes from a variety of sources including the plasma membrane through clathrin-dependent and Arf6-dependent endocytosis (Moreau et al., 2012; Ravikumar et al., 2010). LC3-II is a highly conserved protein that is used to track the autophagic process and is a homolog of yeast Atg8. LC3-II is involved in the fusion steps of autophagosome formation and is observed in phagophores and fully formed autophagosomes (Mizushima et al., 2008; Ravikumar et al., 2009; Xie and Klionsky, 2007). Furthermore, LC3-II is strongly correlated with number of

autophagosomes present within a cell (Kabeya, 2000; Klionsky et al., 2008), which can be increased by inhibiting autophagosome-lysosome fusion by treatment with chloroquine or bafilomycin A1 (Klionsky et al., 2008; Ravikumar et al., 2009; Redmann et al., 2017). The treatment of HeLa cells expressing pmRFP-LC3 with chloroquine was consistent with this theory. Under chloroquine treatment, the number of LC3 -positive punctate structures increased considerably. Moreau et al., (2012) also observed that *Hs*Arf6 partially co-localised LC3-positive vesicles suggesting that *Hs*Arf6 plays a role in phagophore formation and is present on autophagosomes following homotypic fusion of phagophores. Similarly, the number of instances of co-localisation between pmRFP-LC3 and *Pf*Arf6-GFP increased under chloroquine treatment. Lastly, Moreau et al. (2012) observed that *Hs*Arf6 levels appear to be upregulated when autophagy is induced (in their case, by amino acid and serum starvation). Expression of *Pf*Arf6-GFP in HeLa cells under chloroquine treatment led to the impression that there was a marked increase in *Pf*Arf6-GFP structures, but this observation was not quantified, nor subjected to statistical analysis. Altogether, the findings suggested that *Pf*Arf6 may participate in autophagy, or at least is present on LC3-positive autophagosomes.

Based on the knowledge derived from the HeLa cell surrogate model, the possible native, cellular functions of *Pf*Arf6 in parasites that should be explored are *Hs*Arf6-dependent endocytosis and autophagocytosis. It worth noting that in response to the recent advancements in the understanding of malarial autophagy, it has been tagged as a possible target in future malarial drug discovery campaigns. Currently, specific drug targets within the cellular process are being investigated (reviewed by Singh and Chakraborty, 2016). While an Atg8/LC3 homolog (*Pf*Atg8) is an established autophagy marker in parasites, the autophagic pathway in parasites deviates considerably from some of the typical features of mammalian autophagy. *Pf*Atg8 has been observed in phagophores forming at the plasma membrane, autophagosomes throughout the cell, lysosomes near the food vacuole and is even present inside the food vacuole in the late trophozoite/early schizont parasite lifecycle stages (Cervantes et al., 2014; Sinai and Roepe, 2012; Tomlins et al., 2013). Intriguingly, the reported morphologies and localisations of *Pf*Atg8-positive autophagic organelles is similar to those observed for *Pf*Arf6-GFP expressed in parasites. As previously described, *Pf*Arf6-GFP localised to numerous puncta along the periphery of the parasite in the mature trophozoite life stage in addition to a more central intensely fluorescent single ring-like locus which was insensitive to the Golgi disruptors BFA and Golgicide (T.Swart, M.Sc. dissertation). The effects of *Hs*Arf6 on autophagy is mediated by its role in the generation of PIP_2 and by its ability to induce phospholipase D (PLD) activity. PIP2 and PLD may themselves promote autophagosome biogenesis by influencing the formation of phagophores derived from the plasma membrane (Moreau et al., 2012). It is conceivable then that the puncta observed at the parasite's periphery may represent phagophores forming at the plasma membrane and that the more central fluorescence adjacent to the food vacuole may represent mature autophagosomes or autophago-lysosomes accumulating adjacent to food vacuole in preparation of fusion with this compartment. It

would also then follow that, unlike *Pf*Atg8 that is present in the food vacuole, *Pf*Arf6 dissociates before fusion with this compartment since it was observed adjacent to and not within the food vacuole. It is thus important to co -localise *Pf*Arf6 -GFP with the *Pf*Atg8 marker in parasites. To support this study, specially raised antibodies of *Pf*Atg8 were prepared and immunofluorescence studies are underway. In an alternative approach, that also circumvents the requirement for experimentally-difficult co-transfection experiments in parasites, autophagy could be enhanced in parasites expressing only *Pf*Arf6-GFP to determine whether any change in the localisation pattern occurs. Nutrient deprivation and treatment with an autophagy inducer such as rapamycin should produce the desired effect of enhanced autophagy (although this was not achieved in HeLa cells) (Asano et al., 2014; Parker et al., 2016). Similarly, treatment with chloroquine should result in a greater number of autophagosomes and would also be useful in this pursuit (Redmann et al., 2017).

While several avenues exist to further interrogate the possible roles of *Pf*Arf6 in malarial autophagy, follow-up studies pertaining to the possible roles in a *Pf*Arf6-dependent endocytic pathway are complicated by the fact that, currently, little is known about this pathway in mammalian cells. BLAST searches for sequence similarities in the parasite's genome indicate that homologs of the known cargo proteins that traffic through the *Hs*Arf6-dependent endocytic pathway in mammalian cells do not exist. Furthermore, *Hs*Arf6 (and in addition to the cargo proteins mentioned above) are the established markers for early endocytic invaginations budding at the plasma membrane which subsequently traffic through the Arf6-dependent endocytic pathway (Eyster et al., 2009). However, *Hs*Arf6 is also recruited to recycling endosomes returning membrane and transmembrane proteins back to the cell periphery. In mammalian cells, Rab11 is an established marker protein for these organelles (Mayor et al., 2014) and with the existence of a Rab11 homolog in the parasite's genome (Langsley and Chakrabarti, 1996), it may be worthwhile to pursue co-localisation studies with *Pf*Arf6-GFP in order to investigate whether an Arf6-dependent endocytic pathway may exist in malarial parasites. Since these findings would rely on the assumption that a possible malarial Arf6-dependent endocytic pathway is similar in this respect to the mammalian pathway, it may be worth supplementing these findings with evidence that refutes its role in the classical clathrin-dependent endocytosis. Canonical components of the clathrin-dependent endocytic pathway are present in the parasites genome; such as clathrin, dynamin-like proteins, adaptor protein 2 and EEA1 (Henriques et al., 2015; Suresh and Haldar, 2018; Zhou et al., 2009). Although clathrin coats are absent from endosomal invaginations at the plasma membrane during haemoglobin uptake (Deponte et al., 2012), dynamin-like protein 1 (*Pf*Dyn1) and 2 (*Pf*Dyn2) were shown to play important roles in the haemoglobin uptake pathway of parasites by demonstrating that *Pf*Dyn1/2 GTPase activity is inhibited by dynasore (a dynamin inhibitor) and that treatment of the parasite with dynasore substantially decreased the amount of haemoglobin and hemozoin in parasites (the catabolic product of haemoglobin) (Macia et al., 2006; Sullivan et al., 1996; Zhou et al., 2009). Co-localisation (or immunofluorescence studies) with *Pf*Dyn1/2 could be pursued in this respect. In an alternative

approach, parasites expressing only *Pf*Arf6-GFP could be treated with the inhibitor of *Hs*Arf6, NAV279 to determine whether a change in *Pf*Arf6-GFP localisation pattern is realised. Recall that NAV-2729 is the only known inhibitor that binds directly to Arf6 and is predicted to target the GEF binding region of Arf6 (which is partially conserved in *Pf*Arf6 as will be discussed in detail in Chapter 5) (Yoo et al., 2016).

Since follow-up studies would still critically rely on inefficient and expensive co-localisation (or immunofluorescence) studies, it was decided to first validate *Pf*Arf6 as a suitable drug target. In this regard, the lethal dosage of NAV2729 against parasites was determined as 12.9 μM which is considerably higher than the chloroquine gold-standard of 0.015 μM (D. Laming). This finding did however still warrant subsequent studies in molecular target validation. Historically, the parasites genome has been notoriously difficult to manipulate and as such traditional methods to pursue gene-silencing or -knockouts are not ideal. With the advent of CRISPR/Cas9 gene editing, generation of conditional knockdowns and gene deletion have improved drastically and expected to significantly advanced the field of malaria research (Ghorbal et al., 2014; Wagner et al., 2014). However, CRISPR/Cas9 technologies are not yet routinely used in malarial research and would require considerable time and expenditure to establish and develop protocols for this technique. A more immediate approach would be to exploit the affinity of NAV2729 to its target by cross-linking NAV2729 to a column and passing parasite lysates through. NAV2729 binding partners would subsequently be analysed by mass spectrometry to identify the target. It is worth noting though that it is not always possible to cross-link compounds to a column without loss of its bioactivity (Sinz et al., 2015). So, as a final, more amenable approach it was decided to try develop and establish *Pf*Arf6 assays which could identify novel *Pf*Arf6 inhibitors by high throughput screening of compound libraries. The first goal is to validate *Pf*Arf6 as a suitable drug target. Provided this is achieved, the subsequent goals are to find potent inhibitors that inhibit *Pf*Arf6 in the micromolar range *in vitro* that retain their potency *in vivo.*

Chapter 4: Development of an *in vitro* human Arf6 signalling assay for drug screening of potential anticancer therapeutics.

4.1. Introduction

A second ongoing interest of the research group is the development and implementation of bioassays for drug screening. With the decline of new chemical entities entering the pharmaceutical marketplace, new types of drug targets are being explored and protein-protein interactions are likely to become increasingly prominent in this regard (Schacht et al., 2010). As previously reviewed, Arf6 signalling is a prominent target with broad clinical significance i.e. as possible targets for the therapy of cancer and pathogenic microbial infections. This chapter focuses on the development of high-throughput Arf6 interaction assays for drug screening of novel anticancer therapeutics.

4.1.1. Drug screening methods for Arf6 GTPase signalling

The existing chemical entities that have been identified as inhibitors of Arf6 signalling were established by a variety of screening methods that do not align with the requirement of a high-throughput and cost-effective screening method. *In silico* high-throughput screens used to identify LM11, an inhibitor of Arf1 and cytohesins, required *in vitro* validation using routine fluorescence kinetics and anisotropy measurements and *in vivo* validation using immunofluorescence microscopy and wound-healing/cell sheet migration assays, methods which are not inherently amenable to plate-based high-throughput screening (Viaud et al., 2007). The discovery, confirmation and assessment of the NAV-2729 inhibitory effects on spontaneous and ArfGEF-mediated GTP exchange (more specifically by cytohesins and BRAG) using a fluorometric biochemical assay in plate-based format highlighted a second constraint – the need for highly specialised and exorbitantly expensive reagents. In this assay format GDP/GTP exchange on Arf6 was conducted using GTP-BODIPY FL, a costly GTP derivative containing a fluorescent BODIPY FL attached to the ribose group, which was used to monitor GDP/GTP exchange by an increase in fluorescence intensity in a plate reader (Yoo et al., 2016). Similar cost and equipment limitations are inherent in the RNA aptamer displacement *in vitro* screening methods used to identify the inhibitor of all cytohesins, SecinH3 (Hafner et al., 2006). The remaining high-throughput screening methods were designed to find inhibitors of specific cellular events. Golgicide A, for example, was identified from a high-throughput fluorescence-based screen for small molecules that inhibit intracellular toxin transport in cells hosting intracellular pathogens (Sáenz et al., 2009). Similarly, LG186 and AMF-28 were identified by their ability to perturb endocytosis and inhibit cancer cell growth, respectively. The targets of these inhibitors were later identified as the ArfGEF GBF1 using fluorescence kinetics measurement assays (Boal et al., 2010; Feng et al., 2004; Ohashi et al., 2012). An *in vivo* FRET-based assay to monitor Arf6 activation in mammalian cells has been developed (Hall et

al., 2008) and adopted for the identification and validation of Arf6 signalling inhibitors, but not in a high-throughput format. To date, the only existing high-throughput and cost-effective screening strategy that has been developed is an *in vitro* fluorescence resonance energy transfer system (FRET) for monitoring the activation of Arf1 GTPases (Bill et al., 2011). In the assay Arf1 was fused to CFP and the Arf GTPase binding GAT domain of GGA3 (Golgi-localised, gamma adaptin ear-containing, Arf-binding effector protein) was fused to YFP. GGA3 is a coat protein involved in secretory vesicle formation at the *trans*-Golgi network (TGN) which is recruited by Arf1, but also cross-reacts with Arf6 *in vitro*. The fact that it only binds to active (GTP-bound) Arf GTPases has been exploited particularly in pull-down assays to detect the extent of Arf GTPase activation in cell models (Takatsu et al., 2002). FRET based assays excel is in their ability to monitor the activation and deactivation of Arf GTPases in real-time and in their compliance with high-throughput drug screening. As such, an *in vitro* FRET based approach to study Arf1-GGA and Arf6-GGA interactions is currently under development (A. Ntlansana, M.Sc., dissertation). However, like all scientific methods, FRET has its own set of inherent flaws. Some of these include fluorescence cross-talk and bleed-through which can result in high background fluorescence and poor signal to noise ratios, as well as the fact that energy transfer is highly dependent on the appropriate orientation of the donor and acceptor fluorophores. Fluorescence cross-talk may be particularly problematic in the initial stages of Arf GTPase signalling studies which rely heavily on intrinsic tryptophan fluorescence assays to determine the activation status of Arf GTPases (as described below).

4.1.2. Nucleotide exchange and intrinsic tryptophan fluorescence

As previously described, Arf GTPases act as molecular switches that cycle between inactive GDP-bound forms and active GTP-bound forms. Recombinant Arf GTPases produced in bacterial, yeast or mammalian cells are usually obtained in one or the other form (Macia et al., 2001). Thus, prior to studying Arf GTPase signalling by applying *in vitro* biochemical assays, it is critical to prepare GDP and GTP loaded Arf GTPases as controls. The activation status of Arf GTPases is routinely manipulated using EDTA-mediated nucleotide exchange and is monitored by intrinsic tryptophan fluorescence (Bigay and Antonny, 2006). In EDTA-mediated nucleotide exchange, Arf GTPases are incubated with EDTA and excess GDP/GTP. The Mg^{2+} ions that stabilise the attached nucleotide and hence Arf GTPases in inactive or active forms are chelated by EDTA. The Arf GTPases subsequently favour the binding to nucleotides that are present in excess and are stabilised in these forms by adding millimolar amounts of excess $MgCl_2$ relative to EDTA. These stabilised, 'pre-loaded' Arf GTPases are used to study the deactivation and activation of Arf GTPases, by ArfGAPs and ArfGEFs respectively, and their subsequent interactions with effector proteins. Nucleotide exchange is monitored by intrinsic tryptophan fluorescence measurements. An invariant tryptophan residue (in position 62 of the amino acid sequence of Arf6 homologs) within the switch II region is exposed during the binary conformational shift that occurs when Arf-GDP transitions to Arf-GTP. Upon deactivation of Arf-GTP

the invariant residue is hidden within the protein core. Essentially, the intrinsic tryptophan residue acts as a fluorescent probe of the protein confirmation and hence the activation status of Arf GTPases (Béraud-Dufour et al., 1998; Bigay and Antonny, 2006; Hurtado-Lorenzo et al., 2006). Understandably then, the presence of an additional fluorophore (as is the case in FRET based protein-protein interaction assays) may complicate intrinsic tryptophan fluorescence assays. Furthermore, while the ArfGEF-stimulated GDP/GTP exchange and ArfGAP-stimulated GTP hydrolysis can be studied in real-time using the intrinsic tryptophan fluorescence assays, it is not a method that is amenable to high-throughput screening.

4.1.3. Alternative methods for high-throughput drug screening of compounds targeting Arf6-GTPase signalling

The complication in using tryptophan fluorescence or FRET to measure Arf GTPase activation status in screening experiments is that compounds in the libraries screened may themselves display absorption or fluorescence at wavelengths employed (Ex_{298}/Em_{340} for tryptophan fluorescence; $Ex_{425}/Em_{485,535}$ for FRET). For these reasons, alternative multi-well plate-based assay formats are being explored *in tandem* with the FRET based approach to develop methods for the high-throughput screening of compound libraries against the array of protein interactions that occur during Arf6 signalling (Arf6-effector, Arf6-ArfGEF and Arf6-ArfGAP interactions). Two novel colorimetric assay formats were conceptualised and explored in this study and are described below.

4.1.3.1. Ni-NTA immobilised Arf6-GGA GST interaction assay

In this assay format nickel coated 96-well plates were used. To facilitate the immobilisation of Arf6 on the nickel plate, Arf6 was expressed as a His-tagged recombinant protein (His-*Hs*Arf6). Arf6 was further modified by removing the amphipathic N-terminal α–helix which is post translationally myristoylated and responsible for the recruitment of Arf6 to membranes. The truncation of the first 13 amino acid residues of *Hs*Arf6 is routinely practiced in the preparation of *Hs*Arf6$^{N\Delta13}$, a truncated version of Arf6 with better solubility properties (Bigay et al., 2003). The malarial Arf6 homolog was similarly truncated. Sequence alignments determined that truncation of the first 17 residues was required for the removal of the amphipathic N-terminal α–helix in the putative malarial Arf6 homolog (*Pf*Arf6$^{N\Delta17}$). The His-*Hs*Arf6$^{N\Delta13}$ and His-*Pf*Arf6$^{N\Delta17}$ recombinant proteins were pre-loaded with GDP or/GTP by EDTA mediated nucleotide exchange and immobilised on the nickel plate. The Arf GTPase binding domain (GAT domain) of the Arf GTPase effector protein GGA3 (GGA^{GAT}) was used in the early development of the assay. GGA^{GAT} was be fused to glutathione-S-transferase (GST-GGA^{GAT}) and incubated with the immobilised Arf6 on the nickel plate. To detect the Arf6-GGA a standard GST enzyme assay was used. Following incubation of GST-GGA^{GAT} with immobilised His-*Hs*Arf6$^{N\Delta13}$, the nickel plate was washed several times to remove unbound proteins and excess inhibitor. The plate was then incubated with GST substrate solution containing 1-chloro-2,4-dintrobenzene (CDNB) and

reduced L-glutathione (GSH). The dinitrophenyl thioether (GS-DNB) conjugation product produced by active GST was measured at an absorbance of 340 nm. Based on the observation that GGA only interacts with Arf6 in its active state, it was expected that a significant GST signal would be observed where Arf6-GTP was immobilised on the plate. Conversely, no signal, or a lesser signal was expected where Arf6-GDP was immobilised to the plate (**Figure 8**). The extent of GST activity in the wells would thus correlate with Arf6 activation status.

4.1.3.2. Glutathione immobilised GGA-Arf6 HRP interaction assay

In a reverse assay format, the effector protein GST-GGA^{GAT} was immobilised on a glutathione plate and incubated with inactive and active human and malarial Arf6. The His tag on His-*Hs*Arf6$^{N\Delta13}$ and His-*Pf*Arf6$^{N\Delta17}$ was detected using nickel-HRP (horse radish peroxidase). A standard HRP enzyme assay was conducted where 3,3',5,5'-tetramethylbenzidine (TMB) was oxidised to the TMB/diimine blue complex by HRP activity. The chromogenic oxidation product, TMB/diimine blue complex, could be detected at absorbance 630nm. Again, based on the observation that GGA only interacts with Arf6 in its active state, it was expected that a significant HRP signal would be observed where immobilised GST-GGA^{GAT} was incubated with Arf6-GTP. Conversely, no signal, or a lesser signal was expected where immobilised GST-GGA^{GAT} was incubated with Arf6-GDP (**Figure 9**). The reverse assay was explored as an alternative with greater signal sensitivity.

4.1.3.3. The incorporation of ArfGEFs and ArfGAPs

Once the Arf6-GGA interaction assays were established, it necessarily implied that the assays could determine the activation status of Arf6. The Arf6 interaction assay was then be adopted to interrogate the activation status of Arf6 following incubation with ArfGEFs and ArfGAPs. In this way the assay was extended as a tool to study Arf6-ArfGEF and Arf6-ArfGAP interactions in addition to Arf6-effector interactions. In the interrogation of the ArfGAP and ArfGEF assays human ArfGAP1 (GAP domain) and human ARNO (Sec7 domain) were chosen as candidates. These accessory proteins were chosen since their ability to stimulate GTP hydrolysis and GDP/GTP exchange on Arf6 has been established in *in vitro* assays respectively. While full-length ARNO appears to stimulate GDP/GTP exchange on Arf6 *in vivo*, the ARNO (Sec7 domain) has limited but detectable activity on Arf6 *in vitro* (Hurtado-Lorenzo et al., 2006; Macia et al., 2001). Furthermore, although ArfGAP1 has demonstrated the *in vitro* ability to stimulate GTP hydrolysis on Arf6, it has not yet been established whether ArfGAP1 and Arf6 interact within a cellular context (Zhang et al., 2007; Zhu et al., 2012). These candidates were chosen because chemical inhibitors of the Arf6-ARNO and Arf6-ArfGAP1 exist, namely SecinH3 and QS11 respectively (Hafner et al., 2006; Zhang et al., 2007). These inhibitors were used in the chemical validation of the assays measuring ArfGEF-mediated GDP/GTP exchange and ArfGAP-mediated GTP hydrolysis of Arf6. Following the initial validation of the assays, more suitable ArfGEF and ArfGAP

candidates will be chosen for screening purposes. Furthermore, the interactions with Arf6 and alternative effector proteins (other than GGA) was explored.

The assays may be suitable for high-throughput screening but were not designed to monitor the real-time activation or deactivation Arf6. ArfGEF activation and ArfGAP deactivation assays were conducted in 96-well round bottom plates and the activation status of Arf6 was determined using the novel immobilisation assay described above. Thus, using GTP-loaded Arf6 and an ArfGAP, the loss of output signals would indicate ArfGAP-stimulated GTP hydrolysis activity. Conversely, using GDP-loaded Arf6 and an ArfGEF, an increase in the output signal would indicate ArfGEF-stimulated activation (GDP/GTP exchange) of Arf6. Since the focus of the study was to develop the interaction assays for the high-throughput screening of novel anticancer and antimalarial therapeutics human homologs and the putative malarial homologs of Arf6, ArfGEFs and ArfGAPs respectively were explored.

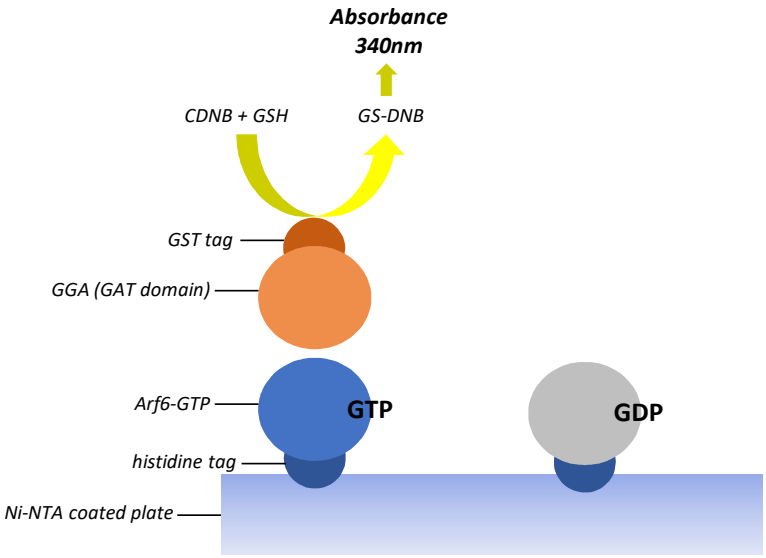

Figure 8: Schematic of the Ni-NTA immobilised Arf6-GGA interaction assay. Inactive Arf6-GDP (*grey*) and active Arf6-GTP (*blue*) were expressed as recombinant, His-tagged (*dark blue*) proteins and immobilised on Ni-NTA coated 96-well plates. The effector protein, the GAT domain of GGA (*light orange*), was expressed as a recombinant GST-tagged (*dark orange*) protein (^{GAT}GGA-GST). Following incubation of ^{GAT}GGA-GST with immobilised Arf6 GTPases, the nickel plate was washed several times to reduce non-specific binding. The plate was then incubated in GST substrate solution containing CDNB and GSH and the GS-DNB conjugation product produced by active GST was measured at an absorbance of 340 nm. Since ^{GAT}GGA-GST selectively binds to active Arf6-GTP, measurements at an absorbance of 340 nm were indicative of active Arf6-GGA interaction.

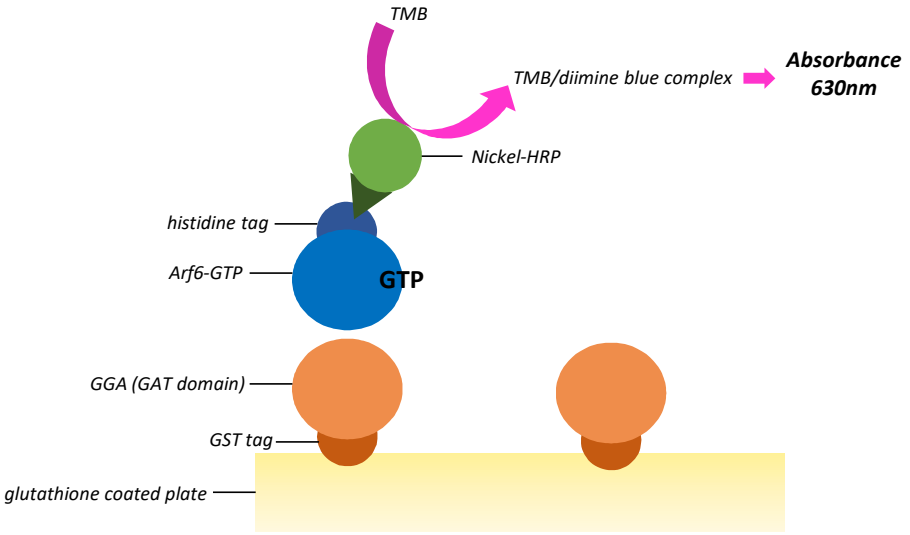

Figure 9: Schematic of the glutathione immobilised GGA-Arf6 HRP interaction assay. The effector protein, the GAT domain of GGA (*light orange*), was expressed as a recombinant GST-tagged (*dark orange*) protein (^{GAT}GGA-GST) and immobilised on glutathione coated 96-well plates. Inactive Arf6-GDP and active Arf6-GTP (*blue*) were expressed as recombinant, His-tagged (*dark blue*) proteins. Following incubation of immobilised ^{GAT}GGA-GST with Arf6 GTPases, the nickel plate was washed several times to reduce non-specific binding. The plate was incubated in blocking solution containing nickel-HRP, and once again washed several times to reduce non-specific binding. The plate was incubated in the TMB substrate which HRP oxidizes to the coloured TMB/diimine complex which was detected at 630 nm. Since ^{GAT}GGA-GST selectively binds to active Arf6-GTP, measurements at an absorbance of 630 nm were indicative of active Arf6-GGA interaction.

4.2. Aims and objectives

Aim of the study. To support the goal of developing assays to identify novel inhibitors of *Pf*Arf6, the novel plate-based assays were established using human Arf6. assays were first established using human Arf6 and human accessory proteins since the corresponding malarial accessory proteins have not been characterised and known inhibitors of human Arf GTPases could be used to validate the assay. An additional advantage is that the assay with the human proteins could be used to identify Arf6 inhibitors for cancer drug discovery purposes.

Specific questions/objectives and experimental approaches:

1. Can the recombinant proteins required in the assay be expressed in soluble and pure forms? All proteins were expressed as His or GST-tagged proteins under small-scale conditions to determine the solubility of each protein. Small-scale conditions were scaled up and the protein expressed and purified by Ni-NTA affinity or glutathione-affinity chromatography.
2. Can the conditions required for EDTA-mediated nucleotide exchange be established and can the activation status of Arf6 be detected by intrinsic tryptophan fluorescence using a standard plate reader? To prepare active and inactive forms of His-*Hs*Arf6$^{N\Delta13}$, nucleotide exchange conditions were optimized, and measured on a standard plate reader.
3. Can significant signal to noise ratios be achieved in the primary Ni-NTA immobilised Arf6-GGA GST interaction assay? To determine the signal to noise ratios the interaction assay using GTP-loaded Arf6 was conducted alongside background and negative controls. The background control consisted of only GST-GGA^{GAT} to determine the contributions of its non-specific binding to the nickel-coated plate to the GST signal output. GDP-loaded Arf6 was added to the negative control to account for the binding of GST-GGA^{GAT} to inactive Arf6.
4. Can significant signal to noise ratios be achieved in the secondary glutathione immobilised GGA-Arf6 HRP interaction assay? Here, the background control consisted of His-*Hs*Arf6$^{N\Delta13}$ only to determine the contributions of its non-specific binding to the glutathione coated plate, to the HRP signal output. The negative control measured of GDP-loaded Arf6 binding to immobilised GST-GGA^{GAT}.
5. Can the primary Ni-NTA immobilised Arf6-GGA GST assay detect the activation status of Arf6 GTPase following ArfGEF-stimulated GDP/GTP exchange and ArfGAP-stimulated GTP hydrolysis? ArfGEF and ArfGAP assays were conducted by incubating recombinant ARNO Sec7 domain and ArfGAP1 GAP domain with Arf6 in round-bottom well plates and then the activation status of the reaction products were analysed using the Ni-NTA immobilised Arf6-GGA GST assay. To validate the ArfGAP1-stimulated GTP hydrolysis on Arf6, the ArfGAP assays were conducted in the presence of QS11, a known ArfGAP1 inhibitor.

4.3. Results

Preparation of the DNA constructs used in the development of the human Arf6 signalling assay. For the expression of the putative human Arf6 (*Hs*Arf6) in *E. coli*, the coding sequence for human Arf6 (*Hs*Arf6) was amplified by PCR from a pARF6-CFP construct obtained from Addgene and cloned into pET-28a-CFP (previously prepared by F.Khan, 2017). To prepare the N-terminally truncated human Arf6 coding sequence (*Hs*Arf6$^{N\Delta13}$), PCR amplification was conducted using a forward primer that omitted amplification of the N-terminal hydrophobic extension and incorporated a *Nhe*I restriction site at the 5' end of the coding sequence. The reverse primer was designed to incorporate a terminal stop codon (to prevent the subsequent expression of CFP) followed by a *Bgl*II restriction site. A *Bgl*II restriction site was chosen because, an internal *Bam*HI restriction site present within the *Hs*Arf6 coding sequence would result in the internal digestion of the *Hs*Arf6 coding sequence. The PCR amplicon was analysed by agarose gel electrophoresis. The approximate sizes of PCR and restriction digestion products were determined by preparing log (base pair) against the relative migration distance plots of the DNA ladder used (*results not shown*). The PCR amplicon was approximately 500 bp (**Figure 10A**) which corresponded to the 486 bp predicted size of the *Hs*Arf6$^{N\Delta13}$ amplicon. The *Hs*Arf6$^{N\Delta13}$ amplicon digested with *Nhe*I and *Bgl*II was subcloned into pET-28a-CFP construct digested with *Nhe*I and *Bam*HI. The ligation reaction was transformed into XL-10 gold competent *E. coli* cells, propagated by overnight culture, purified by alkaline lysis, digested with *Nhe*I and *Xho*I and analysed by agarose gel electrophoresis. The pET-28a-CFP-*Hs*Arf6 $^{N\Delta13}$ construct was digested with *Nhe*I and *Xho*I (as opposed to *Nhe*I and *Bgl*II/BamHI) since ligation of the *Bgl*II and *Bam*HI overhangs resulted in a sequence which was not capable of digestion by either of the isoschizomers (*results not shown*). Theoretically, digestion of the pET-28a-CFP-*Hs*Arf6 $^{N\Delta13}$ construct by *Nhe*I and *Xho*I should result in two linearized bands representing the pET-28a vector (5369 bp) and the CFP-*Hs*Arf6 $^{N\Delta13}$ coding sequences (1203 bp). Two digestions products of approximately 1300 bp and 5500 bp were observed, which correlated with the predicted digestion pattern (**Figure 10B**). The pGEX-4T-2/hGGA3^{GAT} construct in **Figure 10C** was obtained as a DH5α *E. coli* bacterial stab which was propagated as an overnight culture. The pGEX-4T1-JIP4^{LZII}, pET-28a-ArfGAP1^{GAP} and pET-28a-ARNO^{Sec7} constructs were obtained as lyophilized powders, resuspended in water, transformed into XL-10 gold competent *E. coli* cells and propagated as overnight cultures. Constructs subcloned into pGEX-4T1/or 2 and pET-28a vectors were selected for with ampicillin and kanamycin respectively. Purified constructs were obtained from overnight cultures by alkaline lysis. Constructs were subjected to restriction digestion and analysed by agarose gel electrophoresis. The pGEX-4T-2/hGGA3^{GAT} construct was digested by *Sal*I and *Eco*RV. In principle, the diagnostic restriction digestion should have yielded two digestion products of 3169 bp and 2339 bp (**Figure 10C**). The actual diagnostic restriction digestion produced two digestion products of approximately 3200 bp and 2600 bp (**Figure 10D**) which correlated with the predicted digestion.

The pET-28a-ArfGAP1^{GAP} construct was digested with *Nhe*I and *Xho*I and produced two digestion products of approximately 450 bp and 5500 bp (**Figure 11A**). The digestion products correlated with the theoretical sizes of the ArfGAP1^{GAP} coding sequence (435 bp) and the pET-28a vector (5369 bp). Similarly, the pET-28a vector (5369 bp) and the ARNO^{Sec7} coding sequence (624 bp) bands expected for pET-28a-ARNO^{Sec7} construct digestion with *Nhe*I and *Xho*I agreed with the two digestions products of approximately 5500 bp and 600 bp observed (**Figure 11B**). Finally, digestion of the pGEX-4T1-JIP4^{LZII} construct with *Xho*I and *Bam*HI produced two DNA bands at 350 and 5000 bp, which likely represented the JIP4^{LZII} coding sequence (306 bp) and the pGEX-4T1 vector (4969 bp) respectively (**Figure 11C**).

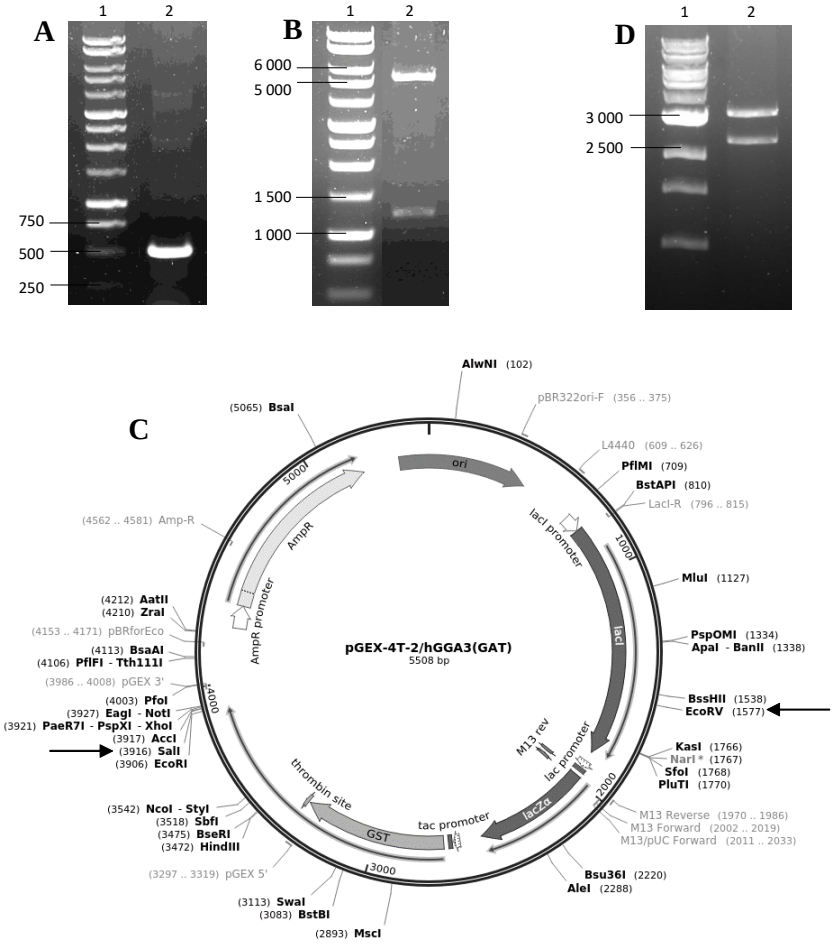

Figure 10: Diagnostic restriction digestions of the pET-28a-CFP-*Hs*Arf6 $^{N\Delta13}$ and pGEX-4T-2/hGGA3^{GAT} constructs. All PCR amplicons and diagnostic restriction digestion products were analysed on 0.8% (w/v) agarose gels run at 90V for approximately 1 hour. DNA bands were visualised under UV light and photographed. Lane 1: Promega 1kb DNA ladder was run alongside each sample (sizes in base pairs). **A**: Lane 2: PCR amplification of the *Hs*Arf6 $^{N\Delta13}$ coding sequence using pARF6-CFP construct as template. **B**: Lane 2: The *Hs*Arf6 $^{N\Delta13}$ coding sequence cloned into pET-28a-CFP and digested using *Xho*I and *Nhe*I. **C**: pGEX-4T-2/hGGA3^{GAT} construct map. **D**: Lane 2: The pGEX-4T-2/hGGA3^{GAT} construct digested using *Eco*RV and *Sal*I.

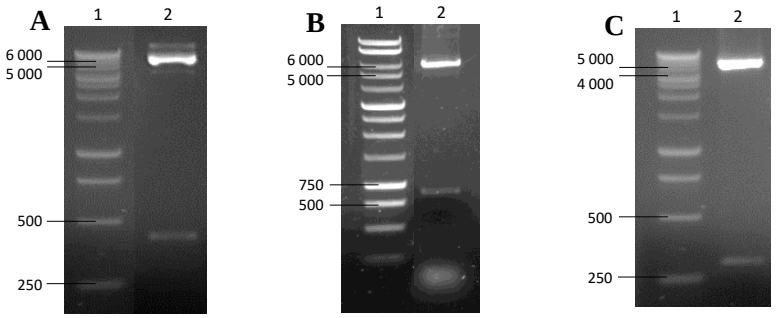

Figure 11: Diagnostic restriction digestions of the pET-28a-ARNO^{Sec7}, pET-28a-ArfGAP1^{GAP} and pGEX-4T1-JIP4^{LZII} constructs. All diagnostic restriction digestion products were analysed on 0.8% (w/v) agarose gels run at 90V for approximately 1 hour. Lane 1: Promega 1kb DNA ladder was run alongside each sample (sizes in base pairs). The restriction profiles were visualised under UV light and photographed. **A**: Lane 2: The pET-28a-ArfGAP1^{GAP} construct digested with *Nhe*I and *Xho*I. **B**: Lane 2: The pET-28a-ARNO^{Sec7} construct digested with *Nhe*I and *Xho*I. **C**: Lane 2: The pGEX-4T1-JIP4^{LZII} construct digested with *Bam*HI and *Xho*I.

Optimization of the small-scale expression of proteins used in the human Arf6 signalling assay. The expression constructs were transformed into T7 Express lysY/Iq competent *E. coli* cells and propagated as an overnight culture. Small-scale expression cultures were prepared by inoculating 8 mL Luria broth containing kanamycin or ampicillin with the overnight cultures. Once the expression cultures reached the exponential growth phase, protein expression was induced with IPTG. Induced *E. coli* cells were collected and lysed and the soluble and insoluble fractions analysed by SDS-PAGE. The approximate sizes of overexpressed proteins of interest were determined by preparing log (molecular weight) against the relative migration distance plots of the molecular weight ladder used (*results not shown*). The His-tagged $^{N\Delta13}$*Hs*Arf6 fusion protein had a predicted molecular weight of 22 kDa. An overexpressed protein of approximately 22 kDa was present in the induced soluble fraction of the small-scale expression profile of *E. coli* cells harbouring the pET-28a-CFP-*Hs*Arf6 $^{N\Delta13}$ construct (**Figure 12A** *indicated by arrow*). The overexpressed protein was not present in the uninduced soluble and insoluble fractions. The His-tagged human ARNO (Sec7 domain) fusion protein had a predicted molecular weight of 26 kDa. An overexpressed protein of approximately 25 kDa was present in the induced soluble fraction of the small-scale expression profile of *E. coli* cells harbouring the pET-28a-ARNO^{Sec7} construct (**Figure 12B** *indicated by arrow*). The overexpressed protein was not present in the uninduced soluble and insoluble fractions. The His-tagged human ArfGAP1 (GAP domain) fusion protein had a predicted molecular weight of 18 kDa. An overexpressed protein of approximately 17 kDa was present in the induced insoluble fraction (**Figure 12C** *indicated by left arrow*) of the small-scale expression profile of *E. coli* cells harbouring the pET-28a-ArfGAP1^{GAP} construct. A similar band was observed in the induced soluble fraction but was less prominent (**Figure 12C** *indicated by right arrow*). However, a less intensely stained band was also present in the uninduced soluble fraction in the same molecular weight range (**Figure 12C**). Thus, to confirm the presence of soluble His-tagged

ArfGAP1^{GAP} in the small-scale expression profile, the samples were analysed by western blotting. The proteins resolved on an SDS-PAGE gel were transferred to a nitrocellulose membrane and probed for His-tagged proteins using nickel-HRP followed by incubation in TMB membrane peroxidase substrate. While a more prominent band was observed in the insoluble fraction, His-tagged ArfGAP1^{GAP} was detected in the soluble fraction (**Figure 12D** *indicated by arrow*).

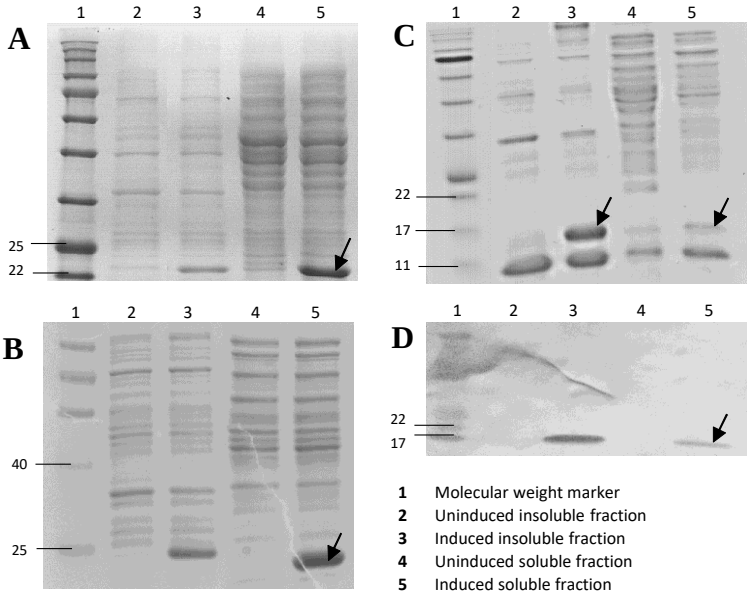

Figure 12: Small-scale protein expression of the His-tagged ArfGAP1^{GAP}, ARNO^{Sec7} and *Hs*Arf6$^{N\Delta13}$ proteins. All expression constructs were transformed into competent *E. coli* (T7 LysY/Iq) cells. Transformed cells were cultured at 37ºC until logarithmic growth phase. Protein expression was induced by 1 mM IPTG and was conducted at 37ºC for 4 hours. The uninduced and induced expression cultures were lysed and the soluble and insoluble fractions of each was separated by centrifugation. All fractions were prepared in SDS sample loading buffer and resolved on polyacrylamide gels run at 120V for approximately 1.5 hours. Lane 1: Molecular weight marker (sizes in kDa). Lane 2: Uninduced insoluble fraction. Lane 3: Induced insoluble fraction. Lane 4: Uninduced soluble fraction. Lane 5: Induced soluble fraction (proteins of interest *indicated by arrows*). **A**: His-tagged *Hs*Arf6$^{N\Delta13}$ samples. **B**: His-tagged ARNO^{Sec7} samples. **C**: His-tagged ArfGAP1^{GAP} samples. **D**: Western blot analysis of the ArfGAP1^{GAP} samples. Resolved proteins were transferred to a nitrocellulose membrane. The membrane was probed nickel-HRP and followed by incubation in TMB membrane peroxidase substrate.

The GST-tagged human GGA (GAT domain) fusion protein had a predicted molecular weight of 44 kDa. An overexpressed protein of approximately 42 kDa was present in the induced soluble fraction of the small-scale expression profile of *E. coli* cells harbouring the pGEX-4T-2/hGGA3^{GAT} construct (**Figure 13A** *indicated by top arrow*). An additional prominent band approximately 26 kDa in size was observed in the induced soluble fraction (**Figure 13A** *indicated by bottom arrow*) that was absent from the uninduced soluble fraction. The GST-tagged human JIP4 (LZII domain) fusion protein had a predicted molecular weight of 36 kDa. An overexpressed protein of approximately 34 kDa was present in the induced soluble fraction of the small-scale expression profile of *E. coli* cells harbouring the

pGEX-4T1-JIP4^{LZII} construct (**Figure 13C** *indicated by top arrow*). An additional prominent band approximately 26 kDa in size was observed in the induced soluble fraction (**Figure 13C** *indicated by bottom arrow*) that was absent from the uninduced soluble fraction. The hypothesis was that the additional bands represented truncated GST proteins since they correlated in size to GST. To test the hypothesis a western blot was conducted. The small-scale expression profile of GST-tagged GGA^{GAT} was resolved on an SDS-PAGE gel, transferred to a nitrocellulose membrane and probed for GST using anti-GST rabbit primary antibodies and anti-rabbit secondary antibodies conjugated to HRP. Although a band approximately 26 kDa in size cross-reacted with the anti-GST antibodies in all fractions, slightly larger GST-positive bands (42 kDa and 26 kDa) were observed only in the induced fractions, particularly the soluble fraction (**Figure 13B** *indicated by arrows*). These observations suggested that soluble GST fusion protein was subjected to proteolytic cleavage in the intact *E. coli* cells or degraded by released proteases in the lysate. In summary, the results indicated that sufficient quantities of each protein was expressed in soluble form to warrant large scale purification. However, additional protease inhibitors should be included during large scale purification of the GST-tagged GGA^{GAT} and JIP4^{LZII} recombinant proteins to prevent or reduce the amount of degraded GST fusion proteins in the final purified fraction.

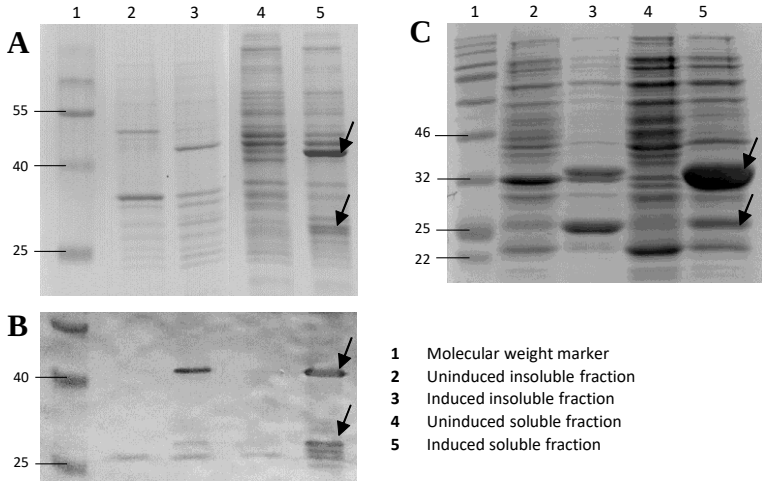

Figure 13: Small-scale protein expression of the GST-tagged JIP4^{LZII} and GGA^{GAT} proteins. All expression constructs were transformed into competent *E. coli* (T7 LysY/Iq) cells. Transformed cells were cultured at 37^{o}C until logarithmic growth phase. Protein expression was induced by 1 mM IPTG and was conducted at 37^{o}C for 4 hours. The uninduced and induced expression cultures were lysed and the soluble and insoluble fractions of each was separated by centrifugation. All fractions were prepared in SDS sample loading buffer and resolved on polyacrylamide gels run at 120V for approximately 1.5 hours. Lane 1: Molecular weight marker (sizes in kDa). Lane 2: Uninduced insoluble fraction. Lane 3: Induced insoluble fraction. Lane 4: Uninduced soluble fraction. Lane 5: Induced soluble fraction (proteins of interest *indicated by arrows*). **A**: GST-tagged GGA3^{GAT} samples. **B**: Western blot analysis of the GST-tagged GGA3^{GAT} samples. Resolved proteins were transferred to a nitrocellulose membrane. The membrane was probed with anti-GST rabbit primary antibodies and anti-rabbit HRP conjugated secondary antibodies followed by incubation in TMB membrane peroxidase substrate. **C**: GST-tagged JIP4^{LZII} samples.

Large scale purification of proteins used in the human Arf6 signalling assay. The optimal expression conditions determined during small-scale expression screening were adopted for large scale expression in 250 mL cultures. The *E.coli* harvested from the expression cultures were lysed, and the soluble and insoluble fractions separated. His-tagged ArfGAP1^{GAP}, ARNO^{Sec7} and *Hs*Arf6 $^{N\Delta13}$ were purified using Ni-NTA affinity chromatography while GST-tagged JIP4^{LZII} and GGA^{GAT} were purified using glutathione affinity chromatography. The purified proteins were desalted into assay buffer and the protein concentrations were determined by Bradford assay (using BSA standard curves of $R^2 > 0.99$). If necessary, the final fraction was concentrated by ultrafiltration, and the Bradford assay repeated. The purification profile was analysed by SDS-PAGE to assess the purity of the final, desalted fraction. The approximate sizes of purified proteins were determined by preparing log (molecular weight) against the relative migration distance plots of the molecular weight ladder used (*results not shown*). Proteins were routinely expressed and purified, and the average yields obtained are described below. Soluble His-tagged *Hs*Arf6 $^{N\Delta13}$ was purified and observed as a band approximately 22 kDa in size (**Figure 14A** *indicated by arrow*). Approximately 6.3 mg of was purified from a single 250 mL culture with negligible amounts of non-specific proteins in the desalted eluate (the polyacrylamide gel presented in **Figure 14A** contains samples from the purification profile of His-tagged *Hs*Arf6 $^{N\Delta13}$ that have been diluted for the purposes of preventing gel overloading and correctly sizing the bands). Soluble His-tagged ARNO^{Sec7} was purified and observed as a band approximately 24 kDa in size (**Figure 14B** *indicated by arrow*). Approximately 6.6 mg of His-tagged ARNO^{Sec7} was purified from a single 250 mL culture with negligible amounts of non-specific proteins in the desalted eluate. Soluble His-tagged ArGAP1^{GAP} was purified but required concentration for better detection by SDS-PAGE analysis. The concentrated desalted eluate of His-tagged ArGAP1^{GAP} was observed as a band approximately 16 kDa in size (**Figure 14C** *indicated by arrow*). Approximately 0.54 mg of His-tagged ArGAP1^{GAP} was purified from a single 250 mL culture with negligible amounts of non-specific proteins in the desalted eluate. Soluble GST-tagged GGA^{GAT} was purified and observed as a band approximately 40 kDa in size (**Figure 15A** *indicated by top arrow*). However, considerable amounts of free GST was present in the desalted eluate (**Figure 15A** *indicated by lower arrow*). Approximately 3.0 mg of GST-tagged GGA^{GAT} and free GST was detected in the desalted eluate in each routine purification. Soluble GST-tagged JIP4^{LZII} was purified and observed as a band approximately 31 kDa in size (**Figure 15B** *indicated by arrow*). Approximately 3.8 mg of GST-tagged JIP4^{LZII} was purified from a single 250 mL culture with negligible amounts of non-specific proteins in the desalted eluate.

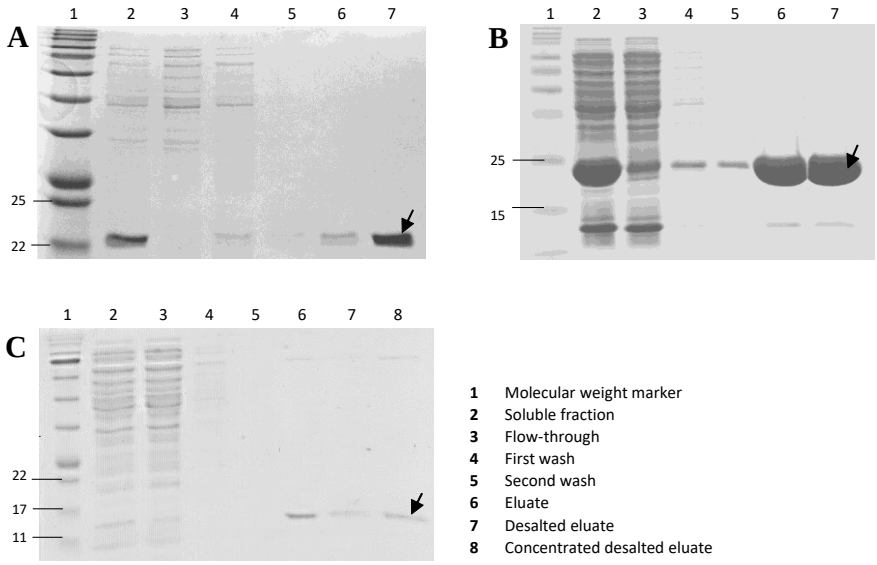

Figure 14: Purification of His-tagged ArfGAP1^{GAP}, ARNO^{Sec7} and *Hs*Arf6 $^{N\Delta13}$ by Ni-NTA affinity chromatography. All expression constructs were transformed into competent *E. coli* (T7 LysY/Iq) cells. Pre -cultures were grown until the logarithmic growth phase was reached and protein expression was induced using IPTG. The expression cultures incubated at 37^{o}C for 4 hours were lysed, and the soluble fractions were collected by centrifugation. His-tagged proteins were purified from the soluble fraction by Ni-NTA column chromatography and the purification profile was analysed by SDS-PAGE. For all gels Lane 1: Molecular weight marker (sizes in kDa). Lane 2: whole soluble fraction. Lane 3: flow-through. Lane 4: first wash. Lane 5: second wash. Lane 6: eluate. Lane 7: desalted eluate. **A**: His-tagged *Hs*Arf6 $^{N\Delta13}$. **B**: His-tagged ARNO^{Sec7}. **C**: His-tagged ArfGAP1^{GAP}.

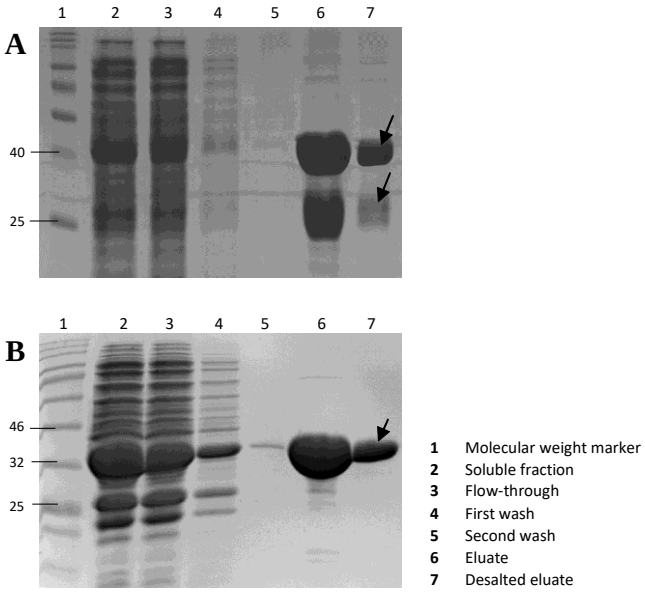

Figure 15: Purification of the GST-tagged JIP4^{LZII} and GGA^{GAT} by glutathione affinity chromatography. All expression constructs were transformed into competent *E. coli* (T7 LysY/Iq) cells. Pre -cultures were grown until the logarithmic growth phase was reached and protein expression was induced using IPTG. The expression cultures incubated at 37^{o}C for 4 hours were lysed, and the soluble fractions were collected by centrifugation. GST -tagged proteins were purified from the soluble fraction by glutathione affinity column chromatography and the purification profile was analysed by SDS-PAGE. For all gels Lane 1: Molecular weight marker (sizes in kDa). Lane 2: whole soluble fraction. Lane 3: flow-through. Lane 4: first wash. Lane 5: second wash. Lane 6: eluate. Lane 7: desalted eluate. **A**: GST-tagged GGA^{GAT}. **B**: GST-tagged JIP4^{LZII}.

Optimization of human Arf6 nucleotide exchange reaction. For the sake of simplicity, the His-tagged $^{N\Delta13}$*Hs*Arf6 recombinant protein will simply be referred to as $^{N\Delta13}$*Hs*Arf6. The inactive form will be referred to as $^{N\Delta13}$*Hs*Arf6-GDP and the active form $^{N\Delta13}$*Hs*Arf6-GTP. Since only active Arf GTPases bind effector proteins, it was necessary to prepare active $^{N\Delta13}$*Hs*Arf6-GTP for the interaction assay. It was also necessary to prepare inactive $^{N\Delta13}$*Hs*Arf6-GDP to serve as a negative control for the interaction assay. EDTA-mediated nucleotide exchange was conducted by incubating 1 µM $^{N\Delta13}$*Hs*Arf6 with 2 mM EDTA and 50 µM GDP/GTP at 25ºC for 60 minutes with gentle agitation. $^{N\Delta13}$*Hs*Arf6-GDP and $^{N\Delta13}$*Hs*Arf6-GTP complexes were stabilised by the addition of 3 mM $MgCl_2$ and incubating the reaction mixtures for an additional 5 minutes at 25ºC with gentle agitation. Nucleotide exchange was assessed by intrinsic tryptophan fluorescence (excitation at 298 nm and emission at 340 nm) as an end-point reading since the samples could not be continuously agitated in the available plate reader. There was no significant difference in the intrinsic tryptophan fluorescence between $^{N\Delta13}$*Hs*Arf6 incubated with GDP and $^{N\Delta13}$*Hs*Arf6 incubated with GTP (ρ = 0.8538, n = 3) (**Figure 16A**). This result suggested that nucleotide exchange did not occur. It was hypothesized that a higher concentration of EDTA may better promote the dissociation of nucleotides bound to $^{N\Delta13}$*Hs*Arf6 after purification from *E. coli* cells. Furthermore, Padovani *et al*. (2013) suggested that nucleotide exchange of $^{N\Delta13}$*Hs*Arf6 is better promoted at 37ºC. Therefore, EDTA-mediated nucleotide exchange was promoted by incubating 1 µM $^{N\Delta13}$*Hs*Arf6 with 5 mM EDTA and 50 µM GDP/GTP at 37ºC for 60 minutes with gentle agitation. $^{N\Delta13}$*Hs*Arf6-GDP and $^{N\Delta13}$*Hs*Arf6-GTP complexes were stabilised by the addition of 20 mM $MgCl_2$ and incubating the reaction mixtures for an additional 5 minutes at 37ºC with gentle agitation. The difference in intrinsic tryptophan fluorescence between $^{N\Delta13}$*Hs*Arf6 incubated with GDP and $^{N\Delta13}$*Hs*Arf6 incubated with GTP was statistically significant (ρ = 0.001, n = 3) **(Figure 16B)**. This result suggested that $^{N\Delta13}$*Hs*Arf6-GDP and $^{N\Delta13}$*Hs*Arf6-GTP complexes were formed. Nucleotide exchange of $^{N\Delta13}$*Hs*Arf6 was reproducible using the abovementioned methods and was used for the remainder of the study. $^{N\Delta13}$*Hs*Arf6-GDP and $^{N\Delta13}$*Hs*Arf6-GTP were either prepared immediately before use in a subsequent assay or were stored at -20ºC until use.

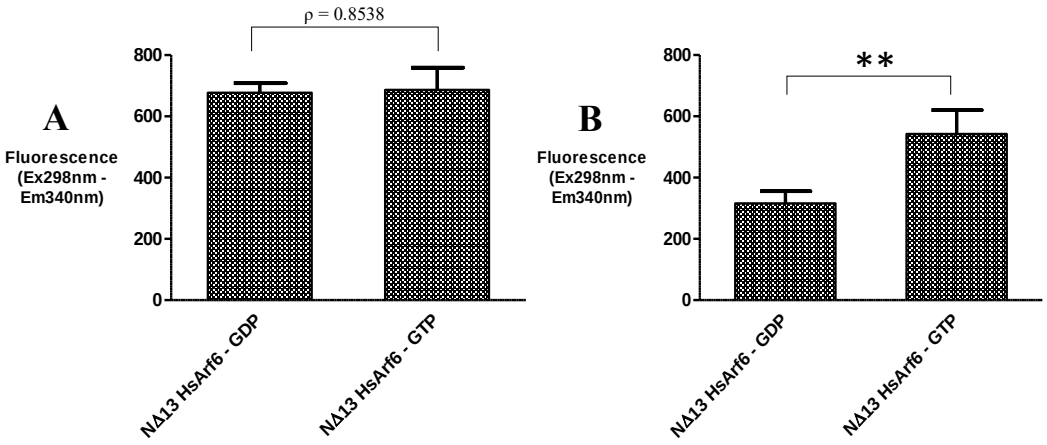

Figure 16: EDTA-mediated nucleotide exchange of $^{N\Delta13}$*Hs*Arf6 measured by tryptophan fluorescence. Nucleotide exchange was conducted by incubating 1 μM $^{N\Delta13}$*Hs*Arf6 in GDP/GTP in the presence of EDTA for 60 minutes with gentle agitation. $^{N\Delta13}$*Hs*Arf6-GDP and $^{N\Delta13}$*Hs*Arf6-GTP complexes were stabilised by incubating the reactions with excess $MgCl_2$ for 5 minutes with gentle agitation. Intrinsic tryptophan fluorescence was measured as an end-point reading in a plate reader at an excitation wavelength of 298 nm and an emission wavelength of 340 nm. **A**: Nucleotide exchange on $^{N\Delta13}$*Hs*Arf6 was not promoted at 25°C using 2 mM EDTA, 50 μM GDP/GTP and 3 mM $MgCl_2$ since a discernible difference in intrinsic tryptophan fluorescence was not observed ($\rho = 0.8538$). **B**: Nucleotide exchange on $^{N\Delta13}$*Hs*Arf6 was promoted at 37°C using 5 mM EDTA, 50 μM GDP/GTP and 20 mM $MgCl_2$ since a discernible difference in intrinsic tryptophan fluorescence was observed ($\rho < 0.01$). Each bar represents the mean and standard deviation of readings obtained from 3 replicate wells (n = 3).

Optimization of the immobilized human Arf6-GGA interaction assay. For the purposes of medium to high-throughput screening it is important to establish the minimal amount of interacting proteins required to produce robust signals in the assay format in order to reduce the demand for purified recombinant proteins. In addition, before embarking on the establishment of the Arf6 activation assay, it was important to control that the nickel-coated plates used were capable of capturing His-tagged proteins and that GST enzyme activity could be robustly detected using our intended protocol and reagents. To determine the minimal concentration of active GST required to produce a signal that is significant from background interference, a range of GST concentrations were tested in the assay format. A His-tagged GST fusion protein (hereafter referred to as His-GST) (prepared by L. Wambua, M.Sc. dissertation) was used for immobilization of GST to the pre-blocked nickel plate. To the nickel plate, 1, 2 and 5 μM His-GST were added in technical triplicate. The negative control lacking His-GST (although, in hindsight, using equivalent amounts of GST would have been a more appropriate control) was included to determine background noise. The reactions were incubated on the plate, removed and the wells washed several times. GST substrate (containing CDNB and GSH) was incubated in the wells for 30 minutes and the GS-DNB conjugation product produced by active immobilised GST was detected as an end-point absorbance reading of 340 nm. The GST signal for 1 μM His-GST ($\rho = 0.0018$, n =3), 2 μM His-GST ($\rho = 0.0008$, n = 3), 5 μM His-GST ($\rho = 0.0015$, n = 3) were all statistically significantly

different from the background control lacking GST and produced high absorbance readings (**Figure 17A**). This result suggested that 1 µM of GST-tagged GGA^{GAT} (hereafter referred to as GST-GGA^{GAT}) bound to immobilised $^{N\Delta13}$*Hs*Arf6 could potentially provide robust signals. To test the hypothesis that 1 µM of GST-GGA^{GAT} bound to immobilised $^{N\Delta13}$*Hs*Arf6 could provide robust signals, the interaction assay was conducted using 1 µM immobilised $^{N\Delta13}$*Hs*Arf6-GTP against a range of GST-GGA^{GAT} concentrations. Based on the stoichiometry of Arf6-GGA interaction (one Arf6 molecule binds to one GGA molecule), it was decided to use the range of 1, 2 and 5 µM GST-GGA^{GAT}. The assay was conducted under the conditions which would subsequently be used for the remainder of the study. In triplicate, 1 µM $^{N\Delta13}$*Hs*Arf6-GTP was immobilised to the nickel-coated plate by incubating for 30 minutes at 4ºC with gentle agitation. The background control wells consisted of assay buffer lacking $^{N\Delta13}$*Hs*Arf6-GTP, added in triplicate. Subsequently, a final concentration of 1, 2 and 5 µM GST-GGA^{GAT} was added to the experimental wells, while a final concentration of 5 µM GST-GGA^{GATA} was added to the background control. $^{N\Delta13}$*Hs*Arf6-GTP and GST-GGA^{GAT} binding was conducted by incubating for 90 minutes at 4ºC with gentle agitation. All solutions were removed, the plate washed several times, GST substrate solution was added and left to incubate for 30 minutes at room temperature before the absorbance at 340 nm was measured. The GST signals for 1 µM GST-GGA^{GAT} ($\rho = 0.0041$, $n = 3$), 2 µM GST-GGA^{GAT} ($\rho = 0.0014$, $n = 3$) and 5 µM GST-GGA^{GAT} ($\rho = 0.0019$, $n = 3$) were all statistically significantly higher than those obtained in the background control wells (**Figure 17B**). Furthermore, the difference in the GST signal between 1 µM and 5 µM GST-GGA^{GAT} was not statistically significant ($\rho = 0.6965$, $n = 3$) (**Figure 17B**). This suggested that any excess use of GST-GGA^{GAT} would not significantly improve the strength of the signal. The result indicated that 1 µM of immobilised $^{N\Delta13}$*Hs*Arf6-GTP interacting with 1 µM GST-GGA^{GAT} was sufficient to produce robust signals in the interaction assay format adopted. These conditions were used in the remainder of the study. The only modification was the reduction of the final concentration of GST-GGA^{GAT} used in the background control to 1 µM so that it would be directly comparable to the experimental wells. The final validation for the development of the immobilised Arf6-GGA interaction assay was to determine whether the assay could distinguish inactive $^{N\Delta13}$*Hs*Arf6-GDP from active $^{N\Delta13}$*Hs*Arf6-GTP. The assay was conducted according to the optimized conditions using $^{N\Delta13}$*Hs*Arf6-GDP and $^{N\Delta13}$*Hs*Arf6-GTP as bait proteins. The difference in the signals measured for inactive $^{N\Delta13}$*Hs*Arf6-GDP and active $^{N\Delta13}$*Hs*Arf6-GTP were statistically significant ($\rho = 0.004$, $n = 3$) (**Figure 17C**). This suggested that the novel assay concept was functional and that the immobilised $^{N\Delta13}$*Hs*Arf6 and GST-GGA^{GAT} interaction could indicate the activation status of $^{N\Delta13}$*Hs*Arf6.

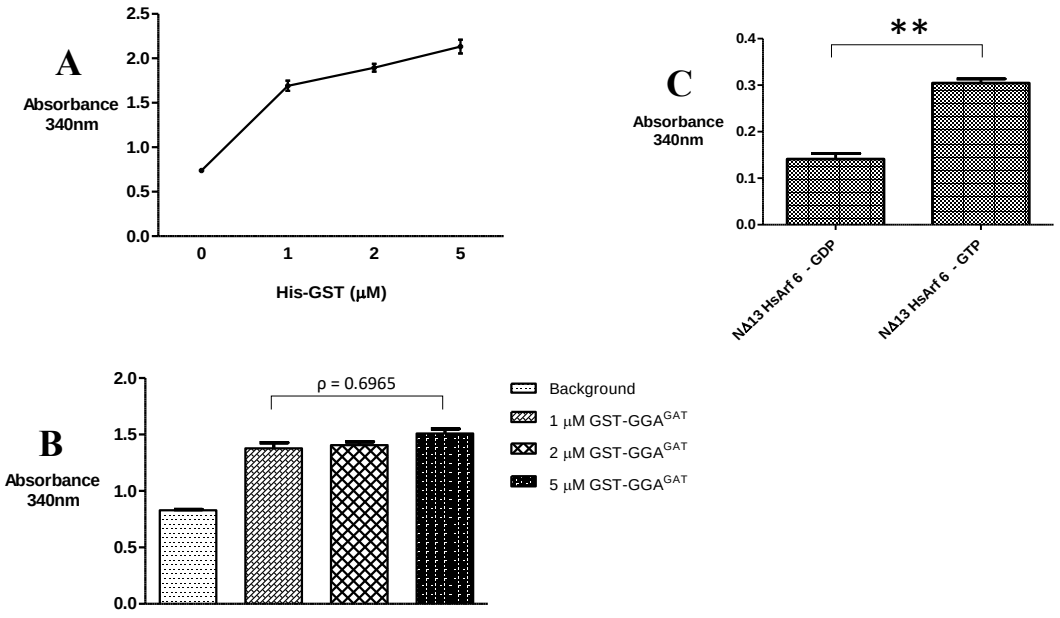

Figure 17: The Ni-NTA immobilised *Hs*Arf6-GGA interaction assay can distinguish inactive and active *Hs*Arf6. **A**: The concentration of GST required to provide a significant signal to background ratio was assessed by incubating 0 (background control), 1, 2 and 5 μM His-GST on the nickel-coated plate. The signals for 1 μM, 2 μM and 5 μM His-GST ($\rho < 0.01$) were all statistically significant from the background reaction lacking His-GST. **B**: The concentration of GST-GGA^{GAT} required to provide a significant signal to background ratio in the Ni-NTA immobilised *Hs*Arf6-GGA interaction assay. The background control lacked $^{N\Delta13}$*Hs*Arf6-GTP and was incubated with a final concentration of 5 μM GST-GGA^{GAT}. The signals for 1 μM, 2 μM and 5 μM GST-GGA^{GAT} ($\rho < 0.01$) were all statistically significantly higher than those from the background control. The difference in the GST signal between 1 μM and 5 μM GST-GGA^{GAT} was not statistically significant ($\rho = 0.6965$). **C**: The Ni-NTA immobilised *Hs*Arf6-GGA interaction assay using active and inactive $^{N\Delta13}$*Hs*Arf6. The background control lacked $^{N\Delta13}$*Hs*Arf6 and was incubated with a final concentration of 1 μM GST-GGA^{GAT}. The GST signals were corrected by the average background readings. The difference in the signals measured for inactive $^{N\Delta13}$*Hs*Arf6-GDP and active $^{N\Delta13}$*Hs*Arf6-GTP were statistically significant ($\rho < 0.01$). Each bar represents the mean and standard deviation of readings obtained from 3 replicate wells.

ARNO-mediated activation of Arf1, but not of Arf6, was capable of detection by the immobilised Arf-GGA interaction assay. Since the immobilised human Arf6-GGA interaction could distinguish the activation status of $^{N\Delta13}$*Hs*Arf6 chemically pre-loaded with GDP/GTP, the next question was whether the assay could distinguish the activation status of $^{N\Delta13}$*Hs*Arf6 following ArfGEF-mediated activation. To investigate this possibility the Sec7 domain of the ArfGEF, ARNO was used. The ARNO^{Sec7}-mediated activation assay was conducted by incubating 1 μM $^{N\Delta13}$*Hs*Arf6-GDP with 0.1 μM ARNO^{Sec7} in the presence of 100 μM GTP for 30 minutes at 28ºC with gentle agitation. A negative control was conducted under the same conditions except that ARNO^{Sec7} was omitted. The reactions were transferred to a nickel plate and the immobilised Arf6-GGA interaction assay conducted as usual. Since *in vitro* ARNO-mediated GDP/GTP exchange on Arf6 is typically demonstrated alongside Arf1 (owing to the greater activation observed on Arf1) it was decided to use $^{N\Delta17}$*Hs*Arf1 as a control. The pET-28a-CFP-*Hs*Arf1$^{N\Delta17}$ construct (**Figure S37A**) - previously prepared by T.Swart (PhD, thesis in preparation)

and provided for this study, was transformed into competent T7 Express lysY/Iq *E. coli* cells. The *E. coli* cells harbouring the construct were used for large scale expression and purification of $^{N\Delta17}$*Hs*Arf1 (**Figure S37B**). $^{N\Delta17}$*Hs*Arf1 was pre-loaded with GDP (**Figure S37C**). The ARNO^{Sec7}-mediated activation assay was conducted as described above using $^{N\Delta13}$*Hs*Arf6-GDP and $^{N\Delta17}$*Hs*Arf1-GDP. The reactions were transferred to a nickel plate and the immobilised Arf6-GGA interaction assay conducted as usual. The difference in the signals measured for $^{N\Delta17}$*Hs*Arf1-GDP incubated with GTP in the presence of ARNO^{Sec7} were statistically significant from those obtained where $^{N\Delta17}$*Hs*Arf1-GDP was incubated with GTP in the absence of ARNO^{Sec7} ($\rho = 0.002$, n =3) (**Figure 18A**). This result suggested that the activation of $^{N\Delta17}$*Hs*Arf1-GDP was a result of ARNO^{Sec7} catalytic activity (stimulation of GDP/GTP exchange on the Arf1 protein). Although higher signals were obtained for the reaction containing ARNO, the difference failed to reach statistical significance ($\rho = 0.0622$, n =3) (**Figure 18B**). Even though **Figure 18B** represents a single biological replicate, the statistically significance varied between replicates and thus it could not be concluded that the apparent activation of $^{N\Delta13}$*Hs*Arf6-GDP was mediated by of ARNO^{Sec7}, nor could the assay be reliably repeated.

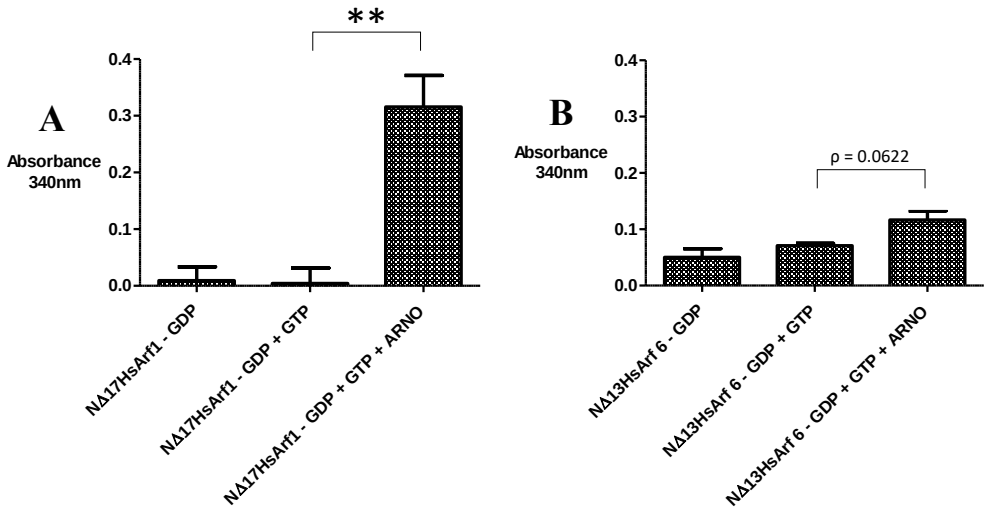

Figure 18: The Ni-NTA immobilised *Hs*Arf-GGA interaction assay can detect ARNO-mediated activation of human Arf1 but not Arf6. As a negative control *Hs*Arf-GDP was incubated alone. As a spontaneous GDP/GTP exchange control *Hs*Arf6-GDP was incubated with only GTP. In the experiment *Hs*Arf-GDP was incubated with GTP in the presence of ARNO^{Sec7}. The immobilised *Hs*Arf-GGA interaction assay was employed to detect the activation status of *Hs*Arf-GDP following ArfGEF mediated activation. **A**: The difference in GST signals measured for $^{N\Delta17}$*Hs*Arf1-GDP incubated with GTP in the presence of ARNO^{Sec7} were statistically significantly higher from those obtained where $^{N\Delta17}$*Hs*Arf1-GDP was incubated with GTP in the absence of ARNO^{Sec7} ($\rho < 0.01$). **B**: A representative example of several biological replicates. The difference in GST signals measured for $^{N\Delta13}$*Hs*Arf6-GDP incubated with GTP in the presence of ARNO^{Sec7} were usually not statistically different from those obtained where $^{N\Delta13}$*Hs*Arf6-GDP was incubated with GTP in the absence of ARNO^{Sec7} ($\rho = 0.0622$). Each bar represents the mean and standard deviation of readings obtained from 3 replicate wells.

Human ArfGAP1 deactivation of Arf6 was detectable in the Arf6-GGA interaction assay. Since the immobilised human Arf6-GGA interaction could distinguish the activation status of $^{N\Delta13}$*Hs*Arf6 chemically pre-loaded with GDP/GTP, the next question was whether the assay could distinguish the activation status of $^{N\Delta13}$*Hs*Arf6 following ArfGAP stimulated deactivation (hydrolysis of the Arf-bound GTP to GDP). To investigate this possibility the GAP domain of ArfGAP1 was used. The ArfGAP1^{GAP} deactivation assay was conducted by incubating 1 μM $^{N\Delta13}$*Hs*Arf6-GTP with 0.1 μM ArfGAP1^{GAP} for 30 minutes at 28^{o}C with gentle agitation. The initial study showed an apparent decrease in the absorbance at 340nm (i.e. GST-GGA^{GAT} binding) where $^{N\Delta13}$*Hs*Arf6-GTP was incubated with ArfGAP1^{GAP} (*results not shown*). To further explore the possibility that ArfGAP1^{GAP} was deactivating $^{N\Delta13}$*Hs*Arf6-GTP, higher concentrations of ArfGAP1^{GAP} (0.1, 0.15 and 0.20 μM) were used and the assay repeated. Decreases in Arf6-GGA binding, in comparison the positive control ($^{N\Delta13}$*Hs*Arf6-GTP in the absence of ArfGAP1^{GAP}) showed that 0.15 μM and 0.20 μM ArfGAP1^{GAP} significantly deactivated $^{N\Delta13}$*Hs*Arf6-GTP ($\rho = 0.004$ and $\rho = 0.0001$ respectively, n = 3 for both *t*-tests) (**Figure 19A**). However, further validation of the deactivation studies was crucial since during the immobilisation of $^{N\Delta13}$*Hs*Arf6-GTP to the nickel-coated plate, it was possible that the His-tagged ArfGAP1^{GAP} may also bind to the nickel coated wells and compete with the Arf protein for binding. This would result in an artefactual decrease in Arf6 concentration and GST-GGA^{GAT} immobilisation in the plate wells. To interrogate whether the decrease in Arf6-GGA interaction signal was owing to the ArfGAP1^{GAP}-stimulated GTP hydrolysis of $^{N\Delta13}$*Hs*Arf6-GTP or simply the displacement of a proportion of $^{N\Delta13}$*Hs*Arf6-GTP by ArfGAP1^{GAP} bound to the nickel plate, validation studies were conducted using an ArfGAP1 inhibitor QS11. For validation of the ArfGAP1^{GAP} mediated deactivation of $^{N\Delta13}$*Hs*Arf6-GTP, three reactions were prepared in conjunction with the background control (wells incubated with GST-GGA^{GAT}). In the positive control $^{N\Delta13}$*Hs*Arf6-GTP was incubated alone. In the negative control $^{N\Delta13}$*Hs*Arf6-GTP was incubated with 0.15 μM ArfGAP1^{GAP} in the absence of QS11, whereas in the experiment they were incubated in the presence of 50 μM QS11. The assay was conducted, in triplicate, as previously described. The deactivation of $^{N\Delta13}$*Hs*Arf6-GTP was inhibited by QS11 ($\rho = 0.004$, n = 3) (**Figure 19B**). This result suggested that the decrease in Arf6-GGA interaction signals was as a result of ArfGAP1^{GAP}-stimulated GTP hydrolytic activity.

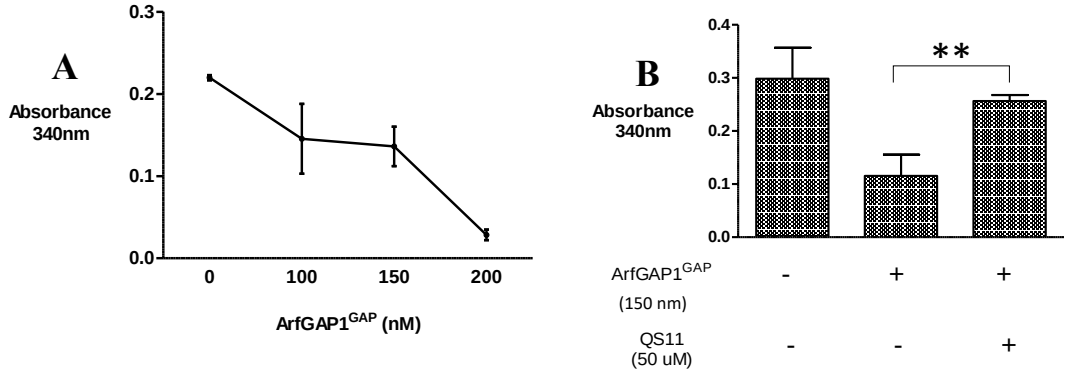

Figure 19: The immobilised *Hs*Arf6-GGA interaction assay can detect ArfGAP1-mediated deactivation of *Hs*Arf6. *Hs*ArfGAP1^{GAP} -stimulated GTP hydrolysis of $^{N\Delta13}$*Hs*Arf6 -GTP was conducted by incubating $^{N\Delta13}$*Hs*Arf6-GTP with *Hs*ArfGAP1^{GAP}. The immobilised *Hs*Arf6 -GGA interaction assay was employed to detect the activation status of $^{N\Delta13}$*Hs*Arf6 following *Hs*ArfGAP1^{GAP}-stimulated deactivation. As a positive control $^{N\Delta13}$*Hs*Arf6-GTP incubated without *Hs*ArfGAP1^{GAP} was used. **A**: To determine the concentration of *Hs*ArfGAP1^{GAP} required to significantly reduce *Hs*Arf6 -GGA binding 100, 150 and 200 nm *Hs*ArfGAP1^{GAP} was incubated with 1 µM $^{N\Delta13}$*Hs*Arf6-GTP. *Hs*Arf6-GGA binding was significantly reduced by 150 nM *Hs*ArfGAP1^{GAP} ($\rho < 0.01$) and 200 nM *Hs*ArfGAP1^{GAP} ($\rho < 0.01$). **B**: Chemical validation of *Hs*ArfGAP1^{GAP} GTP hydrolytic activity. Deactivation was conducted by incubating 1 µM $^{N\Delta13}$*Hs*Arf6-GTP with 150 nM *Hs*ArfGAP1^{GAP} in the presence or absence of 50 µM QS11. The difference in GST signals between *Hs*ArfGAP1^{GAP} deactivation of $^{N\Delta13}$*Hs*Arf6-GTP in the presence and absence of QS11 was statistically significant ($\rho < 0.01$). Each bar represents the mean and standard deviation of readings obtained from 3 replicate wells.

JIP4 can distinguish human Arf6 from human Arf1 in the immobilised Arf-GGA interaction assay. Membrane-tethered membrane type 1-matrix metalloproteinase (MT1-MMP) is a key protease in collagen breakdown which contributes to the degradation of the extracellular matrix and subsequent cancer cell migration. MT1-MMP is delivered to the surface of tumour cells in regulated secretory vesicles. The interaction between JNK cascade kinase 4 (JIP4) and Arf6 is considered a critical regulator of this cellular process and thus the interaction is a prominent target for the inhibition of cancer cell invasion and metastasis (Marchesin *et al.,* 2015*).* To investigate whether the immobilised Arf6 assay could be employed in development of an Arf6-JIP4 interaction assay to screen for novel cancer therapeutics GST-JIP4^{LZII} was used. The assay was conducted as previously described using $^{N\Delta17}$*Hs*Arf1 and $^{N\Delta13}$*Hs*Arf6 as bait proteins (Arf1 was used as a negative control to control for the specificity of JIP4 for Arf6) but where GST-GGA^{GAT} was replaced with GST-JIP4^{LZII}. The difference is GST signals between $^{N\Delta17}$*Hs*Arf1-GTP and $^{N\Delta13}$*Hs*Arf6-GTP was statistically significant ($\rho = 0.0001$, n =3) which indicated that JIP4^{LZII} could distinguish between active Arf1 and active Arf6. In addition, the statistically significant difference in GST signal between $^{N\Delta13}$*Hs*Arf6-GDP and $^{N\Delta13}$*Hs*Arf6-GTP ($\rho = 0.0009$, n =3) supported the fact that JIP4^{LZII} binds only to active Arf6 (**Figure 20**). It also suggested that the assay format may be useful for determining the Arf-specificity and comparative binding affinities of effector proteins.

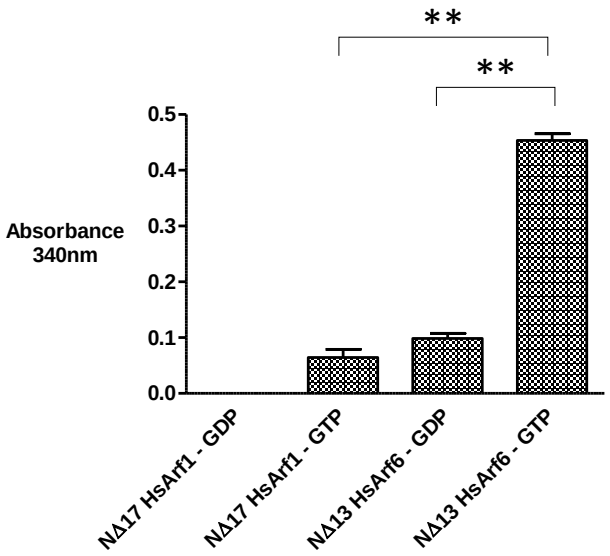

Figure 20: The immobilised Arf6 interaction assay can detect binding of the Arf6 specific effector protein JIP4. The immobilised *Hs*Arf interaction assay was conducted using purified GST-JIP4^{LZII} as an alternative, Arf6 -specific effector protein. Active and inactive $^{N\Delta13}$*Hs*Arf6 and $^{N\Delta17}$*Hs*Arf1 were used a bait proteins. GST-JIP4L^{ZII} has greater binding affinity for active Arf6 than active Arf1 ($\rho < 0.01$). GST-JIP4L^{ZII} also has lower binding affinity to inactive Arf6 than active Arf6 ($\rho < 0.01$). Each bar represents the mean and standard deviation of readings obtained from 3 replicate wells.

Optimization of an alternative glutathione plate-based human Arf6-JIP4 interaction assay. The reverse assay format where the GST-tagged effector protein was used as an immobilised bait protein on glutathione-coated plates to capture the His-tagged Arf6 was investigated as an alternative assay with greater sensitivity. In this scenario, binding of $^{N\Delta13}$*Hs*Arf6-GTP to the immobilised effector protein would be detected using nickel conjugated HRP and a colorimetric HRP substrate. Although it was originally hypothesized that the assay could be developed using GST-GGA^{GAT} as a suitable effector protein, it was later speculated that the considerable amount of free GST in the GST-GGA^{GAT} purified fraction (**Figure 15A**) would adversely affect the signal outputs in the alternative assay format by competing for glutathione binding sites on the plate. Theoretically, free GST could also be immobilised to the glutathione coated plate, thus reducing the amount of the GST-GGA^{GAT} bait protein immobilised on the glutathione plate. While the greater sensitivity of the assay signal may compensate for the competitive binding of free GST to the plate, it was decided to conduct the initial optimization of the assay using GST-JIP4^{LZII}. To determine whether Nickel-HRP could detect His-tagged proteins captured on glutathione plates, a range of His-tagged GST (His-GST) concentrations were tested in the assay format which was used for the reminder of the study. To a pre-blocked glutathione plate, a range of His-GST solutions prepared in assay buffer were added to the plate in technical triplicate. The background control lacked His-GST. His-GST was immobilised by incubating for 60 minutes at 25^{o}C with gentle agitation. The protein solutions were removed, and the wells washed three times. Nickel-HRP in

blocking buffer was added to each well and incubated for 60 minutes at 25ºC before being removed from the wells and washed three times. Nickel-HRP bound to His was detected by incubating in TMB substrate solution for 30 minutes at room temperature. The chromogenic oxidation product of TMB was measured as an end-point reading at an absorbance of 630 nm. The signals for 0.1 μM His-GST (ρ = 0.0027, n =3), 0.5 μM His-GST (ρ = 0.0001, n =3), 1 μM His-GST (ρ = 0.0029, n =3), 2 μM His-GST (ρ = 0.0003, n =3) and 5 μM His-GST (ρ = 0.0022, n =3) were all statistically significantly different from the background reaction lacking His-GST. There was no statistically significant difference in the signals between 0.5 μM and 5 μM His-GST (ρ = 0.2214, n =3) (**Figure 21A**). Taken together, the results suggested that 0.5 μM of GST-tagged effector protein was sufficient to produce a robust signal.

To determine the concentration of $^{N\Delta13}$*Hs*Arf6-GTP required to produce significant interaction signals, 1 μM of the effector protein GST-JIP4^{LZII} was used. A range of 0.1, 0.5, 1.0 and 2 μM $^{N\Delta13}$*Hs*Arf6-GTP concentrations were incubated with 1.0 μM GST-JIP4^{LZII} for 30 minutes at 25ºC with gentle agitation. The protein solutions were transferred to the glutathione plate alongside a background control containing only 2 μM $^{N\Delta13}$*Hs*Arf6-GTP. The assay was continued as previously described. Only the signals for 1 μM $^{N\Delta13}$*Hs*Arf6-GTP (ρ = 0.0203, n =3) and 2 μM $^{N\Delta13}$*Hs*Arf6-GTP (ρ = 0.0006, n =3) were statistically significantly higher than the background reaction which lacked GST-JIP4^{LZII} (**Figure 21B**). The assay was thereafter conducted using 1.0 μM GST-JIP4^{LZII} and 2 μM $^{N\Delta13}$*Hs*Arf6-GTP.

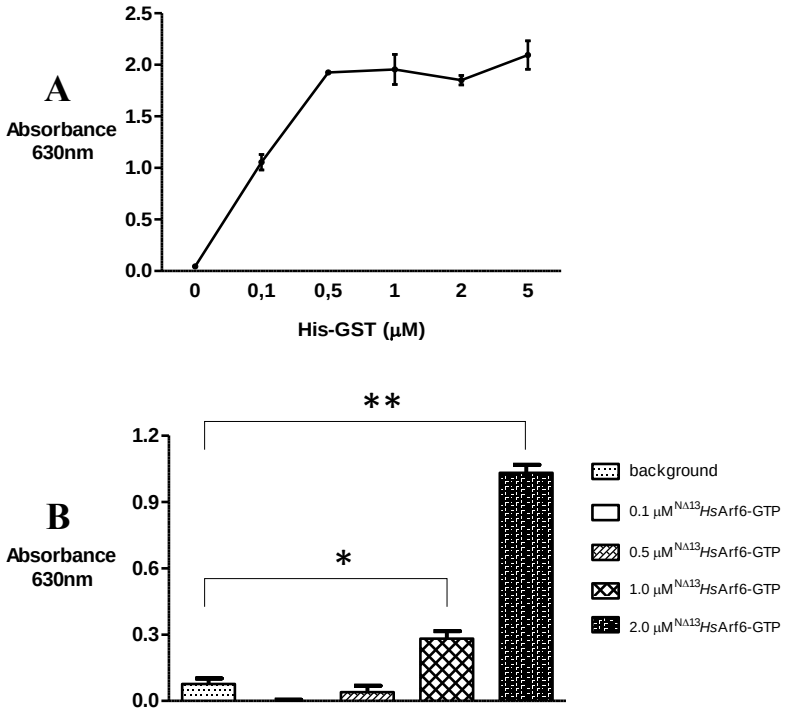

Figure 21: Optimization of the glutathione immobilised JIP4-*Hs*Arf6 interaction assay. **A**: The concentration of histidine tag required to provide a significant signal to background ratio in the HRP assay format was assessed by incubating 0 (background control), 0.1, 0.5, 1.0, 2.0 and 5.0 µM His-GST on the glutathione-coated plate. The signals for 0.1 µM, 0.5 µM, 1 µM, 2 µM and 5 µM His-GST ($\rho < 0.01$) were all statistically significantly different from the background reaction lacking His-GST. However, there was no statistically significant difference in the signals between 0.5 µM and 5.0 µM His-GST ($\rho = 0.2214$). **B**: The concentration of GST-JIP4^{LZII} required to provide a significant signal to background ratio in the interaction assay was determined by incubating 0.5 µM $^{N\Delta13}$*Hs*Arf6-GTP with 0.1, 0.5, 1.0 or 2.0 µM GST-JIP4^{LZII}. The background control lacked $^{N\Delta13}$*Hs*Arf6-GTP and was incubated with a final concentration of 5 µM GST-JIP4^{LZII}. Only the signals for 1 µM $^{N\Delta13}$*Hs*Arf6-GTP ($\rho < 0.05$) and 2 µM $^{N\Delta13}$*Hs*Arf6-GTP ($\rho < 0.01$) were statistically significantly different from the background reaction. Each bar represents the mean and standard deviation of readings obtained from 3 replicate wells.

The immobilised JIP4 -*Hs*Arf6 interaction is detectable on a glutathione plate, but not the immobilised GGA -*Hs*Arf6 interaction. Two final hypotheses were tested concurrently. Firstly could the assay distinguish active and inactive forms of $^{N\Delta13}$*Hs*Arf6? Secondly could the assay produce interaction assay signals using GST-GGA^{GAT} as the effector protein despite the excess free GST present in the purified GST-GGA^{GAT} fraction? The assay was therefore conducted using 2 µM $^{N\Delta13}$*Hs*Arf6-GDP and 2 µM $^{N\Delta13}$*Hs*Arf6-GTP against 1 µM GST-GGA^{GAT} or 1 µM GST-JIP4^{LZII}. The assay was conducted as previously described. Active Arf6 was not distinguishable from inactive Arf6 in the immobilised GGA-Arf6 interaction assay on a glutathione plate (ρ = 0.9064, n =3). However, active Arf6 was robustly distinguishable from inactive Arf6 in the immobilised JIP4-Arf6 interaction assay on a glutathione plate (ρ = 0.0013, n =3) (**Figure 22**). As previously hypothesized, the result suggested that the excess free GST may have hindered the immobilization of sufficient amounts GST-GGA^{GAT} to the glutathione coated plate. Ultimately this suggested that the reverse assay was viable when GST-JIP4^{LZII} was used as an effector protein for Arf6.

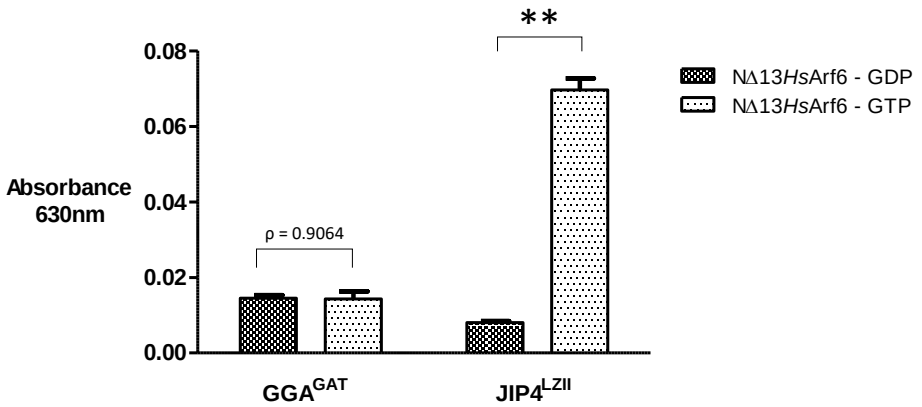

Figure 22: Active and inactive Arf6 can be distinguished by the glutathione immobilised JIP4-*Hs*Arf6 interaction assay, but not the GGA-*Hs*Arf6 interaction assay. The glutathione immobilised *Hs*Arf6 interaction assay was conducted using GST-GGA^{GAT} and GST-JIP4^{LZII} as prey proteins while active and inactive forms of $^{N\Delta13}$*Hs*Arf6 were used as bait proteins. Active, $^{N\Delta13}$*Hs*Arf6 -GTP, is not distinguishable from inactive, $^{N\Delta13}$*Hs*Arf6 -GDP in the glutathione immobilised *Hs*Arf6 interaction assay format (ρ = 0.9064). Active Arf6 is distinguishable from inactive Arf6 in the immobilised JIP4-Arf6 interaction assay on a glutathione plate (ρ < 0.01). Each bar represents the mean and standard deviation of readings obtained from 3 replicate wells.

4.4. Discussion and future work

The aim of the study was to develop a robust, immobilised Arf6 interaction assay that could be employed for high-throughput screening (HTS) of compound libraries to identify novel inhibitors of Arf-effector, Arf-ArfGEF and Arf-ArfGAP interactions at a cost-effective rate.

The immobilised *Hs*Arf6-GGA interaction assay was developed, and subsequently used to measure ARNO^{Sec7}-mediated GDP/GTP exchange on *Hs*Arf1 and *Hs*ArfGAP1^{GAP}-stimulated GTP hydrolysis on *Hs*Arf6 thus extending the assay format as a tool to screen drugs for inhibitory effects on Arf-ArfGEF and Arf-ArfGAP interactions. Consistency between biological replicates in the *Hs*ArfGAP1^{GAP}-stimulated GTP hydrolysis of *Hs*Arf6 assay indicated that it was reproducible, and inhibition using QS11 was used to chemically validate the assay format. In future work a more suitable *Hs*ArfGAP with clinical significance in Arf6 signalling should be used to conduct similar pilot studies before screening compound libraries against the potential ArfGAP cancer drug target (possible ArfGAP candidates are reviewed in Chapter 1: Section 6.1).

On the other hand, ARNO^{Sec7}-mediated GDP/GTP exchange on *Hs*Arf6 was not robustly detected using the immobilised *Hs*Arf6-GGA assay. Since Macia et al. (2001) were able to detect minimal ARNO activity towards *Hs*Arf6 by alternative methods, it raised the possibility that the immobilisation assay format was simply not sufficiently sensitive for these purposes. ArfGEF-mediated GDP/GTP exchange activity on *Hs*Arf6-GDP should, hereafter, be explored using an alternative ArfGEF with greater specificity for *Hs*Arf6. EFA6, an ArfGEF that has previously demonstrated high specificity and high levels of activity towards *Hs*Arf6-GDP *in vitro*, is a possible candidate although a small molecule inhibitor to validate the assay does not exist (Macia et al., 2001). BRAG2/GEP100, which has also been flagged as potential anticancer drug target, is another contender. It has demonstrated *in vivo* activation of *Hs*Arf6-GDP and is inhibited by SecinH3 (Grossmann et al., 2013a). Provided BRAG2/GEP100-mediated activation can be detected in an *in vitro* assay format, it can be chemically validated using SecinH3.

In addition to being reproducible, the Arf6-GGA3 and Arf6-JIP4 interaction assays are also suitable for high-throughput screening (HTS). The Z-factor is a biostatistical measurement routinely used to predict whether smaller, pilot studies of an assay are suitable for HTS by determining whether the background is sufficiently distinguishable from the assay signal. Z-factor scores greater than 0.5 define the assay as an 'excellent' assay for HTS (Zhang et al., 1999). The high-throughput screening potential of the immobilised *Hs*Arf6 assays (using GGA or JIP4 as the effector proteins carrying the GST assay signal) are detailed below in **Table 3**. The immobilised *Hs*Arf6-GGA and *Hs*Arf6-JIP4 interaction assays were

both reproducible and defined as 'excellent' assays for HTS purposes owing to their Z-factor scores of 0.694 and 0.878 respectively.

Table 3: High-throughput screening potential of the immobilised Arf6 interaction assays

	Z-factor
Immobilised *Hs*Arf6-GGA^{GAT} GST assay	0.694
Immobilised *Hs*Arf6-JIP4^{LZII} GST assay	0.878

*Z-factor formulas are described in the supplementary material

However, the immobilised *Hs*Arf6-JIP4 interaction assay improved GST signals intensities by approximately 161.7% above those observed for *Hs*Arf6-GGA (**Figure S4**) and could discriminate *Hs*Arf6-GDP from *Hs*Arf6-GTP more robustly. *Hs*Arf6-GDP binding to GST-GGA^{GAT} was approximately 45.6% of *Hs*Arf6-GTP binding to GST-GGA^{GAT}, whereas *Hs*Arf6-GDP binding to GST-JIP4^{LZII} was approximately 21.7% of *Hs*Arf6-GTP binding to GST-JIP4^{LZII}. An alternative implication of these preliminary findings may be that the immobilised *Hs*Arf6 assay could be used to compare relative binding affinities of effector proteins to both active and inactive forms of *Hs*Arf6.

The immobilised *Hs*Arf6-JIP4 interaction assay has not yet been employed to determine the activation status of *Hs*Arf6 following ArfGEF activation and ArfGAP deactivation assays, but considering its superior performance, it may be worth rather using this assay format in subsequent studies. Lastly, unlike the *Hs*Arf6-GGA interaction which has no significance in a cellular context, the *Hs*Arf6-JIP4 interaction is significant to cancer therapy, and in its current form, is ready for screening compounds with anticancer properties (future work pertaining to screening will be discussed shortly).

The reverse assay format, where the effector protein is immobilised to a glutathione plate as the bait protein and *Hs*Arf6 is the prey protein carrying the HRP assay signal, was not suitable for detecting GGA-*Hs*Arf6 binding but was for JIP4-*Hs*Arf6 binding. It was explored for its potential to deliver greater signal sensitivity. Although this was not achieved in this pilot study, future studies could explore further optimisation of reagent concentrations used and alternative His-tag detection reagents (e.g. HRP-conjugated anti-His antibodies).

A second aim was to produce *Hs*Arf6 (and *Pf*Arf6 – discussed in the next chapter) interaction assays in a format amenable to high-throughput screening (HTS) that could be conducted at a cost-effective rate. For these purposes, we roughly compared the relative costs of each assay format. The costs of vector preparation, protein production and purchase of compound libraries were omitted since these would be incurred by all *in vitro* protein-protein interaction assay formats. Also, the cost of reagents that contributed negligibly to the overall cost of screening were omitted. Examples are standard 96-well plates and standard reagents used in GST assays such as CDNB. Apart from the FRET-based approach

under development (A. Ntlansana, MSc ongoing) which is expected to be the most cost-effective approach for HTS, the assay used to identify NAV2729 (using the fluorescent GTP derivative GTP-BODIPY) as an inhibitor of *Hs*Arf6 via high-throughput screens is, currently, the only comparable assay format. The most expensive component of this assay format is GTP-BODIPY which will be compared to reagents that contribute significantly to the total cost of HTS in our assay formats. The estimated costs for screening 80 compounds (alongside relevant controls) on a 96-well plate are described in **Table 4**. The data indicates that the immobilised GGA/JIP4-*Hs*Arf6 interaction assay is the cheapest assay format for HTS, but only marginally so compared too the reverse immobilised *Hs*Arf6-GGA/JIP4 assay format. Both are at least 2.9 times less expensive than the published HTS assay which exploits the exorbitantly expensive reagent, GTP-BODIPY (Yoo et al., 2016). Furthermore, T. Swart (PhD dissertation, ongoing), has demonstrated that nickel-coated plates can be re-used by stripping bound proteins and recharging the nickel particles in a fashion similar to the recharging of Ni-NTA conjugated resins. Reusability has been demonstrated for at least seven rounds of screening before plates are exhausted. The implication thereof is that the cost of the immobilised *Hs*Arf6 assays could, in theory, be reduced at least seven-fold by reusing plates. Presumably, glutathione-coated plates could also be prepared for reuse much like glutathione agarose is prepared for repeated usage in other applications; however, this has not yet been explored experimentally. As a final option to further reduce costs, methods for the production of nickel- and/or glutathione coated plates are available and could be used to prepare plates in-house, as opposed to purchasing commercial products (Murray et al., 1998; Paborsky et al., 1996).

Since *Hs*Arf6 and its signalling machineries are gaining traction as potential drug targets with broad clinical significance, the assay may be adopted for screening libraries against a plethora of ArfGEFs and ArfGAPs derived from a variety of organisms (as will be discussed in more detail in the overall conclusion) and thus achieving minimal costs becomes crucial.

Table 4: Relative cost of the Arf6 interaction assays compared to the cheapest available alternative

	GTP-BODIPY assay (Yoo et al., 2016)	Immobilised *Hs*Arf6-GGA/JIP4 interaction assay	Immobilised GGA/JIP4-*Hs*Arf6 interaction assay
GTP-BODIPY	139.2[4]	-	-
Nickel-coated plate	-	47.8[1]	-
Glutathione-coated plate	-	-	38.1[2]
Nickel-HRP HisDetector	-	-	7.8[3]
Total cost per 96-well plate ($)	139.2	47.8	45.9

1. Qiagen Ni-NTA HisSorb 96-well plates $239.0 for 5 plates.
2. Pierce Glutathione-coated 96-well plates $190.5 for 5 plates.
3. Qiagen Ni-NTA conjugate $320 per 500 mL recommended working solution. Requiring 12 mL per 96-well plate allows for forty-one 96-well plates to be screened.
4. ThermoFisher Scientific GTP-BODIPY trisodium salt $290 to prepare 100 µL of 5 mM solution. According to the 20 µM concentration used by Yoo et al. (2016). In 96-well assay format would require 100 µL of 20 µM per well.

The immobilised *Hs*Arf6-JIP4 interaction assay is ready for HTS of compounds that inhibit this Arf-effector interaction and may have potential anticancer activity. Alternative ArfGEF and ArfGAP candidates for cancer drug discovery (reviewed in chapter 1, section 6.1) still need to be studied in smaller, pilot studies using the assays developed here before HTS can commence. Screening for compounds that inhibit *Hs*Arf6-JIP4 binding will begin using a BioFocus α-helix mimetic (potential protein interaction inhibitors) library, in addition to a repurposing library (LOPAC library of FDA approved compounds). Hit compounds should subsequently be screened for cytotoxicity and screened for repression of cell migration. Recall that disruption of *Hs*Arf6-JIP4 binding should, in theory, reduce the secretion of proteases that contribute to the degradation of the extracellular matrix (ECM) (Marchesin et al., 2015). The influence of hit compounds on cell migration could be evaluated using inexpensive, rapid and convenient scratch assays (Liang et al., 2007), in conjunction with the more widely accepted cell migration assay technique – the Boyden Chamber technique (Zengel et al., 2011). Any hit compounds that demonstrate promising *in vitro* repression of cell migration should also be captured by X-ray crystallography in complex with *Hs*Arf6-JIP4. X-ray crystallographic studies are crucial in understanding the precise molecular mechanisms by which inhibitors exert their activity.

Lastly, and in addition to its relevance in cancer drug discovery, the relative strength and selectivity of *Hs*Arf6-JIP4 binding could be exploited commercially. Currently, Arf pull-down assays use GGA as a prey protein. GGA binds to Arf1, and Arf6 (amongst other proteins in the cell lysate) which are detected

by Western blot using Arf1 or Arf6 antibodies respectively (Boulay et al., 2008; Yoon et al., 2006). Although immunodetection using Arf6 antibodies would still be required (to detect Arf6 from other interactors of JIP4), JIP4 as a prey protein may produce greater yields of active Arf6 and in turn, higher yields of additional interactors in complex with *Hs*Arf6 that may have previously gone undetected. However, to test this hypothesis, one would need to prepare GST-JIP4^{LZII} and GST-GGA^{GAT} conjugated beads and compare the profile of the protein complexes isolated by each method.

In summary, we have developed immobilised *Hs*Arf6-GGA and *Hs*Arf6-JIP4 interaction assay that can discriminate *Hs*Arf6-GDP from *Hs*Arf6-GTP. Furthermore, the *Hs*Arf6-GGA interaction assay was successfully employed to determine the activation status of Arf following incubation with ArfGEFs (in this case ARNO-mediated GDP/GTP exchange on *Hs*Arf1) and ArfGAPs (*Hs*ArfGAP1-stimulated GTP hydrolysis on *Hs*Arf6). Now that the assay format has been validated with human proteins, and will be exploited for cancer drug discovery, can it be applied to the malarial counterparts for use in identifying novel antimalarial drugs that target *Pf*Arf6 and its signalling machineries?

Chapter 5: Development of an *in vitro* malarial Arf6 signalling assay for drug screening of potential anti-malarial therapeutics.

5.1. Introduction

5.1.1. Malarial Arf signalling system

Several participants in malarial Arf signalling have been identified and characterised to varying degrees. *Pf*Arf1, which, to date, is the most highly characterised, was initially identified by Stafford and colleagues in 1996. They concluded that *Pf*Arf1 mRNA levels reached a maximum during nuclear division towards the end of the intraerythrocytic cycle, suggesting that Arfs are developmentally regulated and they subsequently purified a recombinant *Pf*Arf1 protein from *E. coli*. The purified protein was capable of stimulating cholera-toxin catalysed ADP-ribosyltransferase activity (the defining characteristic of Arfs). Finally, they determined that *Pf*Arf1 was expressed and purified in GDP-bound form which lead to Cook et al. (2010) crystalizing and resolving the structure for *Pf*Arf1-GDP. Leber et al. (2009) also demonstrated that *Pf*Arf1 was capable of activating a unique malarial PIP5K homolog, much like Arf1 derived from other eukaryotic organisms. T.Swart (M.Sc., dissertation) expressed *Pf*Arf1 fused to GFP in parasites and observed that *Pf*Arf1-GFP localised to a structure reminiscent of the Golgi apparatus – a single punctate locus in trophozoites which multiplies during the schizont stage as the nucleus and parasite divides and dissipates upon treatment with the Arf1 inhibitor Golgicide, and Brefeldin A (BFA) (T. Swart, manuscript in preparation). BFA inhibits the activity of a subset of Sec7 domain Arf GEFs by stabilizing an abortive to an Arf-GDP-ArfGEF complex (Peyroche et al., 1999). This raised the possibility that BFA could also disrupt *Pf*Arf1 via its effects on a malarial ArfGEF.

Baumgartner et al. (2001) and Wiek et al. (2004) have identified a single unusual malarial Sec7 domain in the parasite genome and suggested its protein product may be a functional ArfGEF targeted by BFA by generating a BFA resistant parasite line and showing it contains a critical point mutation in the sequence. As further evidence, parasites in which the wild-type putative Sec7 domain was replaced with a mutant sequence by homologous recombination gained BFA resistance.

As far as potential ArfGAPs are concerned, Senkovich and Chattopadhyay (2004) identified a malarial ArfGAP (which we have assigned the name *Pf*ArfGAP1) based on sequence homology with human ArfGAP1 They were able to express the GAP domain of *Pf*ArfGAP1 in *E. coli* and purify it in soluble form. Cook et al (2011) subsequently resolved the crystal structure and noted that although the overall structure of the GAP domain was similar to that of mammalian ArfGAPs, several amino acid residues involved in Arf1 binding were different from that of the mammalian counterpart. No functional studies

were carried out to confirm that the protein possessed GAP activity. In addition to *Pf*ArfGAP1, we have identified a second, putative malarial ArfGAP which has yet to be studied, which will be referred to as *Pf*ArfGAP2 (PlasmoDB code: PF3D7_0526200.1).

In the initial stages of assay development, cytotoxicity screens were conducted using well known Arf signalling inhibitors on parasites. Unexpectedly, QS11 - a human ArfGAP1 inhibitor - was toxic to parasites but not HeLa cells (D. Laming, unpublished results). In yeast it has been demonstrated that single knockouts of the ArfGAPs Gcs1 and Glo3 are non-lethal since these ArfGAPs provide overlapping functions in COPI transport. However, in double knockout experiments, the yeast were unable to survive (Poon et al., 1999). Similarly, the mammalian homolog of Gcs1, ArfGAP1 (Cukierman et al., 1995; Makler et al., 1995) as well as the mammalian homologs of Glo3, ArfGAP2 and ArfGAP3 (Frigerio et al., 2007) have all been shown to be involved in COPI trafficking, and consistent with the findings in yeast, triple knockout of these genes was lethal to mammalian cells. Mammalian cells could survive when only ArfGAP1 or both ArfGAP2 and ArfGAP3 were silenced (Weimer et al., 2008). The differential sensitivity of *P. falciparum* parasites and HeLa cells to QS11 led us to the hypothesis that perhaps *Pf*ArfGAP1 and *Pf*ArfGAP2 do not have overlapping functions and cannot functionally compensate for one another (or at least the alternative ArfGAP cannot compensate for the ArfGAP which is the target of QS11), while in HeLa cells, inhibition of a sub-population of ArfGAPs may be compensated for by alternative ArfGAPs. It also raises the possibility that perhaps the *Pf*ArfGAPs have unique functions, and that one may be involved in terminating *Pf*Arf1 function in the Golgi apparatus, while the other acts on *Pf*Arf6 closer to the plasma membrane.

Cytotoxicity studies indicated that NAV2729 (an inhibitor of human Arf6) was lethal to both mammalian cells and parasites (D. Laming). While the target of NAV2729 in parasites is unknown, a possible candidate could be the putative *Pf*Arf6. As mentioned previously, localisation of *Pf*Arf6-GFP in parasites under NAV2729 treatment is currently underway to investigate this possibility. Other than being identified as a possible second Arf in the parasites genome in the original studies by Stafford and Colleagues (1996), no further studies have been conducted on *Pf*Arf6 other than those presented here and the localisation of *Pf*Arf6-GFP in parasites (T.Swart, M.Sc, dissertation). Hypotheses presented in the discussion above will be explored as part of the development of the *Pf*Arf6 assays.

5.1.2. PfArf6 assay development considerations

In this chapter we explored whether the high-throughput immobilised interaction assays developed for human Arf6 signalling could be extended as a tool to screen for inhibitors of the putative malarial Arf6 signalling system. As previously discussed, the activation status of Arf GTPases is routinely manipulated using EDTA-mediated nucleotide exchange and is monitored by intrinsic tryptophan fluorescence (Bigay & Antonny, 2005). Naturally then, it was essential to first determine whether the

intrinsic tryptophan residue (which acts as a fluorescent probe for the activation of Arf GTPases) was conserved in the putative *Pf*Arf6 protein sequence. The conservation of the residues involved in binding to effector proteins (which carry the GST/HRP assay signal) was also critical for the development of the immobilised *Pf*Arf6 interaction assays. BLAST analyses suggested that there are no homologous GGA and JIP4 effector proteins within the parasite's proteome. As such it is important to remember that the $^{N\Delta17}$*Pf*Arf6-GGA or $^{N\Delta17}$*Pf*Arf6-JIP4 interactions are not significant in a cellular context, but rather provide a tool to study $^{N\Delta17}$*Pf*Arf6 signalling in a high-throughput screening format. In this chapter, these interactions were explored as a base assay which could be used to study ArfGEF and ArfGAP activation and deactivation of *Pf*Arf6, as well as for drug screening.

5.2. Aims and objectives

Aim of the study: To establish plate-based *Pf*Arf6 assays that can be used to screen compounds for inhibitors that can in the longer term be used to chemically validate *Pf*Arf6 (and its related machineries) as malaria drug targets.

Specific questions/objectives and experimental approaches:

1. Can the recombinant proteins required in the assay be expressed in soluble and pure forms? All proteins were expressed as His-tagged proteins under small-scale conditions to determine the solubility of each protein. The small-scale conditions were scaled up and the protein expressed and purified by Ni-NTA affinity chromatography.
2. Can the conditions required for EDTA-mediated nucleotide exchange be established and can the activation status of *Pf*Arf6 be detected by intrinsic tryptophan fluorescence? The nucleotide exchange conditions required to prepare active $^{N\Delta17}$*Pf*Arf6-GTP and inactive $^{N\Delta17}$*Pf*Arf6-GDP proteins were explored by varying the EDTA and temperature conditions and monitoring exchange by intrinsic tryptophan fluorescence.
3. Can the putative *Pf*Arf6 protein interact with the effector proteins GGA and/or JIP4? And can these interactions be exploited to develop a high-throughput drug screening method following the same assay formats developed for human Arf6 signalling? Conservation of the amino acid residues of human Arf6 involved in binding to GGA and JIP4 was explored by protein sequence alignments with *Pf*Arf6. The *in vitro* binding capabilities were also explored by conducting the immobilised plate assays using *Pf*Arf6 as the binding partner for GGA and/or JIP4.
4. Can the primary Ni-NTA immobilised *Pf*Arf6-GGA GST assay and/or the glutathione immobilised JIP4-*Pf*Arf6 HRP enzyme assay detect the activation status of *Pf*Arf6 GTPase following ArfGEF-stimulated GDP/GTP exchange and ArfGAP-stimulated GTP hydrolysis? ArfGEF and ArfGAP assays were conducted by incubating *Pf*ArfGEF^{Sec7}, *Pf*ArfGAP1^{GAP} and/or *Pf*ArfGAP2^{GAP} with *Pf*Arf6 in round-bottom well plates. The reaction products were subsequently analysed using the immobilised plate assays.

5.3. Results

Preparation of the DNA constructs used in the development of the malarial Arf6 signalling assay. For the expression of the putative malarial Arf6 (*Pf*Arf6) in *E. coli*, the coding sequence was amplified by PCR from a human codon-optimised sequence previously custom synthesised and cloned by Genscript. The N-terminally truncated malarial *Pf*Arf6$^{N\Delta17}$ coding sequence was amplified using a forward primer that omitted amplification of the N-terminal hydrophobic extension and incorporated a *Nhe*I restriction site at the 5' end of the coding sequence. The reverse primer was designed to incorporate a terminal stop codon followed by a *Bam*HI restriction site. The PCR amplicon was analysed by agarose gel electrophoresis. The approximate sizes of PCR and restriction digestion products were determined by preparing log (base pair) against the relative migration distance plots of the DNA ladder used (*results not shown*). The PCR amplicon was approximately 500 bp (**Figure 23A**) which corresponded to the 483 bp predicted size of the *Pf*Arf6$^{N\Delta17}$ amplicon. The *Pf*Arf6$^{N\Delta17}$ amplicon digested with *Nhe*I and *Bam*HI was subcloned into a pET-28a-CFP construct (previously prepared by F.Khan, 2017) digested with *Nhe*I and *Bam*HI. The terminal stop codon was incorporated into the reverse primer to prevent the expression of CFP following the *Pf*Arf6$^{N\Delta17}$ coding sequence. The ligation reaction was transformed into XL-10 gold competent *E. coli* cells, propagated by overnight culture, purified by alkaline lysis miniprep, digested with *Nhe*I, *Xho*I and *Bam*HI and analysed by agarose gel electrophoresis. Theoretically, digestion of the pET-28a-CFP- *Pf*Arf6$^{N\Delta17}$ construct by *Nhe*I, *Xho*I and *Bam*HI should have resulted in three linearized bands representing the pET-28a vector (5369 bp), the CFP coding sequence (717 bp) and the *Pf*Arf6$^{N\Delta17}$ coding sequence (483 bp). Three digestions products of approximately 5 300 bp, 750 bp and 500 bp were observed, which correlated with the predicted digestion pattern (**Figure 23B**). For the *E. coli* expression of the GAP domain of the malarial ArfGAP identified by Cook *et al*., (2001) (*Pf*ArfGAP1^{GAP}), the coding sequence was amplified by PCR from *P. falciparum* genomic DNA (donated by Travis Basson). The PCR amplicon amplified using forward and reverse primers which contained *Nhe*I/*Xho*I restriction sites was analysed by agarose gel electrophoresis. The PCR amplicon was approximately 500 bp (**Figure 23C**) which corresponded to the 483 bp predicted size of the *Pf*ArfGAP1^{GAP} amplicon. The *Pf*ArfGAP1^{GAP} amplicon digested with *Nhe*I and *Xho*I was subcloned into the pET-28a construct digested with *Nhe*I and *Xho*I. The ligation reaction was transformed into XL-10 gold competent *E. coli* cells, propagated by overnight culture, purified by alkaline lysis miniprep, digested with *Nhe*I and *Xho*I and analysed by agarose gel electrophoresis. Theoretically, digestion of the pET-28a-*Pf*ArfGAP1^{GAP} construct by *Nhe*I and *Xho*I should result in two linearized bands representing the pET-28a vector (5369 bp) and the *Pf*ArfGAP1^{GAP} coding sequence (483 bp). Two digestions products of approximately 5 000 bp and 500 bp were observed, which correlated with the predicted digestion pattern (**Figure 23D**).

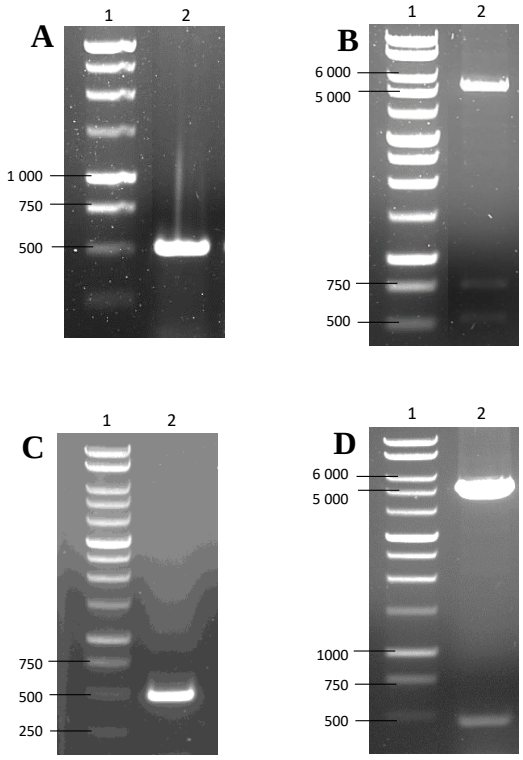

Figure 23: Diagnostic restriction digestions of the pET-28a-CFP- *Pf*Arf6$^{N\Delta17}$ and pET-28a-*Pf*ArfGAP1^{GAP} constructs. All PCR amplicons and diagnostic restriction digestion products were analysed on 0.8% (w/v) agarose gels run at 90V for approximately 1 hour. DNA bands were visualised under UV light and photographed. Lane 1: Promega 1kb DNA ladder was run alongside each sample (sizes in base pairs). **A**: Lane 2: PCR amplification of the truncated *Pf*Arf6$^{N\Delta17}$coding sequence using a pBluescript-*Pf*Arf6 construct as template. **B**: Lane 2: The *Pf*Arf6$^{N\Delta17}$ coding sequence cloned into pET-28a-CFP and digested using *Xho*I, *Bam*HI and *Nhe*I. **C**: Lane 2: PCR amplification of the *Pf*ArfGAP1^{GAP} coding sequence using malarial gDNA as template. **D** Lane 2: The *Pf*ArfGAP1^{GAP} coding sequence cloned into pET-28a and digested using *Xho*I and *Nhe*I.

For the *E. coli* expression of the predicted GAP domain of the putative *Pf*ArfGAP annotated as such by PlasmoDB (*Pf*ArfGAP2^{GAP}) and of the predicted Sec7 domain of the putative *Pf*ArfGEF (Baumgartner *et al*., 2001; *Pf*ArfGEF^{Sec7}), the pET-28a-*Pf*ArfGAP2^{GAP} and pET-28a-*Pf*ArfGEF^{Sec7} constructs were custom synthesised (*E. coli* codon bias), cloned and provided by Genscript as lyophilized powders. These were resuspended in water, transformed into XL-10 gold competent *E. coli* cells and propagated as overnight cultures containing kanamycin as a selection agent. Purified constructs were obtained from overnight cultures by alkaline lysis miniprep. For the *E. coli* expression of *Pf*Arf1, the pET-28a-CFP-*Pf*Arf1$^{N\Delta17}$ construct previously prepared by T.Swart (PhD, thesis in preparation) was provided for this study as an alkaline lysis miniprep. All constructs were subjected to restriction digestion and analysed by agarose gel electrophoresis. The pET-28a-CFP- *Pf*Arf1$^{N\Delta17}$ construct was digested with *Nhe*I, *Xho*I and *Bam*HI. Theoretically, this should have yielded three linearized bands representing the pET-28a vector (5369 bp), the CFP coding sequence (717 bp) and the *Pf*Arf1$^{N\Delta17}$ coding sequence (495 bp). Three digestions products of approximately 5000 bp and 750 bp and 510 bp were observed, which correlated with the predicted digestion pattern (**Figure 24A**). Digestion of the pET-28a-*Pf*ArfGEF^{Sec7}

construct with *Nhe*I and *Xho*I. was expected to result in two linearized bands representing the pET-28a vector (5369 bp) and the *Pf*ArfGEF^{Sec7} coding sequence (1629 bp), which agreed with the two digestions products of approximately 4800 bp and 1500 bp observed (**Figure 24B**). Similarly, the pET-28a vector (5369 bp) and the *Pf*ArfGAP2^{GAP} coding sequence (642 bp) bands expected for pET-28a-*Pf*ArfGAP2^{GAP} construct digestion with *Nhe*I and *Xho*I agreed with thetwo digestions products of approximately 4800 bp and 500 bp observed (**Figure 24C**).

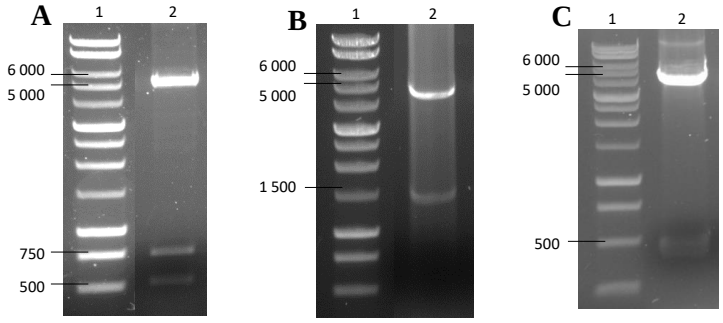

Figure 24: Diagnostic restriction digestions of the pET-28a-CFP- *Pf*Arf1^{NΔ17}, pET-28a-*Pf*ArfGEF^{Sec7} and pET-28a-*Pf*ArfGAP2^{GAP} constructs. All diagnostic restriction digestion products were analysed on 0.8% (w/v) agarose gels run at 90V for approximately 1 hour. Lane 1: Promega 1kb DNA ladder was run alongside each sample (sizes in base pairs). The restriction profiles were visualised under UV light and photographed. **A**: Lane 2: The *Pf*Arf1^{NΔ17} coding sequence cloned into pET-28a-CFP and digested using *Xho*I, *Bam*HI and *Nhe*I. **B**: The *Pf*ArfGEF^{Sec7} coding sequence cloned into pET-28a and digested using *Xho*I and *Nhe*I. **C**: The *Pf*ArfGAP2^{GAP} coding sequence cloned into pET-28a and digested using *Xho*I and *Nhe*I.

Optimization of the small-scale expression of proteins used in the malarial Arf6 signalling assay.

The expression constructs were transformed into T7 Express lysY/Iq competent *E. coli* cells and propagated as an overnight culture. Small-scale expression cultures were prepared by inoculating 8 mL Luria broth containing kanamycin with the overnight cultures. Once the expression cultures reached the exponential growth phase, protein expression was induced with IPTG. Induced *E. coli* cells were collected and lysed and the soluble and insoluble fractions analysed by SDS-PAGE. The approximate sizes of overexpressed proteins of interest were determined by preparing log (molecular weight) against the relative migration distance plots of the molecular weight ladder used (*results not shown*). The His-tagged *Pf*Arf6^{NΔ17} had a predicted molecular weight of 23.9 kDa. In **Figure 25A**, an overexpressed protein approximately 23 kDa in size was present in the induced soluble fraction (*indicated by arrow*) that was absent from the uninduced soluble fraction (lane 4). A more prominent, equivalent protein band in the induced insoluble fraction (lane 3) suggested that His-tagged *Pf*Arf6^{NΔ17} was predominantly insoluble. Conversely, more prominent bands in the induced soluble fractions (*indicated by arrows*) of His-tagged *Pf*Arf1^{NΔ17} (**Figure 25B**) and *Pf*ArfGEF^{Sec7} (**Figure 25C**) suggested that these fusion proteins were predominantly soluble. The sizes of the overexpressed His-tagged *Pf*Arf1^{NΔ17} (20 kDa)

and *Pf*ArfGEF^{Sec7} (60 kDa) correlated with the predicated molecular weights of 21.2 kDa and 64.7 kDa respectively. The His-tagged *Pf*ArfGAP2^{GAP} fusion protein, with a predicted molecular weight of 24.2 kDa was expressed in soluble form. Even though the uninduced soluble fraction (lane 4) was over-loaded relative to the induced soluble fraction (lane 5) a more prominent, overexpressed protein band was observed in the induced soluble fraction at approximately 24 kDa (**Figure 25D**; *indicated by arrow*). Lastly, the His-tagged *Pf*ArfGAP1^{GAP} had a predicted molecular weight of 18.4 kDa. In **Figure 25E**, an overexpressed protein approximately 23 kDa in size was present in the induced soluble fraction (*indicated by arrow*) that was absent from the uninduced soluble fraction (lane 4). A more prominent, equivalent protein band in the induced insoluble fraction (lane 3) suggested that His-tagged *Pf*ArfGAP1^{GAP} was predominantly insoluble.

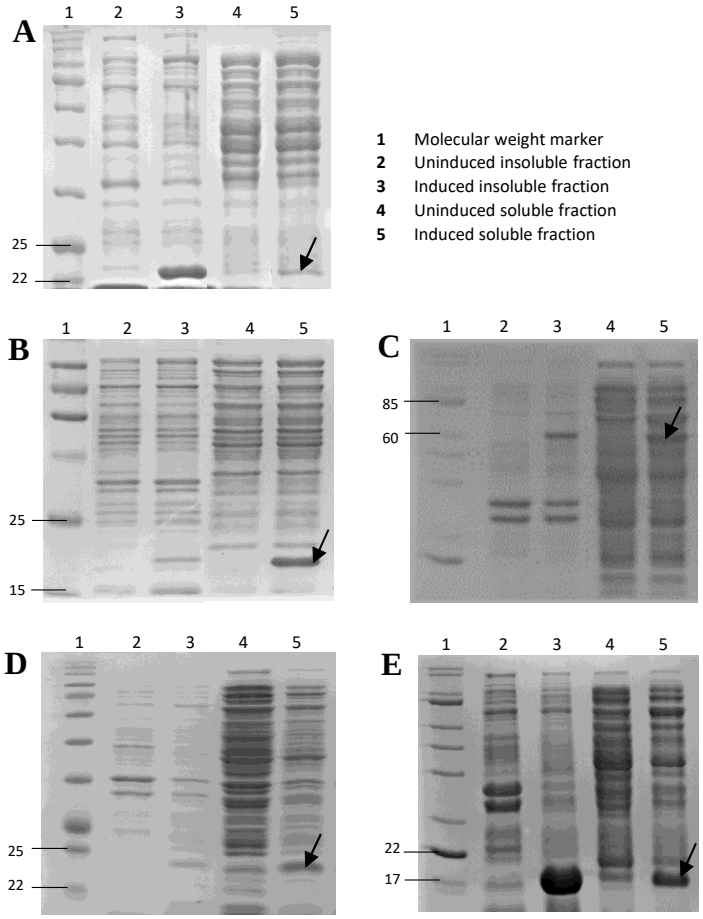

Figure 25: Small-scale protein expression of the His-tagged *Pf*ArfGEF^{Sec7}, *Pf*Arf1^{NΔ17}, *Pf*ArfGAP2^{GAP} and *Pf*ArfGAP1^{GAP} proteins. All expression constructs were transformed into competent *E. coli* (T7 LysY/Iq) cells. Transformed cells were cultured at 37ºC until logarithmic growth phase. Protein expression was induced by 1 mM IPTG and was conducted at 37ºC for 4 hours. The uninduced and induced expression cultures were lysed and the soluble and insoluble fractions of each was separated by centrifugation. All fractions were prepared in SDS sample loading buffer and resolved on polyacrylamide gels run at 120V for approximately 1.5 hours. Lane 1: Molecular weight marker (sizes in kDa). Lane 2: Uninduced insoluble fraction. Lane 3: Induced insoluble fraction. Lane 4: Uninduced soluble fraction. Lane 5: Induced soluble fraction (proteins of interest *indicated by arrows*). **A**: His-tagged *Pf*Arf6^{NΔ17} samples. **B**: His-tagged *Pf*Arf1^{NΔ17} samples. **C**: His-tagged *Pf*ArfGEF^{Sec7} samples. **D**: His-tagged *Pf*ArfGAP2^{GAP} samples. **E**: His-tagged *Pf*ArfGAP1^{GAP} samples.

Large scale purification of proteins used in the malarial Arf6 signalling assay. The optimal expression conditions determined during small-scale expression screening were adopted for large scale expression in 250, or 500 mL cultures. The *E.coli* harvested from the expression cultures were lysed, and the soluble and insoluble fractions separated. His-tagged *Pf*Arf6$^{N\Delta17}$, *Pf*ArfGEF^{Sec7}, *Pf*Arf1$^{N\Delta17}$, *Pf*ArfGAP2^{GAP} and *Pf*ArfGAP1^{GAP} were purified using Ni-NTA affinity chromatography, desalted into assay buffer by size exclusion chromatography and the protein concentrations were determined by Bradford assay (using BSA standard curves of $R^2 > 0.99$). The purification profiles were analysed by SDS-PAGE to assess the purity of the final, desalted fraction. The approximate sizes of purified proteins were determined by preparing log (molecular weight) against the relative migration distance plots of the molecular weight ladder used (*results not shown*). Proteins were routinely expressed and purified, and the average yields obtained are described below. The protein yields obtained from large scale purification of His-tagged *Pf*Arf6$^{N\Delta17}$ from 250 mL expression cultures were not sufficient (*results not shown*). As such 500 mL expression cultures were used. Sufficient amounts of soluble His-tagged *Pf*Arf6$^{N\Delta17}$ was purified from 500 mL cultures and observed as a band approximately 23 kDa in size (**Figure 26A** *indicated by arrow*). Approximately 0.49 mg of protein was purified from a single 500 mL culture with negligible amounts of non-specific proteins in the desalted eluate. Sufficient amounts of soluble His-tagged *Pf*Arf1$^{N\Delta17}$ was purified from 250 mL cultures and observed as a band approximately 23 kDa in size (**Figure 26B** *indicated by arrow*), yielding approximately 0.82 mg of protein purified from a single 250 mL culture with negligible amounts of non-specific proteins in the desalted eluate. Although the small-scale expression profile of *E. coli* cells harbouring the pET-28a-*Pf*ArfGEF^{Sec7} construct suggested that a protein of the approximate size of His-tagged *Pf*ArfGEF^{Sec7} was expressed when induced by IPTG (**Figure 26A**), the putative His-tagged *Pf*ArfGEF^{Sec7} protein was not purified from a subsequent large-scale expression culture (**Figure 26C**), despite the presence of an appropriate band at approximately 60 kDa in the cell lysate, flow-through and first wash (**Figure 26B** *indicated by arrows*) of the purification process. A possible working hypothesis was that the expression of an N-terminally His-tagged *Pf*ArfGEF^{Sec7} recombinant protein resulted in a fusion protein where the His-tag was obscured by the overall protein conformation (as such the Ni-NTA resin would not have access to the His-tag which was necessary for purification of the protein from a lysate on the basis of bio affinity), or that the His tag had been removed from the protein by proteolytic degradation. This could be explored by Western-blotting with His-tag antibodies/probes and by including an uninduced expression culture analysed in parallel with the remainder of the protein purification profile. Time did not permit for these additional experiments to be conducted at the time of dissertation preparation. The protein yields obtained from large scale purification of His-tagged *Pf*ArfGAP2^{GAP} from 250 mL expression cultures were not sufficient (*results not shown*). As such 500 mL expression cultures were used. Sufficient amounts of soluble His-tagged *Pf*ArfGAP2^{GAP} was purified from 500 mL cultures and observed as a band approximately 23 kDa in size (**Figure 26D** *indicated by arrow*). Approximately 0.16 mg of protein was purified from a single 500 mL culture with negligible amounts of non-specific

proteins in the desalted eluate. Sufficient amounts of soluble His-tagged *Pf*ArfGAP1^{GAP} was purified from 250 mL cultures and observed as a band approximately 20 kDa in size (**Figure 26E** *indicated by arrow*). Approximately 1.1 mg of protein was purified from a single 250 mL culture. Several high molecular weight non-specific proteins were present in the desalted eluate but approximately 95% of total protein compromised the 20 kDa, putative *Pf*ArfGAP1^{GAP} protein.

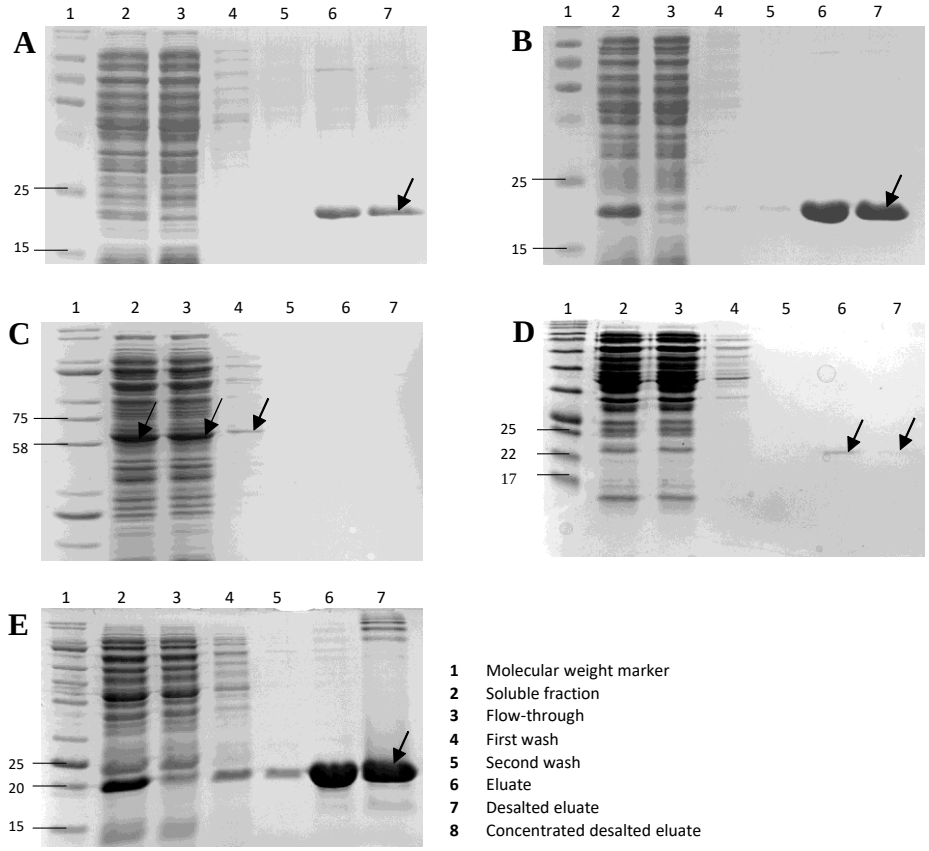

Figure 26: Purification of His-tagged *Pf*Arf6^{NΔ17}, *Pf*ArfGEF^{Sec7}, *Pf*Arf1^{NΔ17}, *Pf*ArfGAP2^{GAP} and *Pf*ArfGAP1^{GAP} by Ni-NTA affinity chromatography. All expression constructs were transformed into competent *E. coli* (T7 LysY/Iq) cells. Pre-cultures were grown until the logarithmic growth phase was reached and protein expression was induced using IPTG. The expression cultures incubated at 37ºC for 4 hours were lysed, and the soluble fractions were collected by centrifugation. His-tagged proteins were purified from the soluble fraction by Ni-NTA column chromatography and the purification profile was analysed by SDS-PAGE. For all gels Lane 1: Molecular weight marker (sizes in kDa). Lane 2: whole soluble fraction. Lane 3: flow-through. Lane 4: first wash. Lane 5: second wash. Lane 6: eluate. Lane 7: desalted eluate. **A**: His-tagged *Pf*Arf6^{NΔ17}. **B**: His-tagged *Pf*Arf1^{NΔ17}. **C**: His-tagged *Pf*ArfGEF^{Sec7}. **D**: His-tagged *Pf*ArfGAP2^{GAP}. **E**: His-tagged *Pf*ArfGAP1^{GAP}.

The tryptophan residue used to monitor nucleotide exchange is conserved in the putative *Pf*Arf6. Sequence alignment with human Arf6 was conducted to investigate whether the tryptophan residue which acts as an intrinsic fluorescent probe to monitor Arf GTPase activation was conserved in the putative *Pf*Arf6 protein sequence. The human Arf6 protein sequence (accession number: CAG46737.1) was obtained from NCBI and the putative malarial Arf6 sequence (PlasmoDB code: *PF*10_0337) was

obtained from PlasmoDB. The pairwise sequence alignment was conducted using the EMBOSS Water alignment tool (EMBL-EBI) and viewed using MEGA software. **Figure 27** demonstrates that the relevant tryptophan residue at position 66 of the protein sequence of human Arf6 (*yellow*) was conserved in the protein sequence of the putative *Pf*Arf6 protein sequence (*blue*).

Figure 27: Conservation of the tryptophan residue used to monitor nucleotide exchange of Arf GTPases in a putative malarial Arf6 GTPase. The putative malarial Arf6 protein sequence (PlasmoDB code: *PF*10_0337) was aligned with human Arf6 (accession number: CAG46737.1) using the EMBOSS water pairwise alignment tool. The alignment was viewed using MEGA software and edited in Microsoft Excel. The tryptophan residue at position 66 (*yellow*) which acts as a fluorescent probe to monitor nucleotide exchange in human Arf6 is conserved in the putative malarial Arf6 at position 66 of the protein sequence (*blue*).

Nucleotide exchange assays may destabilise the *Pf*Arf6 protein. Nucleotide exchange assays monitored by tracking the intrinsic tryptophan fluorescence were employed in the preparation of inactive $^{N\Delta17}$*Pf*Arf6-GDP and active $^{N\Delta17}$*Pf*Arf6-GTP. The fact that $^{N\Delta13}$*Hs*Arf6 and $^{N\Delta17}$*Hs*Arf1 were loaded with GDP and/or GTP under different concentrations of EDTA and temperatures (as described in the previous chapter) suggested that each Arf GTPase may require a unique set of conditions to successfully mediate nucleotide exchange. It was therefore decided to test a range of EDTA concentrations and temperatures for the nucleotide exchange assay of $^{N\Delta17}$*Pf*Arf6. EDTA-mediated nucleotide exchange was first conducted by incubating 1 µM $^{N\Delta17}$*Pf*Arf6 with 2.5, 5.0 or 10 mM EDTA and 50 µM GDP/GTP at 37°C for 60 minutes with gentle agitation. $^{N\Delta17}$*Pf*Arf6-GDP and $^{N\Delta17}$*Pf*Arf6-GTP complexes were stabilised by the addition of 5.0, 10.0 and 20.0 mM $MgCl_2$ respectively and incubating the reaction mixtures for an additional 5 minutes at 37°C with gentle agitation. Nucleotide exchange was assessed by intrinsic tryptophan fluorescence (excitation at 298 nm and emission at 340 nm) as an end-point reading since the samples could not be continuously agitated in the available plate reader. There was no significant difference in the intrinsic tryptophan fluorescence between $^{N\Delta17}$*Pf*Arf6 incubated with GDP and $^{N\Delta17}$*Pf*Arf6 incubated with GTP at any of the EDTA concentrations used (**Figure 28A**). In addition to the lack of statistical significance, the standard deviation between technical replicates was considerably higher than those usually obtained during routine nucleotide exchange assays with other Arf GTPases. This led to the hypothesis that $^{N\Delta17}$*Pf*Arf6 may lose stability at 37°C, and thus a lower temperature was opted for in subsequent optimization studies. The EDTA-mediated nucleotide exchange was conducted as previously described, except that the temperature was lowered to 25°C. The difference in intrinsic tryptophan fluorescence between $^{N\Delta17}$*Pf*Arf6 incubated with GDP and $^{N\Delta17}$*Pf*Arf6 incubated with GTP where 2.5 mM or 10.0 mM EDTA was used was statistically significant ($\rho = 0.0327$ and 0.0148, respectively $n = 3$), but this was not the case with 5.0 mM EDTA ($\rho = 0.2512$, $n = 3$) (**Figure 28B**). However, the statistical significance in the intrinsic tryptophan

fluorescence signals between GDP pre-loaded and GTP pre-loaded $^{N\Delta17}$*Pf*Arf6 were not consistently observed between biological replicates which suggested that the results obtained in the representative graphs may be poorly reproducible. Again, this raised the possibility that perhaps the $^{N\Delta17}$*Pf*Arf6 protein was not stable. To test the hypothesis EDTA-mediated nucleotide exchange was conducted as previously described, at 25ºC without continuous agitation using 2.5 mM EDTA. Continuous agitation was forfeited in order to obtain intrinsic tryptophan readings recorded every five minutes over the time course. A final modification of the method was the extension of stabilisation with $MgCl_2$ to a 20-minute incubation as opposed to the 5-minute incubation previously used. EDTA-mediated nucleotide exchange of $^{N\Delta17}$*Pf*Arf6 was conducted alongside the positive control $^{N\Delta17}$*Hs*Arf1 (since $^{N\Delta13}$*Hs*Arf6 required loading at 37ºC as opposed to 25ºC). **Figure 28C** demonstrates the change in intrinsic tryptophan fluorescence over time when nucleotide exchange occurred on $^{N\Delta17}$*Hs*Arf1. The loading of GDP onto $^{N\Delta17}$*Hs*Arf1 resulted in a steady decrease in intrinsic tryptophan fluorescence (*left*) while the loading of GTP onto $^{N\Delta17}$*Hs*Arf1 resulted in an initial decrease followed by steady kinetics over the remainder of the time course (*right*). These findings were compatible with the theoretical principles of the technique i.e. in the inactive, GDP-bound form the relevant tryptophan residue becomes hidden within the Arf GTPase protein core and a loss of intrinsic tryptophan fluorescence would be expected. Conversely, in the active, GTP-bound form the intrinsic tryptophan becomes exposed from within the Arf GTPase protein core during the conformational shift and an increase in intrinsic tryptophan fluorescence would be expected. The $^{N\Delta17}$*Hs*Arf1-GTP loading profile considered along with these principles suggested that $^{N\Delta17}$*Hs*Arf1 was already GTP-bound (i.e. was expressed in GTP-bound form) since, rather than an increase, steady fluorescence kinetics was observed (**Figure 28C**, *right*). Using the $^{N\Delta17}$*Hs*Arf1 nucleotide exchange profile as a model (**Figure 28C**), one can make inferences about $^{N\Delta17}$*Pf*Arf6 nucleotide exchange. The loading of GDP (*left*) and GTP (*right*) onto $^{N\Delta17}$*Pf*Arf6 resulted in a steady increase in intrinsic tryptophan fluorescence over time (**Figure 28D**). Since GTP was not present in both reactions, it was unlikely that the increase represented the loading of GTP onto $^{N\Delta17}$*Pf*Arf6. Again, the working hypothesis was that the $^{N\Delta17}$*Pf*Arf6 was unstable and undergoing nucleotide-independent conformational changes during the incubation. The question remained whether the protein was destabilised during the EDTA-mediated nucleotide exchange process. This may have been caused by the chelation of the Mg^{2+} required to stabilise nucleotide binding but may also, in the case of *Pf*Arf6, be necessary to maintain its conformation.

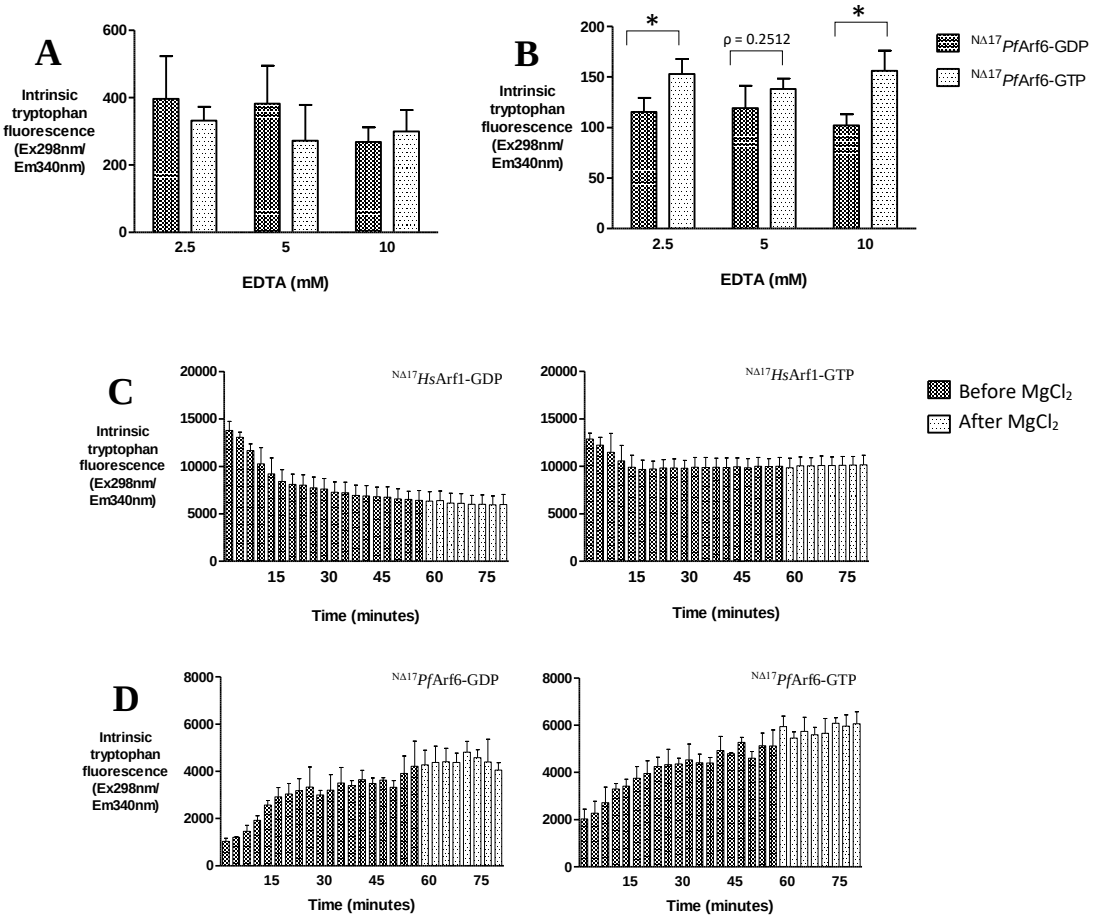

Figure 28: EDTA-mediated nucleotide exchange of $^{N\Delta17}$*Pf*Arf6 measured by tryptophan fluorescence. A-B: Nucleotide exchange was promoted by incubating 1 μM $^{N\Delta17}$*Pf*Arf6 in GDP/GTP in the presence of 2.5, 5.0 and 10.0 mM EDTA for 60 minutes with gentle agitation. $^{N\Delta17}$*Pf*Arf6-GDP and $^{N\Delta17}$*Pf*Arf6-GTP complexes were stabilised by incubating the reactions with excess $MgCl_2$ for 5 minutes with gentle agitation. Intrinsic tryptophan fluorescence was measured as an end-point reading in a plate reader at an excitation wavelength of 298 nm and an emission wavelength of 340 nm. A: Nucleotide exchange conducted at 37°C. B: Nucleotide exchange conducted at 25°C ($\rho < 0.05$, $\rho = 0.2512$, $\rho < 0.05$; n =3). C-D: Nucleotide exchange was promoted by incubating 1 μM $^{N\Delta17}$*Pf*Arf6 in GDP/GTP in the presence of 2.5 mM EDTA for 60 minutes. $^{N\Delta17}$*Pf*Arf6-GDP and $^{N\Delta17}$*Pf*Arf6-GTP complexes were stabilised by incubating the reactions with excess $MgCl_2$ for 20 minutes. Intrinsic tryptophan fluorescence was measured every 5 minutes over the time course. C: Nucleotide exchange profile for $^{N\Delta17}$*Hs*Arf1 as a positive control. *Left*: Incubation of $^{N\Delta17}$*Hs*Arf1 with GDP. *Right*: Incubation of $^{N\Delta17}$*Hs*Arf1 with GTP. D: Nucleotide exchange profile for $^{N\Delta17}$*Pf*Arf6. *Left*: Incubation of $^{N\Delta17}$*Pf*Arf6 with GDP. *Right*: Incubation of $^{N\Delta17}$*Pf*Arf6 with GTP. Each bar represents the mean and standard deviation of readings obtained from 3 replicate wells.

To test this possibility, it was decided to try mediate nucleotide exchange enzymatically (using an ArfGEF) in the presence of Mg^{2+}, rather than chemically (using EDTA). ARNO-mediated GDP/GTP exchange was conducted and the intrinsic tryptophan fluorescence was monitored over time. Time-course readings were chosen to avoid the possibility of false-positive results as were observed in the initial end-point readings obtained for the $^{N\Delta17}$*Pf*Arf6 nucleotide exchange assays (**Figure 28B**). Time-course readings, which allow for the real-time observation of ARNO-mediated GDP/GTP exchange, are usually expressed as a percentage increase in tryptophan fluorescence over time. The percentage

increase in tryptophan fluorescence is determined by dividing the intrinsic tryptophan fluorescence of Arf-GTP by that of Arf-GDP (GTP/GDP relative fluorescence). To conduct the experiment, 1 μM $^{N\Delta17}$*Pf*Arf6 was incubated with50 μM GDP/GTP and 0.1 μM ARNO^{Sec7} at 25ºC for 25 minutes, where the intrinsic tryptophan fluorescence was measured every 5 minutes. Parallel reactions using $^{N\Delta17}$*Hs*Arf1 were used as a positive control and $^{N\Delta13}$*Hs*Arf6 as a negative control (since *in vitro* ARNO-mediated GDP/GTP exchange on $^{N\Delta13}$*Hs*Arf6 was minimal, **Figure 18B**). The GTP/GDP relative fluorescence for $^{N\Delta17}$*Hs*Arf1 usually increased to approximately 252% over time, while no apparent increased was observed for $^{N\Delta13}$*Hs*Arf6. Interestingly, the GTP/GDP relative fluorescence for $^{N\Delta17}$*Pf*Arf6 usually increased to approximately 178% over time (**Figure 29**). Taken together, these results suggested that although EDTA-mediated nucleotide exchange appeared to destabilise $^{N\Delta17}$*Pf*Arf6, the GDP/GTP exchange of $^{N\Delta17}$*Pf*Arf6 by ARNO-stimulation was not compromising the protein's stability. It was therefore possible that an unfolding/destabilisation of $^{N\Delta17}$*Pf*Arf6 over time during GDP and GTP chemical loading was occurring due to Mg^{2+} chelation, resulting in the gradual exposure of the intrinsic tryptophan residues and the subsequent increase in intrinsic tryptophan fluorescence that was observed.

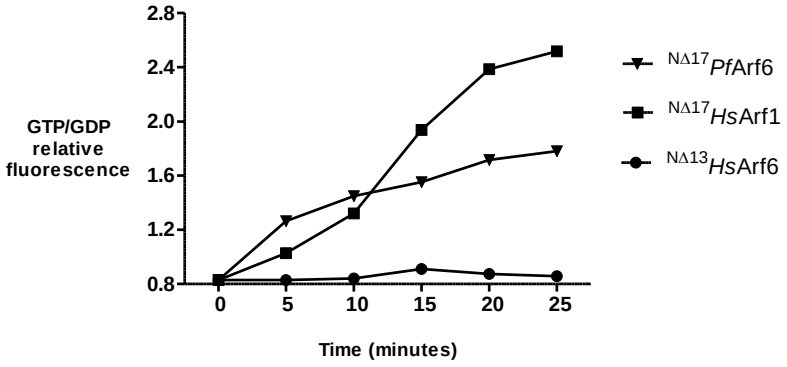

Figure 29: ARNO-mediated nucleotide exchange of $^{N\Delta17}$*Pf*Arf6 measured by tryptophan fluorescence in real-time. The GTP/GDP relative fluorescence was calculated by dividing the Arf-GTP intrinsic tryptophan fluorescence readings by those obtained for Arf-GDP. To 1 μM $^{N\Delta17}$*Pf*Arf6, 50 μM GDP/GTP and 0.1 μM ARNO^{Sec7} was added. The reactions were incubated at 25ºC for 25 minutes, where the intrinsic tryptophan fluorescence was measured every 5 minutes. Parallel reactions using $^{N\Delta17}$*Hs*Arf1 were used as a positive control and $^{N\Delta13}$*Hs*Arf6 as a negative control. No discernible increase in GTP/GTP fluorescence was observed for $^{N\Delta13}$*Hs*Arf6 (●), while a clear increase was observed for $^{N\Delta17}$*Hs*Arf1 (■) which culminated in a total increase of approximately 252% after the 25-minute period. An increase was observed for $^{N\Delta17}$*Pf*Arf6 (▼) which culminated in a total increase of approximately 178% after the 25-minute period. Each point represents the mean of readings obtained from 3 replicate wells containing GTP reactions divided by the mean of readings obtained from 3 replicate wells containing GDP reactions.

The putative GGA and JIP4 binding residues in *Hs*Arf6 are only partially conserved in the putative *Pf*Arf6. Since there are, currently, no known effector proteins for the putative $^{N\Delta17}$*Pf*Arf6, the GGA^{GST} and JIP4^{GST} proteins were used for the interaction assay. Prior to development of the immobilised $^{N\Delta17}$*Pf*Arf6-GGA or $^{N\Delta17}$*Pf*Arf6-JIP4 interaction assays, the conservation of the binding residues was explored. The residues involved in Arf-GGA binding were obtained from the Arf1_5_like protein (NCBI accession number: cd04150) and determined by Zhu *et al.* (2005). Pairwise sequence

alignment with human Arf6 protein sequence (accession number: CAG46737.1) suggested that these residues were conserved in *Hs*Arf6 (*results not shown*). Pairwise sequence alignment between *Hs*Arf6 and the putative *Pf*Arf6 (PlasmoDB code: *PF*10_0337) was conducted using the EMBOSS Water alignment tool (EMBL-EBI) and viewed using MEGA software (**Figure 30A**). The Val49, Gly50 and Phe51 residues within the switch I domain of *Hs*Arf6 (*yellow*) are conserved in *Pf*Arf6 (*blue*). However, the Lys73 and His80 residues in *Hs*Arf6 (*yellow*) involved in GGA binding within the Switch II region are not functionally conserved in *Pf*Arf6 (*red*). The residues involved in *Hs*Arf6-JIP4 binding determined by Isabet *et al*. (2009) were used to investigate the suitability of JIP4 as a binding partner of *Pf*Arf6. Pairwise sequence alignment between *Hs*Arf6 and the putative *Pf*Arf6 (PlasmoDB code: *PF*10_0337) was conducted using the EMBOSS Water alignment tool (EMBL-EBI) and viewed using MEGA software (**Figure 30B**). The Lys62 residue within the interswitch region is the only functionally conserved residue involved in JIP4 binding in the *Pf*Arf6 sequence (*blue*). The Thr57, Asn64 and Thr83 residues involved in JIP4 binding are not functionally conserved in *Pf*Arf6 (*red*).

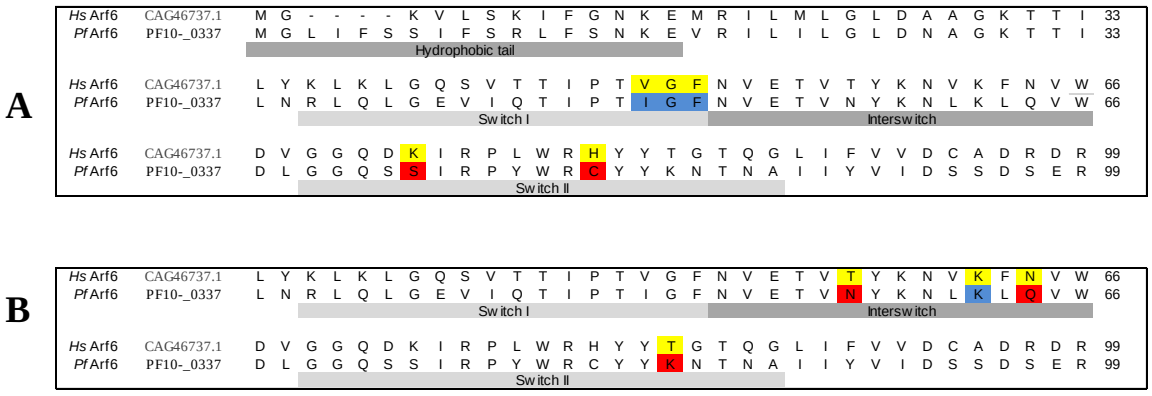

Figure 30: Partial conservation of *Hs*Arf6 effector binding sites in *Pf*Arf6. The putative malarial Arf6 protein sequence (PlasmoDB code: *PF*10_0337) was aligned with human Arf6 (accession number: CAG46737.1) using the EMBOSS water pairwise alignment tool. The alignment was viewed using MEGA software and edited in Microsoft Excel. **A**: The residues involved in *Hs*Arf6-GGA binding obtained from the Arf1_5_like protein (NCBI accession number: cd04150) and determined by Zhu *et al*. (2005) are partially conserved in *Pf*Arf6. The Val49, Gly50 and Phe51 residues within the switch I domain of *Hs*Arf6 (*yellow*) are conserved in *Pf*Arf6 (*blue*). However, the Lys73 and His80 residues in *Hs*Arf6 (*yellow*) involved in GGA binding within the Switch II region are not conserved in *Pf*Arf6 (*red*). **B**: The residues involved in *Hs*Arf6-JIP4 binding determined by Isabet *et al*. (2009) are partially conserved in *Pf*Arf6. The Lys62 residue within the interswitch region is the only conserved residue involved in JIP4 binding in the *Pf*Arf6 sequence (*blue*). The Thr57, Asn64 and Thr83 residues involved in JIP4 binding are not conserved in *Pf*Arf6 (*red*).

The interaction of $^{N\Delta17}$*Pf*Arf6-GGA is not detectable using the nickel-coated plate immobilisation GST assay. Although it was difficult to predict how the non-conservation of binding residues would affect $^{N\Delta17}$*Pf*Arf6-GGA or $^{N\Delta17}$*Pf*Arf6-JIP4 interaction, it was decided to attempt the $^{N\Delta17}$*Pf*Arf6-GGA binding assay (which, at the time, could only be conducted on a nickel-coated plate) since there was a greater conservation of the GGA binding residues as opposed to those involved in JIP4 binding. Since $^{N\Delta17}$*Pf*Arf6-GDP and $^{N\Delta17}$*Pf*Arf6-GTP could not be prepared by EDTA-mediated nucleotide exchange,

the immobilised interaction assay was explored using $^{N\Delta17}$*Pf*Arf6-GTP prepared by ARNO-mediated GDP/GTP exchange alongside relevant controls. To 2 μM $^{N\Delta17}$*Pf*Arf6, 50 μM GTP was added along with 0.2 μM ARNO^{Sec7}. The reaction was incubated for 25 minutes at 25^{o}C with gentle agitation. Two negative controls were also prepared in parallel. In the first negative control ARNO^{Sec7} was omitted, and in the second both ARNO^{Sec7} and GTP were omitted. To confirm that the ARNO-mediated exchange was successful before transferring to the nickel-coated plate, the GTP/GDP relative fluorescence was assessed, as described in the previous section (*not shown*). The reaction products were applied to a nickel-coated plate and the immobilisation assay was conducted as previously described for *Hs*Arf6 (chapter 2). The only alteration to the method was that the final concentration GST-GGA^{GAT} was increased to 5 μM to compensate for the potentially weaker interaction of $^{N\Delta17}$*Pf*Arf6-GGA as opposed to $^{N\Delta13}$*Hs*Arf6-GGA. The difference in the GST signals measured for $^{N\Delta17}$*Pf*Arf6 incubated in the presence and absence of ARNO^{Sec7} was not statistically significant ($\rho = 0.5966$, n =3) (**Figure 31**). This raised the possibility that the $^{N\Delta17}$*Pf*Arf6-GGA interaction was too weak to discriminate $^{N\Delta17}$*Pf*Arf6-GTP from $^{N\Delta17}$*Pf*Arf6 that had not been loaded with the nucleotide.

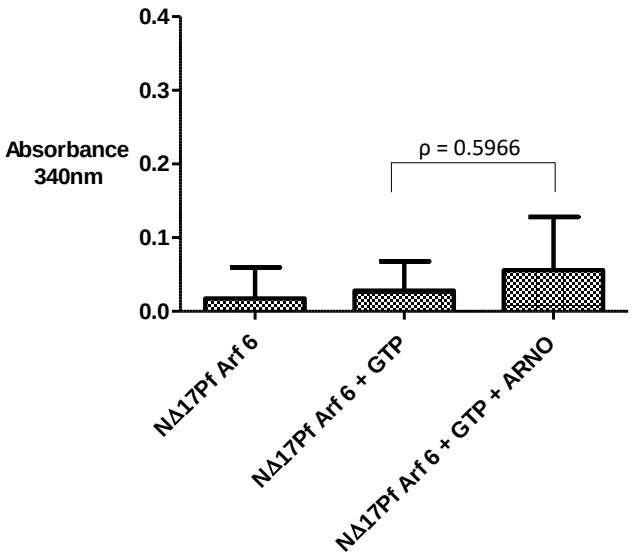

Figure 31: The interaction of $^{N\Delta17}$*Pf*Arf6-GGA is not detectable using the nickel-coated immobilisation assay. As a negative control $^{N\Delta17}$*Pf*Arf6-GTP was incubated alone. As a spontaneous GDP/GTP exchange control $^{N\Delta17}$*Pf*Arf6-GTP was incubated with only GTP. In the experiment $^{N\Delta17}$*Pf*Arf6-GTP was incubated with GTP in the presence of ARNO^{Sec7}. The immobilised *Pf*Arf6-GGA GST interaction assay was employed to detect the activation status of $^{N\Delta17}$*Pf*Arf6 following ArfGEF mediated activation. After subtracting background control readings, the difference in the GST signals measured for $^{N\Delta17}$*Pf*Arf6 incubated in the presence and absence of ARNO^{Sec7} was not statistically significant ($\rho = 0.5966$). Each bar represents the mean and standard deviation of readings obtained from 3 replicate wells.

The interaction of $^{N\Delta17}$*Pf*Arf6-JIP4 is detectable using the glutathione-coated immobilisation assay. In an attempt to enhance the detection of $^{N\Delta17}$*Pf*Arf6-GTP vs. $^{N\Delta17}$*Pf*Arf6 that had not been loaded with a nucleotide, the nickel-HRP enzyme capture assay on a glutathione plate was adopted since it was designed for the purpose of obtaining greater signal sensitivity (the HRP enzyme reaction has a higher

rate and product molar absorption than the corresponding GST assay used to detect interactions in the nickel plate assay). In previous studies done using human Arf6 (Chapter 3), the GST-GGA^{GAT} immobilised on a glutathione plate could not discriminate active $^{N\Delta13}$*Hs*Arf6-GTP from inactive $^{N\Delta13}$*Hs*Arf6-GDP. This was possibly due to the excess free GST in the purified GST-GGA^{GAT} fraction which may have competed with GST-GGA^{GAT} for immobilisation on the glutathione plate. By contrast, GST-JIP4^{LZII} could robustly distinguish between GTP- and GDP loaded human Arf6. It was therefore decided to conduct the nickel-HRP enzyme assay on a glutathione plate using GST-JIP4^{LZII} as the bait protein even though very little conservation of JIP4 binding residues was observed in the *Pf*Arf6 protein sequence. Once again, 50 μM GTP and 0.2 μM ARNO^{Sec7} was added to 2 μM $^{N\Delta17}$*Pf*Arf6 and the reaction was incubated for 25 minutes at 25ºC with gentle agitation. To confirm that the ARNO-mediated exchange was successful before transferring to the nickel-coated plate, the same reaction was conducted using GDP and the GTP/GDP relative fluorescence was assessed by intrinsic tryptophan fluorescence (*not shown*). Two negative controls for the immobilisation assay were also prepared in parallel. In the first negative control ARNO^{Sec7} was omitted, and in the second both ARNO^{Sec7} and GTP were omitted. $^{N\Delta17}$*Pf*Arf6 was diluted to 1 μM by adding a final concentration of 5 μM GST-JIP4^{LZII} and the mixture added to the glutathione plate. The immobilised glutathione plate assay was conducted as usual, except that a 1: 2 000 dilution of Nickel-HRP was used as opposed to 1: 10 000 that was usually used. The reagent concentration was increased to try enhance signals from the potentially weaker $^{N\Delta17}$*Pf*Arf6-JIP4 interaction. The difference in the HRP signals measured for $^{N\Delta17}$*Pf*Arf6 incubated in the presence and absence of ARNO^{Sec7} was statistically significant ($\rho = 0.0001$, n =3) (**Figure 32**). This suggested that although the $^{N\Delta17}$*Pf*Arf6-JIP4 interaction may be weak, under the conditions used in the assay, $^{N\Delta17}$*Pf*Arf6-GTP was distinguishable from $^{N\Delta17}$*Pf*Arf6 that had not been loaded with a nucleotide.

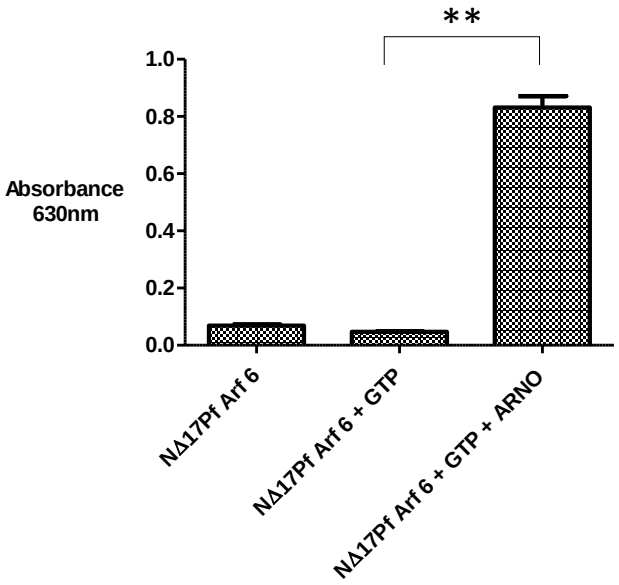

Figure 32: The interaction of $^{N\Delta17}$*Pf*Arf6-JIP4 is detectable using the glutathione-coated plate immobilisation assay. GTP and ARNO^{Sec7} was added to $^{N\Delta17}$*Pf*Arf6. The reaction was incubated alongside parallel reactions lacking ARNO^{Sec7} or lacking both ARNO^{Sec7} and GTP were also conducted. The reaction products were incubated on a glutathione plate containing immobilised GST-JIP4^{LZII} and detected using Nickel-HRP. HRP oxidation product, TMB/diimine complex was detected at an absorbance of 630nm. The difference in the HRP signals measured for $^{N\Delta17}$*Pf*Arf6 incubated in the presence and absence of ARNO^{Sec7} was statistically significant ($\rho < 0.01$). Each bar represents the mean and standard deviation of readings obtained from 3 replicate wells.

The putative GEF interaction site in *Hs*Arf6 is partially conserved in *Pf*Arf6. Since ARNO-stimulated activation of *Pf*Arf6 was possible and detectable using the glutathione-coated immobilisation assay, it implied that ArfGEF interaction sites in *Pf*Arf6 are conserved and that the high-throughput screening format could be adopted for the screening of novel inhibitors of ArfGEF-mediated GDP/GTP exchange on *Pf*Arf6. For this purpose, it may be more relevant to use a malaria ArfGEF rather than a human protein (e.g. ARNO). An attempt was therefore made to obtain the predicted Sec7 domain of a *Pf*ArfGEF. As described earlier, while the protein was expressed in *E. coli*, purification by nickel-affinity chromatography was unsuccessful. Although alternative strategies to purify *Pf*ArfGEF^{Sec7} are currently being explored, *in silico* predictions suggest that the putative ArfGEF interaction sites in *Hs*Arf6 are at least partially conserved in the putative *Pf*Arf6. The specific residues involved in this interaction were obtained from NMR spectroscopy studies of the *Hs*Arf1-ARNO^{Sec7} complex (Kremer *et al*., 2004), and extrapolated by multiple sequence alignments including alignment with the human Arf6 protein sequence (accession number: CAG46737.1). Pairwise sequence alignment between *Hs*Arf6 and the putative *Pf*Arf6 (PlasmoDB code: *PF*10_0337) was conducted using the EMBOSS Water alignment tool (EMBL-EBI) and viewed using MEGA software (**Figure 33**). Of the fourteen residues involved in the *Hs*Arf6-ARNO^{Sec7} interaction, only three are not conserved in *Pf*Arf6. These residues included Asn57, Ser73 and Cys80 (**Figure 33,** *red*). While there is no *a priori* evidence that the putative *Pf*ArfGEF^{Sec7} is able to activate *Pf*Arf6 or that its interaction sites will be similar to those

involved in ArfGEF interaction of human Arf GTPases, the JIP4 interaction assay described above and subsequent X-ray crystallographic determinations could be conducted in the future to explore this.

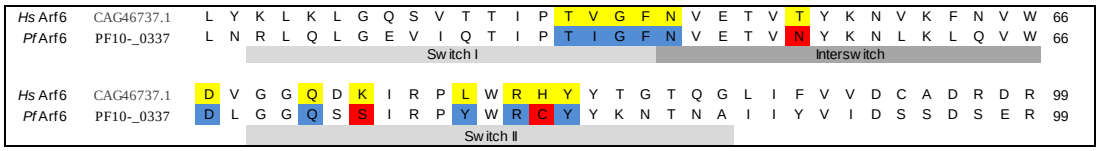

Figure 33: Partial conservation of *Hs*Arf6 putative ArfGEF interaction sites in *Pf*Arf6. The putative ArfGEF interaction sites were obtained from NMR spectroscopy studies of the *Hs*Arf1-ARNO^{Sec7} complex (Kremer *et al*., 2004), and extrapolated by multiple sequence alignments including alignment with human Arf6 protein sequence (accession number: CAG46737.1). The putative malarial Arf6 protein sequence (PlasmoDB code: *PF*10_0337) was aligned with human Arf6 (accession number: CAG46737.1) using the EMBOSS water pairwise alignment tool. The alignment was viewed using MEGA software and edited in Microsoft Excel. Of the fourteen residues involved in the *Hs*Arf6-ARNO^{Sec7} interaction (*yellow*), only the Asn57, Ser73 and Cys80 (*red*) are not conserved. The remaining eleven residues are functionally conserved (*blue*).

The immobilised *Pf*Arf1-GGA GST enzyme assay can be used to study *Pf*ArfGAP1- and *Pf*ArfGAP2-mediated *Pf*Arf1 deactivation.

While the *Pf*Arf6-JIP4 interaction on a glutathione-coated plate may provide a suitable high-throughput assay model for screening compounds with inhibitory effects on ArfGEF-mediated *Pf*Arf6 activation (GDP/GTP exchange), it would not be suitable for drug screening to find inhibitors of ArfGAP-mediated deactivation (GTP hydrolysis) of *Pf*Arf6 using the GAP domains of the putative malaria ArfGAPs, *Pf*ArfGAP1^{GAP} and *Pf*ArfGAP2^{GAP}. In order to study ArfGAP-stimulated GTP hydrolytic activity, one would require Arf GTPases in their Arf-GTP active form. Since EDTA-mediated nucleotide exchange was not achieved through the course of the study using *Pf*Arf6 (as described earlier), it was decided to rather use the *Pf*Arf1-GGA interaction model for the development of *Pf*ArfGAP1^{GAP} and *Pf*ArfGAP2^{GAP} deactivation assays in high-throughput format. $^{N\Delta17}$*Pf*Arf1-GDP and $^{N\Delta17}$*Pf*Arf1-GTP were prepared by EDTA-mediated nucleotide exchange as measured by intrinsic tryptophan fluorescence assays (**Figure S39A**). The preferential binding of GST-GGA^{GAT} to active $^{N\Delta17}$*Pf*Arf1-GTP (as opposed to $^{N\Delta17}$*Pf*Arf1-GDP) on a nickel-coated plate (**Figure S39B**) was also confirmed prior to using $^{N\Delta17}$*Pf*Arf1-GTP in the *Pf*ArfGAP1/2^{GAP}-mediated deactivation studies. To investigate whether the assay could distinguish the activation status of $^{N\Delta17}$*Pf*Arf1 following *Pf*ArfGAP1-stimulated deactivation (hydrolysis of the Arf-bound GTP to GDP) the GAP domain of *Pf*ArfGAP1^{GAP} was used. The *Pf*ArfGAP1^{GAP} deactivation assay was conducted by incubating 1 µM $^{N\Delta17}$*Pf*Arf1-GTP with 0.1, 0.15 and 0.20 µM *Pf*ArfGAP1^{GAP} for 30 minutes at 28ºC with gentle agitation. The remainder of the nickel-coated interaction assay was conducted as described previously (immobilisation of *Pf*Arf1 on a nickel-coated plate, followed by incubation with GST-GGA^{GAT} and a

colorimetric GST enzyme assay). Decreases in *Pf*Arf1-GGA binding, in comparison the positive control ($^{N\Delta17}$*Pf*Arf1-GTP in the absence of *Pf*ArfGAP1^{GAP}) showed that 0.10, 0.15 and 0.20 μM *Pf*ArfGAP1^{GAP} significantly deactivated $^{N\Delta17}$*Pf*Arf1-GTP ($\rho = 0.0009$, $\rho = 0.0024$ and $\rho = 0.0001$ respectively, n = 3 for each *t*-test) (**Figure 34A**). To interrogate whether the decrease in *Pf*Arf1-GGA interaction signal was owing to the *Pf*ArfGAP1^{GAP}-stimulated GTP hydrolysis of $^{N\Delta17}$*Pf*Arf1-GTP or simply the displacement of a proportion of $^{N\Delta17}$*Pf*Arf1-GTP bound to the nickel plate by *Pf*ArfGAP1^{GAP}, validation studies were conducted using a human ArfGAP1 inhibitor QS11. Three reactions were prepared in conjunction with the background control (wells incubated with GST-GGA^{GAT} only). In the positive control $^{N\Delta17}$*Pf*Arf1-GTP was incubated alone. In the negative control $^{N\Delta17}$*Pf*Arf1-GTP was incubated with 0.20 μM *Pf*ArfGAP1^{GAP} in the absence of QS11, whereas in the experiment they were incubated in the presence of 50 μM QS11. The deactivation of $^{N\Delta17}$*Pf*Arf1-GTP was inhibited by QS11 ($\rho = 0.05$, n = 3) (**Figure 34B**). This result suggested that the decrease in *Pf*Arf1-GGA interaction signals was as a result of *Pf*ArfGAP1^{GAP}-stimulated GTP hydrolytic activity and further suggested that *Pf*ArfGAP1^{GAP} may be the target of QS11.

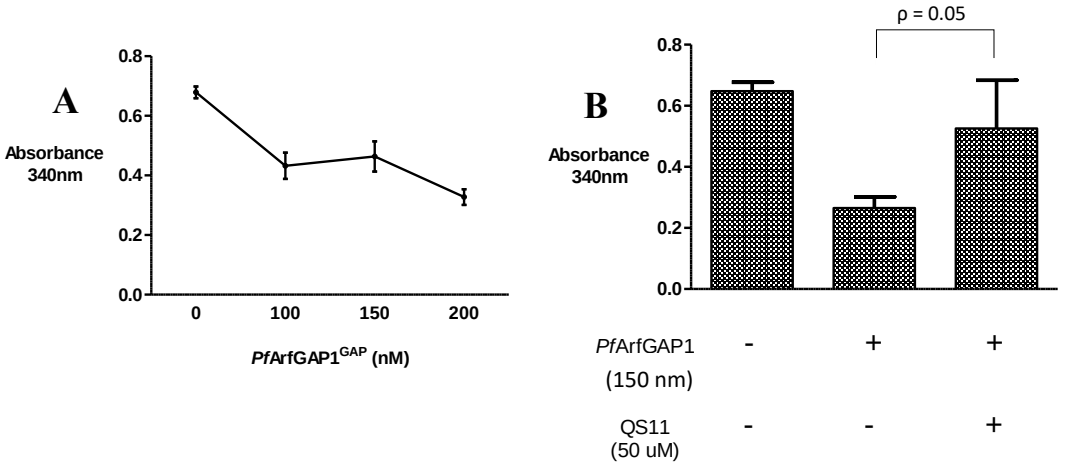

Figure 34: The immobilised *Pf*Arf1-GGA interaction assay can detect *Pf*ArfGAP1-mediated deactivation of malarial Arf1. **A**: *Pf*ArfGAP1^{GAP}-stimulated GTP hydrolysis of $^{N\Delta17}$*Pf*Arf1-GTP was conducted by incubating $^{N\Delta17}$*Pf*Arf1-GTP with *Pf*ArfGAP1^{GAP}. The immobilised *Pf*Arf1-GGA interaction assay was employed to detect the activation status of $^{N\Delta17}$*Pf*Arf1 following *Pf*ArfGAP1^{GAP}-stimulated deactivation. As a positive control $^{N\Delta17}$*Pf*Arf1-GTP incubated without *Pf*ArfGAP1^{GAP} was used. To determine the concentration of *Pf*ArfGAP1^{GAP} required to significantly reduce *Pf*Arf1-GGA binding 100, 150 and 200 nm *Pf*ArfGAP1^{GAP} was incubated with 1 μM $^{N\Delta17}$*Pf*Arf1-GTP. *Pf*Arf1-GGA binding was significantly reduced by all *Pf*ArfGAP1^{GAP} concentrations ($\rho < 0.01$). **B**: Chemical validation of *Pf*ArfGAP1^{GAP} GTP hydrolytic activity. Deactivation was conducted by incubating 1 μM $^{N\Delta17}$*Pf*Arf1-GTP with 200 nM *Pf*ArfGAP1^{GAP} in the presence or absence of 50 μM QS11. difference in GST signals between *Pf*ArfGAP1^{GAP} deactivation of $^{N\Delta17}$*Pf*Arf1-GTP in the presence and absence of QS11 was statistically significant ($\rho = 0.05$). Each bar represents the mean and standard deviation of readings obtained from 3 replicate wells.

To investigate whether the assay could distinguish the activation status of $^{N\Delta17}$*Pf*Arf1 following *Pf*ArfGAP2-stimulated deactivation (hydrolysis of the Arf-bound GTP to GDP) the GAP domain of the putative *Pf*ArfGAP2^{GAP} was used. The *Pf*ArfGAP2^{GAP} deactivation assay was conducted as described for *Pf*ArfGAP1^{GAP} by incubating 1 μM $^{N\Delta17}$*Pf*Arf1-GTP with 0.1, 0.15 and 0.20 μM *Pf*ArfGAP2^{GAP} for 30 minutes at 28ºC with gentle agitation. The remainder of the nickel-coated interaction assay was conducted as usual. Decreases in *Pf*Arf1-GGA binding, in comparison the positive control ($^{N\Delta17}$*Pf*Arf1-GTP in the absence of *Pf*ArfGAP1^{GAP}) showed that 0.15 and 0.20 μM *Pf*ArfGAP2^{GAP} significantly deactivated $^{N\Delta17}$*Pf*Arf1-GTP ($\rho = 0.0104$ and $\rho = 0.0004$ respectively, $n = 3$ for each *t*-test) (**Figure 35A**). As done previously, QS11 was used to determine whether it was capable of inhibiting *Pf*ArfGAP2 and to interrogate whether the decrease in *Pf*Arf1-GGA interaction signal was owing to the *Pf*ArfGAP2^{GAP}-stimulated GTP hydrolysis of $^{N\Delta17}$*Pf*Arf1-GTP and not simply the displacement of a proportion of $^{N\Delta17}$*Pf*Arf1-GTP bound to the nickel plate by *Pf*ArfGAP2^{GAP}. The assay was carried out using $^{N\Delta17}$*Pf*Arf1-GTP alone, $^{N\Delta17}$*Pf*Arf1-GTP incubated with 0.20 μM *Pf*ArfGAP1^{GAP} and $^{N\Delta17}$*Pf*Arf1-GTP incubated with 0.20 μM *Pf*ArfGAP1^{GAP} in the presence of 50 μM QS11, in conjunction with a background control (wells incubated with GST-GGA^{GAT} in the absence of *Pf*Arf1). In contrast to the previous result obtained with *Pf*ArfGAP1, the deactivation of $^{N\Delta17}$*Pf*Arf1-GTP was not inhibited by QS11 ($\rho = 0.7189$, $n = 3$) (**Figure 35B**). While this result raised the possibility that QS11 selectively inhibited *Hs*ArfGAP1 and *Pf*ArfGAP1 (the significance of which will be discussed later), the *Pf*ArfGAP2^{GAP}-stimulated GTP hydrolytic activity still required validation. As an alternative validation strategy $^{N\Delta17}$*Pf*Arf1 was chemically loaded with GTP on the one hand, or GTPγS (a non-hydrolysable analogue of GTP) on the other, and the *Pf*ArfGAP2^{GAP} deactivation assay repeated as described above. As a positive control, $^{N\Delta17}$*Pf*Arf1-GTP and $^{N\Delta17}$*Pf*Arf1-GTPγS were incubated in the absence of *Pf*ArfGAP2^{GAP} (**Figure 35C**). *Pf*ArfGAP2^{GAP} caused a statistically significant ($\rho = 0.0004$, $n = 3$) 60% decrease in the ability of GTP-loaded $^{N\Delta17}$*Pf*Arf1 to bind to GST-GGA^{GAT}. By contrast, in the case of $^{N\Delta17}$*Pf*Arf1 loaded with GTPγS, *Pf*ArfGAP2^{GAP} incubation only decreased GST-GGA^{GAT} binding by 17% ($\rho = 0.0189$, $n = 3$). This suggested that the reduced binding of GST-GGA^{GAT} by $^{N\Delta17}$*Pf*Arf1-GTP after incubation with *Pf*ArfGAP2^{GAP} was indeed due to GAP-stimulated GTP hydrolysis by the Arf GTPase, since the process was inhibited when $^{N\Delta17}$*Pf*Arf1 contained the non-hydrolysable analogue GTPγS.

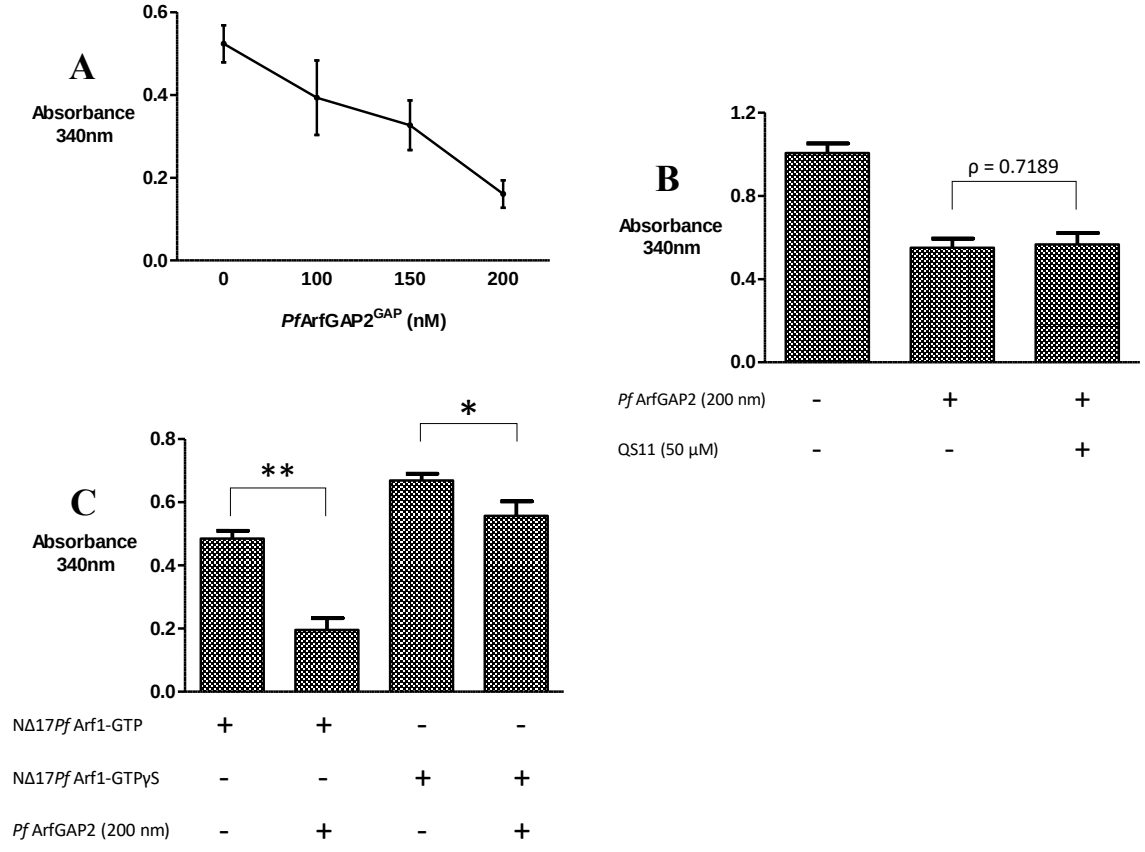

Figure 35: The immobilised *Pf*Arf1-GGA interaction assay can detect *Pf*ArfGAP2-mediated deactivation of malarial Arf1. **A**: *Pf*ArfGAP2^{GAP}-stimulated GTP hydrolysis of $^{N\Delta17}$*Pf*Arf1-GTP was conducted by incubating $^{N\Delta17}$*Pf*Arf1-GTP with *Pf*ArfGAP2^{GAP}. The immobilised *Pf*Arf1-GGA interaction assay was employed to detect the activation status of $^{N\Delta17}$*Pf*Arf1 following *Pf*ArfGAP2^{GAP}-stimulated deactivation. As a positive control $^{N\Delta17}$*Pf*Arf1-GTP incubated without *Pf*ArfGAP2^{GAP} was used. To determine the concentration of *Pf*ArfGAP2^{GAP} required to significantly reduce *Pf*Arf1-GGA binding 100, 150 and 200 nm *Pf*ArfGAP2^{GAP} was incubated with 1 µM $^{N\Delta17}$*Pf*Arf1-GTP. *Pf*Arf1-GGA binding was significantly reduced by 150 and 200 nM *Pf*ArfGAP2^{GAP} ($\rho < 0.05$ and $\rho < 0.01$ respectively). **B**: QS11 did not inhibit *Pf*ArfGAP2^{GAP} GTP hydrolytic activity. Deactivation was conducted by incubating 1 µM $^{N\Delta17}$*Pf*Arf1-GTP with 200 nM *Pf*ArfGAP2^{GAP} in the presence or absence of 50 µM QS11. The difference in GST signals between *Pf*ArfGAP1^{GAP} deactivation of $^{N\Delta17}$*Pf*Arf1-GTP in the presence and absence of QS11 was not statistically significant ($\rho = 0.7189$). **C**: Validation of *Pf*ArfGAP2^{GAP} GTP-hydrolytic activity using a non-hydrolysable analog of GTP, GTPγS. $^{N\Delta17}$*Pf*Arf1-GTP and $^{N\Delta17}$*Pf*Arf1-GTPγS were incubated in the presence and absence of *Pf*ArfGAP2^{GAP}. The decrease in the binding signals between $^{N\Delta17}$*Pf*Arf1-GTP and GST-GGA^{GAT} in the presence and absence of *Pf*ArfGAP2^{GAP} was statistically significant ($\rho < 0.01$, n = 3), as was the difference between the binding signals of $^{N\Delta17}$*Pf*Arf1-GTPγS and GST-GGA^{GAT} in the presence and absence of *Pf*ArfGAP2^{GAP} ($\rho < 0.05$, n = 3)..Each bar represents the mean and standard deviation of readings obtained from 3 replicate wells.

5.4. Discussion and future work

The aim of the study was to develop a robust, *Pf*Arf6 interaction assay that could be employed for high-throughput screening (HTS) of compound libraries to identify novel inhibitors of malarial Arf-effector, Arf-ArfGEF and Arf-ArfGAP interactions. Despite the GST-based assay format being well-suited for the development of human Arf6 signalling interaction assays, it was not compatible with *Pf*Arf6 signalling assays owing to weak interaction signals. As initially intended, the HRP-based assay using JIP4 as an effector protein, appeared to improve signal outputs as required and may be a potential candidate as a *Pf*Arf6-JIP4 interaction assay for HTS. Based on the cost analyses conducted in Chapter 4, we can conclude that the assay may be cost-effective, but we have not yet appropriately validated the assay format.

Owing to time constraints, the reproducibility and high-throughput screening potential (Z-factor) of the immobilised JIP4-*Pf*Arf6 (HRP-based) assay has not yet been properly assessed. The initial findings were promising, in that the assay could distinguish *Pf*Arf6 that had not been specifically pre-loaded with a guanine nucleotide (but presumed to represent *Pf*Arf6-GDP, as discussed shortly) from *Pf*Arf6-GTP that was prepared by ARNO-mediated GDP/GTP exchange. However, the assay has only been tested under one set of conditions (stoichiometry between *Pf*Arf6, JIP4 and ARNO and nickel-HRP antibody dilutions have not been optimised) and extensive repetitions of the assay were not conducted. Thus, it is crucial that the continuation of the project begins by testing the reproducibility of the assay by conducting additional biological replicates. SecinH3 could also be used to validate the ARNO-mediated GDP/GTP exchange of *Pf*Arf6 (SecinH3 is an inhibitor of all cytohesins including ARNO; Hafner et al., 2006).

Provided the initial finding is not a false-positive, the assay conditions should be optimized, and the Z-factor score determined to ascertain whether the assay is suitable for HTS (Zhang et al., 1999). Considering the low background to signal ratio of the single biological replicate, it is unlikely that the assay will fail in terms of its HTS potential.

The potential immobilised JIP4-*Pf*Arf6 interaction assay may be suitable as an Arf-effector base assay that can be extended as a tool to conduct HTS of compounds with inhibitory effects on *Pf*Arf6-*Pf*ArfGEF and *Pf*Arf6-*Pf*ArfGAP interactions, but the *Pf*Arf6-JIP4 interaction itself it is not significant in the cellular context. It may be worth identifying alternative malarial effector proteins that are part of a native *Pf*Arf6-effector interaction within the parasite. Identification of novel effectors could be explored by pull-down assays. His-tagged *Pf*Arf6 pre-loaded to GTPγS (a non-hydrolysable analog of GTP) bound to nickel-coated beads would be used for pull-downs from parasite cell lysates (potential methods for pre-loading *Pf*Arf6 with GTPγS will be discussed shortly). Eluted proteins would then be

analysed by mass-spectrometry, alongside routine pull-down assay controls and an additional control to account for interactors of inactive *Pf*Arf6-GDP (Brymora et al., 2004). Identified malarial effector proteins would serve in the development of additional *Pf*Arf6-effector interaction assays for HTS and may provide insights into the possible functions of *Pf*Arf6 (as was explored in Chapter 3). These findings may support or refute our current hypothesis that *Pf*Arf6 may be a participant in parasite autophagy or a *Pf*Arf6-depdenent endocytic pathway.

A major hurdle in the development of *Pf*Arf6-*Pf*ArfGEF and *Pf*Arf6-*Pf*ArfGAP interaction assays was the inability to prepare *Pf*Arf6-GDP and *Pf*Arf6-GTP by EDTA-mediated nucleotide exchange. These experiments appeared to destabilise the protein structure irreversibly. On the other hand, ARNO-mediated GDP/GTP exchange on *Pf*Arf6 was successfully conducted and assessed by tryptophan fluorescence assays. An increase in fluorescence over time indicates the conformational transition from Arf-GDP to Arf-GTP associated with GDP/GTP nucleotide exchange (Bigay and Antonny, 2006). Conversely, a decrease in fluorescence over time represents the conformation shift from Arf-GTP to Arf-GDP associated with ArfGAP-stimulated GTP hydrolysis (Weimer et al., 2008). Since an increase in fluorescence over time was observed when *Pf*Arf6 was incubated with GTP and ARNO^{Sec7}, it implies that *Pf*Arf6 must have been, at least partially, purified from *E. coli* in a GDP-bound form. This is not an unusual phenomenon, since most Arfs are expressed and purified in either GDP- or GTP-bound forms (Bigay and Antonny, 2006); an example is *Hs*Arf6 which is predominantly expressed in its GTP-bound form (Macia et al., 2001). If *Pf*Arf6 is expressed as *Pf*Arf6-GDP, then EDTA-mediated nucleotide exchange is not required to prepare *Pf*Arf6-GDP for *Pf*ArfGEF^{Sec7} GDP/GTP exchange activity assays. However, while most of the proteins used in the study were successfully purified to an acceptable level of homogeneity, the only exception was the His-tagged *Pf*ArfGEF^{Sec7} recombinant protein, and hence this interaction assay has not yet been examined. The presence of soluble His-tagged *Pf*ArfGEF^{Sec7} in small scale expression studies suggested that the protein was successfully expressed but could not be isolated from the soluble cell lysate by Ni-NTA chromatography. It is possible that the histidine tag fused to *Pf*ArfGEF^{Sec7} is obscured in the final conformation of the recombinant protein and, as a result the Ni-NTA resin cannot gain access to the tag. One possible solution is to change the placement of the His-tag to the C-terminus, as opposed to the N-terminus (as was conducted in this was study) and repeat the Ni-NTA affinity chromatography purification. The fusion of a red fluorescent tag to a yeast Sec7 domain did not appear to affect Sec7 catalytic activity (Losev et al., 2006). Furthermore, a general lack of evidence against C-terminal tags on the Sec7 domain suggests that this fusion is unlikely to disrupt *Pf*ArfGEF^{Sec7} GDP/GTP exchange activity. If the *Pf*ArfGEF^{Sec7} purification issues can be resolved, and if the *Pf*ArfGEF^{Sec7} GDP/GTP exchange activity assays perform as expected then this assay format will be ready for HTS after optimization. As a final note, the highly unusual Sec7 domain of *Pf*ArfGEF makes the assignment of this malarial homolog to one of the human ArfGEF families very difficult. Consequently, while it would be interesting to investigate whether SecinH3 (an

inhibitor of cytohesins and GEP100; Grossmann et al., 2013; Hafner et al., 2006) can inhibit the malarial homolog, it cannot be used as definitive chemical validation.

On the other hand, if *Pf*Arf6 is expressed as *Pf*Arf6-GDP, then the preparation of *Pf*Arf6-GTP is still required for *Pf*ArfGAP^{GAP}-stimulated GTP hydrolysis assays. This issue was initially circumvented by employing the *Pf*Arf1-GGA interaction assay to assess the GTP hydrolytic potential of *Pf*ArfGAP1^{GAP} and the putative *Pf*ArfGAP2^{GAP} (*Pf*Arf1-GDP and *Pf*Arf1-GTP can be prepared by routine EDTA-mediated nucleotide exchange experiments, and *Pf*Arf1 can bind to GGA in the GST-based assay format). *Pf*ArfGAP1^{GAP}-stimulated GTP hydrolysis on *Pf*Arf1-GTP was successfully observed and validated by inhibiting this activity with QS11. This result suggested that *Pf*ArfGAP1^{GAP} may be the molecular target of QS11 in parasites. Interestingly, *Pf*ArfGAP2^{GAP}-stimulated GTP hydrolysis on *Pf*Arf1-GTP was not perturbed by QS11 (*Pf*ArfGAP2^{GAP}-stimulated GTP hydrolysis was instead validated using GTPγS).

This result shows that the GAP domains of *Pf*ArfGAP1 and *Pf*ArfGAP2 are sufficiently different that we may be able to identify unique inhibitors for each protein. Currently, there is no evidence that *Pf*ArfGAP2 is necessarily a good drug target i.e. inhibition of *Pf*ArfGAP2 has not been linked to parasite cell death simply because potent inhibitors have not yet been identified. Likewise, parasite death under QS11 treatment is only effectuated at micromolar concentrations (7 µM), which may warrant further investigation, but does not qualify QS11 as a potent antimalarial. Oftentimes, certain ArfGAPs have demonstrated the ability to compensate for the loss-of-function of an alternative ArfGAP by participating in overlapping functions (Weimer et al., 2008). It is conceivable then that *Pf*ArfGAP2 may be compensating for the inhibition of *Pf*ArfGAP1 and thus reduce the observed potency of QS11 against malaria parasites, and that the dual-inhibition of both *Pf*ArfGAPs may abolish the opportunity for compensatory effects and significantly improve the potency of the individual inhibitors (drug synergy studies by isobologram analysis may be employed to explore this). Using the *Pf*Arf1-GGA interaction assay, HTS for compounds with inhibitory effects on both *Pf*ArfGAPs should commence immediately. Coupled with cytotoxicity screens, single-inhibitor effects and dual-inhibitor effects should be tested and if the dual-inhibition hypothesis is correct, antimalarials containing both active compounds could continue through the drug discovery pipeline. On the contrary, these malarial ArfGAPs may have non-overlapping functions or simply exist in spatially distinct locations with the parasite. It is possible that one ArfGAP may be involved in terminating *Pf*Arf1 function in the Golgi apparatus, while the other acts on *Pf*Arf6 closer to the plasma membrane. The alternative theory could be concurrently explored by co-localisation studies of *Pf*Arf1 and *Pf*Arf6 with each *Pf*ArfGAP.

Although the *Pf*Arf1-GGA interaction assay is available to immediately begin HTS for potent inhibitors of the *Pf*ArfGAPs, it may still be worth establishing the methods to prepare *Pf*Arf6-GTP for the eventual development of *Pf*Arf6-*Pf*ArfGAP GTP hydrolysis assays. While *in vitro* activity of ArfGAPs and

ArfGEFs is not always linked with *in vivo* interactions (as is the case with *Hs*Arf6 and *Hs*ArfGAP1; Zhang et al., 2007; Zhu et al., 2012) the development of the assays could still be used to assess the GTP hydrolytic potential of *Pf*ArfGAP1^{GAP} and the putative *Pf*ArfGAP2^{GAP} towards *Pf*Arf6. As previously mentioned, ARNO-mediated nucleotide exchange was used to prepare *Pf*Arf6-GTP. The shortcoming of this method is that ARNO^{Sec7} would be present in the *Pf*Arf6-GTP sample used for subsequent *Pf*ArfGAP deactivation studies. To circumvent this issue purified *Pf*Arf6 could be loaded with GTP by incubating with ARNO fused to an alternative tag (for example GST) which could then be removed using a glutathione column. *Pf*Arf6-GTP in the eluate could then be used in subsequent *Pf*ArfGAP assays. As previously alluded to, this method could also be applied to the production of *Pf*Arf6-GTPγS for the proposed endogenous effector pull-down experiments using parasite lysates.

In summary, the work described in this chapter suggests there are two assay formats that can currently be used in screening experiments by exploiting *Pf*Arf6-JIP4 interaction: screening for inhibitors of the interaction, and screening for inhibitors of ARNO-mediated *Pf*Arf6 GTP loading (activation). However, the former presupposes that endogenous *Pf*Arf6-effector interactions share the molecular features of the *Pf*Arf6-JIP4 interaction, which seems unlikely. This can be addressed by identifying endogenous parasite effectors by pull-down assays, as discussed above. Likewise, the latter presupposes that *Pf*Arf6-ARNO interaction mimics endogenous *Pf*Arf6-*Pf*ArfGEF interactions. To circumvent this pitfall, purification of the *Pf*ArfGEF Sec7 domain should be further explored. Nonetheless, the activation of *Pf*Arf6 by ARNO paves the way for the development of *Pf*Arf6-*Pf*ArfGAP assays, using approaches proposed above. Finally, the work demonstrates that both the two putative malarial ArfGAPs have GAP activity when used in conjunction with *Pf*Arf1. The assays described here can be exploited to screen for inhibitors of *Pf*Arf1 deactivation by either of the *Pf*ArfGAPs in the immediate future.

Overall conclusions

The initial hypothesis of the research was that the putative *Pf*Arf6 may be a possible target for antimalarial therapy since its human counterpart, *Hs*Arf6, plays essential roles in cellular protein trafficking in human cells. The functional exploration of *Pf*Arf6 in parasites requires the use of methodologically demanding and inefficient research methods, which prompted the development of the HeLa cell surrogate model (HCSM). Although it cannot be confirmed whether the native function of *Pf*Arf6 is realised in HeLa cells, the findings in the HCSM suggested possible roles in a *Pf*Arf6-dependent endocytic pathway and autophagocytosis. Co-localisation of *Pf*Arf6 with available autophagy markers could be explored in parasites. In addition to the requirement of using highly inefficient malarial co-transfection methods, co-localisation studies of *Pf*Arf6 in endocytosis are also complicated by the lack of markers for this pathway. Despite the findings of the HCSM study, functional assignment of *Pf*Arf6 would still critically rely on the malaria experimental practices that are difficult to achieve using current methodology.

Thus, the second goal of the study was to identify a potent inhibitor of *Pf*Arf6. Coupled with endocytosis and autophagocytosis assays, the inhibitor may provide evidence to support or refute our hypotheses on the possible roles of *Pf*Arf6 in parasites. More importantly, a potent inhibitor of *Pf*Arf6 would serve as a tool to validate *Pf*Arf6 as a potential drug target for antimalarial therapy. We aimed to establish plate-based *Pf*Arf6 assays that can be used to screen compounds for potent *Pf*Arf6 inhibitors, as well as its associated signalling machineries. To support this second goal, a novel plate-based assay was first established using human Arf6 and its related accessory machineries since regulatory proteins (ArfGEFs and ArfGAPs) of human Arf6 and effector proteins that bind to it are known and established Arf signalling inhibitors could be used to validate the assay. In addition, the assay format could subsequently be exploited for cancer drug discovery. In this regard we established an *Hs*Arf6-GGA interaction assay with high throughput screening (HTS) potential (owing to its Z-score rating). This base assay was used to establish the *Hs*ArfGAP1 deactivation assay. The *Hs*ArfGAP1 deactivation assay was chemically validated using the known ArfGAP inhibitor QS11. However, while it is useful as a model experimental system, *Hs*ArfGAP1 interaction with *Hs*Arf6 is not thought to occur *in vivo* and may thus not be a significant cancer target. On the other hand, the interaction of ARNO with *Hs*Arf6 does have significance in the cellular context, but we were not able to establish the ARNO activation assay owing to the limited *in vitro* activity of ARNO towards *Hs*Arf6. As it stands, the assay can now be employed to explore alternative ArfGEF and ArfGAP activation and deactivation assays with regulatory proteins relevant to Arf6 function in cells. The handful of ArfGEFs and ArfGAPs that have been validated as cancer drug targets (as discussed in chapter 2) should be examined first, but with the increasing popularity of Arf6 and its signalling machineries as cancer drug targets it is important to frequently review literature for additional candidates. These studies will commence by conducting smaller pilot

studies to assess the individual Z-scores of each assay, before commencing with HTS. The *Hs*Arf6-JIP4 interaction assay, however, is ready for screening in the immediate future for inhibitors of this *in vivo* relevant Arf6-effector interaction. This format also showed significant improvement in assay performance, when compared to the *Hs*Arf6-GGA interaction assay. A suitable Z-score and significance in cancer cell invasion and metastasis qualifies this assay for HTS to identify compounds with anticancer properties.

The development of the *Hs*Arf6 interaction assays paved the way for *Pf*Arf6 interaction assay development. To date we have established the *Pf*Arf6-JIP4 interaction assay which, seemingly, has HTS potential but does not have significance in the parasite's biology. However, the activation of *Pf*Arf6 by ARNO suggests that the *Pf*ArfGEF activation assay may be developed provided the issues surrounding the purification of the malarial ArfGEF can be resolved. We were unable to prepare *Pf*Arf6-GTP for the development of *Pf*ArfGAP deactivation assays, but several working solutions are still available (notably preloading *Pf*Arf6 with GTP using ARNO). If *Pf*Arf6-GTPγS can also be prepared by these means, then pulldown assays using *Pf*Arf6 as bait could help in the identification of native *Pf*Arf6 effector proteins. These effectors could be used to develop additional *Pf*Arf6 interaction assays and may provide insights about the cellular functions in which *Pf*Arf6 is participating in parasites. In the immediate future, the *Pf*Arf1-GGA interaction assay can be used to screen for inhibitors of *Pf*ArfGAP1 and *Pf*ArfGAP2. Both deactivation assays have been appropriately validated and hence HTS can commence immediately. It is important to remember that the malarial Arf signalling machineries have not been properly validated as malarial targets (although human Arf inhibitors have been shown to cause parasite death), so inhibitors identified here would also serve as a tool to validate these machineries as drug targets. Similarly, very little functional characterisation studies on these proteins has been conducted, and these inhibitors may be exploited for these purposes.

In addition to the discovery of potential anticancer and antimalarial compounds, the Arf6 assays can be extended as a tool identify inhibitors of Arf6 signalling (Arf6-effector, Arf6-ArfGAP and Arf6-ArfGEF interactions) in other clinical contexts. Briefly, as an example, the interaction between *Hs*Arf6 and the bacterial effector protein EspG has been shown as essential for enteropathogenic and enterohaemorrhagic *Escherichia coli* (EPEC/EHEC) (which causes diarrhea, haemorrhagic colitis, hemolytic uremic syndrome and acute renal failure in children) to establish infection in the cells of the gut mucosa (Wong et al., 2011). By simply expressing and purifying the EspG protein, an *Hs*Arf6-EspG interaction assay could be prepared. As another example, *Legionella pneumophila* (causative agent of Legionnaires' disease) and *Rickettsia prowazekii* (the causative agent of typhus), express and secrete RalF, a bacterial ArfGEF which manipulates host Arf machineries to facilitate their pathogenesis (Nagai et al., 2002). Once again, establishing a high-throughput assay for RalF would only require the initial purification of RalF and basic assay optimization.

In its broadest context, the assay may even be extended to other small GTPase families which behave by similar mechanisms i.e. via GDP/GTP cycling and selectively binding to effectors in their GTP-bound state (Cherfils and Zeghouf, 2013b). Several examples exist, for which, the small GTPase effector interaction has been determined. Examples include the small GTPase Ras and its effector protein Ral1 (Ras-RalI), small GTPases Rac1 and Cdc42 both bind to the effector protein Pak1 (Rac1-Pak1; Cdc42-Pak1), Rho small GTPase with the effector Rhotekin (Rho-Rhotekin), RalGDS for small GTPase Rap1 (RalGDS-Rap1) and finally Ral for RalI small GTPase (Ral-RalI) (Bos et al., 2001; Ito et al., 2018; Lee et al., 2015; M'Rabet et al., 1998; Moshfegh et al., 2014; Noser et al., 2007; Schmölders et al., 2017). In addition to these base interaction assays, any significant cognate GEFs and GAPs could be incorporated, although a review of the importance of such interactions has not been conducted.

We anticipate that the development of this cost-effective and simple screening strategy can be tailored to the need of the researcher (be it in the field of Arf GTPases or alternative small GTPases) and could serve as a useful tool to the scientific community to drive our fundamental understanding of Arfs and their signalling machineries in a range of organisms and provide candidates suitable for lead optimization studies in the future.

Supplementary material

Chapter 3:

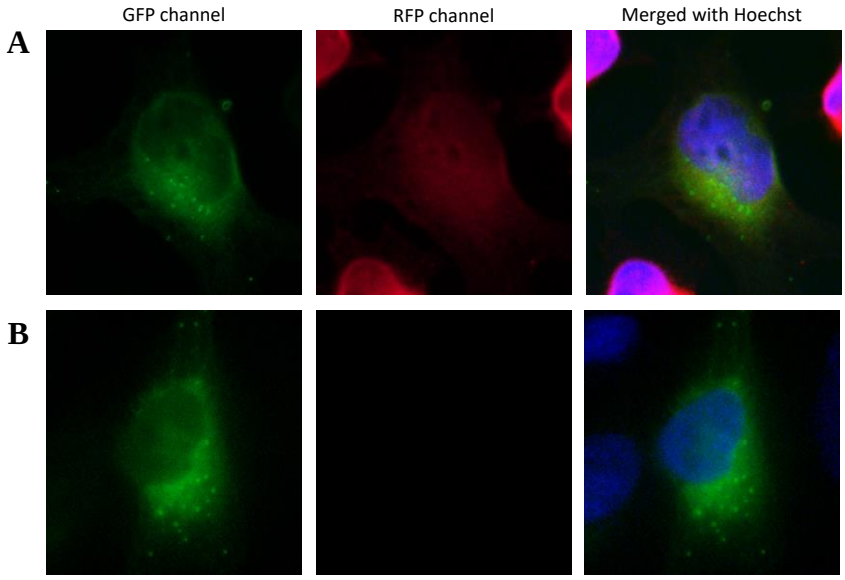

Figure S36: Validation of haemoglobin internalization in HeLa cells. HeLa cells were transfected with *Pf*Arf6-GFP and incubated with culture medium containing free haemoglobin for 1 hour. The haemoglobin suspension was removed, and the coverslips were washed three times with PBS. Cells were fixed with paraformaldehyde and cellular membranes were permeabilised with Triton X-100. Fixed cells were incubated with rabbit anti-haemoglobin primary antibodies, and then anti-rabbit TRITC conjugated secondary antibodies. Nuclei were stained with Hoechst 33342 and the cells were viewed on an Olympus BX61 upright fluorescent microscope with a 100X objective and immersion oil. *Pf*Arf6-GFP was detected by visualisation in the GFP channel (excitation at 489nm, emission at 508 nm). TRITC was detected by visualisation in the RFP channel (excitation at 543nm, emission at 569nm). **A**: HeLa cells incubated in culture media free of haemoglobin. *Pf*Arf6-GFP puncta are observed in the GFP channel (*left panel*). Non-specific fluorescence is detected in the RFP channel (*middle panel*). **B**: HeLa cells incubated in culture media containing free haemoglobin. Primary antibodies were omitted in immunodetection. Secondary antibodies were used. *Pf*Arf6-GFP puncta are observed in the GFP channel (*left panel*). No fluorescence is detected in the RFP channel (*middle panel*). Taken together, the result suggests that the primary antibody is binding to permeabilised cells and is being detected in the RFP channel. Although fluorescence is detected, distinct haemoglobin-containing structures are not observed in the controls.

Chapter 4

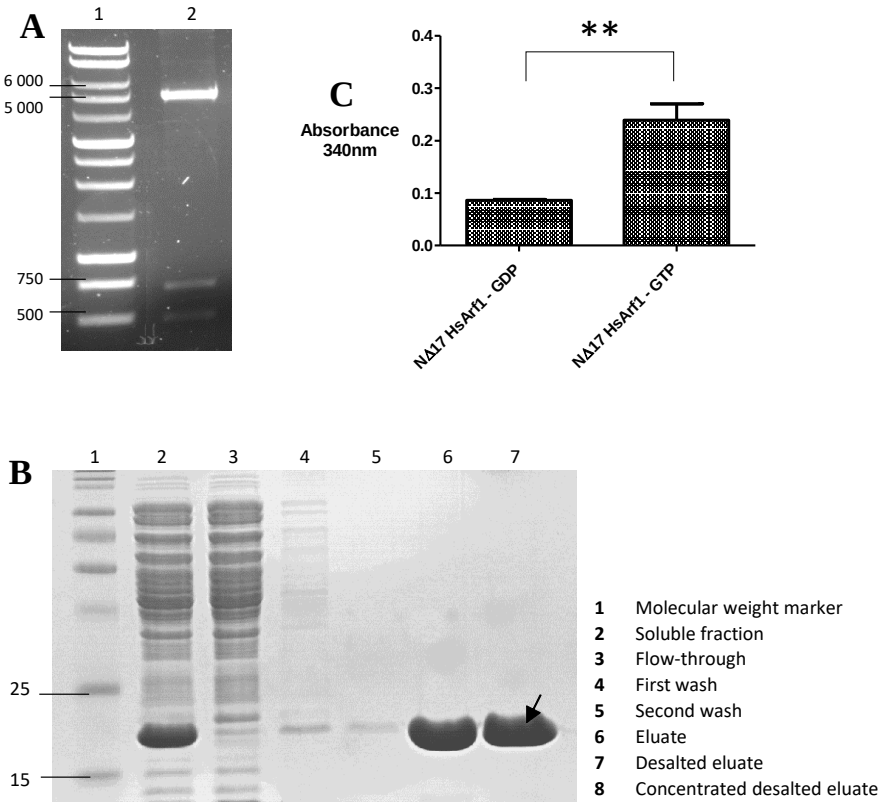

Figure S37: Diagnostic restriction digestion, protein purification and EDTA-mediated nucleotide exchange of $^{N\Delta17}$*Hs*Arf1. **A**: Diagnostic restriction digestion of pET-28a-CFP-*Hs*Arf1$^{N\Delta17}$. The pET-28a-CFP-*Hs*Arf1$^{N\Delta17}$ construct was digested using *Nhe*I, *Xho*I and *Bam*HI. The digestion products were analysed on 0.8% (w/v) agarose gel run at 90V for approximately 1 hour. Lane 1: Promega 1kb DNA ladder (sizes in base pairs). Lane 2: Three bands at approximately 5300 bp, 750 bp and 500 bp that correspond to the theoretical sizes of the pET-28a vector, CFP coding sequence and *Hs*Arf1 coding sequence. **B**: Purification profile of His-tagged *Hs*Arf1$^{N\Delta17}$. Lane 1: Lonza ProSieve Quadcolor protein marker, 4.5 kDa to 300 kDa). Lane 2: whole soluble fraction. Lane 3: flow-through. Lane 4: first wash. Lane 5: second wash. Lane 6: eluate. Lane 7: desalted eluate. A single protein at approximately 21 kDa (*indicated by arrow*) which correlated with the theoretical size of His-tagged *Hs*Arf1$^{N\Delta17}$. **C**: Nucleotide exchange on $^{N\Delta17}$*Hs*Arf1 was promoted at 25°C using 2 mM EDTA, 50 µM GDP/GTP and 3 mM $MgCl_2$ since a discernible difference in intrinsic tryptophan fluorescence was observed ($\rho < 0.01$). Each bar represents the mean and standard deviation of readings obtained from 3 replicate wells (n = 3).

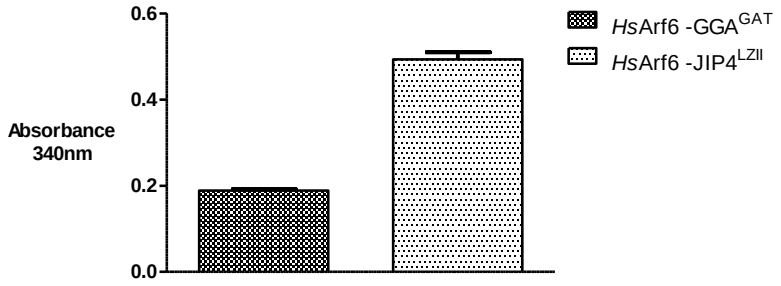

Figure S38: $^{N\Delta13}$*Hs*Arf6 binding to JIP4^{LZII} produces greater GST signals than $^{N\Delta13}$*Hs*Arf6 binding to GGA^{GAT} in the immobilised *Hs*Arf6 assays. Preliminary findings suggested that the immobilised Arf6-JIP4^{LZII} assay can increase the GST signal intensities of the immobilised GGA^{GAT} assay by as much as 261.7%. Each bar represents the mean and standard deviation of readings obtained from 3 replicate wells (n = 3).

Chapter 5:

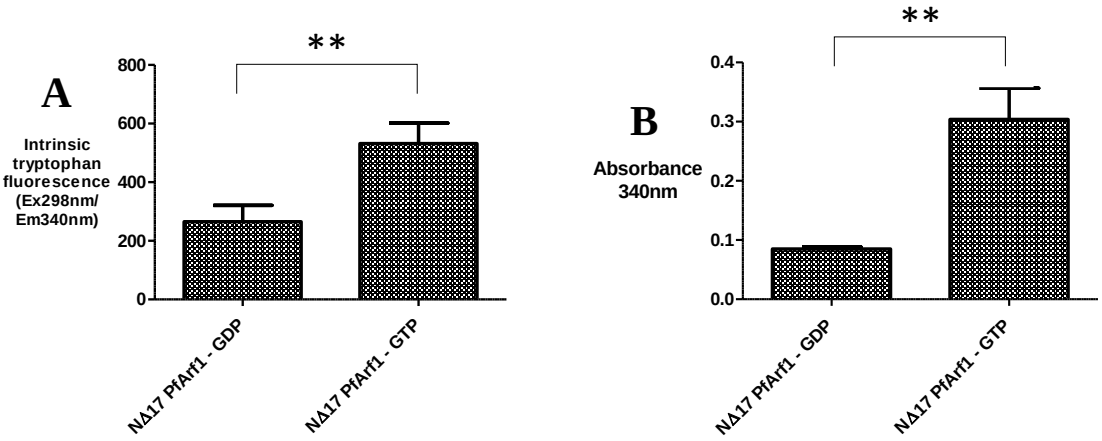

Figure S39: Nucleotide exchange of $^{N\Delta17}$*Pf*Arf1 and the preferential binding of $^{N\Delta17}$*Pf*Arf1-GTP to GST-GGA^{GAT}. **A**: Nucleotide exchange on $^{N\Delta17}$*Pf*Arf1 was promoted at 25ºC using 2 mM EDTA, 50 μM GDP/GTP and 3 mM $MgCl_2$ since a discernible difference in intrinsic tryptophan fluorescence was observed ($\rho < 0.01$). **B**: The immobilised Arf-GGA interaction GST assay can distinguish between active and inactive $^{N\Delta17}$*Pf*Arf1. The difference in the signals measured for inactive $^{N\Delta17}$*Pf*Arf1-GDP and active $^{N\Delta17}$*Pf*Arf1-GTP were statistically significant ($\rho < 0.01$). Each bar represents the mean and standard deviation of readings obtained from 3 replicate wells (n = 3).

Z-factor score (adapted from Zhang et al. (1999))

Formula:

$$\text{Z-factor} = 1 - \frac{3(\sigma_p + \sigma_n)}{|\mu_p - \mu_n|}$$

Where

σ_p = standard deviation of the positive control

σ_n = standard deviation of the negative control

μ_p = mean of the positive control

μ_n = mean of the negative control

Interpretation:

Z factor = 1.0	Ideal
1.0 > Z factor > 0.5	Excellent assay
0.0 > Z factor > 0.5	Marginal assay
Z factor < 0	Assay format is not useful

Example of molecular size determination for PCR and restriction digestion products:

Example using the agarose gel presented in Figure 10A:

DNA ladder bands (bp)	log MW	Relative migration distance	Migration distance
10000	4	0.061538462	4
8000	3.90309	0.107692308	7
6000	3.778151	0.169230769	11
5000	3.69897	0.2	13
4000	3.60206	0.261538462	17
3000	3.477121	0.323076923	21
2500	3.39794	0.384615385	25
2000	3.30103	0.446153846	29
1500	3.176091	0.523076923	34
1000	3	0.630769231	41
750	2.875061	0.707692308	46
500	2.69897	0.815384615	53
250	2.39794	0.938461538	61

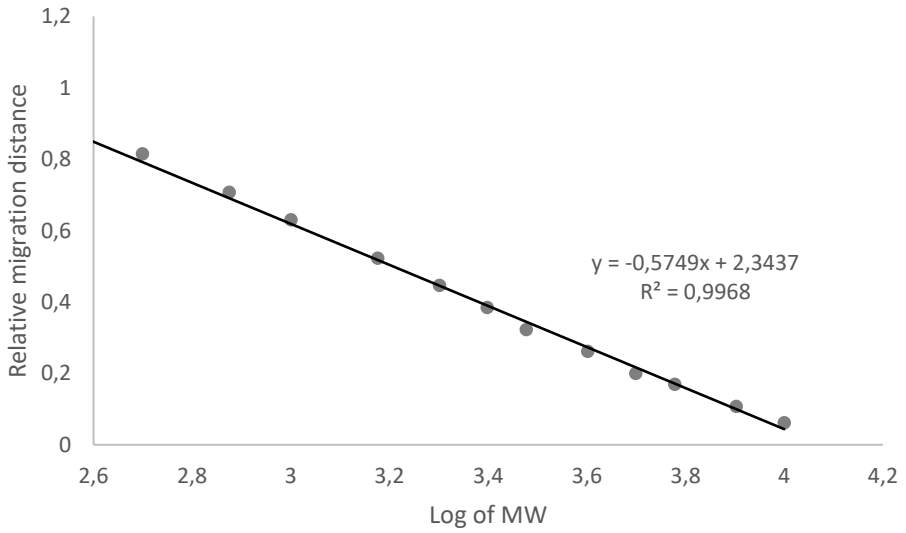

Calculation:

Relative migration distance of the PCR band = $\frac{51.5\ mm}{65\ mm}$ = 0.792308

0.792308 = -0.5749x + 2.3437

x = 2.698543

$10^{2.698543}$ = 500 bp

Example of molecular size determination for protein band sizes:

Example using the polyacrylamide gel presented in Figure 14C:

Protein ladder bands (kDa)	log MW	Relative migration distance	Migration distance
100	2	0.102564103	8
75	1.87506126	0.128205128	10
63	1.79934055	0.192307692	15
48	1.68124124	0.269230769	21
35	1.54406804	0.378205128	29.5
25	1.39794001	0.519230769	40.5
20	1.30103	0.576923077	45
17	1.23044892	0.641025641	50
11	1.04139269	0.801282051	62.5

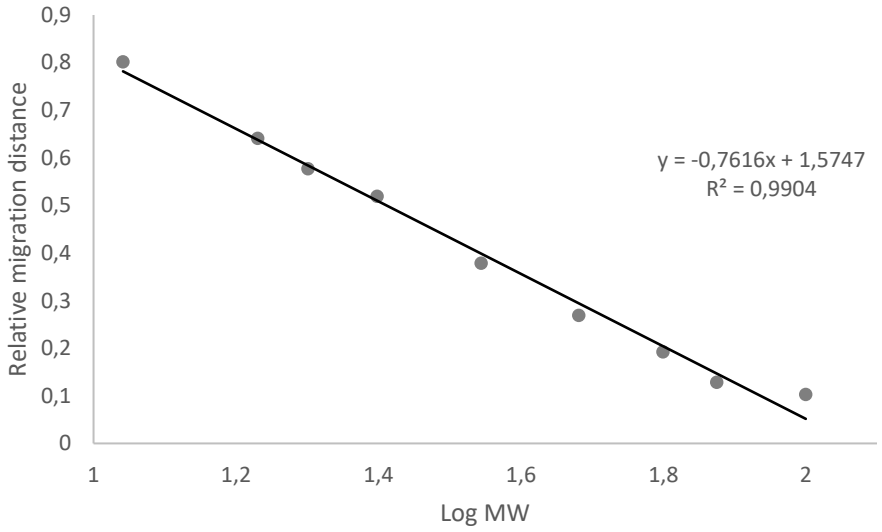

Calculation:

Relative migration distance of the protein band = $\frac{52\ mm}{78\ mm}$ = 0.666666667

0.666666667 = -0.7616x + 1.5747

x = 1.192270658

$10^{1.192270658}$= 15.6 kDa = 16 kDa

References

Ai, E., Poole, D.S., Skop, A., 2010. RACK-1 Directs Dynactin-dependent RAB-11 Endosomal Recycling during Mitosis in Caenorhabditis elegans. Seikagaku. https://doi.org/10.1091/mbc.E08

Aikawa, M., Hepler, P.K., Huff, C.G., Sprinz, H., 1966. The feeding mechanism of avian malarial parasites. J. Cell Biol. https://doi.org/10.1083/jcb.28.2.355

Aikawa, Y., Martin, T.F.J., 2003. ARF6 regulates a plasma membrane pool of phosphatidylinositol(4,5)bisphosphate required for regulated exocytosis. J. Cell Biol. 162, 647–659. https://doi.org/10.1083/jcb.200212142

Al-Awar, O., Radhakrishna, H., 2000. Separation of Membrane Trafficking and Actin Remodeling Functions of ARF6 with an Effector Domain Mutant. … Cell. Biol. 20, 5998–6007. https://doi.org/10.1128/MCB.20.16.5998-6007.2000

Antonny, B., Beraud-Dufour, S., Chardin, P., Chabre, M., 1997. N-terminal hydrophobic residues of the G-protein ADP-ribosylation factor-1 insert into membrane phospholipids upon GDP to GTP exchange. Biochemistry 36, 4675–4684. https://doi.org/10.1021/bi962252b

Asano, K., Asano, Y., Ono, H.K., Nakane, A., 2014. Suppression of starvation-induced autophagy by recombinant toxic shock syndrome toxin-1 in epithelial cells. PLoS One. https://doi.org/10.1371/journal.pone.0113018

Austin, C., Boehm, M., Tooze, S.A., 2002. Site-specific cross-linking reveals a differential direct interaction of class 1, 2, and 3 ADP-ribosylation factors with adaptor protein complexes 1 and 3. Biochemistry 41, 4669–4677. https://doi.org/10.1021/bi016064j

Bakar, N.A., Klonis, N., Hanssen, E., Chan, C., Tilley, L., 2010. Digestive-vacuole genesis and endocytic processes in the early intraerythrocytic stages of Plasmodium falciparum. J. Cell Sci. https://doi.org/10.1242/jcs.061499

Balaña, M.E., Niedergang, F., Subtil, A., Alcover, A., Chavrier, P., Dautry-Varsat, A., 2005. ARF6 GTPase controls bacterial invasion by actin remodelling. J.Cell Sci. 118, 2201–2210. https://doi.org/10.1242/jcs.02351

Barral, D.C., Garg, S., Casalou, C., Watts, G.F.M., Sandoval, J.L., Ramalho, J.S., Hsu, V.W., Brenner, M.B., 2012. Arl13b regulates endocytic recycling traffic. Proc. Natl. Acad. Sci. https://doi.org/10.1073/pnas.1218272110

Bartoloni, A., Zammarchi, L., 2012. Clinical aspects of uncomplicated and severe malaria. Mediterr. J. Hematol. Infect. Dis. 4. https://doi.org/10.4084/MJHID.2012.026

Baumgartner, F., Wiek, S., Paprotka, K., Zauner, S., Lingelbach, K., 2001. A point mutation in an unusual Sec7 domain is linked to brefeldin A resistance in a Plasmodium falciparum line generated by drug selection. Mol. Microbiol. https://doi.org/10.1046/j.1365-2958.2001.02572.x

Beare, N.A.V., Taylor, T.E., Harding, S.P., Lewallen, S., Molyneux, M.E., 2006. Malarial retinopathy: A newly established diagnostic sign in severe malaria. Am. J. Trop. Med. Hyg. https://doi.org/75/5/790 [pii]

Bento, C.F., Puri, C., Moreau, K., Rubinsztein, D.C., 2013. The role of membrane-trafficking small GTPases in the regulation of autophagy. J. Cell Sci. 126, 1059–1069. https://doi.org/10.1242/jcs.123075

Béraud-Dufour, S., Robineau, S., Chardin, P., Paris, S., Chabre, M., Cherfils, J., Antonny, B., 1998. A glutamic finger in the guanine nucleotide exchange factor ARNO displaces Mg2+ and the ??-phosphate to destabilize GDP on ARF1. EMBO J. 17, 3651–3659. https://doi.org/10.1093/emboj/17.13.3651

Bergmans, H.E.N., Van Die, I.M., Hoekstra, W.P.M., 1981. Transformation in Escherichia coli: stages in the process. J. Bacteriol. 146, 564–570. https://doi.org/10.1007/BF02342204

Bharti, S., Inoue, H., Bharti, K., Hirsch, D.S., Nie, Z., Yoon, H.-Y., Artym, V., Yamada, K.M., Mueller, S.C., Barr, V.A., Randazzo, P.A., 2007. Src-Dependent Phosphorylation of ASAP1 Regulates Podosomes. Mol. Cell. Biol. 27, 8271–8283. https://doi.org/10.1128/MCB.01781-06

Bigay, J., Antonny, B., 2006. Real-time assays for the assembly-disassembly cycle of COP coats on liposomes of defined size. Methods Enzymol. https://doi.org/10.1016/S0076-6879(05)04010-3

Bigay, J., Gounon, P., Roblneau, S., Antonny, B., 2003. Lipid packing sensed by ArfGAP1 couples COPI coat disassembly to membrane bilayer curvature. Nature. https://doi.org/10.1038/nature02108

Bill, A., Blockus, H., Stumpfe, D., Bajorath, J., Schmitz, A., Famulok, M., 2011. A homogeneous fluorescence resonance energy transfer system for monitoring the activation of a protein switch in real time. J. Am. Chem. Soc. 133, 8372–8379. https://doi.org/10.1021/ja202513s

Billker, O., Dechamps, S., Tewari, R., Wenig, G., Franke-Fayard, B., Brinkmann, V., 2004. Calcium and a calcium-dependent protein kinase regulate gamete formation and mosquito transmission in a malaria parasite. Cell. https://doi.org/10.1007/BF00688886

Boal, F., Guetzoyan, L., Sessions, R.B., Zeghouf, M., Spooner, R.A., Lord, J.M., Cherfils, J., Clarkson, G.J., Roberts, L.M., Stephens, D.J., 2010. LG186: An Inhibitor of GBF1 Function that Causes Golgi Disassembly in Human and Canine Cells. Traffic 11, 1537–1551. https://doi.org/10.1111/j.1600-0854.2010.01122.x

Boehm, M., Aguilar, R.C., Bonifacino, J.S., 2001. Functional and physical interactions of the adaptor protein complex AP-4 with ADP-ribosylation factors (ARFs). EMBO J. 20, 6265–6276. https://doi.org/10.1093/emboj/20.22.6265

Bos, J.L., De Rooij, J., Reedquist, K.A., 2001. Rap1 signalling: Adhering to new models. Nat. Rev. Mol. Cell Biol. https://doi.org/10.1038/35073073

Bos, J.L., Rehmann, H., Wittinghofer, A., 2007. GEFs and GAPs: Critical Elements in the Control of Small G Proteins. Cell. https://doi.org/10.1016/j.cell.2007.05.018

Boshans, R.L., Szanto, S., van Aelst, L., D'Souza-Schorey, C., 2000. ADP-ribosylation factor 6 regulates actin cytoskeleton remodeling in coordination with Rac1 and RhoA. Mol. Cell. Biol. 20, 3685–94. https://doi.org/10.1128/MCB.20.10.3685-3694.2000.Updated

Boulay, P.L., Cotton, M., Melançon, P., Claing, A., 2008. ADP-ribosylation factor 1 controls the activation of the phosphatidylinositol 3-kinase pathway to regulate epidermal growth factor-dependent growth and migration of breast cancer cells. J. Biol. Chem. https://doi.org/10.1074/jbc.M803603200

Bouterfa, H.L., Sattelmeyer, V., Czub, S., Vordermark, D., Roosen, K., Tonn, J.C., 2000. Inhibition of Ras farnesylation by lovastatin leads to downregulation of proliferation and migration in primary cultured human glioblastoma cells. Anticancer Res.

Bowzard, J.B., Cheng, D., Peng, J., Kahn, R.A., 2007. ELMOD2 is an Arl2 GTPase-activating protein that also acts on Arfs. J. Biol. Chem. 282, 17568–17580. https://doi.org/10.1074/jbc.M701347200

Brodsky, F.M., Chen, C.-Y., Knuehl, C., Towler, M.C., Wakeham, D.E., 2001. Biological Basket Weaving: Formation and Function of Clathrin-Coated Vesicles. Annu. Rev. Cell Dev. Biol. https://doi.org/10.1146/annurev.cellbio.17.1.517

Brown, F.D., Rozelle, A.L., Yin, H.L., Balla, T., Donaldson, J.G., 2001. Phosphatidylinositol 4,5-bisphosphate and Arf6-regulated membrane traffic. J. Cell Biol. 154, 1007–1017. https://doi.org/10.1083/jcb.200103107

Brymora, A., Valova, V.A., Robinson, P.J., 2004. Protein-Protein Interactions Identified by Pull-Down Experiments and Mass Spectrometry, in: Current Protocols in Cell Biology. https://doi.org/10.1002/0471143030.cb1705s22

C, D.C.V.M.K.M.M.Z.G.F.V.J.S.J.S., 2001. Cerivastatin, an inhibitor of HMG-CoA reductase, inhibits the signaling pathways involved in the invasiveness and metastatic properties of highly invasive breast cancer cell lines: an in vitro study. Carcinogenesis. https://doi.org/10.1093/carcin/22.8.1139

Caraballo, H., King, K., 2014. Management Of Mosquito- Borne Illness : Malaria, Dengue , And West Nile Virus. Emerg. Med. Pract. 16, 1–24.

Casanova, J.E., 2007. Regulation of Arf activation: The Sec7 family of guanine nucleotide exchange factors. Traffic 8, 1476–1485. https://doi.org/10.1111/j.1600-0854.2007.00634.x

Caumont, A.S., Vitale, N., Gensse, M., Galas, M.C., Casanova, J.E., Bader, M.F., 2000a. Identification of a plasma membrane-associated guanine nucleotide exchange factor for ARF6 in chromaffin cells. Possible role in the regulated exocytotic pathway. J. Biol. Chem. 275, 15637–15644. https://doi.org/10.1074/jbc.M908347199

Caumont, A.S., Vitale, N., Gensse, M., Galas, M.C., Casanova, J.E., Bader, M.F., 2000b. Identification of a plasma membrane-associated guanine nucleotide exchange factor for ARF6 in chromaffin cells. Possible role in the regulated exocytotic pathway. J. Biol. Chem. https://doi.org/10.1074/jbc.M908347199

Cavenagh, M.M., Whitney, J.A., Carroll, K., Zhang, C.J., Boman, A.L., Rosenwald, A.G., Mellman, I., Kahn, R.A., 1996. Intracellular distribution of Arf proteins in mammalian cells: Arf6 is uniquely localized to the plasma membrane. J. Biol. Chem. 271, 21767–21774. https://doi.org/10.1074/jbc.271.36.21767

Cervantes, S., Bunnik, E.M., Saraf, A., Conner, C.M., Escalante, A., Sardiu, M.E., Ponts, N., Prudhomme, J., Florens, L., Le Roch, K.G., 2014. The multifunctional autophagy pathway in the human malaria parasite, Plasmodium falciparum. Autophagy. https://doi.org/10.4161/auto.26743

Chavrier, P., Ménétrey, J., 2010. Toward a structural understanding of Arf family: Effector specificity. Structure 18, 1552–1558. https://doi.org/10.1016/j.str.2010.11.004

Cherfils, J., Zeghouf, M., 2013a. Regulation of Small GTPases by GEFs, GAPs, and GDIs. Physiol. Rev. https://doi.org/10.1152/physrev.00003.2012

Cherfils, J., Zeghouf, M., 2013b. Regulation of Small GTPases by GEFs, GAPs, and GDIs. Physiol. Rev. 93, 269–309. https://doi.org/10.1152/physrev.00003.2012

City, T.S., 2002. GGA proteins associate with Golgi membranes through interaction between their GGAH domains and ADP-ribosylation factors. Cancer Res. 378, 369–378. https://doi.org/10.1042/BJ20020428

Cook, W.J., Smith, C.D., Senkovich, O., Holder, A.A., Chattopadhyay, D., 2010. Structure of Plasmodium falciparum ADP-ribosylation factor 1. Acta Crystallogr. Sect. F Struct. Biol. Cryst. Commun. 66, 1426–1431. https://doi.org/10.1107/S1744309110036997

Cowman, A.F., Berry, D., Baum, J., 2012. The cellular and molecular basis for malaria parasite invasion of the human red blood cell. J. Cell Biol. https://doi.org/10.1083/jcb.201206112

Cukierman, E., Huber, I., Rotman, M., Cassel, D., 1995. The ARF1 GTPase-Activating protein: Zinc finger motif and golgi complex localization. Science (80-.). 270, 1999–2002. https://doi.org/10.1126/science.270.5244.1999

Czech, M.P., 2003. Dynamics of Phosphoinositides in Membrane Retrieval and Insertion. Annu. Rev. Physiol. 65, 791–815. https://doi.org/10.1146/annurev.physiol.65.092101.142522

D'Souza-Schorey, C., Boshans, R.L., McDonough, M., Stahl, P.D., Van Aelst, L., 1997. A role for POR1, a Rac1-interacting protein, in ARF6-mediated cytoskeletal rearrangements. EMBO J. 16, 5445–5454. https://doi.org/10.1093/emboj/16.17.5445

D'Souza-Schorey, C., Chavrier, P., 2006. ARF proteins: Roles in membrane traffic and beyond. Nat. Rev. Mol. Cell Biol. 7, 347–358. https://doi.org/10.1038/nrm1910

D'Souza-Schorey, C., Li, G., Colombo, M.I., Stahl, P.D., 1995. A regulatory role for ARF6 in receptor-mediated endocytosis. Science (80-.). 267, 1175–1178. https://doi.org/10.1126/science.7855600

D'Souza-Schorey, C., Van Donselaar, E., Hsu, V.W., Yang, C., Stahl, P.D., Peters, P.J., 1998. ARF6 targets recycling vesicles to the plasma membrane: Insights from an ultrastructural investigation. J. Cell Biol. 140, 603–616. https://doi.org/10.1083/jcb.140.3.603

David Padro ´n, Renee D. Tall, and M.G.R., 2006. Phospholipase D2 Is Required for Efficient Endocytic Recycling of Transferrin Receptors. Mol. Biol. Cell. https://doi.org/10.1091/mbc.E05

de Curtis, I., 2001. Cell migration: GAPs between membrane traffic and the cytoskeleton. EMBO Rep. 2, 277–281. https://doi.org/10.1093/embo-reports/kve072

Dell'Angelica, E.C., Puertollano, R., Mullins, C., Aguilar, R.C., Vargas, J.D., Hartnell, L.M., Bonifacino, J.S., 2000. GGAs: A family of ADP ribosylation factor-binding proteins related to adaptors and associated with the Golgi complex. J. Cell Biol. 149, 81–93. https://doi.org/10.1083/jcb.149.1.81

Delves, M., Plouffe, D., Scheurer, C., Meister, S., Wittlin, S., Winzeler, E.A., Sinden, R.E., Leroy, D., 2012. The activities of current antimalarial drugs on the life cycle stages of plasmodium: A comparative study with human and rodent parasites. PLoS Med. https://doi.org/10.1371/journal.pmed.1001169

Deponte, M., Hoppe, H.C., Lee, M.C.S., Maier, A.G., Richard, D., Rug, M., Spielmann, T., Przyborski, J.M., 2012. Wherever i may roam: Protein and membrane trafficking in P. falciparum-infected red blood cells. Mol. Biochem. Parasitol. https://doi.org/10.1016/j.molbiopara.2012.09.007

Derrien, V., Couillault, C., Franco, M., Martineau, S., Montcourrier, P., Houlgatte, R., Chavrier, P., 2002. A conserved C-terminal domain of EFA6-family ARF6-guanine nucleotide exchange factors induces lengthening of microvilli-like membrane protrusions. J. Cell Sci. 115, 2867–2879.

Doherty, G.J., McMahon, H.T., 2009. Mechanisms of Endocytosis. Annu. Rev. Biochem. 78, 857–902. https://doi.org/10.1146/annurev.biochem.78.081307.110540

Donaldson, J.G., Cassel, D., Kahn, R.A., Klausner, R.D., 1992. ADP-ribosylation factor, a small GTP-binding protein, is required for binding of the coatomer protein beta-COP to Golgi membranes. Proc. Natl. Acad. Sci. U. S. A. 89, 6408–12. https://doi.org/10.17083/ijsg.v1i3.12

Donaldson, J.G., Jackson, C.L., 2011. ARF family G proteins and their regulators: Roles in membrane transport, development and disease. Nat. Rev. Mol. Cell Biol. 12, 362–375. https://doi.org/10.1038/nrm3117

Donaldson, J.G., Jackson, C.L., 2000. Regulators and effectors of the ARF GTPases. Curr. Opin. Cell Biol. 12, 475–482. https://doi.org/10.1016/S0955-0674(00)00119-8

Dunphy, J.L., Moravec, R., Ly, K., Lasell, T.K., Melancon, P., Casanova, J.E., 2006. The Arf6 GEF GEP100/BRAG2 regulates cell adhesion by controlling endocytosis of β1 integrins. Curr. Biol. 16, 315–320. https://doi.org/10.1016/j.cub.2005.12.032

Elliott, D.A., McIntosh, M.T., Hosgood, H.D., Chen, S., Zhang, G., Baevova, P., Joiner, K.A., 2008. Four distinct pathways of hemoglobin uptake in the malaria parasite Plasmodium falciparum. Proc. Natl. Acad. Sci. https://doi.org/10.1073/pnas.0711067105

ENDO, A., KURODA, M., TSUJITA, Y., 1976. ML-236A, ML-236B, and ML-236C, new inhibitors of cholesterogensis produced by Penicillium citrinum. J. Antibiot. (Tokyo). https://doi.org/10.7164/antibiotics.29.1346

Eyster, C.A., Cole, N.B., Petersen, S., Viswanathan, K., Fruh, K., Donaldson, J.G., 2011. MARCH ubiquitin ligases alter the itinerary of clathrin-independent cargo from recycling to degradation. Mol. Biol. Cell 22, 3218–3230. https://doi.org/10.1091/mbc.E10-11-0874

Eyster, C.A., Higginson, J.D., Huebner, R., Porat-Shliom, N., Weigert, R., Wu, W.W., Shen, R.F., Donaldson, J.G., 2009. Discovery of new cargo proteins that enter cells through clathrin-independent endocytosis. Traffic. https://doi.org/10.1111/j.1600-0854.2009.00894.x

Feng, Y., Jadhav, A.P., Rodighiero, C., Fujinaga, Y., Kirchhausen, T., Lencer, W.I., 2004. Retrograde transport of cholera toxin from the plasma membrane to the endoplasmic reticulum requires the trans-Golgi network but not the Golgi apparatus in Exo2-treated cells. EMBO Rep. 5, 596–601. https://doi.org/10.1038/sj.embor.7400152

Florens, L., Washburn, M.P., Raine, J.D., Anthony, R.M., Grainger, M., Haynes, J.D., Moch, J.K., Muster, N., Sacci, J.B., Tabb, D.L., Witney, A.A., Wolters, D., Wu, Y., Gardner, M.J., Holder, A.A., Sinden, R.E., Yates, J.R., Carucci, D.J., 2002. A proteomic view of the Plasmodium falciparum life cycle. Nature. https://doi.org/10.1038/nature01107

Franco, M., 1999. EFA6, a sec7 domain-containing exchange factor for ARF6, coordinates membrane recycling and actin cytoskeleton organization. EMBO J. 18, 1480–1491. https://doi.org/10.1093/emboj/18.6.1480

Frank, S., Upender, S., Hansen, S.H., Casanova, J.E., 1998. ARNO is a guanine nucleotide exchange factor for ADP-ribosylation factor 6. J. Biol. Chem. 273, 23–27. https://doi.org/10.1074/jbc.273.1.23

Frearson, J.A., Wyatt, P.G., Gilbert, I.H., Fairlamb, A.H., 2007. Target assessment for antiparasitic drug discovery. Trends Parasitol. https://doi.org/10.1016/j.pt.2007.08.019

Frigerio, G., Grimsey, N., Dale, M., Majoul, I., Duden, R., 2007. Two human ARFGAPs associated with COP-I-coated vesicles. Traffic 8, 1644–1655. https://doi.org/10.1111/j.1600-0854.2007.00631.x

Funakoshi, Y., Hasegawa, H., Kanaho, Y., 2011. Regulation of PIP5K activity by Arf6 and its physiological significance. J. Cell. Physiol. 226, 888–895. https://doi.org/10.1002/jcp.22482

Furniss, R.C.D., Slater, S., Frankel, G., Clements, A., 2016. Enterohaemorrhagic E. coli modulates an ARF6:Rab35 signaling axis to prevent recycling endosome maturation during infection. J. Mol. Biol. 428, 3399–3407. https://doi.org/10.1016/j.jmb.2016.05.023

Galas, M.C., Helms, J.B., Vitale, N., Thiersé, D., Aunis, D., Bader, M.F., 1997. Regulated exocytosis in chromaffin cells. A potential role for a secretory granule-associated ARF6 protein. J. Biol. Chem. https://doi.org/10.1074/jbc.272.5.2788

Gallup, J.L., Sachs, J.D., 2001. The economic burden of malaria, in: American Journal of Tropical Medicine and Hygiene. https://doi.org/10.4269/ajtmh.2012.12-0157

Garcia-Exposito, L., Barroso-Gonzalez, J., Puigdomenech, I., Machado, J.-D., Blanco, J., Valenzuela-Fernandez, A., 2011. HIV-1 requires Arf6-mediated membrane dynamics to efficiently enter and infect T lymphocytes. Mol. Biol. Cell. https://doi.org/10.1091/mbc.E10-08-0722

Garza-Mayers, A.C., Miller, K.A., Russo, B.C., Nagda, D. V., Goldberg, M.B., 2015. Shigella flexneri regulation of ARF6 activation during bacterial entry via an IpgD-mediated positive feedback loop. MBio 6, 1–12. https://doi.org/10.1128/mBio.02584-14

Ghorbal, M., Gorman, M., MacPherson, C.R., Martins, R.M., Scherf, A., Lopez-Rubio, J.J., 2014. Genome editing in the human malaria parasite Plasmodium falciparum using the CRISPR-Cas9 system. Nat. Biotechnol. https://doi.org/10.1038/nbt.2925

Gillingham, A.K., Koumanov, F., Pryor, P.R., Reaves, B.J., Holman, G.D., 1999. Association of AP1 adaptor complexes with GLUT4 vesicles. J. Cell Sci.

Gillingham, A.K., Munro, S., 2007. The Small G Proteins of the Arf Family and Their Regulators. Annu. Rev. Cell Dev. Biol. 23, 579–611. https://doi.org/10.1146/annurev.cellbio.23.090506.123209

Goldberg, J., 1999. Structural and functional analysis of the ARF1-aRFGAP complex reveals a role for coatomer in GTP hydrolysis. Cell 96, 893–902. https://doi.org/10.1016/S0092-8674(00)80598-X

Goldfinger, L.E., Ptak, C., Jeffery, E.D., Shabanowitz, J., Hunt, D.F., Ginsberg, M.H., 2006. RLIP76 (RalBP1) is an R-Ras effector that mediates adhesion-dependent Rac activation and cell migration. J. Cell Biol. 174, 877–888. https://doi.org/10.1083/jcb.200603111

Goldstein, J.L., Brown, M.S., 1990. Regulation of the mevalonate pathway. Nature. https://doi.org/10.1038/343425a0

Gommel, D.U., Memon, A.R., Heiss, A., Lottspeich, F., Pfannstiel, J., Lechner, J., Reinhard, C., Helms, J.B., Nickel, W., Wieland, F.T., 2001. Recruitment to Golgi membranes of ADP-ribosylation factor 1 is mediated by the cytoplasmic domain of p23. EMBO J. 20, 6751–6760. https://doi.org/10.1093/emboj/20.23.6751

Grant, B.D., Donaldson, J.G., 2009. Pathways and mechanisms of endocytic recycling. Nat. Rev. Mol. Cell Biol. https://doi.org/10.1038/nrm2755

Grossmann, A.H., Yoo, J.H., Clancy, J., Sorensen, L.K., Sedgwick, A., Tong, Z., Ostanin, K., Rogers, A., Grossmann, K.F., Tripp, S.R., Thomas, K.R., D'Souza-Schorey, C., Odelberg, S.J., Li, D.Y., 2013a. The small GTPase ARF6 stimulates β-catenin transcriptional activity during WNT5A-mediated melanoma invasion and metastasis. Sci. Signal. 6. https://doi.org/10.1126/scisignal.2003398

Grossmann, A.H., Yoo, J.H., Clancy, J., Sorensen, L.K., Sedgwick, A., Tong, Z., Ostanin, K., Rogers, A., Grossmann, K.F., Tripp, S.R., Thomas, K.R., D'Souza-Schorey, C., Odelberg, S.J., Li, D.Y., 2013b. The small GTPase ARF6 stimulates β-catenin transcriptional activity during WNT5A-mediated melanoma invasion and metastasis. Sci. Signal. https://doi.org/10.1126/scisignal.2003398

Guttery, D.S., Holder, A.A., Tewari, R., 2012. Sexual development in plasmodium: Lessons from functional analyses. PLoS Pathog. https://doi.org/10.1371/journal.ppat.1002404

H. Radhakrishna, O. Al-Awar, Z. Khachikian, J.G.D., 1999. ARF6 requirement for Rac ruffling suggests a role for membrane trafficking in cortical actin rearrangements. J. Cell Sci. 866, 855–866. https://doi.org/10.1101/GAD.11.18.2295

Hafner, M., Schmitz, A., Grüne, I., Srivatsan, S.G., Paul, B., Kolanus, W., Quast, T., Kremmer, E., Bauer, I., Famulok, M., 2006. Inhibition of cytohesins by SecinH3 leads to hepatic insulin resistance. Nature 444, 941–944. https://doi.org/10.1038/nature05415

Haldar, K., 1998. Intracellular trafficking in Plasmodium-infected erythrocytes. Curr. Opin. Microbiol. https://doi.org/10.1016/S1369-5274(98)80067-2

Hall, B., McLean, M.A., Davis, K., Casanova, J.E., Sligar, S.G., Schwartz, M.A., 2008. A fluorescence resonance energy transfer activation sensor for Arf6. Anal. Biochem. 374, 243–249. https://doi.org/10.1016/j.ab.2007.11.032

Hanahan, D., Weinberg, R.A., 2011. Hallmarks of cancer: The next generation. Cell. https://doi.org/10.1016/j.cell.2011.02.013

Hanahan, D., Weinberg, R.A., Francisco, S., 2000. 2000-Hanahan.pdf 100, 57–70. https://doi.org/10.1007/s00262-010-0968-0

Hanboonkunupakarn, B., White, N.J., 2016. The threat of artemisinin resistant malaria in Southeast Asia. Travel Med. Infect. Dis. https://doi.org/10.1016/j.tmaid.2016.11.016

Hanssen, E., Knoechel, C., Dearnley, M., Dixon, M.W.A., Le Gros, M., Larabell, C., Tilley, L., 2012. Soft X-ray microscopy analysis of cell volume and hemoglobin content in erythrocytes infected with asexual and sexual stages of Plasmodium falciparum. J. Struct. Biol. https://doi.org/10.1016/j.jsb.2011.09.003

Hasenkamp, S., Wong, E.H., Horrocks, P., 2012. An improved single-step lysis protocol to measure luciferase bioluminescence in Plasmodium falciparum. Malar. J. https://doi.org/10.1186/1475-2875-11-42

Hashimoto, S., Hashimoto, A., Yamada, A., Kojima, C., Yamamoto, H., Tsutsumi, T., Higashi, M., Mizoguchi, A., Yagi, R., Sabe, H., 2004. A novel mode of action of an ArfGAP, AMAP2/PAG3/Papα, in Arf6 function. J. Biol. Chem. 279, 37677–37684. https://doi.org/10.1074/jbc.M404196200

Henriques, G., Van Schalkwyk, D.A., Burrow, R., Warhurst, D.C., Thompson, E., Baker, D.A., Fidock, D.A., Hallett, R., Flueck, C., Sutherland, C.J., 2015. The Mu subunit of Plasmodium falciparum clathrin-associated adaptor protein 2 modulates in vitro parasite response to artemisinin and quinine. Antimicrob. Agents Chemother. https://doi.org/10.1128/AAC.04067-14

Hilpela, P., Oberbanscheidt, P., Hahne, P., Hund, M., Kalhammer, G., Small, J. V., Bähler, M., 2003. SWAP-70 Identifies a Transitional Subset of Actin Filaments in Motile Cells. Mol. Biol. Cell. https://doi.org/10.1091/mbc.E03

Hiroi, T., Someya, A., Thompson, W., Moss, J., Vaughan, M., 2006. GEP100/BRAG2: Activator of ADP-ribosylation factor 6 for regulation of cell adhesion and actin cytoskeleton via E-cadherin and -catenin. Proc. Natl. Acad. Sci. 103, 10672–10677. https://doi.org/10.1073/pnas.0604091103

Hisaeda, H., Yasutomo, K., Himeno, K., 2005. Malaria: Immune evasion by parasites. Int. J. Biochem. Cell Biol. 37, 700–706. https://doi.org/10.1016/j.biocel.2004.10.009

Holman, G.D., Cushman, S.W., 1994. Subcellular localization and trafficking of the GLUT4 glucose transporter isoform in insulin-responsive cells. BioEssays. https://doi.org/10.1002/bies.950161010

Honda, A., Nogami, M., Yokozeki, T., Yamazaki, M., Nakamura, H., Watanabe, H., Kawamoto, K., Nakayama, K., Morris, A.J., Frohman, M.A., Kanaho, Y., 1999. Phosphatidylinositol 4-phosphate 5-kinase α is a downstream effector of the small G protein ARF6 in membrane ruffle formation. Cell. https://doi.org/10.1016/S0092-8674(00)81540-8

Hongu, T., Kanaho, Y., 2014. Activation machinery of the small GTPase Arf6. Adv. Biol. Regul. 54, 59–66. https://doi.org/10.1016/j.jbior.2013.09.014

Hongu, T., Yamauchi, Y., Funakoshi, Y., Katagiri, N., Ohbayashi, N., Kanaho, Y., 2016. Pathological functions of the small GTPase Arf6 in cancer progression: Tumor angiogenesis and metastasis. Small GTPases 7, 47–53. https://doi.org/10.1080/21541248.2016.1154640

Hu, B., Shi, B., Jarzynka, M.J., Yiin, J.J., D'Souza-Schorey, C., Cheng, S.Y., 2009. ADP-ribosylation factor 6 regulates glioma cell invasion through the IQ-domain GTPase-activating protein 1-Rac1-mediated pathway. Cancer Res. 69, 794–801. https://doi.org/10.1158/0008-5472.CAN-08-2110

Hurd, H., Grant, K.M., Arambage, S.C., 2006. Apoptosis-like death as a feature of malaria infection in mosquitoes. Parasitology. https://doi.org/10.1017/S0031182006000849

Hurtado-Lorenzo, A., Skinner, M., El Annan, J., Futai, M., Sun-Wada, G.H., Bourgoin, S., Casanova, J., Wildeman, A., Bechoua, S., Ausiello, D.A., Brown, D., Marshansky, V., 2006. V-ATPase interacts with ARNO and Arf6 in early endosomes and regulates the protein degradative pathway. Nat. Cell Biol. 8, 124–136. https://doi.org/10.1038/ncb1348

Inaba, Y., Tian, Q.B., Okano, A., Zhang, J.P., Sakagami, H., Miyazawa, S., Li, W., Komiyama, A., Inokuchi, K., Kondo, H., Suzuki, T., 2004. Brain-specific potential guanine nucleotide exchange factor for Arf, synArfGEF (Po), is localized to postsynaptic density. J. Neurochem. 89, 1347–1357. https://doi.org/10.1111/j.1471-4159.2004.02440.x

Inoue, H., Randazzo, P.A., 2007. Arf GAPs and their interacting proteins. Traffic 8, 1465–1475. https://doi.org/10.1111/j.1600-0854.2007.00624.x

Ireton, K., 2007. Entry of the bacterial pathogen Listeria monocytogenes into mammalian cells. Cell. Microbiol. 9, 1365–1375. https://doi.org/10.1111/j.1462-5822.2007.00933.x

Isabet, T., Montagnac, G., Regazzoni, K., Raynal, B., Khadali, F. El, England, P., Franco, M., Chavrier, P., Houdusse, A., Ménétrey, J., 2009. The structural basis of Arf effector specificity: The crystal structure of ARF6 in a complex with JIP4. EMBO J. 28, 2835–2845. https://doi.org/10.1038/emboj.2009.209

Ito, H., Morishita, R., Nagata, K.I., 2018. Functions of rhotekin, an effector of rho gtpase, and its binding partners in mammals. Int. J. Mol. Sci. https://doi.org/10.3390/ijms19072121

Jackson, C.L., Casanova, J.E., 2000. Turning on ARF : the Sec7 family of exchange factors. Trends Cell Biol. 6, 60–67.

Janse, C.J., van der Klooster, P.F.J., van der Kaay, H.J., van der Ploeg, M., Prosper Overdulve, J., 1986. DNA synthesis in Plasmodium berghei during asexual and sexual development. Mol. Biochem. Parasitol. https://doi.org/10.1016/0166-6851(86)90029-0

Kabeya, Y., 2000. LC3, a mammalian homologue of yeast Apg8p, is localized in autophagosome membranes after processing. EMBO J. https://doi.org/10.1093/emboj/19.21.5720

Kahn, R.A., Bruford, E., Inoue, H., Logsdon, J.M., Nie, Z., Premont, R.T., Randazzo, P.A., Satake, M., Theibert, A.B., Zapp, M.L., Cassel, D., 2008. Consensus nomenclature for the human ArfGAP domain-containing proteins. J. Cell Biol. 182, 1039–1044. https://doi.org/10.1083/jcb.200806041

Kahn, R.A., Gilman, A.G., 1986. The protein cofactor necessary for ADP-ribosylation of G(s) by cholera toxin is itself a GTP binding protein. J. Biol. Chem. 261, 7906–7911.

Kaiser, C., 2000. Thinking about p24 proteins and how transport vesicles select their cargo. Cell 97, 3783–3785.

https://doi.org/10.1073/pnas.97.8.3783

Kattenberg, J.H., Ochodo, E.A., Boer, K.R., Schallig, H.D., Mens, P.F., Leeflang, M.M., 2011. Systematic review and meta-analysis: Rapid diagnostic tests versus placental histology, microscopy and PCR for malaria in pregnant women. Malar. J. 10, 321. https://doi.org/10.1186/1475-2875-10-321

Kirchhausen, T., 2000. <Nrm1200_187a.Pdf> 1.

Klein, E.Y., 2013. Antimalarial drug resistance: A review of the biology and strategies to delay emergence and spread. Int. J. Antimicrob. Agents. https://doi.org/10.1016/j.ijantimicag.2012.12.007

Klionsky, D.J., Abeliovich, H., Agostinis, P., Agrawal, D.K., Aliev, G., Askew, D.S., Baba, M., Baehrecke, E.H., Bahr, B.A., Ballabio, A., Bamber, B.A., Bassham, D.C., Bergamini, E., Bi, X., Biard-Piechaczyk, M., Blum, J.S., Bredesen, D.E., Brodsky, J.L., Brumell, J.H., Brunk, U.T., Bursch, W., Camougrand, N., Cebollero, E., Cecconi, F., Chen, Y., Chin, L.S., Choi, A., Chu, C.T., Chung, J., Clarke, P.G.H., Clark, R.S.B., Clarke, S.G., Clavé, C., Cleveland, J.L., Codogno, P., Colombo, M.I., Cotomontes, A., Cregg, J.M., Cuervo, A.M., Debnath, J., Demarchi, F., Dennis, P.B., Dennis, P.A., Deretic, V., Devenish, R.J., Di Sano, F., Dice, J.F., DiFiglia, M., Dinesh-Kumar, S., Distelhorst, C.W., Djavaheri-Mergny, M., Dorsey, F.C., Dröge, W., Dron, M., Dunn, W.A., Duszenko, M., Eissa, N.T., Elazar, Z., Esclatine, A., Eskelinen, E.L., Fésüs, L., Finley, K.D., Fuentes, J.M., Fueyo, J., Fujisaki, K., Galliot, B., Gao, F.B., Gewirtz, D.A., Gibson, S.B., Gohla, A., Goldberg, A.L., Gonzalez, R., González-Estévez, C., Gorski, S., Gottlieb, R.A., Häussinger, D., He, Y.W., Heidenreich, K., Hill, J.A., Høyer-Hansen, M., Hu, X., Huang, W.P., Iwasaki, A., Jäättelä, M., Jackson, W.T., Jiang, X., Jin, S., Johansen, T., Jung, J.U., Kadowaki, M., Kang, C., Kelekar, A., Kessel, D.H., Kiel, J.A.K.W., Hong, P.K., Kimchi, A., Kinsella, T.J., Kiselyov, K., Kitamoto, K., Knecht, E., Komatsu, M., Kominami, E., Kondo, S., Kovács, A.L., Kroemer, G., Kuan, C.Y., Kumar, R., Kundu, M., Landry, J., Laporte, M., Le, W., Lei, H.Y., Lenardo, M.J., Levine, B., Lieberman, A., Lim, K.L., Lin, F.C., Liou, W., Liu, L.F., Lopez-Berestein, G., López-Otín, C., Lu, B., Macleod, K.F., Malorni, W., Martinet, W., Matsuoka, K., Mautner, J., Meijer, A.J., Meléndez, A., Michels, P., Miotto, G., Mistiaen, W.P., Mizushima, N., Mograbi, B., Monastyrska, I., Moore, M.N., Moreira, P.I., Moriyasu, Y., Motyl, T., Münz, C., Murphy, L.O., Naqvi, N.I., Neufeld, T.P., Nishino, I., Nixon, R.A., Noda, T., Nürnberg, B., Ogawa, M., Oleinick, N.L., Olsen, L.J., Ozpolat, B., Paglin, S., Palmer, G.E., Papassideri, I., Parkes, M., Perlmutter, D.H., Perry, G., Piacentini, M., Pinkas-Kramarski, R., Prescott, M., Proikascezanne, T., Raben, N., Rami, A., Reggiori, F., Rohrer, B., Rubinsztein, D.C., Ryan, K.M., Sadoshima, J., Sakagami, H., Sakai, Y., Sandri, M., Sasakawa, C., Sass, M., Schneider, C., Seglen, P.O., Seleverstov, O., Settleman, J., Shacka, J.J., Shapiro, I.M., Sibirny, A., Silva-Zacarin, E.C.M., Simon, H.U., Simone, C., Simonsen, A., Smith, M.A., Spanel-Borowski, K., Srinivas, V., Steeves, M., Stenmark, H., Stromhaug, P.E., Subauste, C.S., Sugimoto, S., Sulzer, D., Suzuki, T., Swanson, M.S., Tabas, I., Takeshita, F., Talbot, N.J., Tallóczy, Z., Tanaka, K., Tanaka, K., Tanida, I., Taylor, G.S., Taylor, J.P., Terman, A., Tettamanti, G., Thompson, C.B., Thumm, M., Tolkovsky, A.M., Tooze, S.A., Truant, R., Tumanovska, L. V., Uchiyama, Y., Ueno, T., Uzcátegui, N.L., Van Der Klei, I., Vaquero, E.C., Vellai, T., Vogel, M.W., Wang, H.G., Webster, P., Wiley, J.W., Xi, Z., Xiao, G., Yahalom, J., Yang, J.M., Yap, G., Yin, X.M., Yoshimori, T., Yu, L., Yue, Z., Yuzaki, M., Zabirnyk, O., Zheng, X., Zhu, X., Deter, R.L., 2008. Guidelines for the use and interpretation of assays for monitoring autophagy in higher eukaryotes. Autophagy. https://doi.org/10.4161/auto.5338

Korenromp, E.L., Williams, B.G., De Vlas, S.J., Gouws, E., Gilks, C.F., Ghys, P.D., Nahlen, B.L., 2005. Malaria attributable to the HIV-1 epidemic, sub-Saharan Africa. Emerg. Infect. Dis. 11, 1410–1419. https://doi.org/10.3201/eid1109.050337

Kou, L., Sun, J., Zhai, Y., He, Z., 2013. The endocytosis and intracellular fate of nanomedicines: Implication for rational design. Asian J. Pharm. Sci. 8, 1–8. https://doi.org/10.1016/j.ajps.2013.07.001

Kouranti, I., Sachse, M., Arouche, N., Goud, B., Echard, A., 2006. Rab35 Regulates an Endocytic Recycling Pathway Essential for the Terminal Steps of Cytokinesis. Curr. Biol. https://doi.org/10.1016/j.cub.2006.07.020

Koushika, S.P., 2008. "JIP"ing along the axon: The complex roles of JIPs in axonal transport. BioEssays 30, 10–14. https://doi.org/10.1002/bies.20695

Krai, P., Dalal, S., Klemba, M., 2014. Evidence for a Golgi-to-endosome protein sorting pathway in Plasmodium falciparum. PLoS One. https://doi.org/10.1371/journal.pone.0089771

Laemmli, U.K., 1970. Cleavage of structural proteins during the assembly of the head of bacteriophage T4. Nature. https://doi.org/10.1038/227680a0

Langsley, G., Chakrabarti, D., 1996. Plasmodium falciparum: The small GTPase rab11. Exp. Parasitol. https://doi.org/10.1006/expr.1996.0071

Lawrence, J.T., Birnbaum, M.J., 2001. ADP-ribosylation factor 6 delineates separate pathways used by endothelin 1 and insulin for stimulating glucose uptake in 3T3-L1 adipocytes. Mol. Cell. Biol. 21, 5276–85. https://doi.org/10.1128/MCB.21.15.5276-5285.2001

Lazarus, M.D., Schneider, T.G., Taraschi, T.F., 2008. A new model for hemoglobin ingestion and transport by the human malaria parasite Plasmodium falciparum. J. Cell Sci. https://doi.org/10.1242/jcs.023150

Leber, W., Skippen, A., Fivelman, Q.L., Bowyer, P.W., Cockcroft, S., Baker, D.A., 2009. A unique phosphatidylinositol 4-phosphate 5-kinase is activated by ADP-ribosylation factor in Plasmodium falciparum. Int. J. Parasitol. https://doi.org/10.1016/j.ijpara.2008.11.015

Lee, J.-W., Ryu, Y.-K., Ji, Y.-H., Kang, J.H., Moon, E.-Y., 2015. Hypoxia/reoxygenation-experienced cancer cell migration and metastasis are regulated by Rap1- and Rac1-GTPase activation via the expression of thymosin beta-4. Oncotarget. https://doi.org/10.18632/oncotarget.3218

Lee, S.Y., Yang, J.S., Hong, W., Premont, R.T., Hsu, V.W., 2005. ARFGAP1 plays a central role in coupling COPI cargo sorting with vesicle formation. J. Cell Biol. 168, 281–290. https://doi.org/10.1083/jcb.200404008

Lefort, 2003. Elevated Phospholipase D Activity in H-Ras- but Not K-Ras-Transformed Cells by the Synergistic Action of RalA and ARF6. Mol Cell Biol 23, 645–54. https://doi.org/10.1128/MCB.23.2.645

Legendre-Guillemin, V., Metzler, M., Charbonneau, M., Gan, L., Chopra, V., Philie, J., Hayden, M.R., McPherson, P.S., 2002. HIP1 and HIP12 display differential binding to F-actin, AP2, and clathrin. Identification of a novel interaction with clathrin light chain. J. Biol. Chem. 277, 19897–19904. https://doi.org/10.1074/jbc.M112310200

Lew, V.L., Tiffert, T., Ginsburg, H., 2003. Excess hemoglobin digestion and the osmotic stability of Plasmodium falciparum - Infected red blood cells. Blood. https://doi.org/10.1182/blood-2002-08-2654

Li, J., Peters, P.J., Bai, M., Dai, J., Bos, E., Kirchhausen, T., Kandror, K. V., Hsu, V.W., 2007. An ACAP1-containing clathrin coat complex for endocytic recycling. J. Cell Biol. https://doi.org/10.1083/jcb.200608033

Li, L. V., Kandror, K. V., 2005. Golgi-Localized, γ-Ear-Containing, Arf-Binding Protein Adaptors Mediate Insulin-Responsive Trafficking of Glucose Transporter 4 in 3T3-L1 Adipocytes. Mol. Endocrinol. https://doi.org/10.1210/me.2005-0032

Liang, C.C., Park, A.Y., Guan, J.L., 2007. In vitro scratch assay: A convenient and inexpensive method for analysis of cell migration in vitro. Nat. Protoc. https://doi.org/10.1038/nprot.2007.30

Liu, Y., Kahn, R.A., Prestegard, J.H., 2009. Structure and Membrane Interaction of Myristoylated ARF1. Structure 17, 79–87. https://doi.org/10.1016/j.str.2008.10.020

Liu, Z., Miao, J., Cui, L., 2011. Gametocytogenesis in malaria parasite: Commitment, development and regulation. Future Microbiol. https://doi.org/10.2217/fmb.11.108

Logsdon, J.M., Kahn, R.A., n.d. Chapter 1 THE ARF FAMILY TREE 1–21. https://doi.org/10.1007/1-4020-2593-9_1

Losev, E., Reinke, C.A., Jellen, J., Strongin, D.E., Bevis, B.J., Glick, B.S., 2006. Golgi maturation visualized in living yeast. Nature. https://doi.org/10.1038/nature04717

M'Rabet, L., Coffer, P., Zwartkruis, F., Franke, B., Segal, A.W., Koenderman, L., Bos, J.L., 1998. Activation of the small GTPase rap1 in human neutrophils. Blood.

Macia, E., Chabre, M., Franco, M., 2001. Specificities for the Small G Proteins ARF1 and ARF6 of the Guanine Nucleotide Exchange Factors ARNO and EFA6. J. Biol. Chem. 276, 24925–24930. https://doi.org/10.1074/jbc.M103284200

Macia, E., Ehrlich, M., Massol, R., Boucrot, E., Brunner, C., Kirchhausen, T., 2006. Dynasore, a Cell-Permeable Inhibitor of Dynamin. Dev. Cell. https://doi.org/10.1016/j.devcel.2006.04.002

Majoul, I., Straub, M., Hell, S.W., Duden, R., Söling, H.D., 2001. KDEL-Cargo Regulates Interactions between Proteins Involved in COPI Vesicle Traffic: Measurements in Living Cells Using FRET. Dev. Cell 1, 139–153. https://doi.org/10.1016/S1534-5807(01)00004-1

Makyio, H., Ohgi, M., Takei, T., Takahashi, S., Takatsu, H., Katoh, Y., Hanai, A., Ueda, T., Kanaho, Y., Xie, Y., Shin, H.W., Kamikubo, H., Kataoka, M., Kawasaki, M., Kato, R., Wakatsuki, S., Nakayama, K., 2012. Structural basis for Arf6-MKLP1 complex formation on the Flemming body responsible for cytokinesis. EMBO J. 31, 2590–2603. https://doi.org/10.1038/emboj.2012.89

Maldonado-Báez, L., Cole, N.B., Krämer, H., Donaldson, J.G., 2013. Microtubule-dependent endosomal sorting of clathrin-independent cargo by Hook1. J. Cell Biol. 201, 233–247. https://doi.org/10.1083/jcb.201208172

Marchesin, V., Castro-Castro, A., Lodillinsky, C., Castagnino, A., Cyrta, J., Bonsang-Kitzis, H., Fuhrmann, L., Irondelle, M., Infante, E., Montagnac, G., Reyal, F., Vincent-Salomon, A., Chavrier, P., 2015. ARF6-JIP3/4 regulate endosomal tubules for MT1-MMP exocytosis in cancer invasion. J. Cell Biol. 211, 339–358. https://doi.org/10.1083/jcb.201506002

Maxfield, F.R., McGraw, T.E., 2004. Endocytic recycling. Nat. Rev. Mol. Cell Biol. 5, 121–132. https://doi.org/10.1038/nrm1315

Mayor, S., Parton, R.G., Donaldson, J.G., 2014. Clathrin-independent pathways of endocytosis. Cold Spring Harb. Perspect. Biol. 6, 1–20. https://doi.org/10.1101/cshperspect.a016758

Melendez, A.J., Harnett, M.M., Allen, J.M., 2001. Crosstalk between ARF6 and protein kinase Cα in Fcγ/RI-mediated activation of phospholipase D1. Curr. Biol. 11, 869–874. https://doi.org/10.1016/S0960-9822(01)00260-3

Ménétrey, J., Perderiset, M., Cicolari, J., Dubois, T., Elkhatib, N., Khadali, F. El, Franco, M., Chavrier, P., Houdusse, A., 2007. Structural basis for ARF1-mediated recruitment of ARHGAP21 to Golgi membranes. EMBO J. 26, 1953–1962. https://doi.org/10.1038/sj.emboj.7601634

Meyers, J.A., Sanchez, D., Elwell, L.P., Falkow, S., 1976. Simple agarose gel electrophoretic method for the identification and characterization of plasmid deoxyribonucleic acid. J. Bacteriol. 127, 1529–1537.

Millar, C.A., Powell, K.A., Hickson, G.R.X., Bader, M.F., Gould, G.W., 1999. Evidence for a role for ADP-ribosylation factor 6 in insulin-stimulated glucose transporter-4 (GLUT4) trafficking in 3T3-L1 adipocytes. J. Biol. Chem. https://doi.org/10.1074/jbc.274.25.17619

Mittal, R., Ahmadian, M.R., Goody, R.S., Wittinghofer, A., 1996. Formation of a transition-state analog of the Ras GTPase reaction by Ras·Gdp, tetrafluoroaluminate, and GTPase-activating proteins. Science (80-.). https://doi.org/10.1126/science.273.5271.115

Mizushima, N., Levine, B., Cuervo, A.M., Klionsky, D.J., 2008. Autophagy fights disease through cellular self-digestion. Nature. https://doi.org/10.1038/nature06639

Montagnac, G., Sibarita, J.B., Loubéry, S., Daviet, L., Romao, M., Raposo, G., Chavrier, P., 2009. ARF6 Interacts with JIP4 to Control a Motor Switch Mechanism Regulating Endosome Traffic in Cytokinesis. Curr. Biol. 19, 184–195. https://doi.org/10.1016/j.cub.2008.12.043

Moorthy, V., Reed, Z., Smith, P.G., 2007. Measurement of malaria vaccine efficacy in phase III trials: Report of a WHO consultation, in:

Vaccine. https://doi.org/10.1016/j.vaccine.2007.01.085

Moreau, K., Ravikumar, B., Puri, C., Rubinsztein, D.C., 2012. Arf6 promotes autophagosome formation via effects on phosphatidylinositol 4,5-bisphosphate and phospholipase D. J. Cell Biol. 196, 483–496. https://doi.org/10.1083/jcb.201110114

Morishige, M., Hashimoto, S., Ogawa, E., Toda, Y., Kotani, H., Hirose, M., Wei, S., Hashimoto, A., Yamada, A., Yano, H., Mazaki, Y., Kodama, H., Nio, Y., Manabe, T., Wada, H., Kobayashi, H., Sabe, H., 2008. GEP100 links epidermal growth factor receptor signalling to Arf6 activation to induce breast cancer invasion. Nat. Cell Biol. 10, 85–92. https://doi.org/10.1038/ncb1672

Moshfegh, Y., Bravo-Cordero, J.J., Miskolci, V., Condeelis, J., Hodgson, L., 2014. A Trio-Rac1-Pak1 signalling axis drives invadopodia disassembly. Nat. Cell Biol. https://doi.org/10.1038/ncb2972

Moss, J., Vaughan, M., 1995. Structure and function of ARF proteins. Activators of cholera toxin and critical components of intracellular vesicular transport processes. J. Biol. Chem. https://doi.org/10.1074/jbc.270.21.12327

Mukherjee, S., Gurevich, V. V, Jones, J.C., Casanova, J.E., Frank, S.R., Maizels, E.T., Bader, M.F., Kahn, R.A., Palczewski, K., Aktories, K., Hunzicker-Dunn, M., 2000. The ADP ribosylation factor nucleotide exchange factor ARNO promotes beta-arrestin release necessary for luteinizing hormone/choriogonadotropin receptor desensitization. Proc. Natl. Acad. Sci. U. S. A. 97, 5901–6. https://doi.org/10.1073/pnas.100127097

Mullis, K., Faloona, F., Scharf, S., Saiki, R., Horn, G., Erlich, H., 1986. Specific enzymatic amplification of DNA in vitro: The polymerase chain reaction. Cold Spring Harb. Symp. Quant. Biol. https://doi.org/10.1101/SQB.1986.051.01.032

Murphy, D.A., Courtneidge, S.A., 2011. The "ins" and "outs" of podosomes and invadopodia: Characteristics, formation and function. Nat. Rev. Mol. Cell Biol. 12, 413–426. https://doi.org/10.1038/nrm3141

Murphy, J.A., Jensen, O.N., Walikonis, R.S., 2006. BRAG1, a Sec7 domain-containing protein, is a component of the postsynaptic density of excitatory synapses. Brain Res. 1120, 35–45. https://doi.org/10.1016/j.brainres.2006.08.096

Murray, A.M., Kelly, C.D., Nussey, S.S., Johnstone, A.P., 1998. Production of glutathione-coated microtitre plates for capturing recombinant glutathione S-transferase fusion proteins as antigens in immunoassays. J. Immunol. Methods. https://doi.org/10.1016/S0022-1759(98)00114-8

Nadjm, B., Behrens, R.H., 2012. Malaria: An Update for Physicians. Infect. Dis. Clin. North Am. https://doi.org/10.1016/j.idc.2012.03.010

Nagai, H., Kagan, J.C., Zhu, X., Kahn, R.A., Roy, C.R., 2002. A bacterial guanine nucleotide exchange factor activates ARF on Legionella phagosomes. Science (80-.). 295, 679–682. https://doi.org/10.1126/science.1067025

Naslavsky, N., 2003. Convergence of Non-clathrin- and Clathrin-derived Endosomes Involves Arf6 Inactivation and Changes in Phosphoinositides. Mol. Biol. Cell. https://doi.org/10.1091/mbc.02

Neafsey, D.E., 2013. Genome sequencing sheds light on emerging drug resistance in malaria parasites. Nat. Genet. https://doi.org/10.1038/ng.2648

Neu, M., Brachvogel, V., Oschkinat, H., Zerial, M., Metcalf, P., 1997. Rab7: NMR and kinetics analysis of intact and C-terminal truncated constructs. Proteins Struct. Funct. Genet. 27, 204–209. https://doi.org/10.1002/(SICI)1097-0134(199702)27:2<204::AID-PROT6>3.0.CO;2-F

Nguyen, D.X., Bos, P.D., Massagué, J., 2009. Metastasis: From dissemination to organ-specific colonization. Nat. Rev. Cancer 9, 274–284. https://doi.org/10.1038/nrc2622

Nickel, W., Brugger, B., Wieland, F.T., 2002. Vesicular transport: the core machinery of COPI recruitment and budding. J. Cell Sci. 115, 3235–3240.

Nie, Z., Hirsch, D.S., Randazzo, P.A., 2003. Arf and its many interactors. Curr. Opin. Cell Biol. 15, 396–404. https://doi.org/10.1016/S0955-0674(03)00071-1

Niedergang, F., Colucci-Guyon, E., Dubois, T., Raposo, G., Chavrier, P., 2003. ADP ribosylation factor 6 is activated and controls membrane delivery during phagocytosis in macrophages. J. Cell Biol. 161, 1143–1150. https://doi.org/10.1083/jcb.200210069

Nishi, K., Saigo, K., 2007. Cellular internalization of green fluorescent protein fused with herpes simplex virus protein VP22 via a lipid raft-mediated endocytic pathway independent of caveolae and Rho family GTPases but dependent on dynamin and Arf6. J. Biol. Chem. https://doi.org/10.1074/jbc.M703810200

Noser, J.A., Mael, A.A., Sakuma, R., Ohmine, S., Marcato, P., Lee, P.W.K., Ikeda, Y., 2007. The RAS/Raf1/MEK/ERK signaling pathway facilitates VSV-mediated oncolysis: Implication for the defective interferon response in cancer cells. Mol. Ther. https://doi.org/10.1038/sj.mt.6300193

O'Neal, C.J., Jobling, M.G., Holmes, R.K., Hol, W.G.J., 2005. Structural basis for the activation of cholera toxin by human ARF6-GTP. Science (80-.). 309, 1093–1096. https://doi.org/10.1126/science.1113398

Ohashi, Y., Iijima, H., Yamaotsu, N., Yamazaki, K., Sato, S., Okamura, M., Sugimoto, K., Dan, S., Hirono, S., Yamori, T., 2012. AMF-26, a novel inhibitor of the Golgi system, targeting ADP-ribosylation factor 1 (Arf1) with potential for cancer therapy. J. Biol. Chem. 287, 3885–3897. https://doi.org/10.1074/jbc.M111.316125

Okada, R., Yamauchi, Y., Hongu, T., Funakoshi, Y., Ohbayashi, N., Hasegawa, H., Kanaho, Y., 2015. Activation of the Small G Protein Arf6 by Dynamin2 through guanine nucleotide exchange factors in endocytosis. Sci. Rep. 5, 1–11. https://doi.org/10.1038/srep14919

Ooi, C.E., Dell'Angelica, E.C., Bonifacino, J.S., 1998. ADP-ribosylation factor 1 (ARF1) regulates recruitment of the AP-3 adaptor complex to membranes. J. Cell Biol. 142, 391–402. https://doi.org/10.1083/jcb.142.2.391

Paborsky, L.R., Dunn, K.E., Gibbs, C.S., Dougherty, J.P., 1996. A nickel chelate microtiter plate assay for six histidine-containing proteins. Anal. Biochem. https://doi.org/10.1006/abio.1996.0050

Palacios, F., D'Souza-Schorey, C., 2003. Modulation of Rac1 and ARF6 activation during epithelial cell scattering. J. Biol. Chem. 278, 17395–17400. https://doi.org/10.1074/jbc.M300998200

Palacios, F., Price, L., Schweitzer, J., Collard, J.G., D'Souza-Schorey, C., 2001. An essential role for ARF6-regulated membrane traffic in adherens junction turnover and epithelial cell migration. EMBO J. 20, 4973–4986. https://doi.org/10.1093/emboj/20.17.4973

Palacios, F., Schweitzer, J.K., Boshans, R.L., D'Souza-Schorey, C., 2002. ARF6-GTP recruits Nm23-H1 to facilitate dynamin-mediated endocytosis during adherens junctions disassembly. Nat. Cell Biol. 4, 929–936. https://doi.org/10.1038/ncb881

Paleotti, O., Macia, E., Luton, F., Klein, S., Partisani, M., Chardin, P., Kirchhausen, T., Franco, M., 2005. The small G-protein Arf6GTPrecruits the AP-2 adaptor complex to membranes. J. Biol. Chem. 280, 21661–21666. https://doi.org/10.1074/jbc.M503099200

Palmer, D.J., Helms, J.B., Beckers, C.J.M., Orci, L., Rothman, J.E., 1993. Binding of coatomer to Golgi membranes requires ADP-ribosylation factor. J. Biol. Chem. 268, 12083–12089.

Paris, S., Béraud-Dufour, S., Robineau, S., Bigay, J., Antonny, B., Chabre, M., Chardin, P., 1997. Role of protein-phospholipid interactions in the activation of ARF1 by the guanine nucleotide exchange factor Arno. J. Biol. Chem. 272, 22221–22226. https://doi.org/10.1074/jbc.272.35.22221

Parker, K.H., Horn, L.A., Ostrand-Rosenberg, S., 2016. High-mobility group box protein 1 promotes the survival of myeloid-derived suppressor cells by inducing autophagy. J. Leukoc. Biol. https://doi.org/10.1189/jlb.3HI0715-305R

Pasqualato, S., Renault, L., Cherfils, J., 2002. Arf, Arl, Arp and Sar proteins: A family of GTP-binding proteins with a structural device for "front-back" communication. EMBO Rep. 3, 1035–1041. https://doi.org/10.1093/embo-reports/kvf221

Perkins, M.D., Bell, D.R., 2008. Working without a blindfold: The critical role of diagnostics in malaria control. Malar. J. 7, 1–9. https://doi.org/10.1186/1475-2875-7-S1-S5

Peters, P.J., Hsu, V.W., Ooi, C.E., Finazzi, D., Teal, S.B., Oorschot, V., Donaldson, J.G., Klausner, R.D., 1995. Overexpression of wild-type and mutant ARF1 and ARF6: Distinct perturbations of nonoverlapping membrane compartments. J. Cell Biol. 128, 1003–1017. https://doi.org/10.1083/jcb.128.6.1003

Peyroche, A., Antonny, B., Robineau, S., Acker, J., Cherfils, J., Jackson, C.L., 1999. Brefeldin A acts to stabilize an abortive ARF-GDP-Sec7 domain protein complex: Involvement of specific residues of the Sec7 domain. Mol. Cell. https://doi.org/10.1016/S1097-2765(00)80455-4

Ploug, T., Van Deurs, B., Ai, H., Cushman, S.W., Ralston, E., 1998. Analysis of GLUT4 distribution in whole skeletal muscle fibers: Identification of distinct storage compartments that are recruited by insulin and muscle contractions. J. Cell Biol. https://doi.org/10.1083/jcb.142.6.1429

Poon, P.P., Cassel, D., Spang, A., Rotman, M., Pick, E., Singer, R.A., Johnston, G.C., 1999. Retrograde transport from the yeast Golgi is mediated by two ARF GAP proteins with overlapping function. EMBO J. https://doi.org/10.1093/emboj/18.3.555

Powelka, A.M., Sun, J., Li, J., Gao, M., Shaw, L.M., Sonnenberg, A., Hsu, V.W., 2004. Stimulation-dependent recycling of integrin β1 regulated by ARF6 and Rab11. Traffic 5, 20–36. https://doi.org/10.1111/j.1600-0854.2004.00150.x

Powner, D.J., Hodgkin, M.N., Wakelam, M.J.O., 2002. Antigen-stimulated Activation of Phospholipase D1b by Rac1, ARF6, and PKC□ in RBL-2H3 Cells. Mol. Biol. Cell. https://doi.org/10.1091/mbc.01

Prati Pal Singh, Purbali Chakraborty, 2016. Malaria: Autophagy as a Potential Therapeutic Target. J. Pharm. Pharmacol. 4, 298–306. https://doi.org/10.17265/2328-2150/2016.07.003

Radhakrishna, H., Donaldson, J.G., 1997. ADP-ribosylation factor 6 regulates a novel plasma membrane recycling pathway. J. Cell Biol. 139, 49–61. https://doi.org/10.1083/jcb.139.1.49

Randazzo, P.A., Hirsch, D.S., 2004. Arf GAPs: Multifunctional proteins that regulate membrane traffic and actin remodelling. Cell. Signal. 16, 401–413. https://doi.org/10.1016/j.cellsig.2003.09.012

Randazzo, P.A., Inoue, H., Bharti, S., 2007. Arf GAPs as regulators of the actin cytoskeleton. Biol. Cell 99, 583–600. https://doi.org/10.1042/BC20070034

Ravikumar, B., Futter, M., Jahreiss, L., Korolchuk, V.I., Lichtenberg, M., Luo, S., Massey, D.C.O., Menzies, F.M., Narayanan, U., Renna, M., Jimenez-Sanchez, M., Sarkar, S., Underwood, B., Winslow, A., Rubinsztein, D.C., 2009. Mammalian macroautophagy at a glance. J. Cell Sci. https://doi.org/10.1242/jcs.031773

Ravikumar, B., Moreau, K., Jahreiss, L., Puri, C., Rubinsztein, D.C., 2010. Plasma membrane contributes to the formation of pre-autophagosomal structures. Nat. Cell Biol. https://doi.org/10.1038/ncb2078

Rea, S., James, D.E., 1997. Moving GLUT4: The biogenesis and trafficking of GLUT4 storage vesicles. Diabetes. https://doi.org/10.2337/diab.46.11.1667

Redmann, M., Benavides, G.A., Berryhill, T.F., Wani, W.Y., Ouyang, X., Johnson, M.S., Ravi, S., Barnes, S., Darley-Usmar, V.M., Zhang, J., 2017. Inhibition of autophagy with bafilomycin and chloroquine decreases mitochondrial quality and bioenergetic function in primary neurons. Redox Biol. https://doi.org/10.1016/j.redox.2016.11.004

REJMAN, J., OBERLE, V., ZUHORN, I.S., HOEKSTRA, D., 2004. Size-dependent internalization of particles via the pathways of clathrin- and caveolae-mediated endocytosis. Biochem. J. 377, 159–169. https://doi.org/10.1042/bj20031253

Renault, L., Guibert, B., Cherfils, J., 2003. Structural snapshots of the mechanism and inhibition of a guanine nucleotide exchange factor. Nature 426, 525–530. https://doi.org/10.1038/nature02197

Riley, E.M., Stewart, V.A., 2013. Immune mechanisms in malaria: New insights in vaccine development. Nat. Med. https://doi.org/10.1038/nm.3083

Rittinger, K., Walker, P.A., Eccleston, J.F., Smerdon, S.J., Gamblin, S.J., 1997. Structure at 1.65 Å of RhoA and its GTPase-activating protein in complex with a transition-state analogue. Nature 389, 758–762. https://doi.org/10.1038/39651

Robinson, M.S., Bonifacino, J.S., 2001. Adaptor-related proteins. Curr. Opin. Cell Biol. 13, 444–453. https://doi.org/10.1016/S0955-0674(00)00235-0

Rothman, J.E., 2002. The machinery and principles of vesicle transport in the cell. Nat. Med. 8, 1059–1062. https://doi.org/10.1038/nm770

Sáenz, J.B., Sun, W.J., Chang, J.W., Li, J., Bursulaya, B., Gray, N.S., Haslam, D.B., 2009. Golgicide A reveals essential roles for GBF1 in Golgi assembly and function. Nat. Chem. Biol. 5, 157–165. https://doi.org/10.1038/nchembio.144

Sakagami, H., 2008. The EFA6 family: guanine nucleotide exchange factors for ADP ribosylation factor 6 at neuronal synapses. Tohoku J. Exp. Med. 214, 191–198. https://doi.org/10.1620/tjem.214.191

Sangar, F., Schreurs, A.S., Umaña-Diaz, C., Clapéron, A., Desbois-Mouthon, C., Calmel, C., Mauger, O., Zaanan, A., Miquel, C., Fléjou, J.F., Praz, F., 2014. Involvement of small ArfGAP1 (SMAP1), a novel Arf6-specific GTPase-activating protein, in microsatellite instability oncogenesis. Oncogene 33, 2758–2767. https://doi.org/10.1038/onc.2013.211

Sannerud, R., Declerck, I., Peric, A., Raemaekers, T., Menendez, G., Zhou, L., Veerle, B., Coen, K., Munck, S., De Strooper, B., Schiavo, G., Annaert, W., 2011. ADP ribosylation factor 6 (ARF6) controls amyloid precursor protein (APP) processing by mediating the endosomal sorting of BACE1. Proc. Natl. Acad. Sci. https://doi.org/10.1073/pnas.1100745108

Santy, L.C., Casanova, J.E., 2001. Activation of ARF6 by ARNO stimulates epithelial cell migration through downstream activation of both Rac1 and phospholipase D. J. Cell Biol. 154, 599–610. https://doi.org/10.1083/jcb.200104019

Santy, L.C., Ravichandran, K.S., Casanova, J.E., 2005. The DOCK180/Elmo complex couples ARNO-mediated Arf6 activation to the downstream activation of Rac1. Curr. Biol. 15, 1749–1754. https://doi.org/10.1016/j.cub.2005.08.052

Sartorius, K., Sartorius, B., Govender, P.S., Sharma, V., Sherriff, A., 2016. The future cost of cancer in South Africa: An interdisciplinary cost management strategy. South African Med. J. https://doi.org/10.7196/SAMJ.2016.v106i10.11375

Sato, M., Sato, K., Liou, W., Pant, S., Harada, A., Grant, B.D., 2008. Regulation of endocytic recycling by C. elegans Rab35 and its regulator RME-4, a coated-pit protein. EMBO J. https://doi.org/10.1038/emboj.2008.54

Schacht, A.L., Lindborg, S.R., Mytelka, D.S., Persinger, C.C., Paul, S.M., Munos, B.H., Dunwiddie, C.T., 2010. How to improve R&D productivity: the pharmaceutical industry's grand challenge. Nat. Rev. Drug Discov. 9, 203–214. https://doi.org/10.1038/nrd3078

Scheffzek, K., Ahmadian, M.R., Kabsch, W., Wiesmüller, L., Lautwein, A., Schmitz, F., Wittinghofer, A., Wiesmoller, L., Wittinghofert, A., 2010. -RESEARCH ARTICLES The Ras-RasGAP Complex : Structural Basis for GTPase Its in Activation and Oncogenic Ras Mutants. Adv. Sci. 277, 333–338.

Schmalzigaug, R., Phee, H., Davidson, C.E., Weiss, A., Premont, R.T., 2007. Differential expression of the ARF GAP genes GIT1 and GIT2 in mouse tissues. J. Histochem. Cytochem. 55, 1039–1048. https://doi.org/10.1369/jhc.7A7207.2007

Schmölders, J., Manske, C., Otto, A., Hoffmann, C., Steiner, B., Welin, A., Becher, D., Hilbi, H., 2017. Comparative Proteomics of Purified Pathogen Vacuoles Correlates Intracellular Replication of *Legionella pneumophila* with the Small GTPase Ras-related protein 1 (Rap1). Mol. Cell. Proteomics. https://doi.org/10.1074/mcp.M116.063453

Schweitzer, J.K., D'Souza-Schorey, C., 2005. A requirement for ARF6 during the completion of cytokinesis. Exp. Cell Res. 311, 74–83. https://doi.org/10.1016/j.yexcr.2005.07.033

Schweitzer, J.K., D'Souza-Schorey, C., 2002. Localization and activation of the ARF6 GTPase during cleavage furrow ingression and cytokinesis. J. Biol. Chem. 277, 27210–27216. https://doi.org/10.1074/jbc.M201569200

Schweitzer, J.K., Sedgwick, A.E., D'Souza-Schorey, C., 2011. ARF6-mediated endocytic recycling impacts cell movement, cell division and lipid homeostasis. Semin. Cell Dev. Biol. 22, 39–47. https://doi.org/10.1016/j.semcdb.2010.09.002

Senkovich, O., Chattopadhyay, D., 2004. Plasmodium falciparum ARFGAP: Expression and crystallization of the catalytic domain. Biochim. Biophys. Acta - Proteins Proteomics 1698, 127–130. https://doi.org/10.1016/j.bbapap.2003.10.007

Shen, Y., Naujokas, M., Park, M., Ireton, K., 2000. InIB-dependent internalization of Listeria is mediated by the Met receptor tyrosine kinase. Cell 103, 501–510. https://doi.org/10.1016/S0092-8674(00)00141-0

Shin, O.H., Couvillon, A.D., Exton, J.H. joh., 2001. Arfophilin is a common target of both class II and class III ADP-ribosylation factors. Biochemistry 40, 10846–10852. https://doi.org/10.1021/bi0107391

Shin, O.H., Ross, A.H., Mihai, I., Exton, J.H., 1999. Identification of arfophilin, a target protein for GTP-bound class II ADP-ribosylation factors. J. Biol. Chem. 274, 36609–36615. https://doi.org/10.1074/jbc.274.51.36609

Sigismund, S., Argenzio, E., Tosoni, D., Cavallaro, E., Polo, S., Di Fiore, P.P., 2008. Clathrin-Mediated Internalization Is Essential for Sustained EGFR Signaling but Dispensable for Degradation. Dev. Cell. https://doi.org/10.1016/j.devcel.2008.06.012

Silva, C.V. da, Silva, E.A. da, Cruz, M.C., Chavrier, P., Mortara, R.A., 2009. ARF6, PI3-kinase and host cell actin cytoskeleton in Toxoplasma gondii cell invasion. Biochem. Biophys. Res. Commun. 378, 656–661. https://doi.org/10.1016/j.bbrc.2008.11.108

Sinai, A.P., Roepe, P.D., 2012. Autophagy in Apicomplexa: A life sustaining death mechanism? Trends Parasitol. https://doi.org/10.1016/j.pt.2012.06.006

Sinden, R.E., Talman, A., Marques, S.R., Wass, M.N., Sternberg, M.J.E., 2010. The flagellum in malarial parasites. Curr. Opin. Microbiol. https://doi.org/10.1016/j.mib.2010.05.016

Singh, M.K., Gao, H., Sun, W., Song, Z., Schmalzigaug, R., Premont, R.T., Zhang, Q., 2015. Structure-activity relationship studies of QS11, a small molecule Wnt synergistic agonist. Bioorganic Med. Chem. Lett. https://doi.org/10.1016/j.bmcl.2015.06.062

Sinz, A., Arlt, C., Chorev, D., Sharon, M., 2015. Chemical cross-linking and native mass spectrometry: A fruitful combination for structural biology. Protein Sci. https://doi.org/10.1002/pro.2696

SLOMIANNY, C., PRENSIER, G., 1990. A Cytochemical Ultrastructural Study of the Lysosomal System of Different Species of Malaria Parasites. J. Protozool. https://doi.org/10.1111/j.1550-7408.1990.tb01247.x

Song, J., Khachikian, Z., Radhakrishna, H., Donaldson, J.G., 1998. Localization of endogenous ARF6 to sites of cortical actin rearrangement and involvement of ARF6 in cell spreading. J. Cell Sci. 111 (Pt 1, 2257–67. https://doi.org/10.1083/JCB.124.3.289

Springer, S., Spang, A., Schekman, R., 1999. Minireview 97, 145–148.

Stahl, P., Schwartz, A.L., 1986. Receptor-mediated endocytosis. J. Clin. Invest. https://doi.org/10.1172/JCI112359

Stamnes, M.A., Rothman, J.E., 1993. The binding of AP-1 clathrin adaptor particles to Golgi membranes requires ADP-ribosylation factor, a small GTP-binding protein. Cell 73, 999–1005. https://doi.org/10.1016/0092-8674(93)90277-W

Stewart, B.W., Wild, C.P., Report, W.C., 2014. World cancer report 2014, World Cancer Report 2014. https://doi.org/9283204298

Sullivan, D.J., Gluzman, I.Y., Goldberg, D.E., 1996. Plasmodium hemozoin formation mediated by histidine-rich proteins. Science (80-.). https://doi.org/10.1126/science.271.5246.219

Suresh, N., Haldar, K., 2018. Mechanisms of artemisinin resistance in Plasmodium falciparum malaria. Curr. Opin. Pharmacol. https://doi.org/10.1016/j.coph.2018.06.003

Szatmari, Z., Kis, V., Lippai, M., Hegedus, K., Farago, T., Lorincz, P., Tanaka, T., Juhasz, G., Sass, M., 2014. Rab11 facilitates cross-talk between autophagy and endosomal pathway through regulation of Hook localization. Mol. Biol. Cell 25, 522–531. https://doi.org/10.1091/mbc.E13-10-0574

Takai, Y., Sasaki, T., Matozaki, T., 2001. Small GTP-Binding Proteins. Physiol. Rev. 81, 153–209. https://doi.org/10.1038/353668a0

Talman, A.M., Domarle, O., McKenzie, F.E., Ariey, F., Robert, V., 2004. Gametocytogenesis: The puberty of Plasmodium falciparum. Malar. J. https://doi.org/10.1186/1475-2875-3-24

Tanabe, K., Kon, S., Natsume, W., Torii, T., Watanabe, T., Satake, M., 2006. Involvement of a novel ADP-ribosylation factor GTPase-activating protein, SMAP, in membrane trafficking: Implications in cancer cell biology. Cancer Sci. 97, 801–806. https://doi.org/10.1111/j.1349-7006.2006.00251.x

Tang, W., Tam, J.H.K., Seah, C., Chiu, J., Tyrer, A., Cregan, S.P., Meakin, S.O., Pasternak, S.H., 2015. Arf6 controls beta-amyloid production by regulating macropinocytosis of the Amyloid Precursor Protein to lysosomes. Mol. Brain 8. https://doi.org/10.1186/s13041-015-0129-7

Teixeira, T.L., Cruz, L., Mortara, R.A., Da Silva, C.V., 2015. Revealing Annexin A2 and ARF-6 enrollment during Trypanosoma cruzi extracellular amastigote-host cell interaction. Parasites and Vectors. https://doi.org/10.1186/s13071-015-1097-6

Tekwani, B., Walker, L., 2005. Targeting the Hemozoin Synthesis Pathway for New Antimalarial Drug Discovery: Technologies for In Vitro β-Hematin Formation Assay. Comb. Chem. High Throughput Screen. https://doi.org/10.2174/1386207053328101

Tomlins, A.M., Ben-Rached, F., Williams, R.A., Proto, W.R., Coppens, I., Ruch, U., Gilberger, T.W., Coombs, G.H., Mottram, J.C., Müller, S., Langsley, G., 2013. Plasmodium falciparum ATG8 implicated in both autophagy and apicoplast formation. Autophagy. https://doi.org/10.4161/auto.25832

Traub, L.M., Ostrom, J.A., Kornfeld, S., 1993. Biochemical dissection of AP-1 recruitment onto Golgi membranes. J. Cell Biol. 123, 561–573. https://doi.org/10.1083/jcb.123.3.561

Tsuchiya, M., Price, S.R., Tsai, S.C., Moss, J., Vaughan, M., 1991. Molecular identification of ADP-ribosylation factor mRNAs and their expression in mammalian cells. J. Biol. Chem. 266, 2772–2777.

Turner, C.E., West, K.A., Brown, M.C., 2001. Paxillin-ARF GAP signaling and the cytoskeleton. Curr. Opin. Cell Biol. 13, 593–599. https://doi.org/10.1016/S0955-0674(00)00256-8

Uchida, B.H., Kondo, A., Yoshimura, Y., Mazaki, Y., Sabe, H., 2001. ADP-Ribosylation Factor (ARF), Regulates ARF6 in Fc □ Receptor

– mediated Phagocytosis of Macrophages. J. Exp. Med 193, 955–966. https://doi.org/10.1084/jem.193.8.955

Utani, A., 2010. Molecular Mechanisms Controlling GLUT4 Intracellular Retention. Seikagaku. https://doi.org/10.1091/mbc.E08

Vanden Broeck, D., Horvath, C., De Wolf, M.J.S., 2007. Vibrio cholerae: Cholera toxin. Int. J. Biochem. Cell Biol. 39, 1771–1775. https://doi.org/10.1016/j.biocel.2007.07.005

Vetter, I.R., Wittinghofer, A., 2001. The guanine nucleotide-binding switch in three dimensions. Science (80-.). 294, 1299–1304. https://doi.org/10.1126/science.1062023

Viaud, J., Zeghouf, M., Barelli, H., Zeeh, J.-C., Padilla, A., Guibert, B., Chardin, P., Royer, C.A., Cherfils, J., Chavanieu, A., 2007. Structure-based discovery of an inhibitor of Arf activation by Sec7 domains through targeting of protein-protein complexes. Proc. Natl. Acad. Sci. 104, 10370–10375. https://doi.org/10.1073/pnas.0700773104

Volpicelli-Daley, L.A., Li, Y., Zhang, C.-J., A., K.R., 2005. Isoform-selective Effects of the Depletion of ADP- Ribosylation Factors 1–5 on Membrane Traffic. Mol. Biol. Cell. https://doi.org/10.1091/mbc.E04

Wagner, J.C., Platt, R.J., Goldfless, S.J., Zhang, F., Niles, J.C., 2014. Efficient CRISPR-Cas9-mediated genome editing in Plasmodium falciparum. Nat. Methods. https://doi.org/10.1038/nmeth.3063

Weimer, C., Beck, R., Eckert, P., Reckmann, I., Moelleken, J., Brügger, B., Wieland, F., 2008. Differential roles of ArfGAP1, ArfGAP2, and ArfGAP3 in COPI traffi cking. J. Cell Biol. https://doi.org/10.1083/jcb.200806140

Wenk, M.R., De Camilli, P., 2004. Protein-lipid interactions and phosphoinositide metabolism in membrane traffic: Insights from vesicle recycling in nerve terminals. Proc. Natl. Acad. Sci. https://doi.org/10.1073/pnas.0401874101

Western, L.M., Rose, S.J., 1991. A novel DNA joining activity catalyzed by T4 DNA ligase. Nucleic Acids Res. 19, 809–813. https://doi.org/10.1093/nar/19.4.809

White, N.J., Sc, D., 2006. Malaria — Time to Act 1956–1957.

Wickham, M.E., Culvenor, J.G., Cowman, A.F., 2003. Selective inhibition of a two-step egress of malaria parasites from the host erythrocyte. J. Biol. Chem. https://doi.org/10.1074/jbc.M305252200

Wiek, S., Cowman, A.F., Lingelbach, K., 2004. Double cross-over gene replacement within the sec 7 domain of a GDP-GTP exchange factor from Plasmodium falciparum allows the generation of a transgenic brefeldin A-resistant parasite line. Mol. Biochem. Parasitol. 138, 51–55. https://doi.org/10.1016/j.molbiopara.2004.06.015

Wieland, F., Harter, C., 1999. Mechanisms of vesicle formation: Insights from the COP system. Curr. Opin. Cell Biol. 11, 440–446. https://doi.org/10.1016/S0955-0674(99)80063-5

Wilson, R.A., Talbot, N.J., 2009. Under pressure: Investigating the biology of plant infection by Magnaporthe oryzae. Nat. Rev. Microbiol. 7, 185–195. https://doi.org/10.1038/nrmicro2032

Wittinghofer, A., 1997. Signaling mechanistics: aluminum fluoride for molecule of the year. Curr. Biol. 7, R682-5. https://doi.org/10.1016/S0960-9822(06)00355-1

Wong, A.R.C., Pearson, J.S., Bright, M.D., Munera, D., Robinson, K.S., Lee, S.F., Frankel, G., Hartland, E.L., 2011. Enteropathogenic and enterohaemorrhagic Escherichia coli: Even more subversive elements. Mol. Microbiol. 80, 1420–1438. https://doi.org/10.1111/j.1365-2958.2011.07661.x

Wong, K.-W., Isberg, R.R., 2003. Arf6 and Phosphoinositol-4-Phosphate-5-Kinase Activities Permit Bypass of the Rac1 Requirement for β_1 Integrin–mediated Bacterial Uptake. J. Exp. Med. 198, 603–614. https://doi.org/10.1084/jem.20021363

Xie, Z., Klionsky, D.J., 2007. Autophagosome formation: Core machinery and adaptations. Nat. Cell Biol. https://doi.org/10.1038/ncb1007-1102

Yamauchi, Y., Miura, Y., Kanaho, Y., 2017. Machineries regulating the activity of the small GTPase Arf6 in cancer cells are potential targets for developing innovative anti-cancer drugs. Adv. Biol. Regul. 63, 115–121. https://doi.org/10.1016/j.jbior.2016.10.004

Yang, J., Zhang, Z., Roe, S.M., Marshall, C.J., Barford, D., 2009. by a Nucleotide Sensor 1398–1403.

Yeganeh, B., Wiechec, E., Ande, S.R., Sharma, P., Moghadam, A.R., Post, M., Freed, D.H., Hashemi, M., Shojaei, S., Zeki, A.A., Ghavami, S., 2014. Targeting the mevalonate cascade as a new therapeutic approach in heart disease, cancer and pulmonary disease. Pharmacol. Ther. https://doi.org/10.1016/j.pharmthera.2014.02.007

Yegorov, S., Galiwango, R.M., Ssemaganda, A., Muwanga, M., Wesonga, I., Miiro, G., Drajole, D.A., Kain, K.C., Kiwanuka, N., Bagaya, B.S., Kaul, R., 2016. Low prevalence of laboratory-confirmed malaria in clinically diagnosed adult women from the Wakiso district of Uganda. Malar. J. 15, 1–8. https://doi.org/10.1186/s12936-016-1604-z

Yoo, J.H., Shi, D.S., Grossmann, A.H., Sorensen, L.K., Tong, Z.Z., Mleynek, T.M., Rogers, A., Zhu, W., Richards, J.R., Winter, J.M., Zhu, J., Dunn, C., Bajji, A., Shenderovich, M., Mueller, A.L., Woodman, S.E., Harbour, J.W., Thomas, K.R., Odelberg, S.J., Ostanin, K., Li, D.Y., 2016. ARF6 Is an Actionable Node that Orchestrates Oncogenic GNAQ Signaling in Uveal Melanoma. Cancer Cell 29, 889–904. https://doi.org/10.1016/j.ccell.2016.04.015

Yoon, H.Y., Bonifacino, J.S., Randazzo, P.A., 2006. In vitro assays of Arf1 interaction with GGA proteins. Methods Enzymol. https://doi.org/10.1016/S0076-6879(05)04028-0

Zengel, P., Nguyen-Hoang, A., Schildhammer, C., Zantl, R., Kahl, V., Horn, E., 2011. µ-Slide Chemotaxis: A new chamber for long-term

chemotaxis studies. BMC Cell Biol. https://doi.org/10.1186/1471-2121-12-21

Zhang, J.H., Chung, T.D.Y., Oldenburg, K.R., 1999. A simple statistical parameter for use in evaluation and validation of high throughput screening assays. J. Biomol. Screen. https://doi.org/10.1177/108705719900400206

Zhang, Q., Major, M.B., Takanashi, S., Camp, N.D., Nishiya, N., Peters, E.C., Ginsberg, M.H., Jian, X., Randazzo, P.A., Schultz, P.G., Moon, R.T., Ding, S., 2007. Small-molecule synergist of the Wnt/beta-catenin signaling pathway. Proc. Natl. Acad. Sci. https://doi.org/10.1073/pnas.0702136104

Zhou, H.C., Gao, Y.H., Zhong, X., Wang, H., 2009. Dynamin like protein 1 participated in the hemoglobin uptake pathway of Plasmodium falciparum. Chin. Med. J. (Engl). https://doi.org/10.3760/cma.j.issn.0366-6999.2009.14.015

Zhu, W., London, N.R., Gibson, C.C., Davis, C.T., Tong, Z., Sorensen, L.K., Shi, D.S., Guo, J., Smith, M.C.P., Grossmann, A.H., Thomas, K.R., Li, D.Y., 2012. Interleukin receptor activates a MYD88-ARNO-ARF6 cascade to disrupt vascular stability. Nature 492, 252–255. https://doi.org/10.1038/nature11603

Zhu, Y., Traub, L.M., Kornfeld, S., 1999. High-Affinity Binding Of The AP-1 Adaptor Complex to Trans-Golgi Network Membranes Devoid Of Mannose 6-Phosphate Receptors. Mol. Biol. Cell 10, 537–549. https://doi.org/10.1091/mbc.10.3.537

Zorzano, A., Munoz, P., Camps, M., Mora, C., Testar, X., Palacin, M., 1996. Insulin-induced redistribution of GLUT4 glucose carriers in the muscle fiber: In search of GLUT4 trafficking pathways, in: Diabetes. https://doi.org/10.1016/j.agee.2015.09.038